Bulletin

of

The Geological Society of America

VOLUME 62 August 1951 NUMBER 8

CONTENTS

	Pages
Deformation of Yule marble:	
Part I—Compression and extension experiments on dry Yule marble at 10,000 atmospheres confining pressure, room temperature. By David Griggs and W. B. Miller	853–862
Part II—Predicted fabric changes. By John W. Handin and David Griggs	863–886
Part III—Observed fabric changes due to deformation at 10,000 atmospheres confining pressure, room temperature, dry. By Francis J. Turner and C. S. Ch'ih	887–906
Mold of a rhinoceros in basalt, Lower Grand Coulee, Washington. By Walter M. Chappell, J. Wyatt Durham, and Donald E. Savage	907–918
Further biogeochemical data from the San Manuel copper deposit, Pinal County, Arizona. By Harry V. Warren, Robert E. Delavault, and Ruth I. Irish	919–930
Mount Lincoln-Castle Peak area, Sierra Nevada, California. By F. S. Hudson	931–952
Nankoweap group of the Grand Canyon Algonkian of Arizona. By C. E. Van Gundy	953–960
Short Note	
Deep-sea sands and submarine canyons. By D. B. Ericson, Maurice Ewing, and B. C. Heezen	961–966

Subscription $15.00 per year.

Publication Office: Mt. Royal & Guilford Aves., Baltimore 2, Md.

Communications for publication should be addressed to The Geological Society of America, Dr. H. R. Aldrich, Secretary, 419 West 117th Street, New York, N. Y.

NOTICE.—Four weeks notice of change of address is necessary. In accordance with the rules established by the Council, claims for non-receipt of the preceding number of the Bulletin must be sent to the Secretary of the Society within three months of the date of the receipt of this number in order to be filled gratis.

Entered as second-class matter at the Post-Office at Baltimore, Md., under the Act of Congress of July 16, 1894.

Accepted for mailing at special rate of postage provided for in Section 1103, Act of October 3, 1917, authorized on July 8, 1918.

PAPERS IN PRESS FOR FORTHCOMING ISSUES

ENGINEERING GEOLOGY OF SAN FRANCISCO BAY, CALIFORNIA. By Parker D. Trask and Jack W. Rolston

ILLINOIAN AND WISCONSIN DRIFFT OF THE SOUTHERN PART OF THE GRAND RIVER LOBE IN EASTERN OHIO. By George W. White

PRECAMBRIAN STRATIGRAPHY OF MINNESOTA. By F. F. Grout, J. W. Gruner, G. M. Schwartz, and G. A. Thiel

PETROLOGY OF THE BALTIMORE GABBRO. By Norman Herz

GLACIAL CLAYS IN STEEP ROCK LAKE, ONTARIO. By Ernst Antevs

SUBMARINE GEOLOGY OF THE GULF OF ALASKA. By H. W. Menard and R. S. Dietz

BULLETIN OF THE GEOLOGICAL SOCIETY OF AMERICA
VOL. 62, PP. 853-862, 4 FIGS., 2 PLS. AUGUST 1951

DEFORMATION OF YULE MARBLE: PART I—COMPRESSION AND EXTENSION EXPERIMENTS ON DRY YULE MARBLE AT 10,000 ATMOSPHERES CONFINING PRESSURE, ROOM TEMPERATURE*

BY DAVID GRIGGS AND W. B. MILLER

ABSTRACT

A co-operative study of the deformation of marble is described in this series of three papers. Part I deals with the experimental deformation of jacketed cylinders of dry Yule marble, at room temperature and under a confining fluid pressure of 10,000 atmospheres. Cylinders cut parallel, normal, and at 45° to the plane of foliation were homogeneously deformed varying amounts in uniaxial compression and extension. The stress-strain curves show the mechanical anisotropy of the original marble in relation to the fabric anisotropy. Applying the analytical methods of Part II, it is found that Taylor's hypothesis of the deformation of granular aggregates when applied to gliding on {01$\bar{1}$2} planes provides an explanation of the observed mechanical anisotropy. This correlation in turn provides evidence that both twin and translation gliding occur under these experimental conditions and that their relative importance depends on the original fabric and the orientation of the applied stress. Parts II and III describe other evidence which points toward similar conclusions.

CONTENTS

	Page		Page
Introduction	853	Interpretation of the results	859
Acknowledgments	854	Summary	862
Technique	854	References cited	862
Experimental results	857		

ILLUSTRATIONS

Figure	Page	Figure	Page
1. Schematic drawing of high-pressure assembly	855	4. Preliminary stress-strain curves of jacketed calcite single crystals	859
2. Mounting of specimen	856	Plate	Facing page
3. Stress-strain curves for Yule marble deformed in compression and extension	858	1. High-pressure apparatus	854
		2. Record of typical experiment	855

TABLES

	Page		
1. Summary of experiments	857	solved shear-stress coefficient	859
2. Correlation between stress and average re-		3. Correlation under homogeneous hypothesis	861

INTRODUCTION

It has been known for fifty years that marble may be deformed plastically under high confining pressure, at room temperature, without the presence of chemical solvents. It has been shown that intragranular gliding is the major and perhaps the only mechanism of deformation under these conditions. Until Bell's (In press) discovery of translation gliding on {01$\bar{1}$2} in calcite the only proven mechanism of deformation was twin gliding on the same plane. Previous experiments by the senior author (Griggs, 1936) and J. R. Balsley (1941) and fabric analysis by E. B. Knopf (1949) have provided evidence still insufficient to define the relative importance of {01$\bar{1}$2} twinning and translation, or to exclude other mechanisms.

Part I of this series of papers describes the experimental phase of a joint program designed

* The term "extension" is here used rather than "tension," as previously used by Bridgman, Balsley, and the senior author. Although we agree with Bridgman's treatment of the subject which considers the stress system as a hydrostatic stress plus a tensile stress, this usage is not in accord with some conventional treatments in the theory of elasticity, and we choose the geometrically descriptive term "extension" used long ago by Bridgman to avoid possible confusion and ambiguity. In any case, the stress system is such that the longitudinal stress is less than the two equal radial stresses, and greater than zero. The difference between the longitudinal and radial stresses is termed the extension stress, since "extensile" is pre-empted by other usage.

to narrow these uncertainties. This program was conceived by E. B. Knopf, F. J. Turner, J. W. Handin, and the senior author. The results to date are due to the background work of Mrs. Knopf and to the close co-operation among individuals working on the three phases of this program. The deformation of marble under the conditions described here does not closely resemble that observed in nature. It is intended that the project now completed will serve as a foundation for work which is now beginning on Yule marble at elevated temperature, high pressure, and in the presence of chemical solvents.

Acknowledgments

Project grants from The Geological Society of America; equipment loaned by the Committee on Experimental Geology at Harvard and by the U. S. Geological Survey, Yule marble supplied by Mrs. E. B. Knopf, a substantial grant from the Office of Naval Research for equipment and operating funds; and support from the Institute of Geophysics all contributed essentially to this program. The excellent craftsmanship of Mr. Fred Banning and Mr. Edwin Perry in our shop was indispensable. It is a pleasure to acknowledge our indebtedness to all.

Technique

The basic apparatus (Fig. 1; Pl. 1) was developed at Harvard in Bridgman's laboratory (Griggs, 1936; Balsley, 1941). The specimen, jacketed with a .005-inch wall annealed copper tube is first subjected to hydrostatic pressure, then the upper piston to which the specimen is attached is moved in or out of the cylinder, compressing or extending the specimen. The liquid pressure is maintained nearly constant by coupled motion of the lower piston of the same diameter bearing only on the fluid.

Measurements of differential force on the specimen and of related strain are made externally on the upper piston. Corrections to these measurements must be made for elastic distortion of elements other than the specimen, for change in cross section of the specimen during an experiment, and for change in hydrostatic pressure. The first correction is obtained from a calibration of the system with a steel specimen. The second is made from the observed strain, on the assumption that the deformation is homogeneous and that the volume remains constant. The third is computed from the measured change in hydrostatic pressure and the area of the piston.

An error can arise from change in friction on the piston as a function of force on the specimen and displacement. This effect was minimized by design of the upper packing, the use of a packing press (Fig. 1), and a polished solid carboloy upper piston, all of which reduced the average friction to 5 per cent of the hydrostatic pressure on the piston. The friction was nearly constant for large displacements of the piston with no force on the specimen. The change in friction with force on the specimen was shown to be small by an experiment in which a hardened steel specimen in two pieces, sealed together with a copper jacket, was pulled apart. The measured force required to separate the two pieces was 3 per cent less than that due to the hydrostatic pressure holding them together.

The hydrostatic pressure was measured by a manganin resistance gauge with wire supplied by Professor Bridgman from his calibrated stock. Measurement of the resistance of the pressure-gauge coil was accomplished automatically by a self-balancing Carey-Foster bridge circuit using a Brown Instrument Company servoamplifier and a precision Helipot. The pressure measurements agree within 1 per cent with the pressure determined from the mean force on the piston in opposite friction measurements. The force on the upper piston was determined by an elastic steel ring whose deflection was measured by a Statham strain gauge and recorded by a Brown potentiometer. This whole system was calibrated by proving

Plate 1. HIGH-PRESSURE APPARATUS

Press at left, motor-driven pump for main cylinders in background. Center foreground: priming pump and packing press pump. Right (top to bottom): strain recorder, force recorder, hydrostatic pressure indicator, temperature regulator (not used in these experiments).

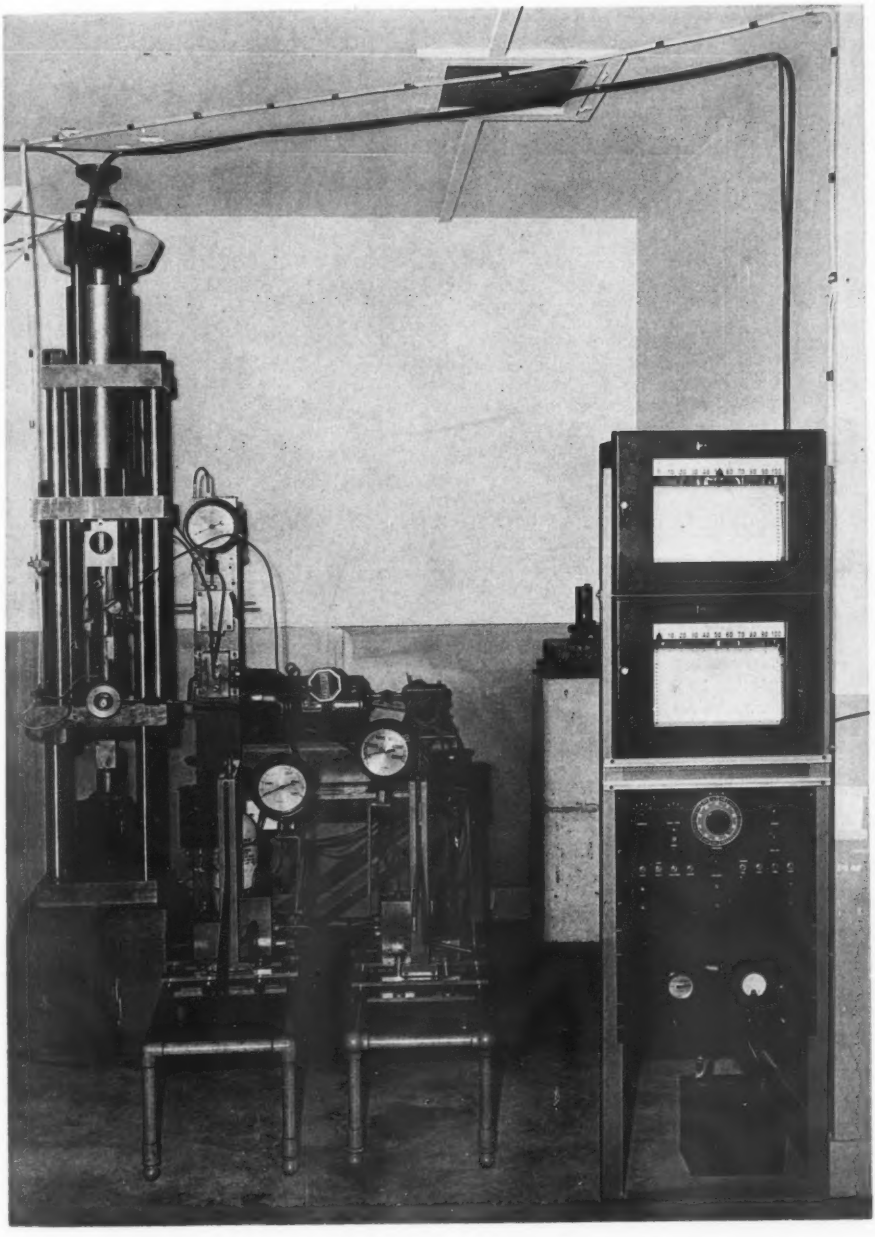

HIGH-PRESSURE APPARATUS

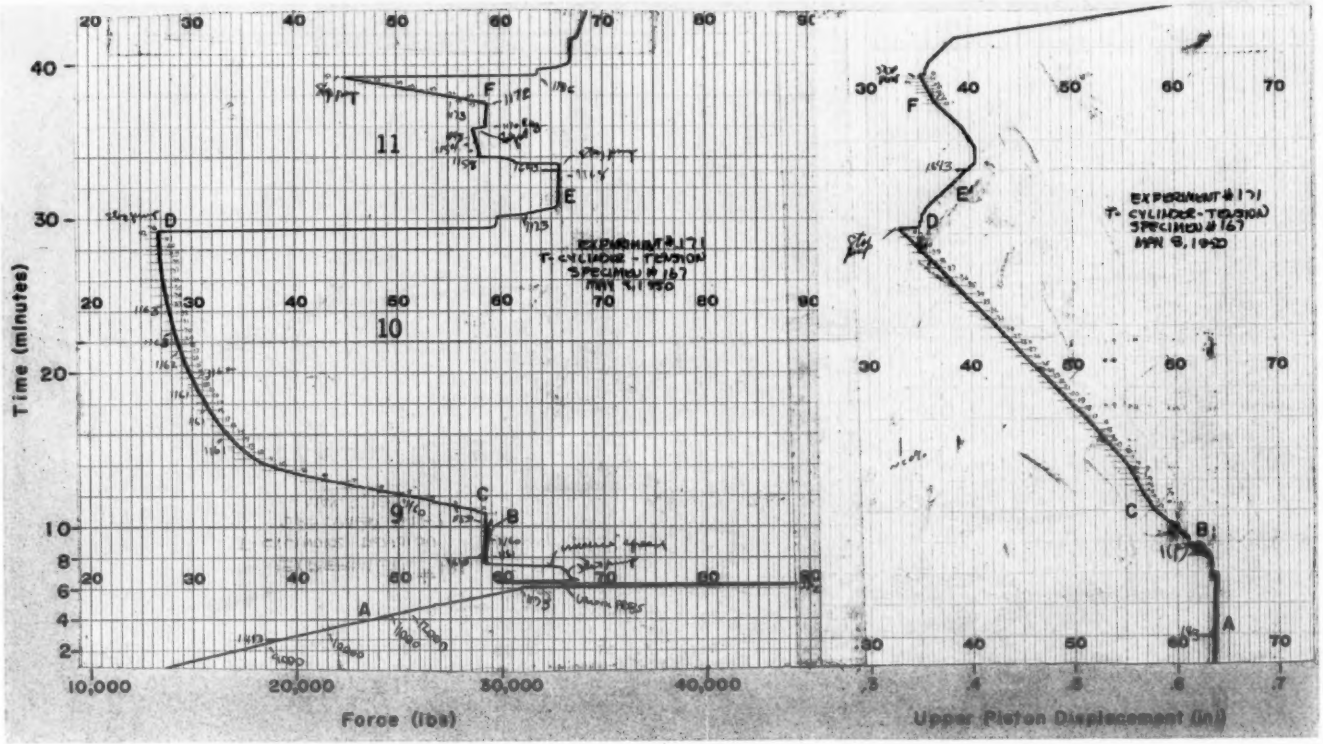

RECORD OF TYPICAL EXPERIMENT

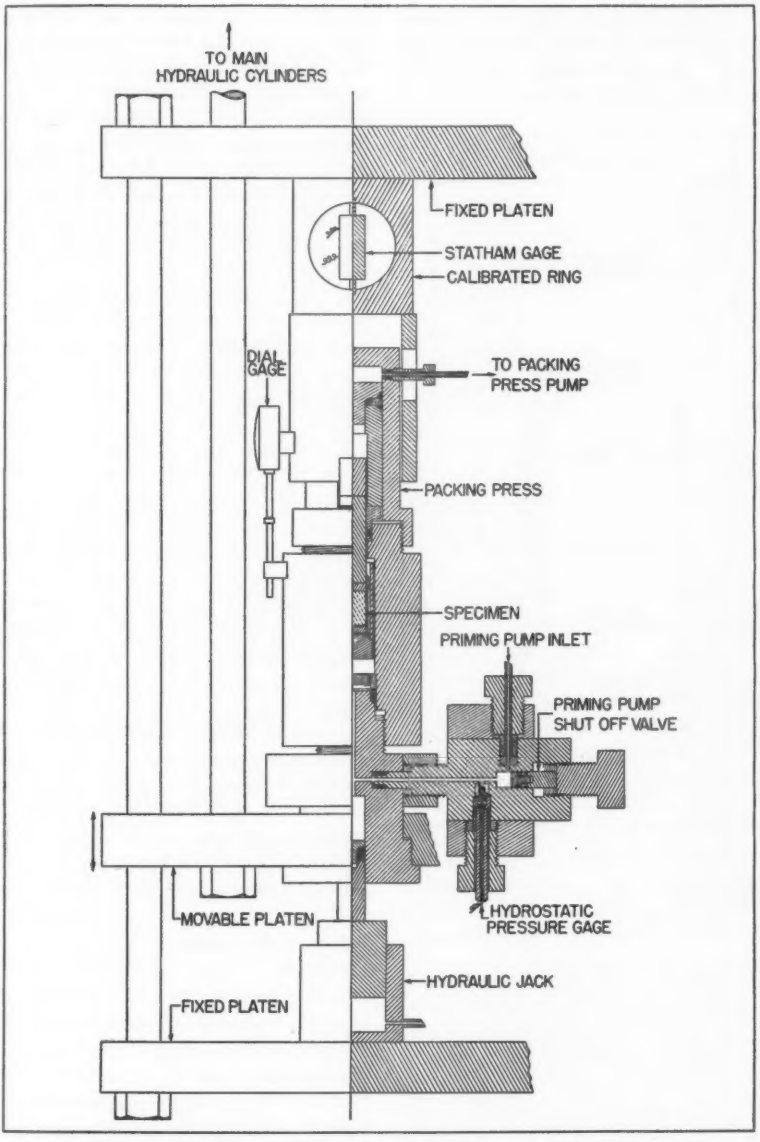

FIGURE 1.—SCHEMATIC DRAWING OF HIGH-PRESSURE ASSEMBLY

rings certified by the Bureau of Standards. The force measurement was linear to half a per cent and reproducible to one-tenth per cent. Piston displacement was measured and recorded by an Ames Dial gauge to the main pinion of which was attached a 5000 ohm one-turn Helipot

PLATE 2. RECORD OF TYPICAL EXPERIMENT

used in a potentiometer circuit to a Brown recorder. Calibrated linearity was within half a per cent, and reproducibility to one-tenth per cent. Sensitivity was .001 inch.

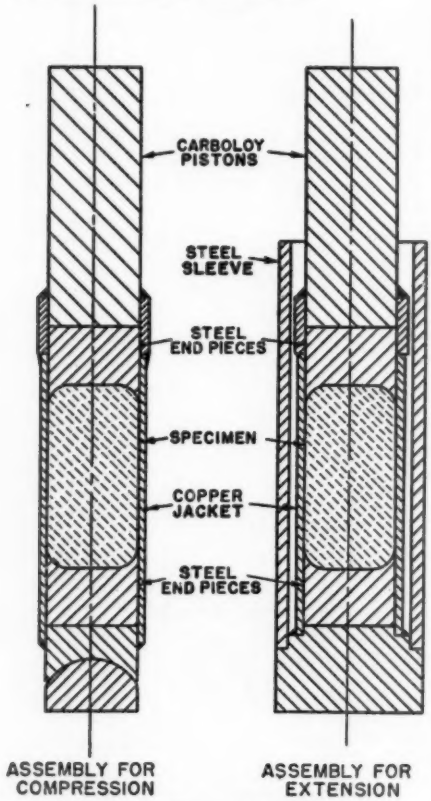

FIGURE 2.—MOUNTING OF SPECIMEN

In an experiment, the piston with specimen attached was fixed in position by locking the main press in such a position that the specimen would be subject only to hydrostatic pressure. The liquid pressure was then raised by pushing in the lower piston until the desired pressure was attained. The main press was then moved at a nearly constant rate in the appropriate direction for compression or extension. Motion of about one fourth of an inch was provided before the specimen holder came in contact with the end of the cylinder which prevented the end of the specimen not attached to the piston from moving farther. Prior to this time the force on the piston is due only to hydrostatic pressure plus friction in the piston packing. This force is taken as the zero point of the applied stress and is corrected only for observed changes in hydrostatic pressure. After contact the force changes rapidly; the difference is taken as the force applied to the specimen. The rate of strain is nearly constant; it changes only as a result of elastic distortion of the apparatus and compressibility of the fluid in the main hydraulic cylinders.

A typical record of an experiment is shown in Plate 2. At *A*, the force increases as the hydrostatic pressure is raised, while the upper piston is stationary. The force remains constant (*B*) while the pistons move freely. This force is that due to the hydrostatic pressure minus friction. The specimen holder hits the end of the cylinder (*C*), and the force borne by the specimen (in extension in this experiment) diminishes the external force on the piston. The extension test at nearly constant strain rate is shown from *C* to *D*. The motion of the piston is reversed at *D*. The force remains nearly constant (*E*) for free motion of the piston in the opposite direction. The force at *E* minus the force at *B* equals the double friction of the upper piston packing. A repeat run measures the residual deformation of the specimen *F*. The displacement at the inflection point, *C*, minus that at *F* equals the residual strain—22 per cent in this case. Final data are obtained by registering the time markers on the two charts, reading force and displacement and correcting for elastic distortion of the apparatus, changes in hydrostatic pressure, and change in cross section of the specimen.

In all these experiments, the liquid pressure was 10,000 atmospheres $\pm$ 5 per cent. During any run, the liquid pressure changes about 0.1 per cent/per cent of strain because the two pistons are not exactly the same size. In addition, distortions of the apparatus cause pressure variations during a run (maximum change 6 per cent, average 2 per cent). No effect on physical properties as a result of these changes in pressure could be found.

From a block of Yule marble supplied by E. B. Knopf cylinders half an inch in diameter by 1 inch long were cut in three orientations (Knopf, 1949; Part III, Fig. 1):

R cylinders—parallel to foliation, normal to c axes maximum;

Q cylinders—normal to foliation, parallel to c axes maximum;

d cylinders—45° to foliation, 45° to c axes maximum.

These cylinders were fitted to steel cups (Fig. 2) to distribute the discontinuity of deformation between piston and specimen over an area large enough to prevent rupture of the copper jacket. The resultant deformation was uniform within a few thousandths of an inch between the cups. The original length of 1 inch was used for calculating the reduction and increase in area during deformation. The derived stresses are consequently somewhat high for compression and low for extension, errors which were partially cancelled by making the end pieces of low-strength steel which would deform to some extent. Measurements of the specimen after deformation indicate that the derived stress is accurate to within a few per cent.

No correction was made for the strength of the .005-inch wall annealed copper tube which was measured under pressure as about 100 pounds, corresponding to a stress on the specimen of 40 kg/cm².

Experimental Results

Knopf and Turner decided that, because of the completely changed pattern of the fabrics measured at 30 per cent compression (Knopf, 1949) and 20 per cent tension (Balsley, 1941), and because of the difficulty of making microscopic determinations at these deformations, it was desirable to carry out a series of experiments yielding smaller strains in all orientations. The senior writer desired to repeat the older experiments (Griggs, 1936; Balsley, 1941; Knopf, 1949) in both extension and compression with improved apparatus to obtain better statistics. Accordingly, 28 specimens were deformed as shown in Table 1.

The shape of the stress-strain curves is a function of the rate of strain in the plastic range. Four creep tests on P cylinders in extension were performed to ascertain the nature of the time-dependent flow. Unlike previous results on unjacketed Solenhofen limestone (Griggs, 1936) no pseudoviscous flow was observed in these creep experiments. Only elastic flow, at a rate decreasing logarithmically with time, was detected at constant stresses up to 6000 kg/cm² applied for an hour. After renewal of the forced strain rate, increase of applied stress was rapid, and the stress-strain relation returned to the value it would have had if the strain rate had not been interrupted.

Table 1.—Summary of Experiments
(In per cent)

R cylinders		*Q* cylinders		*d* cylinders	
Extension	Comp.	Extension	Comp.	Extension	Comp.
5	7	4	3	7	6
5	10.5	6	5.5	12	10.7
6.5	22	6.5	10.5	21	22
7.5	40	9	20		
14		11			
21.5		13			
		22			
		44			

All specimens jacketed, at 10,000 atm confining pressure, room temperature, dry. Rate of strain 1.5 per cent/minute.

Average stress-strain curves for all orientations are shown in Figure 3. The average deviation of individual experiments from the average for all of that orientation was 3 per cent. The initial slopes of these curves are not accurately determined due to lost motion in the apparatus. These curves are arbitrarily adjusted to Lepper's (1949) values for Young's modulus in Yule marble at atmospheric pressure. The change in Young's modulus with confining pressure has not been measured.

Plastic flow only was the rule in these experiments. No experiment was carried to the point of true failure by rupture except possibly in one instance—a Q cylinder stretched 44 per cent by a differential stress of 7900 kg/cm² parted in the central portion of the specimen. The "fracture" had the appearance of a typical tension break, normal to the axis of extension. The possibility could not be excluded that this parting was caused by rupture of the highly deformed copper jacket. Other fractures were occasionally encountered, but they were all traced to imperfections in the grips or eccentric loading in compression. Most specimens were

strained the desired amount and then removed intact, after the pressure had been released.

Each specimen showed evidences of residual stresses after being removed from the pressure chamber, as had been noted in unjacketed specimens (Griggs, 1936). This took the form of longitudinal flow at a logarithmically decreasing rate in the opposite direction to the deformation. The total magnitude could not be measured because of uncertainties as to the effects of release of hydrostatic pressure. The maximum measured amount was 0.2 per cent from 10 minutes to 1 hour after release of pressure. The substantial increase of volume after deformation and release of hydrostatic pressure (Griggs, 1936; Knopf, 1949) was again found, but not measured accurately. The specimens which show the greatest increase in volume are those which have been deformed most, and are weakest, almost to the point of crumbling. It is tentatively suggested that the increase in volume is due to grain separation after relief of pressure as a result of the residual stresses and consequent flow of the grains. This is supported by evidences of grain separation in such specimens, which are impregnated in balsam before thin-sectioning. DeGrossé, who prepares the excellent thin sections, reports that this separation does not occur in the grinding process.

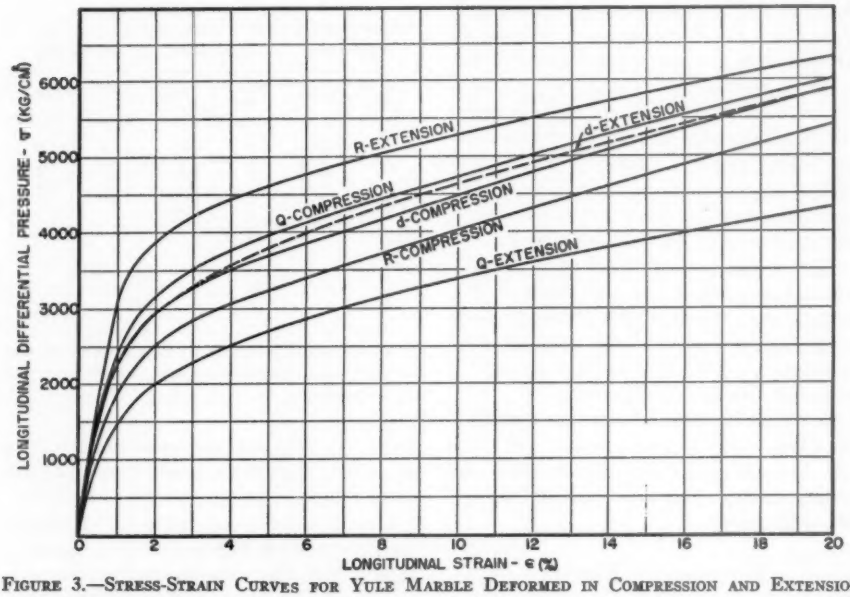

FIGURE 3.—STRESS-STRAIN CURVES FOR YULE MARBLE DEFORMED IN COMPRESSION AND EXTENSION

Normal to R, *Q*, *d* planes. Each curve is an average of three or more tests. All experiments at 10,000 atmospheres confining pressure, jacketed, dry, at room temperature. Rate of strain .015/minute. Stress plotted is the difference between the longitudinal stress and the lateral stress which is equal to the liquid confining pressure.

A program of study of the behavior of calcite single crystals has been undertaken by Griggs and Turner to establish the phenomena of deformation under similar experimental conditions to those discussed above. Two preliminary stress-strain curves of calcite crystals are shown in Figure 4, for compression and for extension parallel to the *c* axis. These are utterly different from those published for unjacketed calcite crystals of other orientations at 10,000 atmospheres (Griggs, 1938). Bell (In press) first demonstrated the existence of $\{01\bar{1}2\}$ translation gliding in calcite single crystals with the same glide direction as for twinning, but under shear in the opposite sense. This discovery has been confirmed in other experiments on calcite

rhombs at lower pressures. Translation gliding on $\{01\bar{1}2\}$ has been shown to function in the calcite single crystal cylinder of Figure 4, compressed parallel to the c axis at 10,000 atmospheres. Twinning is dominant in the case of extension parallel to the c axis (Fig. 4).

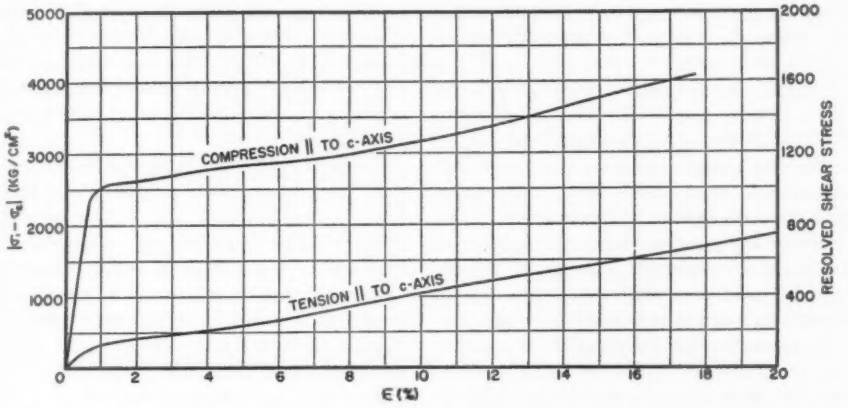

FIGURE 4.—PRELIMINARY STRESS-STRAIN CURVES OF JACKETED CALCITE SINGLE CRYSTALS IN COMPRESSION AND EXTENSION PARALLEL TO THE c AXIS

The Resolved Shear Stress plotted is that on the $\{01\bar{1}2\}$ plane in the twin and translation direction calculated for the undeformed crystal. 10,000 atmospheres confining pressure, room temperature.

INTERPRETATION OF THE RESULTS

Turner and Ch'ih (Part III) report that the overwhelming majority of visible deformation structures in the deformed marble are $\{01\bar{1}2\}$ lamellae. Handin and Griggs (Part II, Fig. 7) determined the resolved shear-stress coefficients in the twin and in the opposite sense for each $\{01\bar{1}2\}$ plane in a representative sample of grains of undeformed Yule marble. It is supposed that, if deformation is due principally to gliding on $\{01\bar{1}2\}$, the observed strength anisotropy shown in Figure 3 would be related to the average resolved shear-stress coefficients in the several directions. A qualitative correspondence is found (Table 2). Except for the two d cylinders, the observed strengths are in the order of decreasing average shear-stress coefficient in the twinning sense, as expected. Efforts to achieve more than this qualitative comparison on the basis of resolved shear stress in the twinning sense only were of no avail.

The next step is to apply hypotheses from other studies of deformation of solids to see if quantitative correlation can be found. Two antithetical hypotheses have been used by metallurgists and physicists in attempts to relate single-crystal properties to those of an aggregate: (a) that the individual crystal grains deform without regard to the restrictions on change of shape imposed by neighboring grains (Cox and Sopwith, 1937); (b) that the contact between grains is rigidly maintained, forcing homogeneous deformation of all grains (Taylor, 1938). In both cases it is further assumed that deformation within the grains is homogeneous and that the stress field on the grain is equal to the external stress field.

TABLE 2.—CORRELATION BETWEEN STRESS AND AVERAGE RESOLVED SHEAR-STRESS COEFFICIENT

Orientation	Longitudinal stress at 3% strain (kg/cm²)	Weighted average resolved shear-stress coefficient	
		Twinning sense	Opposite sense
Q-Extension	2280	.361	.072
R-Compression	2830	.294	.070
d-Extension	3280	.244	.174
d-Compression	3270	.174	.274
Q-Compression	3510	.072	.361
R-Extension	4220	.070	.294

Treatments based on the above hypotheses cannot be strictly correct in view of the following observations on metals:

(1) Deformation is not homogeneous within the grains (Boas and Hargreaves, 1948).
(2) The existence of an "elastic limit" higher than that predicted by either treatment.
(3) No grain separation of the amount required for independent grain deformation has been found.
(4) Different amounts of deformation of individual grains in the same aggregate, conflicting with hypothesis (b).

The deformation of marble under the present experimental conditions is, in all respects that have been investigated, similar to that of metals which deform by intragranular gliding. Many of the above contradictions with hypotheses (a) and (b) have been observed in the case of marble. It seemed not without profit, however, to explore the consequences of subjecting the data for marble to both types of analysis to see what correspondence might result. Specifically, it was hoped that, if a self-consistent treatment could be found for the stress-strain data, the fabric data, and the resolved shear stress analysis, this would be helpful in discovering the relative roles played respectively by twinning and translation on $\{01\bar{1}2\}$.

Hypothesis (a), of independent grain deformation, proved in drastic conflict with most of the data, as follows:

(1) The knee of the stress-strain curves (limit of proportionality) in the several orientations could not be correlated with the resolved shear-stress data.
(2) The shape of each stress-strain curve above the knee was grossly different from any fit obtained on the independent-grain deformation hypothesis.
(3) For low deformations, the fabric changes predicted are very much greater than those actually observed (this point is more fully discussed in Parts II and III).

Hypothesis (a) was strenuously pursued over a period of several months. It was not discarded hurriedly, because some of the observed phenomena were in qualitative accord with this treatment. Full discussion of these efforts to obtain agreement is omitted here because of the weight of quantitative evidence against this hypothesis.

Taylor's hypothesis (b) of homogeneous grain deformation will be treated more fully, since it is more compatible with observations. In his treatment of an aluminum aggregate, based on data from single crystals, Taylor rigorously and laboriously carried out calculations of deformation on the principle of least work for homogeneous grain deformation. He further showed that for exactly homogeneous deformation a minimum of five glide systems in each crystal grain is required.

Calcite is importantly different from aluminum in having lower symmetry, so that, whereas in aluminum gliding occurs on eight planes in three directions with equal ease in both senses, in calcite three $\{01\bar{1}2\}$ planes deform by twinning in only one sense; translation on the same planes in the opposite sense requires considerably more resolved shear stress, and other planes presumably require still more shear stress. In the present analysis, the criterion of resolved shear stress is substituted for the principle of least work. Specifically, the assumptions under which Taylor's hypothesis is applied are as follows:

(1) Gliding on $\{01\bar{1}2\}$ is predominant.
(2) Each grain deforms principally by gliding on that $\{01\bar{1}2\}$ plane on which the resolved shear stress (as computed from the external stress field) is a maximum, with the proviso that resistance to slip in the twinning sense is assumed to be different from that in the opposite sense.

These assumptions are supported by the discovery (Part III) of a strikingly consistent relation between the profusion of $\{01\bar{1}2\}$ glide lamellae and the computed resolved shear stress on the planes in question, and by the fact that in single crystals, even when constrained so that slip on $\{01\bar{1}2\}$ is difficult, this is still the only important mechanism of deformation observed. Secondary gliding on other lamellae in deformed marble is to be expected under Taylor's hypothesis, which is consistent with the small number of $\{02\bar{2}1\}$ lamellae found (Part III).

From the above assumptions, it follows that the applied stress is the average of the stress on all crystals of the aggregate which can now be

expressed in terms of the resolved shear stress and resolved shear-stress coefficient:

$$\sigma = \frac{1}{n}\left[\frac{n_1\tau_1}{S_1} + \frac{n_2\tau_2}{S_2} + \cdots\right] \quad (1)$$

where: σ = applied stress in compression or extension,

τ_1 etc. = shear stress on the functioning slip plane in each crystal in the slip direction,

S_1 etc. = resolved shear stress coefficient = $\sin\chi_0 \cos\chi_0 \cos\phi_0$

where: χ_0 = angle between applied stress axis and slip plane,

ϕ_0 = angle between projection of stress axis on slip plane and the direction of slip (see Part II),

n_1 etc. = number of grains having shear stress factor S_1 etc.,

n = total number of grains.

Consider the $\{01\bar{1}2\}$ planes and neglect all others:

τ_a = resolved shear stress required to produce slip in the twinning sense—constant for a particular amount of shear strain in each crystal,

τ_b = resolved shear stress required to produce slip in the opposite sense—also constant for a given shear strain,

$$\alpha = \frac{\tau_b}{\tau_a}$$

Equation (1) may now be rewritten:

$$\sigma = \frac{\tau_a}{n}\left[\frac{n_1'}{S_1} + \frac{n_2''}{S_2} + \cdots\right] + \alpha\frac{\tau_a}{n}\left[\frac{n_1''}{S_1} + \frac{n_2''}{S_2} + \cdots\right].$$

Defining:

$$F_a = \frac{1}{n}\left[\frac{n_1'}{S_1} + \cdots\right] \text{ and } F_b = \frac{1}{n}\left[\frac{n_1''}{S_1} + \cdots\right],$$

$$\sigma = \tau_a (F_a + \alpha F_b) \quad (2)$$

This construction is now tested for internal consistency on the six stress-strain curves of Figure 3. Since there are two disposable constants, τ_a and α, agreement on all six curves within a small fraction of the initial difference between the curves would imply a high degree of internal consistency, lend plausibility to the above assumptions, and support Taylor's hypothesis.

If there were a sharply defined elastic limit in these curves, this would be the critical point at which to apply the test. Lacking that, an arbitrary point is picked at a strain sufficiently large so that the initial uncertainties of measurement will have diminished, but not so large that a significant fraction of the grains will have twinned completely, changing F_a and F_b. An average shear strain $s = (F_a + F_b)$ of 0.1 is used. This corresponds to extension and compression strains (ϵ) of about 3 per cent.

The sums F_a and F_b are computed from the original data of Part II, iterating until the proper ratio α is found. Thus in each grain, assuming an α, it is determined which $\{01\bar{1}2\}$ plane will function in the twin sense or in the opposite sense for each orientation. The quantities F_a and F_b are then calculated as the sum of the averages of 10 intervals of S from 0 to .50. The values which give the closest fit are:

$$\tau_a = 840 \text{ kg/cm}^2$$
$$\tau_b = 1470 \text{ kg/cm}^2$$
$$\alpha = 1.75$$

Table 3 gives the pertinent values of all the essential quantities:

TABLE 3.—CORRELATION UNDER HOMOGENEOUS HYPOTHESIS

Orientation	F_a	F_b	$F_a + 1.75F_b$	σ Calc	σ Obs. ($s = 0.1$)	$\frac{\sigma \text{ calc}}{\sigma \text{ obs}}$
Q-Comp	.72	2.00	4.22	3540	3680	.96
Q-Tens	2.20	.45	2.99	2505	2530	.99
R-Comp	2.96	.27	3.43	2880	2860	1.01
R-Tens	.64	2.68	5.33	4460	4350	1.03
d-Comp	2.09	1.00	3.84	3220	3280	.98
d-Tens	2.13	1.11	4.07	3410	3365	1.01

The standard deviation of the calculated values from the observed values for applied stress at 0.1 shear strain is 2.0 per cent. This is to be compared with the standard deviation of the observed stresses from their mean, which is 17.5 per cent. It is concluded that Taylor's hypothesis applied to Handin's data in this simplified form results in correlation of the observed anisotropy within the limits of ex-

perimental error in the stress-strain determinations.

It will be noted that the computed average resolved shear stress in the twinning sense τ_a = 840 kg/cm², and in the opposite sense τ_b = 1470 kg/cm² bear no relation to the single-crystal values shown in the preliminary experiments (Fig. 4), and, particularly, the ratio of the two is vastly different. This is not surprising, since our treatment supposes that all the resistance to deformation occurs on the one $\{01\bar{1}2\}$ plane which has the highest shearing strain. The slip necessary on other planes to give homogeneous deformation would contribute importantly to the resistance to deformation. It is perhaps surprising that this simplified treatment gives such a good correlation of the observed strength anisotropy. This may in fact indicate a significant departure from Taylor's hypothesis of rigorously homogeneous deformation.

Summary

Experiments in both compression and extension at 10,000 atmospheres confining pressure on dry Yule marble at room temperature using cylinders of three different orientations have been made with slightly refined apparatus. These experiments are consistent with the earlier experiments of Balsley (1941) in extension on a different block of Yule marble known to have a slightly different pattern of preferred orientation of calcite grains. They have refined the preliminary experiments of Griggs (Knopf, 1949) in compression. The stress-strain data are reproducible for the several orientations.

Preliminary experiments on calcite single crystals have confirmed Bell's discovery of translation on $\{01\bar{1}2\}$ and have disclosed no other mechanism except twinning on $\{01\bar{1}2\}$, which occurs at about one-tenth of the resolved shear stress required to produce translation.

A simplified treatment following Taylor (1938) gives good internal agreement among the six sets of stress-strain relations but does not permit correlation between the properties of single crystals and those of the aggregate. The internal consistency of the data subject to this treatment constitutes evidence for:

(1) nearly homogeneous deformation of each grain in the aggregate under these conditions (2) the dominant role of $\{01\bar{1}2\}$ gliding in both senses on the plane of maximum resolved shear stress as computed from the external stress field.

This analysis does not discriminate between twinning and translation in the twinning sense, but requires a resolved shear stress for gliding in the opposite sense about 1.7 times as great as that for the twinning sense.

This paper contains little of direct application to geological problems. It indicates the complexity of solving the simplest and oldest problem in the laboratory deformation of rocks, "What is the mechanism of deformation of marble?"

It should be reiterated that the conditions of these experiments are not believed to be similar to those under which most marble is deformed in nature. Experiments at elevated temperature and in the presence of solvents are now in progress in an effort to approximate more closely natural conditions.

References Cited

Balsley, J. R. (1941) *Deformation of marble under tension at high pressure*, Am. Geophys. Union, Tr., pt. II, p. 519–525.

Bell, J. F. (In press) *On experimentally produced (01$\bar{1}$2) translation in calcite single crystals.*

Boas, W., and Hargreaves, M. E. (1948) *On the inhomogeneity of plastic deformation in crystals of an aggregate*, Roy. Soc. London, Pr., ser. A., vol. 193, p. 89–97.

Cox, H. L., and Sopwith, D. G. (1937) *The effect of orientation on stresses in single crystals and of random orientation on strength of polycrystalline aggregates*, Phys. Soc. London, Pr., vol. 49, p. 134–151.

Griggs, D. T. (1936) *Deformation of rocks under high confining pressures*, Jour. Geol., vol. 44, p. 541–577.

—— (1938) *Deformation of single calcite crystals under high confining pressures*, Am. Mineral., vol. 23, p. 28–33.

Knopf, E. B. (1949) *Fabric changes in Yule marble after deformation in compression*, Am. Jour. Sci., vol. 247, p. 433–461, 537–569.

Lepper, H. A., Jr. (1949) *Compression tests on oriented specimens of Yule marble*, Am. Jour. Sci., vol. 247, p. 570–574.

Taylor, G. I. (1938) *Plastic strain in metals*, Inst. Metals, Jour., vol. 62, p. 307–324.

Turner, F. J. (1949) *Preferred orientation of calcite in Yule marble*, Am. Jour. Sci., vol. 247, p. 593–621.

Institute of Geophysics, University of California, Los Angeles 24, Calif.

Manuscript Received by the Secretary of the Society, January 17, 1951

Project Grant 201-37

Assisted by ONR Grant.

COMPRESSION

UNDEFORMED

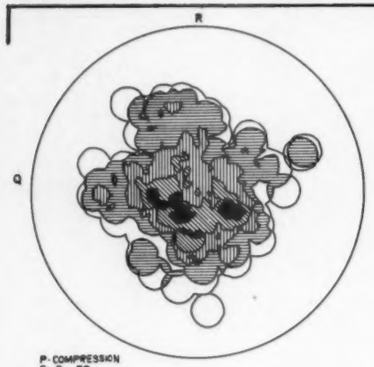

P-COMPRESSION
S= 0 - .50
e= 14.5%

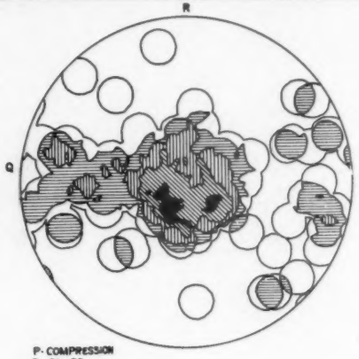

P-COMPRESSION
S= .31-.50
e= 11.4%

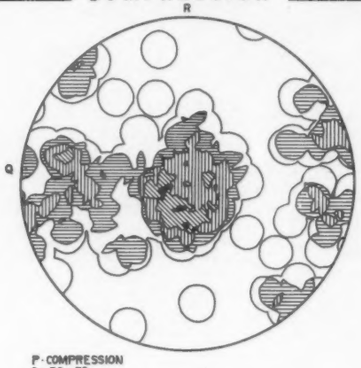

P-COMPRESSION
S= .36-.50
e= 8.8%

P-COMPRESSION
S= 41-.50
e= 4.9%

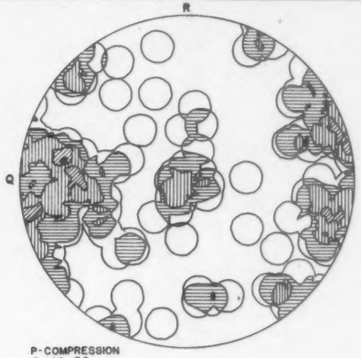

P-COMPRESSION
S= 46-.50
e= 2.1%

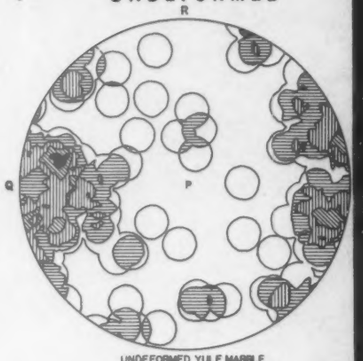

UNDEFORMED YULE MARBLE

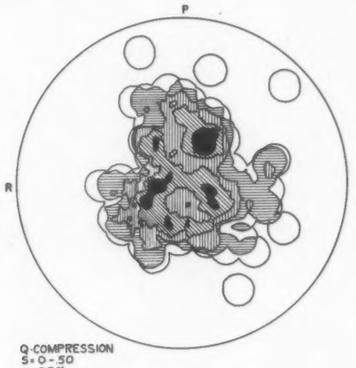

Q-COMPRESSION
S= 0 - .50
e= 3.7%

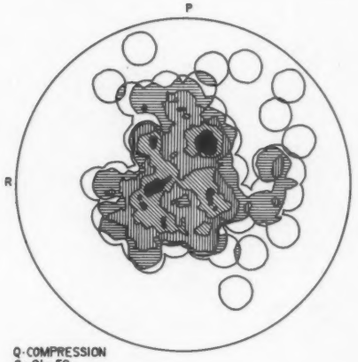

Q-COMPRESSION
S= .31-.50
e= 3.4%

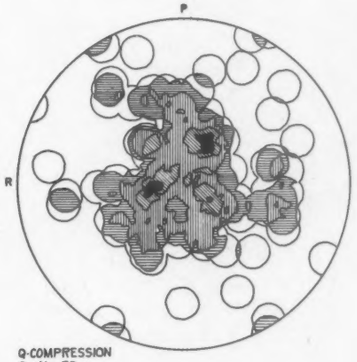

Q-COMPRESSION
S= 41-.50
e= 1.8%

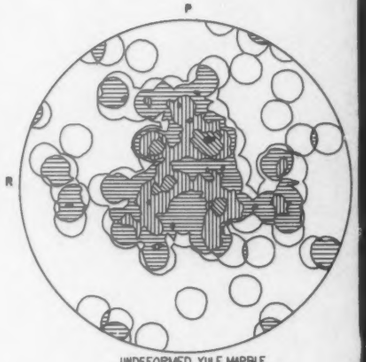

UNDEFORMED YULE MARBLE

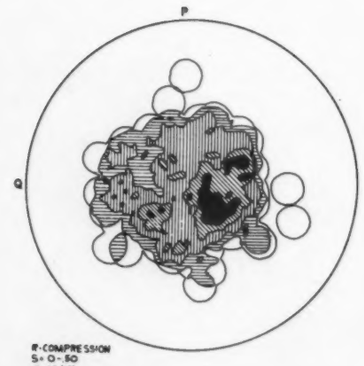

R-COMPRESSION
S= 0 - .50
e= 14.2%

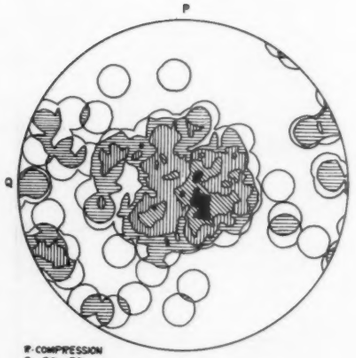

R-COMPRESSION
S= .30 - .50
e= 11.0%

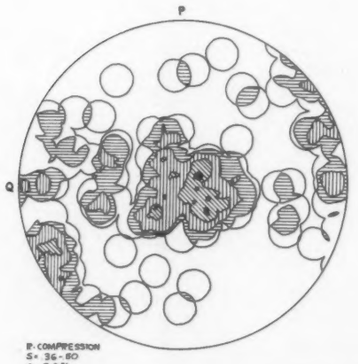

R-COMPRESSION
S= .36 - .50
e= 8.0%

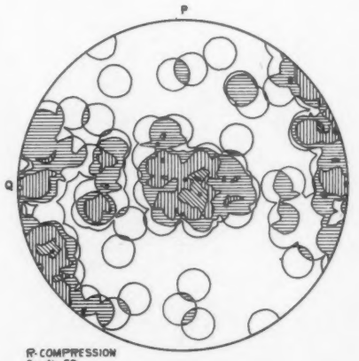

R-COMPRESSION
S= 41-.50
e= 5.9%

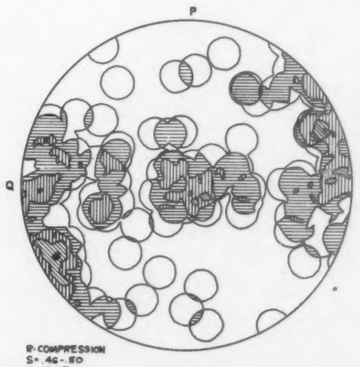

R-COMPRESSION
S= 46-.50
e= 3.8%

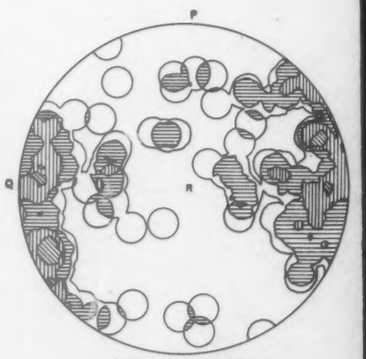

UNDEFORMED YULE MARBLE

PREDICTED FABRICS AS A RESULT OF COMPLETE M

Assuming heterogeneous deformation. 136 *c* axes in each diagram.
corded below each diagram. Contour interval: 0.7, 1.5, 3.5,7 per cent (Und

RESSION

UNDEFORMED

P-COMPRESSION
S=.41-.50
e=4.9%

P-COMPRESSION
S=.46-.50
e=2.1%

UNDEFORMED YULE MARBLE

P-TENSION
S=.41-.50
e=2.90%

P-TENSION
S=.31-.50
e=4.39%

Q-COMPRESSION
S=.31-.50
e=3.4%

Q-COMPRESSION
S=.41-.50
e=1.8%

UNDEFORMED YULE MARBLE

Q-TENSION
S=.49-.50
e=5.5%

Q-TENSION
S=.46-.50
e=13.6%

R-COMPRESSION
S=.41-.50
e=5.9%

R-COMPRESSION
S=.46-.50
e=3.5%

UNDEFORMED YULE MARBLE

R-TENSION
S=.41-.50
e=2.85%

R-TENSION
S=.31-.50
e=4.93%

PREDICTED FABRICS AS A RESULT OF COMPLETE MECHANICAL TWINNING ON $01\bar{1}2$

Assuming heterogeneous deformation. 136 c axes in each diagram. Strain accompanying changes is recorded below each diagram. Contour interval: 0.7, 1.5, 3.5,7 per cent (Undeformed fabrics after F. J. Turner.)

UNDEFORMED

EXTENSION

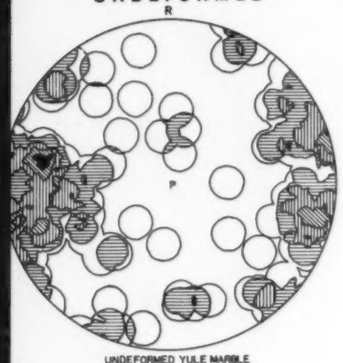

UNDEFORMED YULE MARBLE

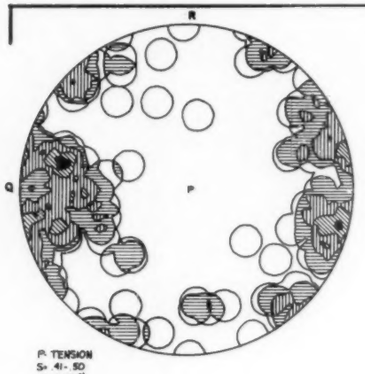

P-TENSION
S=.41-.50
e= 2.90%

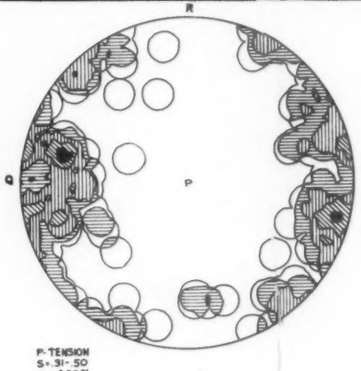

P-TENSION
S=.31-.50
e= 4.39%

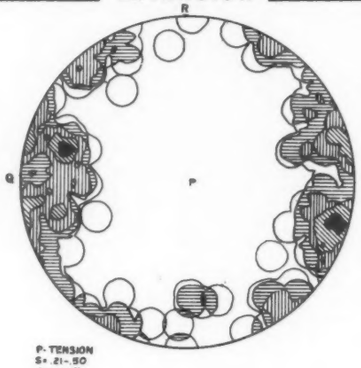

P-TENSION
S=.21-.50
e= 6.27%

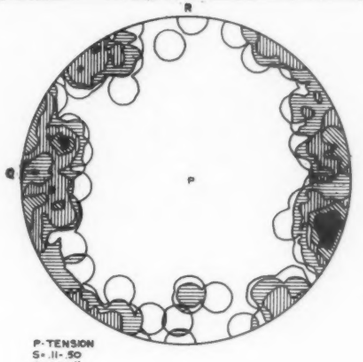

P-TENSION
S=.11-.50
e= 6.90%

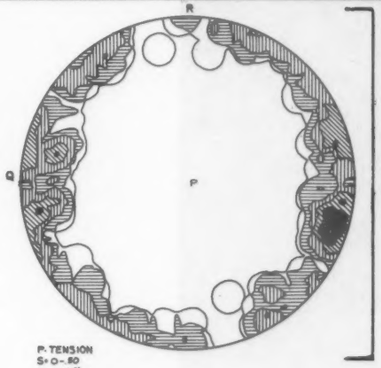

P-TENSION
S=0-.50
e= 6.18%

P

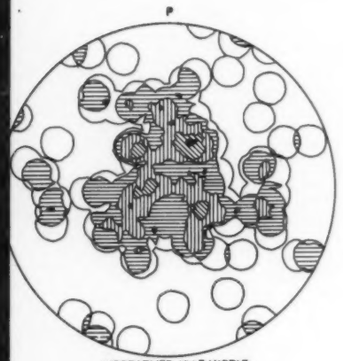

UNDEFORMED YULE MARBLE

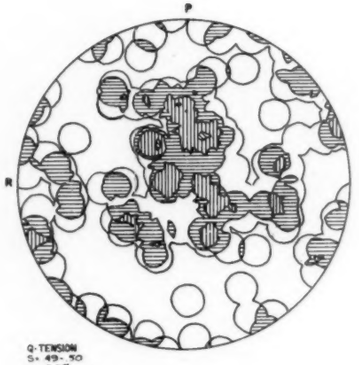

Q-TENSION
S=.49-.50
e= 5.1%

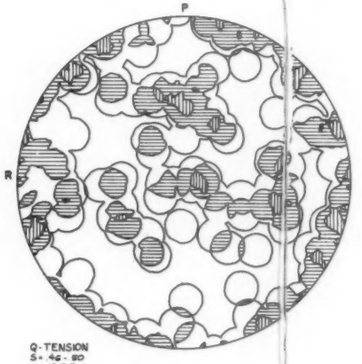

Q-TENSION
S=.45-.50
e= 13.6%

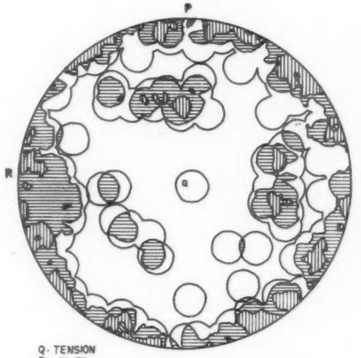

Q-TENSION
S=.41-.50
e=19.6%

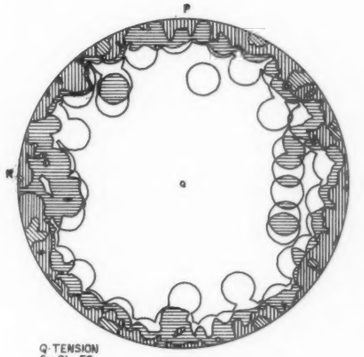

Q-TENSION
S=.21-.50
e=25.2%

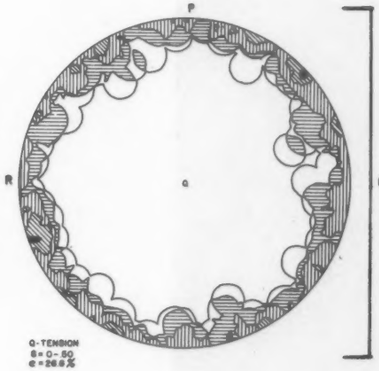

Q-TENSION
S=0-.50
e=26.8%

Q

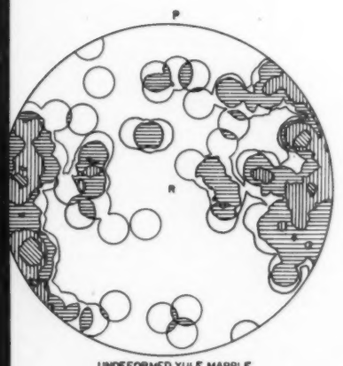

UNDEFORMED YULE MARBLE

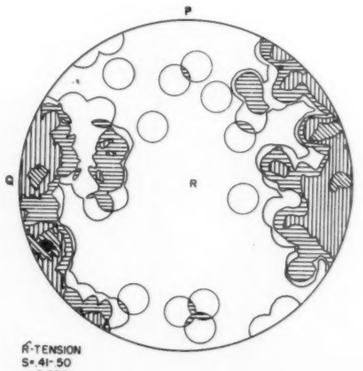

R-TENSION
S=.41-.50
e=2.85%

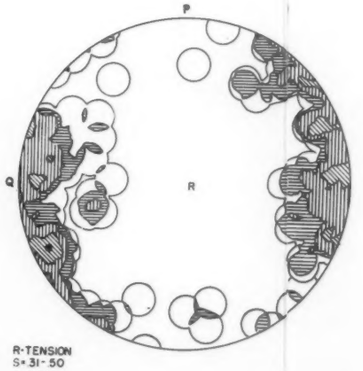

R-TENSION
S=.31-.50
e=4.93%

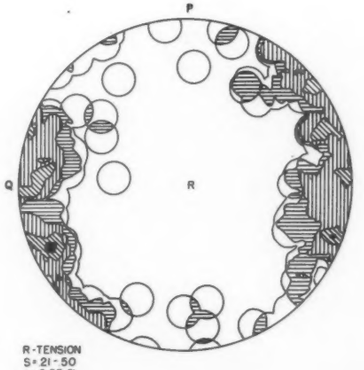

R-TENSION
S=.21-.50
e=6.25%

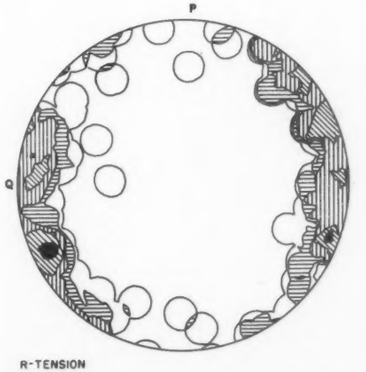

R-TENSION
S=.11-.50
e=7.21%

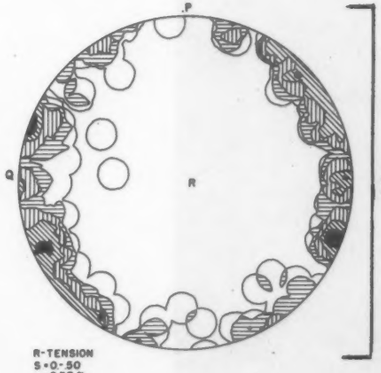

R-TENSION
S=0-.50
e=8.37%

R

ULT OF COMPLETE MECHANICAL TWINNING ON $01\bar{1}2$

rmation. 136 *c* axes in each diagram. Strain accompanying changes is re-
interval: 0.7, 1.5, 3.5,7 per cent (Undeformed fabrics after F. J. Turner.)

BULLETIN OF THE GEOLOGICAL SOCIETY OF AMERICA
VOL. 62, PP. 863-886, 16 FIGS., 2 PLS. AUGUST 1951

DEFORMATION OF YULE MARBLE: PART II—PREDICTED FABRIC CHANGES

BY JOHN W. HANDIN AND DAVID GRIGGS

ABSTRACT

The resolved shear-stress coefficient for twinning and translation was determined graphically for each $\{01\bar{1}2\}$ plane in every grain of two representative fabric samples of Yule marble for six different stress orientations. The rotation of crystal elements in each grain was computed as a function of strain of the aggregate using the methods of metallurgists under two widely different hypotheses of the deformation of granular aggregates: (a) "heterogeneous" and (b) "homogeneous" deformation. Predicted fabrics are then constructed for different stress orientations and different degrees of deformation. Comparison of predicted and observed (Part III) fabrics shows that predictions under the heterogeneous hypothesis are not in agreement with observed fabrics. Fabrics predicted under the homogeneous hypothesis of Taylor are very similar to those observed. This provides evidence for the complementary roles of twinning and translation on $\{01\bar{1}2\}$ and the subordinate roles of other glide planes in the case of calcite marble deformed under the conditions described in Part I.

CONTENTS

	Page
Introduction	863
Geometry of the gliding process	866
Predicted fabrics based on the assumption of heterogeneous deformation	869
General statement	869
Fabrics predicted on hypothesis of twinning on $\{01\bar{1}2\}$	871
Fabrics predicted on hypothesis of translation on $\{01\bar{1}2\}$	877
Fabrics predicted on hypothesis of mechanical twinning on $\{02\bar{2}1\}$	879
Predicted fabrics based on the assumption of homogeneous deformation	880
Conclusion	884
References cited	885

ILLUSTRATIONS

Figure	Page
1. Fabric diagrams of undeformed and deformed marble	865
2. Geometry of the gliding process	866
3. Overlay to be used with a stereographic net	868
4. Geometry of mechanical twinning on $\{01\bar{1}2\}$ in calcite	869
5. Field of complete twinning in tension	870
6. Field of complete twinning in compression	871
7. Histograms showing the distribution of the maximum resolved shear-stress coefficient	873
8. Predicted fabric changes in a d cylinder as a result of twinning alone	875
9. Predicted changes in a axes orientation in a P cylinder in tension as a result of twinning alone	876
10. Predicted orientations of edges $[e{:}e']$	876
11. Ratio of resolved shear-stress coefficient after slip-plane rotation to that before deformation, tension	878
12. Ratio of resolved shear-stress coefficient after slip-plane rotation to that before deformation, compression	879
13. Predicted fabric changes as a result of translation alone	880
14. Predicted fabric changes as a result of translation alone	881
15. Geometry of mechanical twinning (hypothetical) on $\{02\bar{2}1\}$ in calcite	882
16. Strain for complete twinning	883

Plate	Facing page
1. Predicted fabrics as a result of heterogeneous mechanical twinning	863
2. Predicted fabrics as a result of homogeneous mechanical twinning	884

INTRODUCTION

Five decades of work on artificial deformation of marble have failed to define the mechanism of its plastic flow under laboratory conditions. The most recent work by Balsley (1941) and Knopf (1949) made great advances, principally in showing: (1) that the deformation is mainly, if not wholly, due to intragranular gliding, (2) that development of $\{01\bar{1}2\}$ lamellae constitutes the predominant visible effect of this deformation within the calcite

grains. They also reported gross changes in the optic-axis fabric as a result of 30 per cent compression (Knopf, 1949) and 20 per cent tension (Balsley, 1941) which have not been wholly confirmed in present work, but which were influential in its initial direction.

Bell's discovery of $\{01\bar{1}2\}$ translation gliding in calcite (Knopf, 1949, Pl. 4) in a direction sense opposite to that of the well-known mechanical twinning doubled the degrees of freedom of known deformation mechanisms. Taking into account all published data as well as her own extensive work, Knopf (1949, p. 568) concluded: "The relative importance of these two mechanisms of slip (twin- and translation-gliding) on $\{01\bar{1}2\}$ cannot be determined from evidence at hand."

Both Balsley and Knopf suggested that a more extensive analytical study based on principles established by metallurgists and physicists in their work on metals, coupled with more microscopic data on artificially deformed marble, might lead to resolution of this problem. This paper reports the results of such an analytical study, which we believe has been successful, at least in reducing the area of uncertainty. The work has been closely co-ordinated throughout with the current microscopic study of Turner and Ch'ih (Part III) and the experimental program of Griggs and Miller (Part I). It is perhaps appropriate to point out that the extensive work of the metallurgists and physicists on metals, which has yielded so much of value, has not yet established a completely satisfactory theory of the mechanism of deformation of polycrystalline metal aggregates.

The data on which this study is based are the complete crystallographic orientations of an adequate sample of calcite grains in undeformed Yule marble. The individual space co-ordinates were supplied by Turner and Ch'ih. Since Knopf (1949) and Turner (1949) have shown that the fabric of Yule marble is remarkably homogeneous, this fabric sample can then be used as a starting point from which to predict the fabric to be expected in specimens of the same material for any given deformation.

In the derivation of predicted fabrics, hypothetical mechanisms of deformation of the individual crystals were assumed; the reaction of each grain to a given deformation of the aggregate was determined using hypothetical methods developed in the study of metals; from this the change in orientation of any crystal element (*e.g.*, the *c* axis) was predicted; and a new fabric constructed. In practice, fabrics were so constructed for approximately the same orientations and degrees of strain which were achieved experimentally (Part I). Comparison of these predicted fabrics with the observed fabrics of the experimentally deformed specimens (Part III) then served as a check on the hypothetical mechanism of grain deformation and the hypothesis used to relate individual grain deformation to that of the aggregate.

At the outset, a choice had to be made between two widely divergent hypotheses of deformation in polycrystalline metal aggregates. To use simple titles these will be called the "heterogeneous" and "homogeneous" hypothesis respectively. The former, applied in different modifications by many metallurgists, assumes that the individual grains deform in response to the external stress field with negligible or minor restriction on their freedom of motion by neighboring grains. The latter hypothesis, originated by Taylor (1938, p. 319) assumes, on the other hand, that each grain is completely restricted by contact with its neighbors so that, "Each grain suffers exactly the same strain as the surrounding material in bulk." Both of these hypotheses are acknowledged to be over-simplified, and the true situation is probably between the two extremes, but oversimplification is necessary to facilitate the analytical approach to the problem, and trial of both hypotheses may show which is more nearly correct.

In view of the gross fabric changes (Fig. 1) reported at 30 per cent compression by Knopf (1949) and 20 per cent tension by Balsley (1941), it was initially decided that the "heterogeneous" was more promising than the "homogeneous" hypothesis, since the former gives greater fabric changes for small deformations. Study of the amount of axis rotation due to translation quickly showed that translation alone was insufficient to produce fabric changes of the reported magnitude at 20 per cent ex-

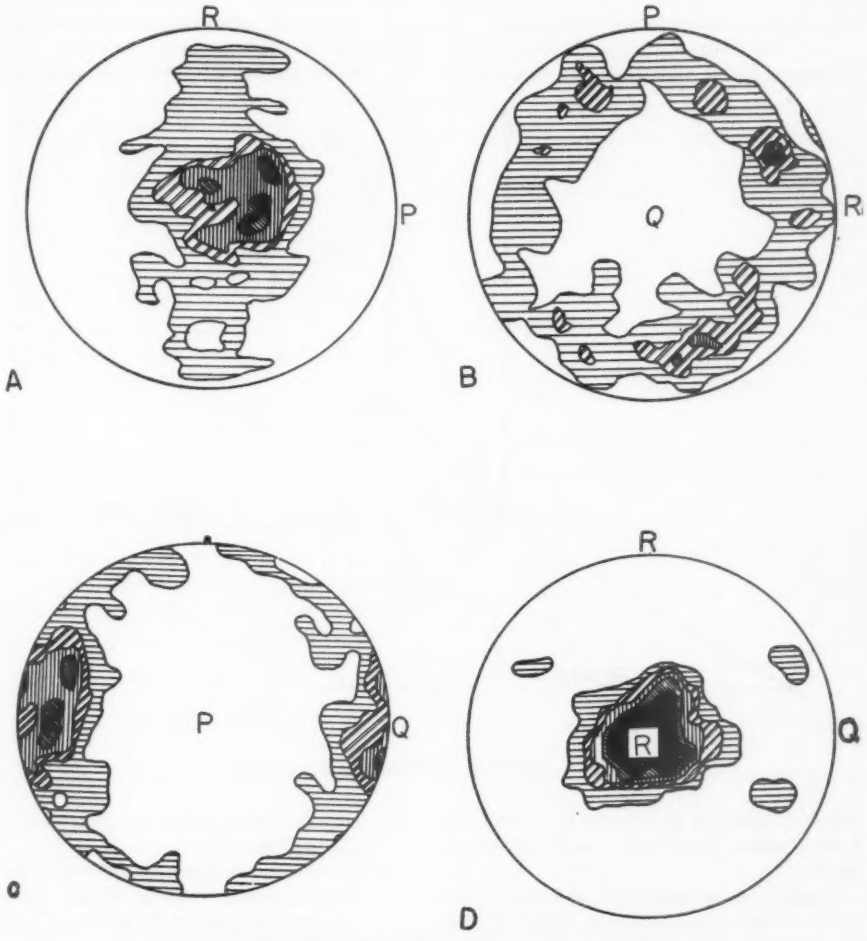

FIGURE 1.—FABRIC DIAGRAMS OF UNDEFORMED AND DEFORMED MARBLE

A. Undeformed Yule marble; 209 *c* axes, contours 1, 3, 5, 7, 9 per cent (After E. B. Knopf).
B. Marble deformed 20 per cent in extension; 200 *c* axes, contours 1, 3, 5, 7 per cent (After J. R. Balsley).
C. Undeformed Yule marble; 209 *c* axes, contours 1, 3, 5, 7, 9 per cent (After E. B. Knopf).
D. Marble deformed 30 per cent in compression; 163 *c* axes, contours 1, 3, 5, 7, 9 per cent (After Snively, Bell, Griggs, and Knopf).

tension. It was thus decided to explore first the capabilities of twinning, which are qualitatively of the right magnitude. Consequently the first and most extensive study was directed toward exploring the consequences of twinning alone under the heterogeneous hypothesis. Only after this phase was completed did Turner and Ch'ih (Part III) discover that Balsley's fabric diagram (Fig. 1B) was in error, due to the extreme difficulty of measuring the optic axes in his section. Had the true fabric been known initially the course of this work might have been different; but it is felt that much was learned in exploring this "blind alley", and the results of this phase of the work are therefore reported in full. Moreover, an approach of this type may

possibly prove fruitful in other materials, or under other conditions of deformation.

Next, the effect of translation alone under the heterogeneous hypothesis was determined.

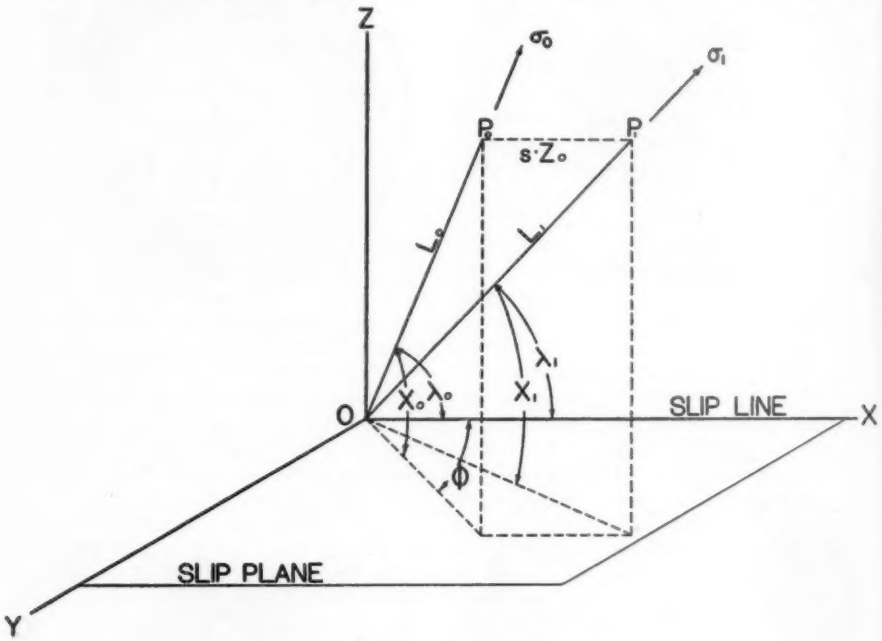

FIGURE 2.—GEOMETRY OF THE GLIDING PROCESS

Other mechanisms of deformation under the heterogeneous hypothesis were considered briefly.

Finally, the homogeneous hypothesis was tested. Under this hypothesis both twinning and translation must operate in general. Indeed, Taylor's rigorous application of the hypothesis requires functioning of at least two more glide planes in addition to the three $\{01\bar{1}2\}$ planes. The relative amount of twinning and translation is then fixed by the original fabric and the amount and orientation of strain.

Other important assumptions common to all phases of this work are necessary to reduce the analytical procedures to manageable proportions. These are also attended by some uncertainty, and their degree of validity may be evaluated by comparison of predicted and observed fabrics. They are:

(1) That the grains on the average are subject to the same stress field as that applied to the specimen as a whole. This means that stress differences caused by grain anisotropy either are unimportant or cancel out.

(2) That the law of maximum resolved shear stress determines which $\{01\bar{1}2\}$ plane will glide in a grain of the aggregate, and in which sense.

Still other assumptions peculiar to the particular case are stated in treatment of the separate cases. Further discussion of how the fabrics predicted on these several assumptions compare with Turner and Ch'ih's observed fabrics will be left until later.

GEOMETRY OF THE GLIDING PROCESSES

Plastic deformation by gliding in a single crystal or grain involves shear on one or more systems of closely spaced parallel glide or slip planes. Since deformation results in a change in shape of the deformed body, the

glide planes must rotate to accommodate themselves to the change. In the analytical treatment of the problem used by metallurgists (*cf.* Schmid and Boas, 1935, p. 61–67), it is convenient to imagine that the glide planes remain fixed and that the stress axis changes position. The geometry is shown in Figure 2 where a stress σ_0 is applied at an angle χ_0 to the glide plane. In tension the stress axis moves from P_0 to P_1 along a line parallel to the glide line or direction of slip, and the angle between the stress axis and the glide plane is then χ_1. In compression the positions of P_0 and P_1 are reversed; P_0 moves to the left instead of to the right. In tension the slip planes rotate toward parallelism with the stress axis, and in compression they rotate away from it, toward the normal. In Figure 2, λ_0 and λ_1 are the angles between the stress axis and the glide direction before and after deformation respectively. The quantity s is the shear, and ϕ is the angle between the glide line and the projection of the stress axis on the glide plane.

σ is the stress or force per unit area on the plane normal to the stress axis. The shear stress on the slip plane in the slip direction, is

$$\tau = \sigma \sin \chi_0 \cos \lambda_0 = \sigma \sin \chi_0 \cos \chi_0 \cos \phi, \quad (1A)$$

and the resolved shear stress coefficient is:

$$S_0 = \frac{\tau}{\sigma} = \sin \chi_0 \cos \lambda_0 = \sin \chi_0 \cos \chi_0 \cos \phi \quad (1B)$$

The strain, ϵ, is determined from the relationships shown in Figure 2. For tension:

$$x_1 = x_0 + z_0 s$$

$$y_1 = y_0$$

$$z_1 = z_0$$

$$x_0 = L_0 \cos \lambda_0$$

$$z_0 = L_0 \sin \chi_0$$

$$\frac{L_1}{L_0} = \sqrt{\frac{x_1^2 + y_1^2 + z_1^2}{x_0^2 + y_0^2 + z_0^2}}$$

$$\frac{L_1}{L_0} = \sqrt{1 + \frac{2s x_0 z_0 + s^2 z_0^2}{L_0^2}}$$

$$1 + \epsilon = \frac{L_1}{L_0}$$

$$= \sqrt{1 + 2s \sin \chi_0 \cos \lambda_0 + s^2 \sin^2 \chi_0}. \quad (2)$$

For compression, $x_1 = x_0 - z_0 s$, and:

$$1 - \epsilon = \frac{L_1}{L_0}$$

$$= \sqrt{1 - 2s \sin \chi_0 \cos \lambda_0 + s^2 \sin^2 \chi_0}. \quad (3)$$

Combining equation (1B) with equations (2) and (3) yields strain in terms of the resolved shear-stress coefficient, S_0, and the angle χ_0. For tension:

$$\frac{L_1}{L_0} = \sqrt{1 + 2sS_0 + s^2 \sin^2 \chi_0}, \quad (4)$$

and for compression:

$$\frac{L_1}{L_0} = \sqrt{1 - 2sS_0 + s^2 \sin^2 \chi_0}. \quad (5)$$

Graphical solutions of equations (1B), (4) and (5) were used to determine the appropriate values for individual grains in the sample fabric supplied by Turner and Ch'ih. Figure 3 is a stereographic projection giving values of S_0 from equation (1B) for the case of twinning and translation on $\{01\bar{1}2\}$ in calcite. The c axis is at the center of the projection, on the .40 contour line. The trace of one $\{01\bar{1}2\}$ plane is shown, coinciding with one 0.0 contour. The normal to this plane is also shown, on the N-S axis, on the other 0.0 contour. The orientation of any uniaxial stress with respect to the c axis and one $\{01\bar{1}2\}$ plane can be represented by a point on this projection. For this stress, the contour through the point gives the magnitude of the resolved shear-stress coefficient (S_0) on that $\{01\bar{1}2\}$ plane. If the applied stress is tensile, and falls in the stippled area, or compressive and in the unstippled area, the sense of the resolved shear stress is such as to produce twinning. Otherwise, the sense is such as to produce translation. In each grain of the sample fabric the magnitude of S_0 and the sense of the resolved shear stress was determined for each of the three $\{01\bar{1}2\}$ planes and for each of the stress orientations considered (P, Q, R, d).

Figure 4 shows the geometry of mechanical twinning on the $\{01\bar{1}2\}$ plane. Arrows show the direction of shear, and it is apparent that twinning occurs not only in a definite crystallographic direction but also in a definite sense. The twinning results in a shift of 52°30′ in the position of the c axis. The shear, which is

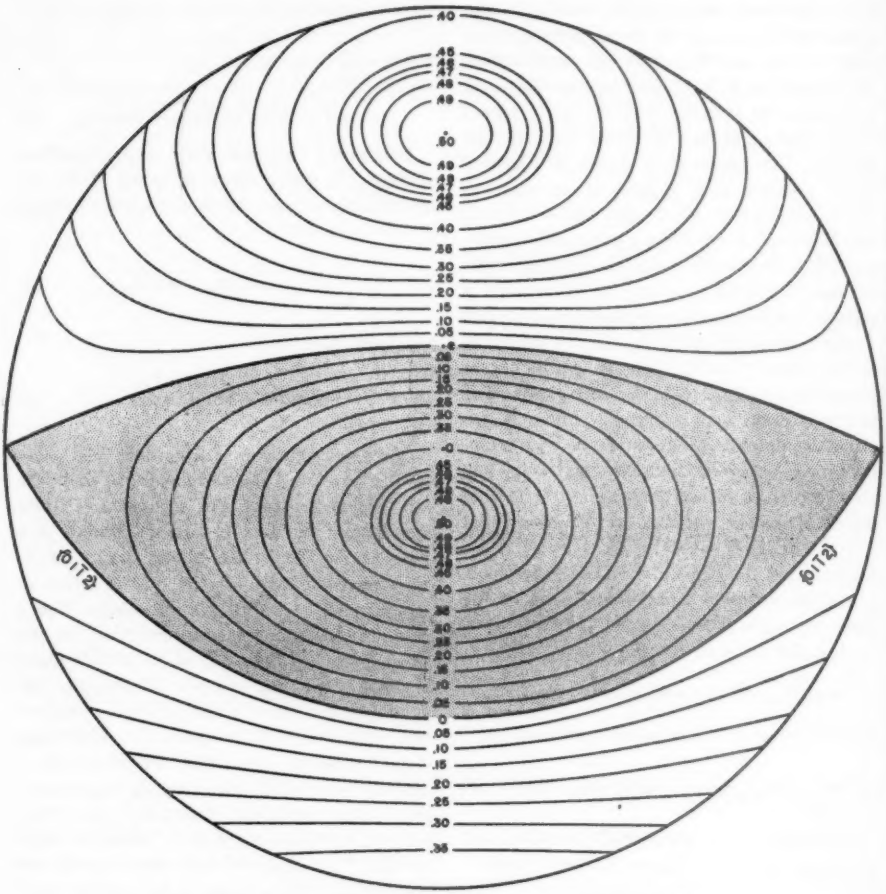

FIGURE 3.—OVERLAY TO BE USED WITH A STEREOGRAPHIC NET

For determining the resolved shear-stress coefficient on the {01$\bar{1}$2} plane in the glide direction of calcite. (c is the *c* axis; e is the pole of an {01$\bar{1}$2} plane. Field of twinning in tension—stippled area.)

always the same for twinning, is given by:

$$s = 2 \tan \frac{\psi}{2} = 0.694. \qquad (6)$$

In tension, as long as the stress axis is oriented so that the resolved shear stress is in the proper sense to produce twinning, there is no restriction on the value χ_0 may take. We find the restriction on χ_0 for compression by setting equation (3) equal to unity. Complete twinning in compression cannot occur if χ_0 is greater than 70° 52′.

To determine the maximum strain in twinning, set $\phi = 0$ (or $\chi_0 = \lambda_0$) and maximize the expression under the radical in equations (2) and (3). Then,

$$\tan \chi_{0\max} = \frac{s}{2} \pm \sqrt{\frac{s^2}{4} + 1} = \frac{L_1}{L_0 \max} \qquad (7)$$

(+ for extension, − for compression). Substituting $s = .694$, the maximum strain in tension is 41 per cent when $\chi_0 = 54° 35′$; in compression, 29 per cent when $\chi_0 = 35° 25′$.

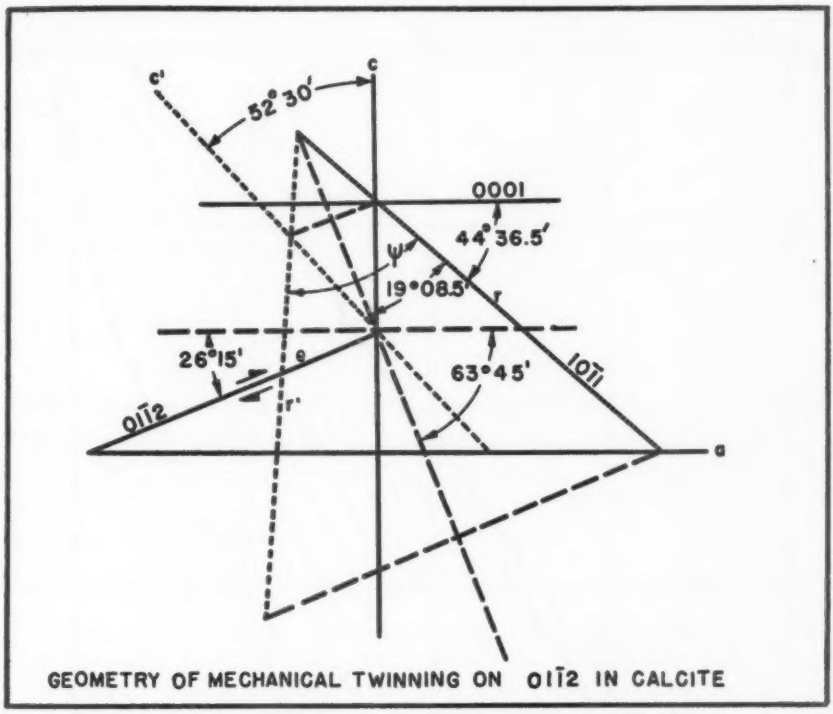

FIGURE 4.—GEOMETRY OF MECHANICAL TWINNING ON {01$\bar{1}$2} IN CALCITE
Showing the shear $s = 2 \tan \psi/2$. (Projection on a-c plane.)

To determine the grain rotation resulting from a single shear produced in tension, the following relation is used (*see* Fig. 2):

$$\frac{L_1}{L_0} = \frac{\sin x_0}{\sin x_1}. \tag{8}$$

For rotation in compression, a different construction is more accurate (*cf.* Schmid and Boas, 1935, p. 67), yielding the relation:

$$\frac{L_1}{L_0} = \frac{\cos x_1}{\cos x_0}. \tag{9}$$

Figures 5 and 6 give graphical solutions of equations (4) and (5) for complete twinning on {01$\bar{1}$2} in calcite, where $s = .694$. While plotting each grain for determination of the resolved shear-stress coefficient, x_0 is also measured. The extension or compression of the grain which would result from complete twinning on any one of the {01$\bar{1}$2} planes may then be determined from Figures 5 and 6.

PREDICTED FABRICS BASED ON THE ASSUMPTION OF HETEROGENEOUS DEFORMATION

General Statement

In this phase of the investigation it was assumed that each grain in the polycrystalline aggregate can deform independently of surrounding grains; that is, the deformation of a grain is assumed to be under no restriction at its boundaries. (*Cf.* Cox and Sopwith, 1937, p. 146.) This implies further that the contribution of each grain to the total deformation of the aggregate is the individual deformation divided by the total number of grains. It is reasonable to suppose also that, if this sort of deformation predominated, those individuals

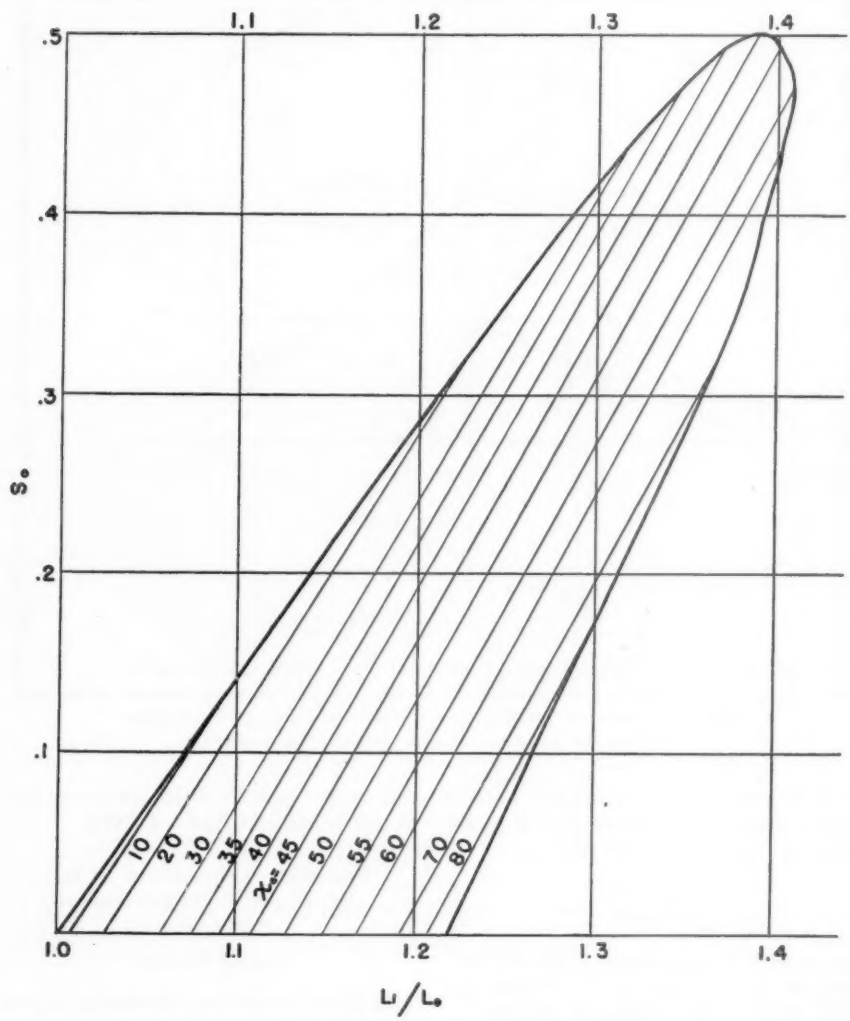

FIGURE 5.—FIELD OF COMPLETE TWINNING IN TENSION
L_1/L_0 as a function of S_0 and χ_0 on $\{01\bar{1}2\}$ in calcite.

in which the resolved shear stress on one set of $\{01\bar{1}2\}$ planes is high would deform first, before grains in which the resolved shear stress has lower values on all $\{01\bar{1}2\}$ planes. It was further assumed:

(1) That there is no work hardening.

(2) That the law of maximum resolved shear stress determines which of the three $\{01\bar{1}2\}$ planes functions and whether in twinning or translation (Gough, 1933, p. 23).

These four basic assumptions are made in deriving all the fabrics described in the next four sections.

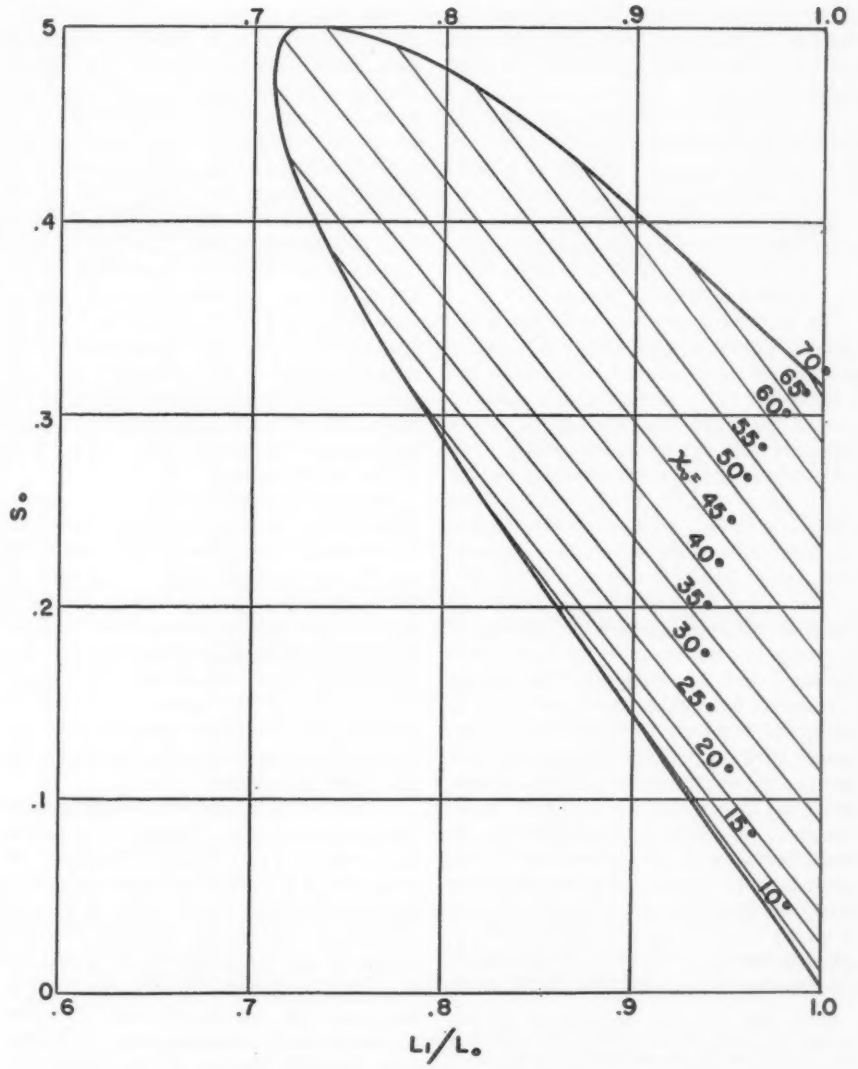

FIGURE 6.—FIELD OF COMPLETE TWINNING IN COMPRESSION
L_1/L_0 as a function of S_0 and χ_0 on $\{01\bar{1}2\}$ in calcite.

Fabrics Predicted on the Hypothesis of Twinning on $\{01\bar{1}2\}$

General considerations.—Turner and Ch'ih furnished complete crystallographic data, determined with the universal stage, on 136 calcite grains measured in an *R* section of undeformed Yule marble and an additional 100 grains measured in an *R* section from a different block also

undeformed.[1] The latter is the block from which cylinders were cut for study in Parts I and III. The data include co-ordinates of the optic axis and one or more $\{01\bar{1}2\}$ lamellae for each grain.

Two important assumptions are made in deriving the deformation fabrics:

(1) Deformation occurs entirely as a result of mechanical twinning on $\{01\bar{1}2\}$.

(2) Each grain twins completely on one and only one plane before twinning occurs in grains for which the resolved shear stress on $\{01\bar{1}2\}$ is lower.

The resolved shear-stress coefficient is determined as indicated for each $\{01\bar{1}2\}$ lamella and for each stress axis, in both extension and compression. The grains are then grouped so that all the grains in a given group have a maximum resolved shear-stress coefficient falling within a certain range of values (for example, S_0 = .46–.50, .41–.45, etc.). Having determined in each grain which $\{01\bar{1}2\}$ plane functions, we measure the angle χ_0 between that plane and the associated stress axis. Knowing the values of S_0 and χ_0, the amount of elongation in extension and the amount of shortening in compression are determined from Figures 5 and 6 respectively. The average deformation for each group of grains is then computed. Beginning with the group in the highest stress interval, we calculate the contribution of each group to the total deformation of the hypothetical fabric. Figure 7 shows histograms of the resolved shear-stress coefficient distribution in 136 grains for three stress orientations *P*, *Q*, and *R* (on the left of the figure) and in 100 grains from a different block of marble for three stress orientations *R*, *Q*, and *d* (on the right). Above the histograms are the hypothetical inverse stress-strain curves for plastic deformation by twinning alone, derived purely geometrically from the calculated deformation as a function of resolved shear stress, taking no account of a critical stress or work hardening. In general the histograms and curves for the *P* and *R* orientations are similar, but those for the *Q* orientation are radically different from the other two. The similarities between the two *R* sections and the two *Q* sections from different blocks indicate that Yule marble is fairly homogeneous with regard to resolved shear stress on $\{01\bar{1}2\}$ planes. Also shown are the weighted mean resolved shear-stress coefficients, $\bar{S}_0$, in the twinning sense for all orientations. The qualitative correlation between $\bar{S}_0$ and strength is shown in Part I, Table 2. The lack of correlation between the hypothetical stress-strain curves and the experimental curves (Part I, Fig. 3) is evident on inspection.

Changes in preferred orientation of c axes.—Three sets of predicted deformation fabrics, one for each of the three orientations *P*, *Q*, and *R*, are shown on Plate 1. The series of fabric changes to be expected in tension is shown to the right of the undeformed fabric; the series in compression to the left. The three undeformed fabrics are plotted from Turner's original data for 136 grains measured in an *R* section. The *P* and *Q* sections show the same grains, the *c* axes having been rotated 90° to the *P* and *Q* positions.

In deriving each series of fabric changes, we begin with the group of grains in the highest S_0 interval and plot the twinned position of the *c* axes for all the grains in this group and the untwinned position for all other grains. The amount of deformation accompanying the change is recorded below each diagram. The procedure is repeated for each group until all the grains that can possibly twin, no matter how small the resolved shear-stress coefficient, have deformed. The last fabric diagram in a series therefore represents the maximum change that can be brought about by twinning, and the corresponding deformation is the greatest possible for twinning alone.

It is necessary to correct the twinned position of the *c* axes for the intragranular rotation of the twin plane resulting from the shearing

[1] After this work was completed, it was discovered that the tentative correlation between *P* and *R* in the two blocks was probably wrong. Some fabric changes derived for *P* orientations in block 2 were intended to correlate with *T* sections from block 3 (the block used in present experiments, *see* Part III). It is now thought that *T* of block 3 most probably correlates with *R* of block 2, so some of the predicted fabrics cannot be directly compared with observed fabrics in Part III. However, since fabric data alone cannot distinguish clearly between *P* and *R*, the comparison of predicted fabric changes in *P* with observed changes in *R* is believed valid.

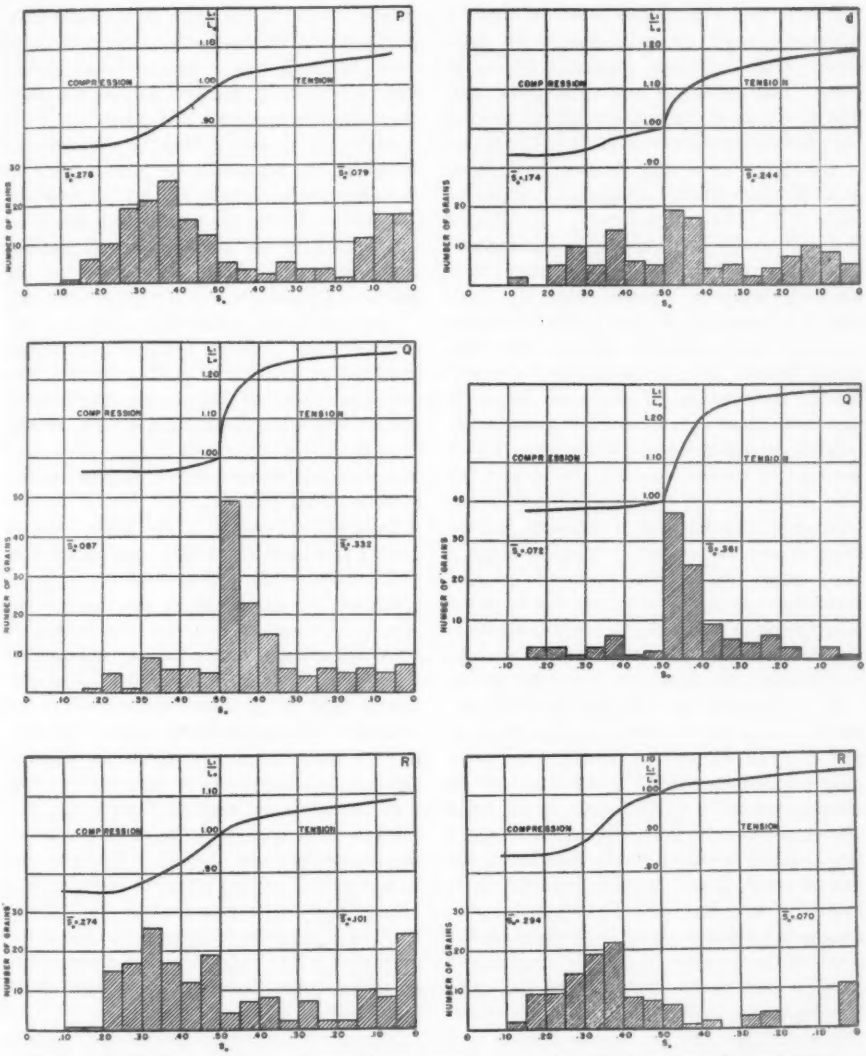

FIGURE 7.—HISTOGRAMS SHOWING THE DISTRIBUTION OF THE MAXIMUM RESOLVED SHEAR-STRESS COEFFICIENT, S_0, FOR $\{01\bar{1}2\}$ TWINNING AND CURVES SHOWING CUMULATIVE DEFORMATION *vs.* S_0 FOR COMPLETE TWINNING

Both calculated on the assumption of heterogeneous deformation. Left: 136 calcite grains from block no. 2 of Yule marble. Right: 100 calcite grains from block no. 3. Note pronounced anisotropy of maximum resolved shear-stress coefficient.

motion. The angle χ_1 between the stress axis and the twin plane after deformation is calculated from equations (8) and (9). The shift in position of the *c* axes due to shearing has an average value of about 10° and is therefore small compared to the shift due to twinning ($52\frac{1}{2}$°).

A comparison of the fabrics of experimen-

tally deformed Yule marble shown in Figure 1 (diagrams based on preliminary work done before 1942) with the predicted fabrics of Plate 1 indicates a fair qualitative agreement. The directions of the changes are the same in the predicted and observed fabrics. The degree of the change is at least large in both cases, although not directly comparable since the amount of deformation involved is different (for a *P* section in compression, a maximum shortening of 14.5 per cent predicted, 27.6 per cent shortening actually observed). However, a comparison of these predicted fabrics with the newly observed fabrics (Part III) shows little or no correspondence for experimental deformations of less than about 15 per cent. Moreover, we predict a maximum possible deformation by twinning alone of 14.5 per cent in compression (*P*) and of 26.6 per cent in tension (*Q*); whereas Yule marble has been artificially deformed 40 per cent in compression and 44 per cent in tension. Even if every grain in the fabric were perfectly oriented with respect to the stress axis, so that twinning would result in the maximum possible deformation (41 per cent in tension, 29 per cent in compression), twinning alone would not suffice.

It is interesting to note that the final predicted fabrics for the three orientations *P*, *Q*, and *R* are all similar with respect to the stress axis: a maximum parallel to the stress axis in compression and a girdle normal to the stress axis in tension. To determine whether or not this behavior is related to the fact that in the case of the *P*, *Q*, and *R* orientations the stress axis is symmetrical with the original fabric, a series of predicted fabrics was derived for the *d* orientation in which the stress is applied at an angle of 45° to the foliation plane. As Figure 8 indicates, the final result is similar: in extension the *c* axes tend to become aligned in a girdle normal to the stress axis; in compression they tend to become aligned parallel to the stress axis. Again for small deformations there is little or no correspondence with the observed fabrics of *d* cylinders (Part III).

Changes in the preferred orientation of a axes.—During the course of our work, the question arose as to whether or not deformation by twinning would result in any appreciable reorientation of the calcite space lattice other than that reflected in changes in position of the *c* axes. Any such reorientations should be obvious in a series of diagrams showing the effect of deformation upon preferred orientation of the crystal axes a_1, a_2, a_3. Making the same assumptions as previously for deformation by twinning alone, we derive a set of predicted deformation fabrics using the same procedures, except that in this case the twinned position of the three axes a_1, a_2, a_3 of each of the 136 grains is plotted for a *P* section in tension.

The undeformed *a* axes fabric (Fig. 9), constructed from Turner's original data, shows preferred orientation of a low degree. The successive predicted deformation fabrics show statistically insignificant changes. The reality of observed preferred orientations of *a* axes in artificially deformed marble is questionable, however (Part III).

Preferred orientation of the edges [*e*:*e*′].—Turner and Ch'ih (Part III) have found that, in *R* cylinders deformed in extension, a strong preferred orientation pattern develops for the edge [*e*:*e*′] between sets of well-developed $\{01\bar{1}2\}$ lamellae in each grain. For other directions of applied stress, the [*e*:*e*′] pattern is totally different. If these observed effects are a result of twinning under the present hypothesis, the mechanism involved is probably as follows: Twinning starts on that $\{01\bar{1}2\}$ plane with the maximum resolved shear stress, and proceeds until work hardening (and to a minor degree intragranular rotation) increases the stress required on that plane for twinning to a value equal to or greater than the critical resolved shear stress for twinning on one of the other two $\{01\bar{1}2\}$ planes in the grain; twinning then proceeds on the new plane or on both planes.

The grains are again divided into groups, but this time according to the resolved shear stress on the *second* plane, and it is assumed that all the second-generation twins that can develop do so regardless of how small the resolved shear stress on the second plane may be. The resulting fabrics are shown in Figure 10. For a *Q* section in tension a girdle develops normal to the axis of tension in agreement with the observed behavior (Part III). For an

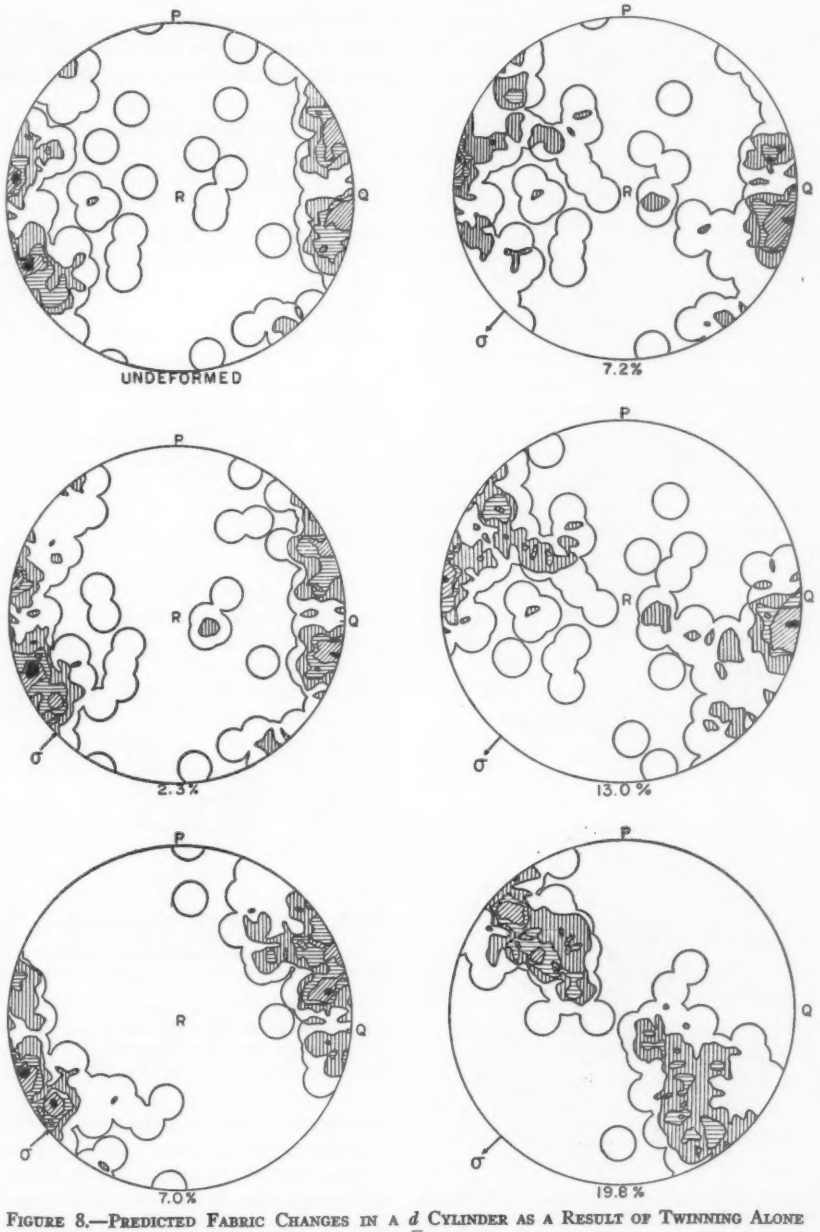

FIGURE 8.—PREDICTED FABRIC CHANGES IN A *d* CYLINDER AS A RESULT OF TWINNING ALONE ON {01$\bar{1}$2}

Assuming heterogeneous deformation. 100 *c* axes in an *R* section of a *d* cylinder. Arrows show directions of applied stress. Strain accompanying changes is recorded below each diagram. Contour interval: 1, 3, 5, 7, 9 per cent. (Undeformed fabric after Turner and Ch'ih.)

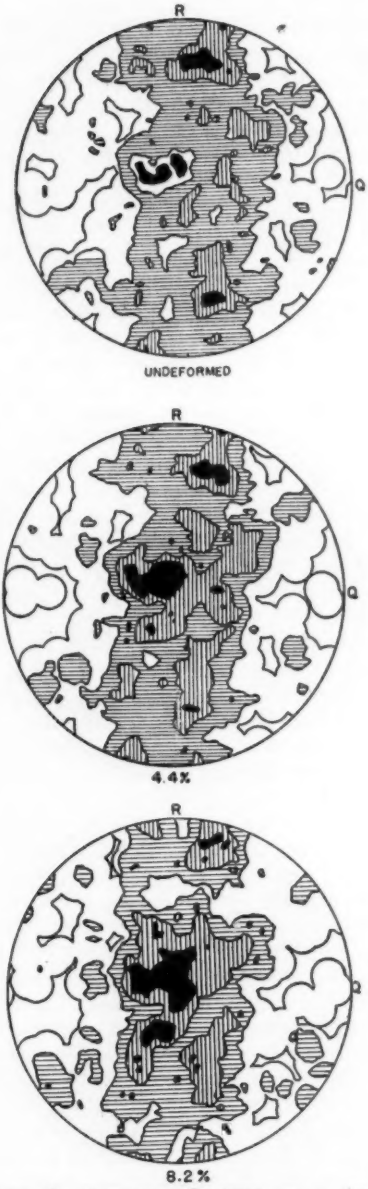

FIGURE 9.—PREDICTED CHANGES IN *a* AXES ORIENTATIONS IN A *P* CYLINDER IN TENSION AS A RESULT OF TWINNING ALONE ON {01$\bar{1}$2}

Assuming heterogeneous deformation. 408 *a* axes in a *P* section of a *P* cylinder. Strain accompanying deformation is recorded below each diagram. Contour interval: 1, 2, 3 per cent. (Undeformed fabric after Turner and Ch'ih.)

R section in compression, a maximum develops normal to the axis of applied stress. Since the work-hardening function for calcite

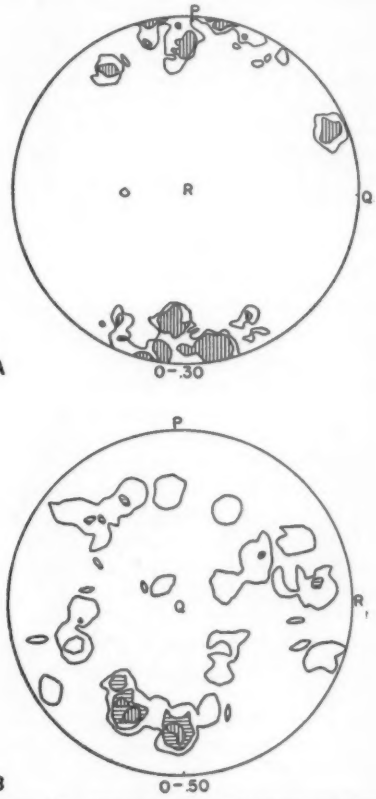

FIGURE 10.—PREDICTED ORIENTATIONS OF EDGES [*e*:*e*'] AFTER TWINNING ON TWO {01$\bar{1}$2} PLANES

Assuming heterogeneous deformation and assuming that all grains that can possibly twin on two planes do so.

A. 75 edges [*e*:*e*'] in a *R* section of an *R* cylinder in compression. Contour interval: 4, 6.5, 9 per cent.

B. 87 edges [*e*:*e*'] in a *Q* section of a *Q* cylinder in tension. Contour interval: 2.3, 4.6, 7 per cent.

twinning is not known under these conditions, a definite value of strain cannot be given.

In a random traverse of a thin section of deformed marble, Turner and Ch'ih (Part III) find at least two sets of {01$\bar{1}$2} lamellae developed in nearly all grains. They show that these lamellae are not residual structures persisting from the original fabric, but are produced by the artificial deformation. Our analy-

sis reveals that, for an R section in tension and a Q section in compression, less than 10 per cent of the grains have two $\{01\bar{1}2\}$ planes with a resolved shear stress in the twinning field. This is of course strong evidence against the twinning theory, and it makes a statistical analysis of $[e{:}e']$ fabrics impossible for those orientations. The fact that all grains appear to take part in the deformation is evidence against the assumption that the deformation is heterogeneous.

Fabrics Predicted on the Hypothesis of Translation on $\{01\bar{1}2\}$

When the work described in this section was begun, there was no conclusive evidence against the hypothesis that translation gliding is the sole mechanism of deformation of marble. Predicted fabrics were, therefore, based on the assumption that deformation occurs entirely as a result of translation gliding in either sense on $\{01\bar{1}2\}$.

The grains were grouped again according to stress intervals, and it was assumed that translation continues on one plane in each grain within the highest interval, until the resolved shear-stress coefficient is reduced by intragranular rotation of the glide plane to the value of the lower limit of the S_0 interval. At this point, grains in the second interval begin to translate, while grains in the higher interval continue translating, and so on for lower intervals. We knew when this analysis was undertaken that a serious weakness of the assumptions is that work hardening from causes other than glide-plane rotation tends to increase the stress required, so that grains with a much lower resolved shear stress could actually begin translating sooner than is assumed. We did not yet have adequate information to take work hardening into account. Our predicted fabrics probably represent the greatest possible changes that can result from translation alone.

Preliminary data for single crystals show that the resolved shear stress necessary to initiate translation in the sense opposite to twinning is of the order of 10 times that required to initiate twinning (Part I, Fig. 4). No translation has been reported in the twinning sense. The strength anisotropy of the Yule marble, and analysis of the stress-strain curves for Yule marble indicate that, if the mechanism of deformation is $\{01\bar{1}2\}$ gliding, the resistance to glide is less in the twin sense. This is not consistent with our assumptions. The departure of the assumptions from reality is greatest for those fabrics in which the majority of grains have orientations favorable for twinning (R in compression, Q in tension). The assumptions are much less objectionable for the fabrics with few grains which can twin (R in tension, Q in compression). In any case it may be instructive to proceed with the predictions to show that the evidence from fabric changes is also against the theory that deformation results from translation alone.

Fabric changes due to translation alone result from intragranular rotation of the glide planes. We wish to relate the amount of deformation to the reduction in resolved shear stress on the glide plane in the glide direction. Let S_0' be the new value of the resolved shear-stress coefficient after rotation. Then,

$$\frac{S_0}{S_0'} = \frac{\sin \chi_0 \cos \lambda_0}{\sin \chi_1 \cos \lambda_1} \tag{10}$$

For tension:

$$\frac{L_1}{L_0} = d = \frac{\sin \lambda_0}{\sin \lambda_1} = \frac{\sin \chi_0}{\sin \chi_1}$$

$$\left(\frac{S_0'}{S_0}\right)^2 = \frac{1}{d^2}\frac{\cos^2 \lambda_1}{\cos^2 \lambda_0} = \frac{1}{d^2}\frac{(1 - \sin^2 \lambda_1)}{\cos^2 \lambda_0}$$

$$= \frac{1}{d^4}\frac{(d^2 - \sin^2 \lambda_0)}{\cos^2 \lambda_0}$$

$$\frac{S_0'}{S_0} = \frac{1}{d^2 \cos \lambda_0}\sqrt{d^2 - \sin^2 \lambda_0}. \tag{11}$$

Having already measured the values of S_0 and χ_0, one can determine λ_0 from equation (1B). The following example indicates the method of calculation of the ratio S_0'/S_0. Suppose the resolved shear-stress coefficient for a certain grain is .48. This grain then falls into the group in the interval .46–.50. We wish to know how much deformation is required to reduce the stress to a point where grains in the next lower stress interval (.41–.45) can begin to translate. This ratio is therefore .45/.48, and we calculate the deformation using equation (11). From equation (8) we compute the value of χ_1, the angle between the stress axis and the glide plane after deformation.

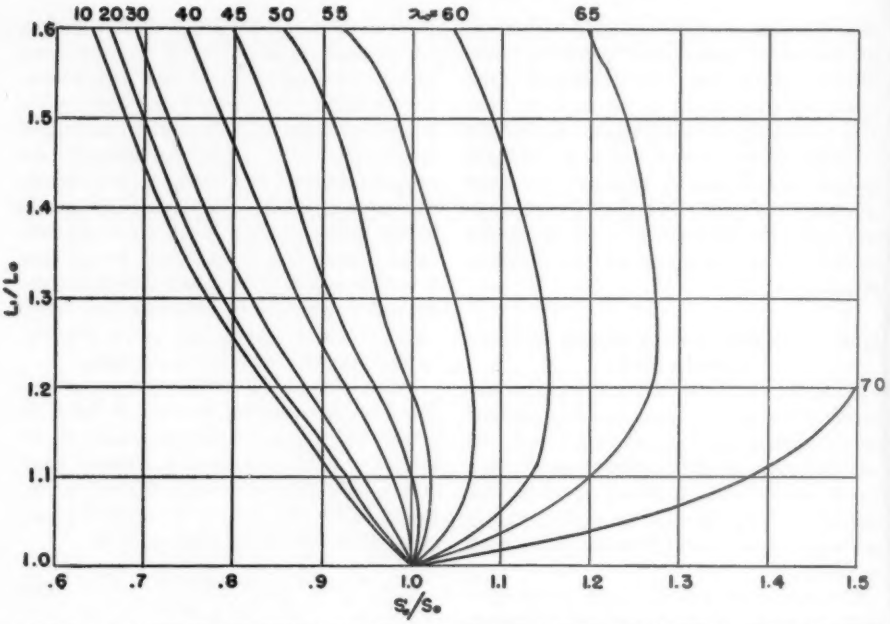

FIGURE 11.—RATIO OF RESOLVED SHEAR-STRESS COEFFICIENT AFTER SLIP-PLANE ROTATION TO THAT BEFORE DEFORMATION, S_0'/S_0
As a function of λ_0 and L_1/L_0 for tension.

For compression:

$$\frac{S_0}{S_0'} = \frac{\sin \chi_0 \cos \lambda_0}{\sin \chi_1 \cos \lambda_1} \tag{12}$$

$$\frac{L_1}{L_0} = d = \frac{\cos \lambda_1}{\cos \lambda_0} = \frac{\cos \chi_1}{\cos \chi_0}$$

$$\left(\frac{S_0'}{S_0}\right)^2 = \frac{\sin^2 \chi_1 d^2}{\sin^2 \chi_0} = \frac{(1 - \cos^2 \chi_1) d^2}{\sin^2 \chi_0}$$

$$= \frac{d^2(1 - d^2 \cos^2 \chi_0)}{\sin^2 \chi_0}$$

$$\frac{S_0'}{S_0} = \frac{d}{\sin \chi_0} \sqrt{1 - d^2 \cos^2 \chi_0}. \tag{13}$$

The values of the ratio S_0'/S_0 and the angle χ_0 are known. We calculate the required deformation using equation (13), and equation (9) gives us the angle χ_1. Graphical solutions of equations (11) and (13) are shown in Figures 11 and 12.

A few calculations were sufficient to show that large deformations are required to produce appreciable fabric changes, and that, even with large deformations, predicted fabrics are not comparable with experimental ones. Consequently, only four predicted diagrams for Q (Fig. 13), and R (Fig. 14) orientations were made: one for a small and one for a large amount of deformation in tension and compression. These diagrams are to be compared with the undeformed Q section of Plate 1, and the undeformed R section of Figure 8.

In a Q section elongated 11.7 per cent, the analysis predicts the development of an incomplete, but distinct girdle lying about 55° from the periphery. When the extension is increased to 54.3 per cent, there is a girdle at about 45°, and the central region of the diagram is completely cleared of c axes. An infinite elongation could shift the girdle outward a maximum of 64° from the center, since the glide planes would then all be parallel to the stress axis, and the c axes lie at an angle of 64° to the glide planes. There is little resemblance between predicted and observed fabrics for a Q section in tension. (*See* Part III, Pl. 1H.)

Figure 13 shows the development of a strong maximum at the center of the diagram for a Q section 8.2 per cent in compression. Increasing the compression to 44.9 per cent results in a

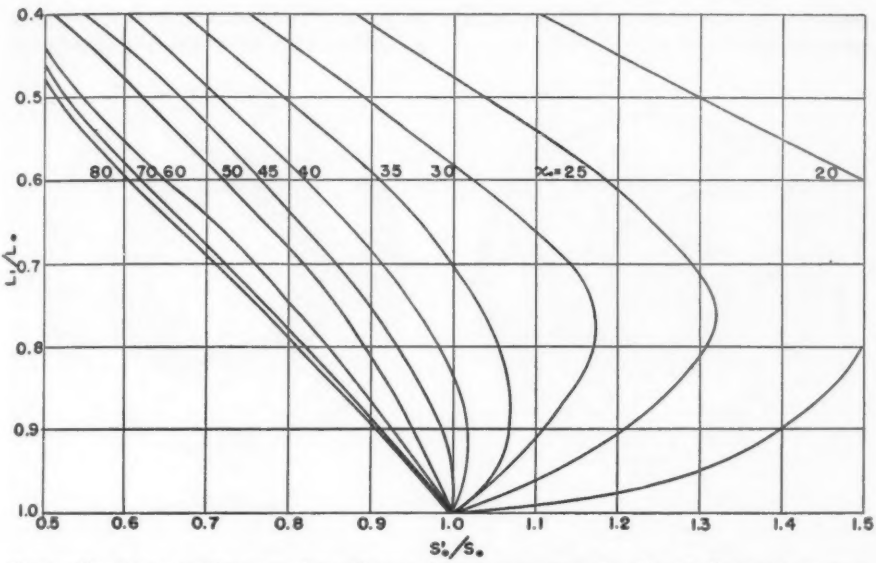

FIGURE 12.—RATIO OF RESOLVED SHEAR-STRESS COEFFICIENT AFTER SLIP-PLANE ROTATION TO THAT BEFORE DEFORMATION, S_0'/S_0
As a function of χ_0 and L_1/L_0 for compression.

stronger maximum and causes the peripheral region to be cleared of *c* axes. We do not expect twinning to be important in this orientation, and translation can well account for most of the fabric change actually observed (Part III, Pl. 1E).

On an *R* section for an elongation of 7.4 per cent, the analysis predicts the sharpening of peripheral maxima and a small shift of the centrally situated *c* axes toward the periphery of the diagram (Fig. 14). When the extension is increased to 34.2 per cent, these effects become more pronounced, but are nevertheless small compared to those observed to occur at only 20 per cent extension (Part III, Pl. 1D).

Figure 14 shows a slight broadening of the peripheral concentration of *c* axes for an *R* section 7.8 per cent in compression. Increasing the compression to 35.5 per cent results in a shift of peripheral maxima toward the center about 40 degrees. These changes too are small compared with those observed (Part III, Pl. 1A).

Fabrics Predicted on the Hypothesis of Mechanical Twinning on $\{02\bar{2}1\}$

Neither mechanical twinning nor translation gliding has been observed to occur in calcite on any but the $\{01\bar{1}2\}$ plane. However, mechanical twinning on $\{02\bar{2}1\}$ is observed in dolomite (Fairbairn and Hawkes, 1941), and both Knopf (1949) and Turner and Ch'ih (Part III) have observed a minor development of $\{02\bar{2}1\}$ lamellae in deformed Yule marble. Accordingly, the effect on the fabric of mechanical twinning on $\{02\bar{2}1\}$ was investigated. The geometry of such twinning is shown in Figure 15. The shearing motion is in the opposite direction from that on $\{01\bar{1}2\}$, but the angle of shear is very nearly the same. Moreover, the angle through which the *c* axis shifts is to a good approximation the supplement of that angle for twinning on $\{01\bar{1}2\}$. Consequently, the series of predicted fabrics of Plate 1 represents the expected changes as a result of twinning on $\{02\bar{2}1\}$ if the fields of tension and compression be reversed. That is, we expect a central concentration of *c* axes to result from tension, and a peripheral one from compression.[2] Such fabric changes are just the opposite of the observed trends, so that the

[2] These opposing characteristics have been used qualitatively by Fairbairn and Hawkes (1941) in their interpretation of a mixed dolomite-calcite fabric from the Plymouth-Rochester area, Vermont.

possibility of important twinning on $\{02\bar{2}1\}$ seems remote.

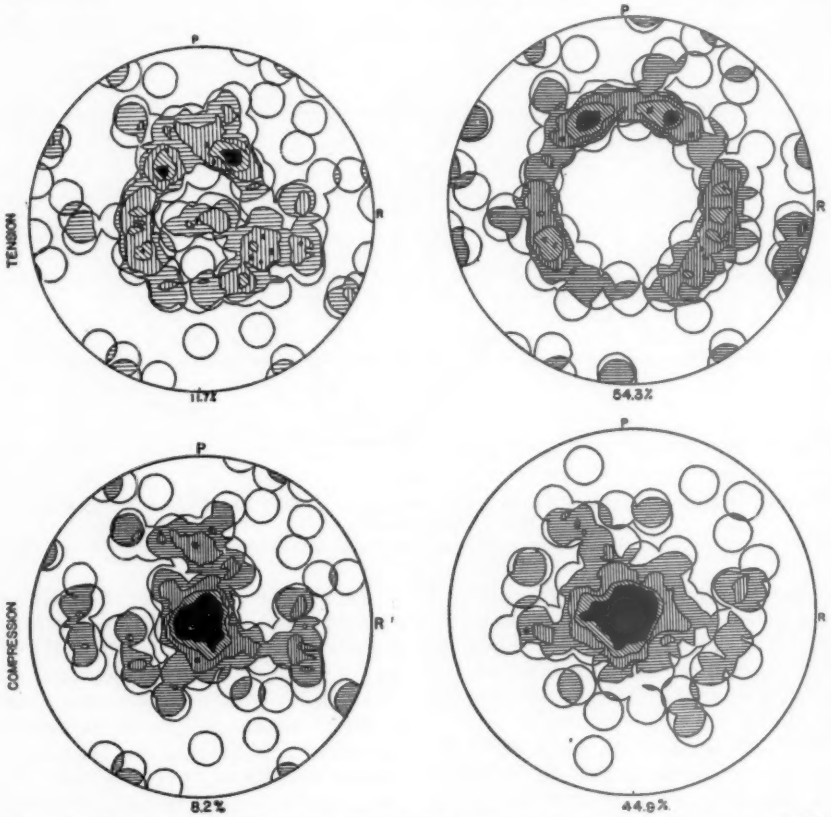

FIGURE 13.—PREDICTED FABRIC CHANGES AS A RESULT OF TRANSLATION ALONE ON $\{0112\bar{}\}$
Assuming heterogeneous deformation. 136 c axes in a Q section of a Q cylinder. Strain accompanying changes is recorded below each diagram. Contour interval: 0.7, 1.5, 3, 5, 7 per cent.

Deformation resulting from gliding on other planes was not investigated analytically in view of the lack of microscopic evidence for such deformation.

PREDICTED FABRICS BASED ON THE ASSUMPTION OF HOMOGENEOUS DEFORMATION

As measurements of fabrics by Turner and Ch'ih progressed, it became apparent that the initial reasoning which led to exploring heterogeneous deformation rested on insecure grounds. Balsley's gross fabric change for Q 20 per cent in extension was shown to be in error (Part III). All fabrics of specimens deformed 10 per cent or less showed surprisingly little change. A principal characteristic of the heterogeneous hypothesis—its ability to yield large fabric changes for small deformations by twinning alone—became less attractive.

When it was found (Part I) that the homogeneous hypothesis was more satisfactory in correlating the stress-strain relations as a function of orientation, the emphasis of the analytical study was shifted to application of that hypothesis. Under this hypothesis all the grains of the aggregate share in the deformation regardless of the resolved shear stress on them.

Each individual deforms relatively little; whereas under the heterogeneous hypothesis those grains with a high resolved shear stress were most affected, and their deformation was relatively large. The homogeneous hypothesis yields small fabric changes for small deformations of the marble, instead of the large changes previously predicted.

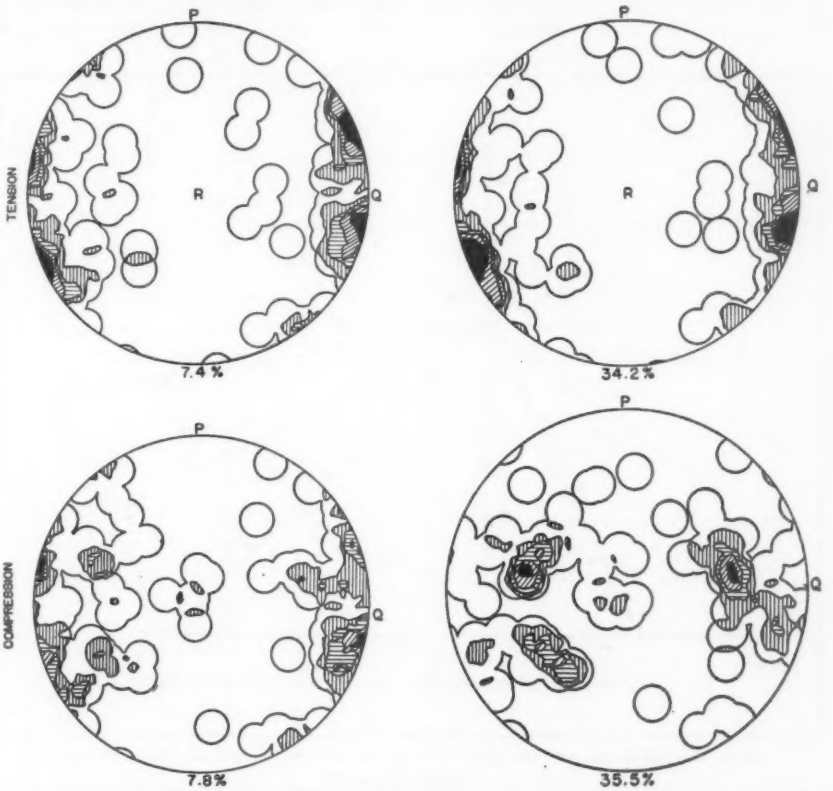

FIGURE 14.—PREDICTED FABRIC CHANGES AS A RESULT OF TRANSLATION ALONE ON $\{01\bar{1}2\}$
Assuming heterogeneous deformation. 100 c axes in an R section of an R cylinder. Strain accompanying changes is recorded below each diagram. Contour interval: 1, 3, 5, 7, 9 per cent.

In deriving fabrics based on the assumption of homogeneous deformation, further assumptions were made, as follows:

(1) The law of maximum resolved shear stress holds; that is, within each grain predominant gliding occurs on the plane with the highest resolved shear stress.
(2) The resistance to glide in the translation sense is 1.7 times as great as that in the twinning sense (Part I).
(3) Both twinning and translation occur on $\{01\bar{1}2\}$ in the same direction, but in opposite senses.
(4) Every grain that can twin at all does so, unless in the grain there is another $\{01\bar{1}2\}$ plane (not favorably oriented for twinning) with a resolved shear-stress coefficient at least 1.7 times greater than that on the twin plane, in which case translation occurs in preference to twinning.
(5) If the deformation of the aggregate is greater than that which can result from twinning in an individual grain, the dif-

ference is made up by translation of the completely twinned individual (after complete twinning, translation is in the opposite sense from twinning).

is very nearly a linear function of resolved shear-stress coefficient, so that grains with a low resolved shear-stress coefficient are the first to twin completely. It is these grains

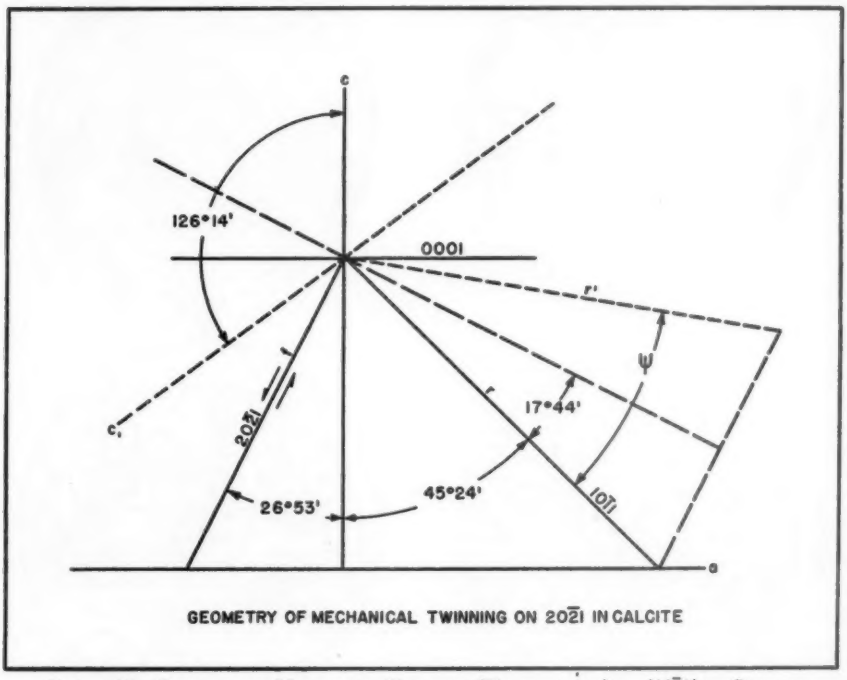

FIGURE 15.—GEOMETRY OF MECHANICAL TWINNING (HYPOTHETICAL) ON $\{02\bar{2}1\}$ IN CALCITE
Compare Figure 4.[3]

(6) If the deformation of the aggregate is less than that resulting from twinning, then an individual is only partly twinned.
(7) If a grain cannot twin at all, it translates so that its deformation is just equal to that of the aggregate as a whole.
(8) In computing strains, only that due to twinning or translation on the predominant plane (1 above) is considered. This is clearly not rigorously true for homogeneous deformation, but should give a fair approximation.

In Figure 16, strain resulting from twinning is plotted as a function of the resolved shear-stress coefficient for all the grains that can twin in six stress orientations: *R*, *Q*, and *d* in tension and in compression. In tension, the strain which are oriented within the marble fabric in such a way that twinning results in a very small apparent change of fabric. In compression, however, twinning strain is not a linear function of the resolved shear-stress coefficient, so that many grains with a comparatively high resolved shear-stress coefficient can twin completely in the early stages of deformation. There should be significant fabric changes even for small deformations in compression, particularly in *R* cylinders.

Translational shifts in the position of the *c* axes are statistically negligible for deformations below 10 per cent and are small for deformations below 20 per cent; so that the effects of translation are neglected in deriving predicted fabrics for deformations up to 20

[3] The $\{02\bar{2}1\}$ plane is incorrectly labelled $20\bar{2}1$ in the illustration.

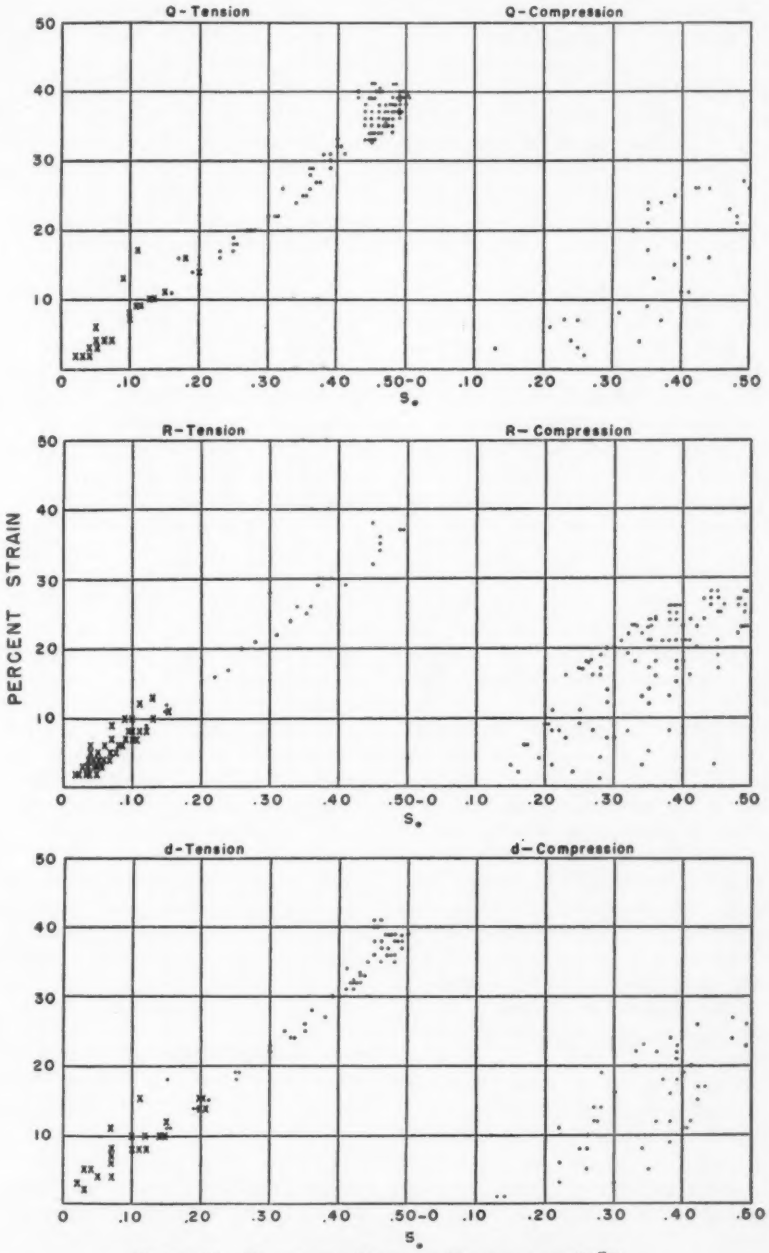

FIGURE 16.—STRAIN, FOR COMPLETE TWINNING ON $\{01\bar{1}2\}$

As a function of resolved shear-stress coefficient for Q, R, and d cylinders in tension and compression. Dots represent grains oriented favorably for twinning. Crosses represent grains with a favorably oriented plane, but which have another $\{01\bar{1}2\}$ plane with a high enough resolved shear stress in the opposite sense, so that the grain deforms by translating in preference to twinning.

per cent in tension where the average shift for all orientations is about 7°, and up to 15 per cent in compression where the average shift is 10°.

Since some grains cannot be completely twinned for deformations of less than 41 per cent in tension and 29 per cent in compression, we adopt a convention for plotting *c* axes as follows:

(1) If a grain is two-thirds or more twinned, the twinned position only is plotted.
(2) If a grain is twinned more than half, but less than two-thirds, both the twinned and untwinned positions are plotted.
(3) If a grain is less than half twinned, only the untwinned position is plotted.

Predicted fabrics for deformations up to 15 per cent in compression and 20 per cent in extension are shown in Plate 2. Thirty per cent compression and 40 per cent extension would yield fabrics similar to the final ones in each series of Plate 1, except that the effects of translation will no longer be negligible. Twinning is complete at these deformations, and further deformation will change the fabric only by the comparatively smaller effects of translation.

Turner and Ch'ih's comparable observed fabrics (Part III, Pl. 1, Fig. 4B) agree with these predicted fabrics as well as can be expected in view of the statistical fluctuations from one fabric measurement to another, and the oversimplified assumptions on which the predicted fabrics were based. In comparing Plate 2 with the *c* axis diagrams of Part III, it must be borne in mind that all the observed fabrics are plotted on an *R* projection, except Figure 4B, while the *Q* series in Plate 2 is plotted on a *Q* projection. Detailed comparison of the predicted and observed fabrics may be summarized as follows:

(1) In the range of deformations covered experimentally, the predicted fabrics show the greatest fabric change in *Q*–20 per cent extension—and *P*–10 per cent compression. The two corresponding observed fabrics also show the greatest change. Furthermore, the observed fabrics are closely similar in pattern to the predicted ones. (*Compare* Part III, Pl. 1A, 4B.) The only important difference between these observed and predicted fabrics is that the amount of twinning observed is somewhat less than that predicted. This is not surprising, since a necessary step in construction of the predicted fabrics was the assumption that all the deformation of each grain was due to gliding on the $\{01\bar{1}2\}$ plane for which the resolved shear stress was highest. This simplification patently overestimates the amount of twinning for a given deformation since under the homogeneous hypothesis gliding on all $\{01\bar{1}2\}$ planes and some others ($\{02\bar{2}1\}$?) must contribute to the deformation in general. Within the limits of accuracy of the prediction on this basis, it is believed that the predictions for these two cases of maximum fabric change are completely consistent with the observed fabrics.

(2) The predicted fabrics show that for all other cases studied the change in fabric is small. The degree of fabric change observed is similar to that predicted in each case, except that the observed fabric of an *R* cylinder elongated 20 per cent (Part III, Pl. 1D) has a central area completely cleared of *c* axes, implying nearly complete twinning of all centrally situated grains; whereas our predicted fabric for the same deformation (Pl. 2) shows several untwinned *c* axes still remaining in the central region of the diagram.

(3) Knopf's fabric for *P*–30 per cent compression (Fig. 1D)—is consistent with expectations under the homogeneous hypothesis.

This agreement between predicted and observed fabrics demonstrates that the behavior of Yule marble, deformed under the conditions described, approximates more closely Taylor's hypothesis of homogeneous deformation than the hypothesis of heterogeneous deformation.

Conclusion

An analytical procedure has been described which permits the prediction of changes resulting in a known fabric from a given amount of deformation under various assumptions as to the mechanism of deformation. Comparison of such predicted fabrics with Turner and Ch'ih's (Part III) observed fabrics repudiates the hypothesis of heterogeneous deformation and substantiates Taylor's homogeneous deformation hypothesis in the case of Yule marble

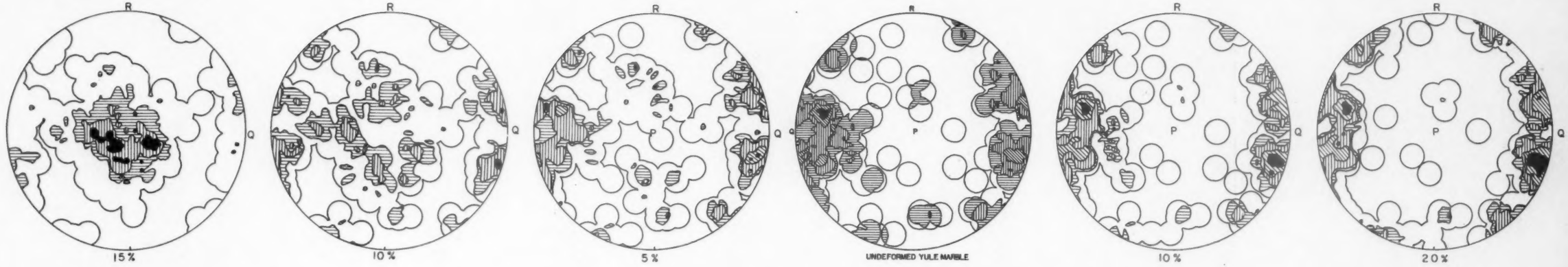

PREDICTED FABRICS AS A RESULT OF MECHANICAL TWINNING ON 0112

Assuming homogeneous deformation. Strain accompanying changes is recorded below each diagram. For undeformed fabrics (after F. J. Turner): 136 *c* axes, contour interval: 0.7, 1.5, 3,5,7 per cent. For *P* sections of *P* cylinders (upper row, tension to the right, compression to the left of the undeformed fabric): 140 to 178 *c* axes, contour interval approximately: 0.7, 2,3,5,7 per cent (15 per cent compression: 0.6, 2.2, 3.9, 5.6 per cent). For *Q* sections of *Q* cylinders (lower row): 136 to 206 *c* axes, contour interval approximately 0.7, 2,3,5,7.

def
10,
A
effi
for
tat
use
tha
wit
cul
als
Ill
str
tw
me
Ill
mu
Gl
as
re
ni
pr
th
th
pl
sh
si
T
fu
0.
in
w
u
3
sh
fa
fa
th
a
b
w
m
st
cl

deformed dry, at room temperature, and under 10,000 atmospheres confining pressure.

Analytical data for resolved shear-stress coefficient on each grain of a measured, undeformed fabric for the six different stress orientations experimentally tested have also been used by Griggs and Miller (Part I) to show that the stress-strain relations are in accord with Taylor's hypothesis. This method of calculating resolved shear-stress coefficient has also been applied by Turner and Ch'ih (Part III) to test the validity of the resolved shear-stress law. It follows from the agreement between predicted and observed fabrics and from measurements of the amount of twinning (Part III) that gliding on $\{01\bar{1}2\}$ in the twin sense must be wholly or predominantly twinning. Glide in the opposite sense must be translation as discovered by Bell. Under this hypothetical reconstruction, the relative importance of twinning, as compared to translation, varies in a predictable manner according to the nature of the original fabric, the stress orientation, and the amount of strain. Twinning would be complete in all favorably oriented grains after a shear strain of 0.7 (40 per cent uniaxial extension or 30 per cent uniaxial compression). Translation would be the main mechanism of further deformation. Shear strains of less than 0.3 would not produce important fabric changes in any calcite marble. Shear strains up to 1.0 would not produce gross fabric changes in an unfavorably oriented marble (*cf.* *Q* compression 30 per cent). In favorably oriented marble a shear strain of 0.5 to 0.7 would produce gross fabric changes. Further strain would change the fabric comparatively little per unit strain. All the above statements about fabric changes apply only to calcite *c* axes fabrics and are based on the fact that twinning—as contrasted with translation—causes much greater movement of the axes for small strains. For shear strains much in excess of 1.0, large fabric changes would result from translation.

This co-operative study has shown how difficult and complex is the problem of determining uniquely the mechanism of deformation under laboratory conditions where the number of variables is limited to two—the amount and the orientation of deformation. It further demonstrates the need for caution in attempts to reconstruct deformation mechanisms from field evidence afforded by deformed rocks.

References Cited

Balsley, J. R. (1941) *Deformation of marble under tension at high pressure*, Am. Geophys. Union, Trs., pt. II, p. 519–525.

Baumhauer, H. (1879) *Über künstliche Kalkspath-Zwillinge nach 1/2 R*, Zeitschr. Krist., vol. 3, p. 588.

Boas, W., and Hargreaves, M. E. (1948) *On the inhomogeniety of plastic deformation in crystals of an aggregate*, Roy. Soc. London, Pr., ser. A, vol. 193, p. 89–97.

Cox, H. L., and Sopwith, D. G. (1937) *The effect of orientation on stresses in single crystals and of random orientation on strength of polycrystalline aggregates*, Phys. Soc. London, Pr., vol. 49, p. 134–151.

Fairbairn, H. W., and Hawkes, H. E. (1941) *Dolomite orientation in deformed rocks*, Am. Jour. Sci., vol. 239, p. 617.

Gough, H. J. (1933) *Crystalline structure in relation to failure in metals—especially by fatigue*, Edgar Marburg Lecture, Am. Soc. Testing Materials.

Griggs, D. T. (1936) *Deformation of rocks under high confining pressures*, Jour. Geol., vol. 44, p. 541–577.

Knopf, E. B. (1949) *Fabric changes in Yule marble after deformation in compression*, Am. Jour. Sci., vol. 247, p. 433–461, 537–569.

Schmid, E., and Boas, W. (1935) *Kristallplastizität*, Berlin.

Taylor, G. I. (1938) *Plastic strain in metals*, Inst. Metals, Jour., vol. 62, p. 307–324.

Turner, F. J. (1949) *Preferred orientation of calcite in Yule marble*, Am. Jour. Sci., vol. 247, p. 593–621.

Exploration and Production Research, Shell Oil Co., Houston, Texas; Institute of Geophysics, University of California, Los Angeles 24, Calif.

Manuscript Received by the Secretary of the Society, January 17, 1951

Assisted by ONR Grant

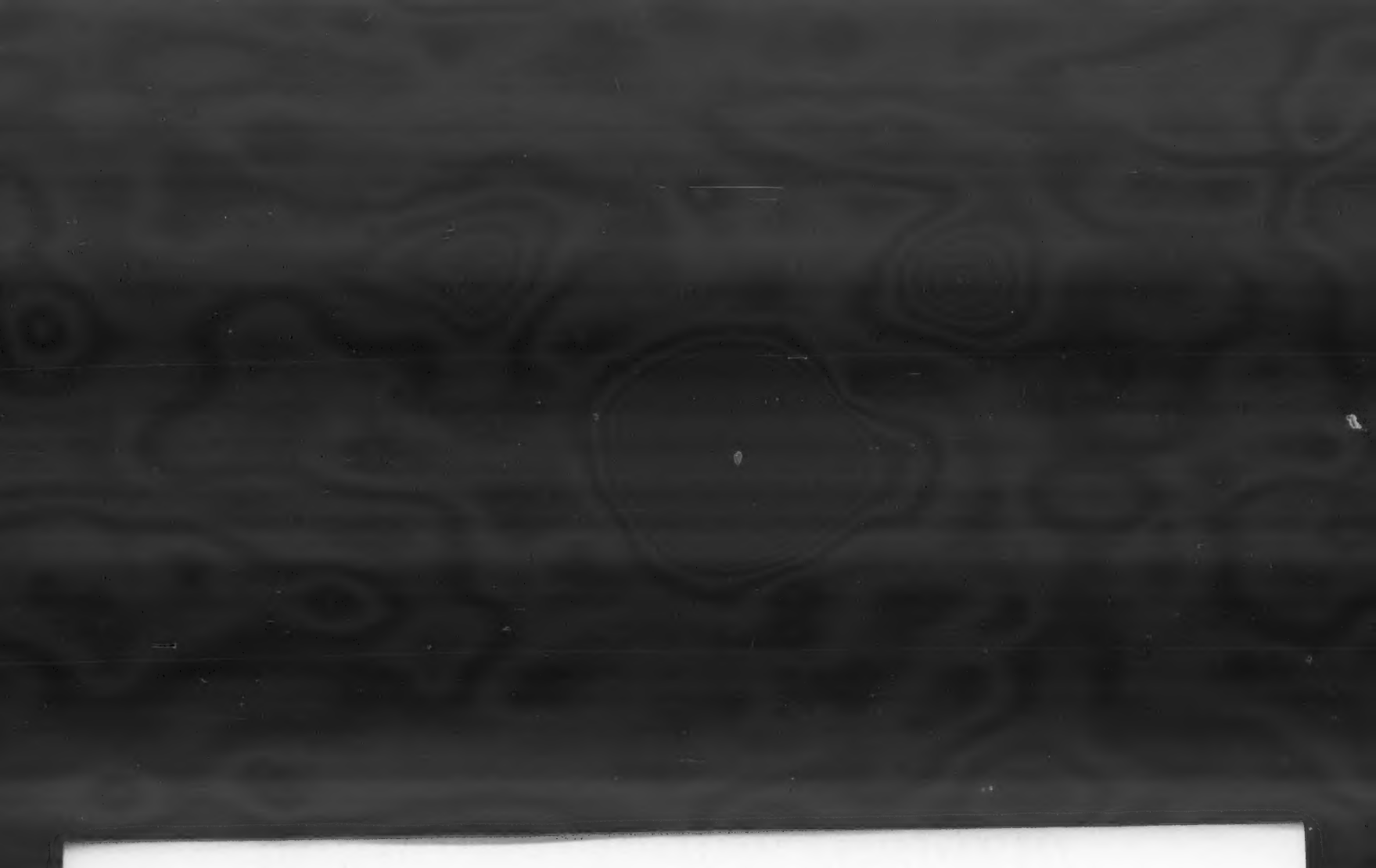

EXPLANATION OF DIAGRAM

T (R) cylinders

- A: Specimen 173, shortened 10.5%. Solid circles=28 measured *c* axes. Open circles=*c* axes as calculated for twinned lattice within best-developed $\{01\bar{1}2\}$ lamellae of each grain. The single cross is a measured *c* axis in what is thought to be an almost completely twinned grain.
- B: Specimen 158, elongated 5%.
- C: Specimen 159, elongated 7.2%.
- D: Specimen 167, elongated 20.5%.

1 (Q) cylinders

- E: Specimen 235, shortened 10.5%.
- F: Specimen 231, elongated 6.8%.
- G: Specimen 232, elongated 9.2%.
- H: Specimen 234, elongated 12%.

d cylinders

- I: Specimen 282, shortened 11%.
- J: Specimen 283, shortened 6%.
- K: Specimen 281, elongated 7%.
- L: Specimen 280, elongated 12.2%.

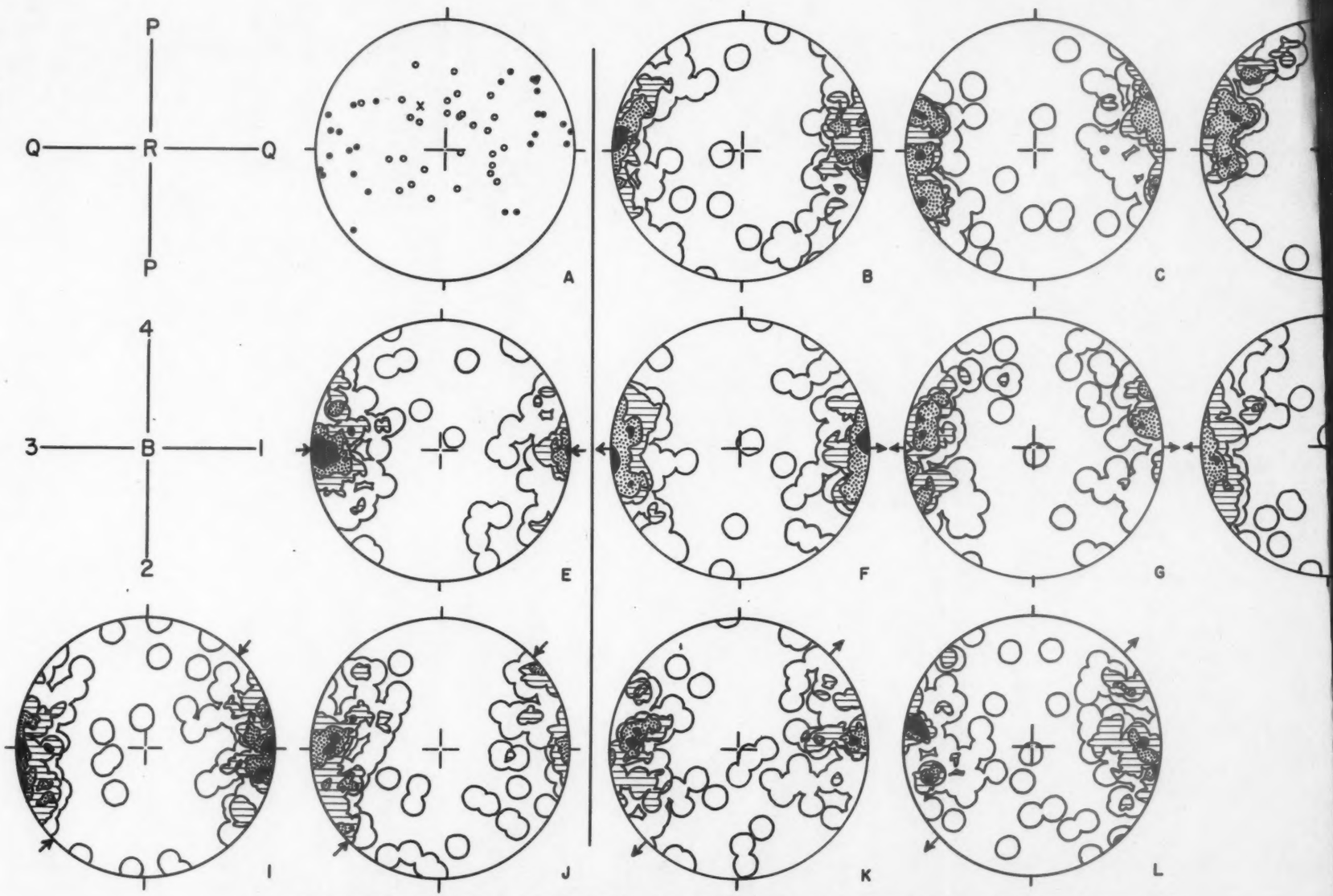

ORIENTATION DIAGRAMS FOR *c* AXES OF CALCITE (100 GRAINS IN EACH, UNLESS OTHERWISE INDICATED) IN DEFORMED YULE MARBLE

Contours 1, 3, 5, 10% per 1% area. All diagrams similarly oriented, as indicated in top, left section. Plane of projection = R; trace of foliation. Plane (Q) is parallel to N-S diameters.

EXPLANATION OF DIAGRAM

T (R) cylinders

- A: Specimen 173, shortened 10.5%. Solid circles=28 measured *c* axes. Open circles=*c* axes as calculated for twinned lattice within best-developed $\{01\bar{1}2\}$ lamellae of each grain. The single cross is a measured *c* axis in what is thought to be an almost completely twinned grain.
- B: Specimen 158, elongated 5%.
- C: Specimen 159, elongated 7.2%.
- D: Specimen 167, elongated 20.5%.

1 *(Q)* cylinders

- E: Specimen 235, shortened 10.5%.
- F: Specimen 231, elongated 6.8%.
- G: Specimen 232, elongated 9.2%.
- H: Specimen 234, elongated 12%.

d cylinders

- I: Specimen 282, shortened 11%.
- J: Specimen 283, shortened 6%.
- K: Specimen 281, elongated 7%.
- L: Specimen 280, elongated 12.2%.

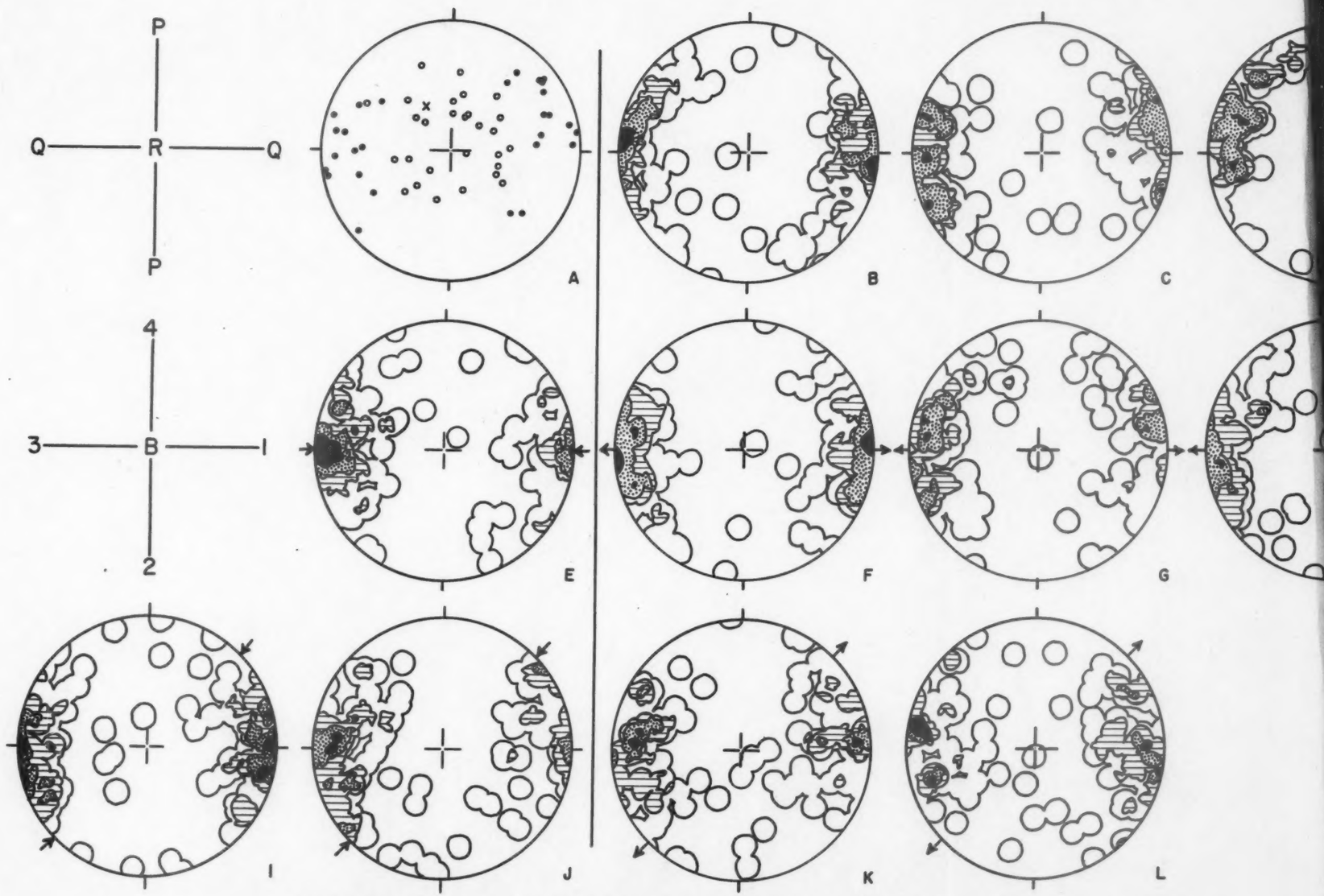

ORIENTATION DIAGRAMS FOR *c* AXES OF CALCITE (100 GRAINS IN EACH, UNLESS OTHERWISE INDICATED) IN DEFORMED YULE MARBLE

Contours 1, 3, 5, 10% per 1% area. All diagrams similarly oriented, as indicated in top, left section. Plane of projection = R; trace of foliation. Plane (Q) is parallel to N-S diameters.

COMPRESSION

EXTENSION

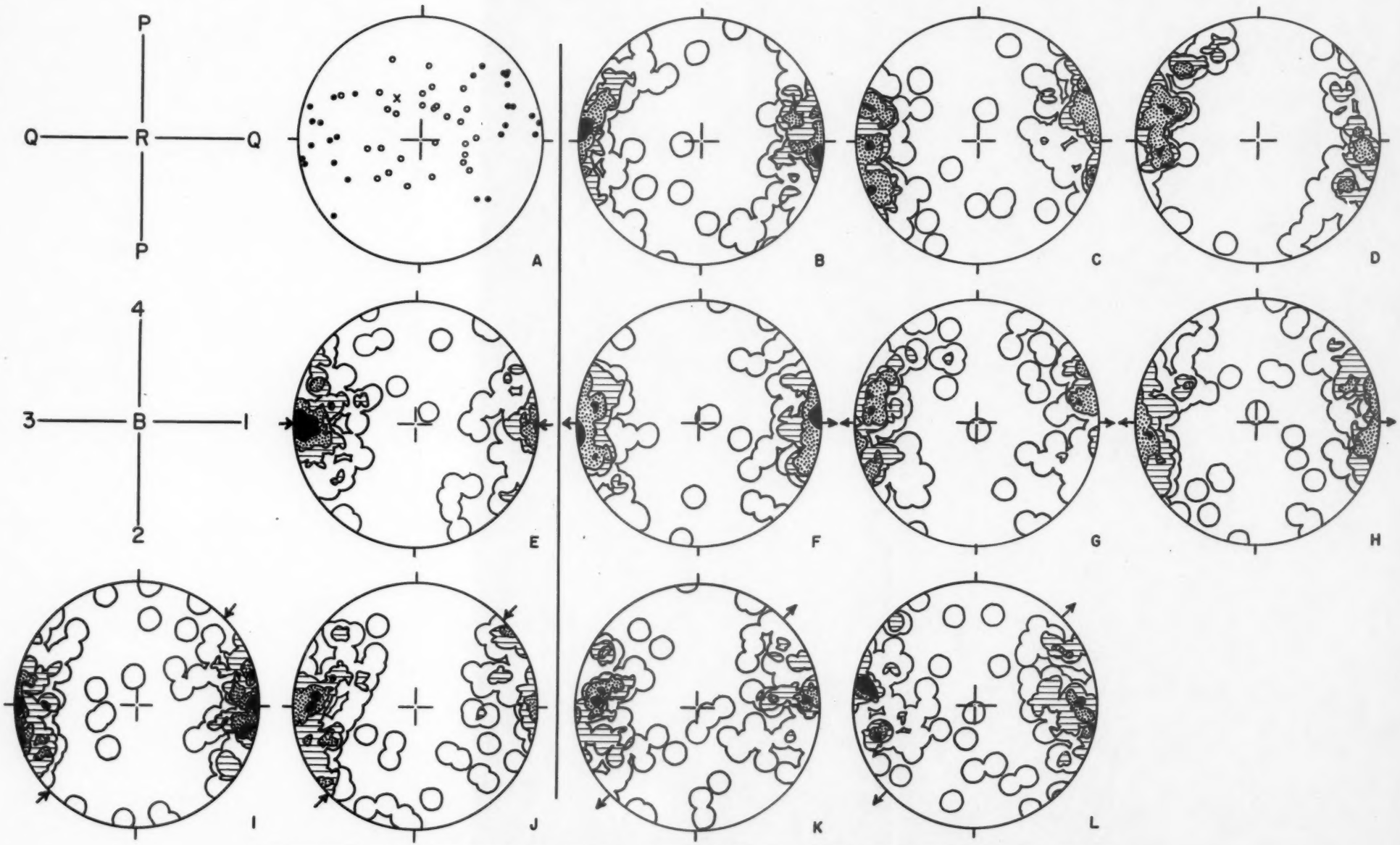

ORIENTATION DIAGRAMS FOR *c* AXES OF CALCITE (100 GRAINS IN EACH, UNLESS OTHERWISE INDICATED) IN DEFORMED YULE MARBLE

Contours 1, 3, 5, 10% per 1% area. All diagrams similarly oriented, as indicated in top, left section. Plane of projection = R; trace of foliation. Plane (Q) is parallel to N-S diameters.

BULLETIN OF THE GEOLOGICAL SOCIETY OF AMERICA
VOL. 62, PP. 887-906 9 FIGS., 2 PLS. AUGUST 1951

DEFORMATION OF YULE MARBLE: PART III—OBSERVED FABRIC CHANGES DUE TO DEFORMATION AT 10,000 ATMOSPHERES CONFINING PRESSURE, ROOM TEMPERATURE, DRY

BY FRANCIS J. TURNER AND C. S. CH'IH

ABSTRACT

Preferred orientation patterns are recorded for c axis, a_1, a_2, a_3 axes, $\{01\bar{1}2\}$ lamellae, edges $[e{:}e']$ between prominent $\{01\bar{1}2\}$ lamellae, and $\{02\bar{2}1\}$ lamellae in Yule marble deformed to various degrees in the laboratory at 10,000 atmospheres confining pressure, room temperature, dry. The changes of fabric observed correspond strikingly with those predicted by Handin and Griggs (Part II) on their hypothesis of homogeneous deformation.

Visible $\{01\bar{1}2\}$ lamellae can be correlated with gliding (probably twinning) in the direction and sense appropriate for twinning. Translation on $\{01\bar{1}2\}$ in the opposite sense, though effective in many cases, leaves no microscopically visible trace. Gliding in the twinning sense on $\{02\bar{2}1\}$ could account for development of relatively insignificant lamellae.

Comments are added regarding interpretation of petrofabric data in general, in the light of the results here recorded.

CONTENTS

	Page
Scope of investigation	888
Acknowledgments	888
Procedure	888
Orientation of specimens, sections and diagrams	888
Microscopic measurements on slightly and moderately deformed material	889
Microscopic measurements on strongly deformed material	890
Results of petrofabric analysis	891
Preferred orientation of optic axis c	891
Variation in undeformed specimens	891
Orientation data for deformed specimens	891
Preferred orientation of axes a_1, a_2, a_3	895
Development and preferred orientation of $\{01\bar{1}2\}$ lamellae	895
General statement	895
Lamellae orientation diagrams	896
Spacing index data	896
Preferred orientation of edges $[e{:}e']$	901
Development and preferred orientation of $\{02\bar{2}1\}$ lamellae	901
Interpretation of fabric data	901
Mechanism of deformation	901
Application to interpretation of petrofabric data in general	904
References cited	905

ILLUSTRATIONS

Figure	Page
1. Yule marble, block No. 3	889
2. Equal-area projection of calcite lattice	889
3. Orientation diagrams for c axes of calcite in undeformed Yule marble	892
4. Orientation diagrams for c axes of calcite in Q cylinder (125) of Yule marble	894
5. Orientation diagrams for observed conspicuous $\{01\bar{1}2\}$ lamellae in calcite of deformed Yule marble	897
6. Relation between spacing index and resolved shear-stress coefficient for $\{01\bar{1}2\}$ lamellae	899
7. Relation between spacing index and resolved shear-stress coefficient for $\{01\bar{1}2\}$ lamellae	900
8. Orientation diagrams for edges $[e{:}e']$ in calcite of deformed Yule marble	902
9. Orientation of poles of all observed $\{02\bar{2}1\}$ lamellae in three d cylinders of deformed Yule marble	903

Plate	Facing page
1. Orientation diagrams for c axes of calcite in deformed Yule marble	887
2. Orientation diagrams for a_1, a_2, a_3 axes of calcite in undeformed and in deformed Yule marble	906

TABLES

	Page
1. Additional data on distribution of optic axes in Plate 1	893
2. Mean spacing index for $\{01\bar{1}2\}$ lamellae	898

Scope of Investigation

The state of preferred orientation of calcite in the marble from Yule Creek, Colorado, has been recorded and discussed in several papers (Knopf, 1949; Turner, 1949; Turner and Ch'ih, 1950). Knopf's paper also summarizes observed changes in preferred orientation of *c* axes and prominent {01$\bar{1}$2} lamellae in the same marble after compression under high confining pressure in the course of earlier laboratory experiments by Griggs (1936) and Balsley (1941).

The present paper records fabric data for a number of test cylinders of Yule marble deformed dry under confining pressure of 10,000 atmospheres at room temperature by Griggs and Miller during 1949 and 1950, as described in Part I. The observed fabrics are compared with those predicted in Part II by Handin and Griggs on a theoretical basis, and certain tentative conclusions on the mechanism of deformation under the specified physical conditions are drawn. The bearing of our observations on interpretation of fabric diagrams for naturally deformed rocks is also discussed briefly.

Acknowledgments

This paper would not be complete without acknowledgment of our debt to Mrs. E. B. Knopf whose persistent encouragement of research on evolution of marble fabrics under controlled laboratory conditions led us to start our current investigations in this field. She has not only supplied us with marble suitable for experimental deformation but has constantly discussed our results and advised us on procedure as the work progressed. We also wish to thank Mr. John de Grosse, who has made the many excellent thin sections necessary for fabric analysis, Mrs. I. Borg for permission to use two of her fabric analyses, and Mr. J. P. Wagner for drafting many of the diagrams. The research has been sponsored and generously financed by the Institute of Geophysics of the University of California.

Procedure

Orientation of Specimens, Sections and Diagrams

In the earlier studies of Yule marble by Knopf, Griggs, and others, deformation was described with reference to three mutually perpendicular planes designated *P*, *Q*, and *R* respectively and defined as follows:

P = vertical surface, striking E.-W., and oriented perpendicular to original foliation;

Q = vertical surface, striking N.-S., and oriented parallel to foliation;

R = horizontal surface, oriented perpendicular to foliation.

The field orientation of the marble block which supplied the material for the present series of experiments is not certainly known. The *Q* plane (= foliation) is easily identified; but the fabric properties of planes *P* and *R* are so nearly identical that distinction between them must be regarded as tentative.

In order to allow unique definition of any plane or direction in the marble block, opposite parallel faces must be distinguished from each other. Accordingly the six boundary faces have been designated 1, 2, 3, 4, *T*, *B*, (Fig. 1) such that:

1 and 3 are parallel to *Q* (foliation);

2 and 4 are probably parallel to *P*;

T and B are probably parallel to *R*.

Fortunately the close similarity of *P* and *R* as regards the initial preferred orientation pattern renders positive identification of these two planes immaterial for the purposes of this study. What is important is that both are normal to the foliation *Q*. Distinction between opposite faces of a parallel pair—e.g., between *T* and *B*—is necessary only in order to compare fabric patterns determined from different microsections.

Material for fabric analysis was selected from cylinders of three different orientations, deformed to various degrees both by compression and by extension:

(1) Cylinders with long axis normal to the foliation, *Q* (= planes 1 and 3); designated *Q* cylinders.

(2) Cylinders with long axis normal to faces *T* and *B* and parallel to the foliation; designated *R* cylinders.

(3) Cylinders with long axes normal to face *d* and inclined at 45° to the foliation; designated *d* cylinders.

Most fabric data were determined in sections cut parallel to faces *T* and *B* (*R* sections); and all fabric diagrams, except those of Figure 4,

represent data either measured in, or rotated into, this plane, and plotted (on the lower hemisphere of projection) looking in the direction T to B.

Microscopic Measurements on Slightly and Moderately Deformed Material

The procedure of petrofabric analysis previously applied to undeformed Yule marble (Turner, 1949, p. 597–602) is satisfactory too in the case of cylinders elongated or shortened by less than about 10 to 15 per cent. Optic axes c, visible lamellae $\{01\bar{1}2\}$, cleavages $\{10\bar{1}1\}$, and rarely parallel fractures or lamellae of other orientations are measured as accurately as possible in 100 grains of clacite, preferably in a section of standard orientation (parallel to face T). From such measurements the orientation of any desired crystallographic direction or plane may be determined—e.g., the c axis, the three crystal axes a_1, a_2, and a_3, the three planes of the form $\{01\bar{1}2\}$, the edge $[e{:}e']$ between observed paired lamellae of the form $\{01\bar{1}2\}$, and so on. The more obvious and consistent features of fabric, and changes in fabric, are brought out by orientation diagrams respectively depicting (1) the c axes, (2) the crystal axes a_1, a_2, and a_3, and (3) edges $[e{:}e']$ between well-developed $\{01\bar{1}2\}$ lamellae observed in any grain. Plots of observed $\{01\bar{1}2\}$ lamellae were made in a number of cases but it is doubtful if some diagrams of this type have recognizable significance.

Nearly all observed lamellae or partings may be positively identified from interfacial angles and zonal relations (*cf.* Fig. 2), as parallel to faces of the forms $\{01\bar{1}2\}$ or $\{10\bar{1}1\}$. In specimens that have been elongated or shortened by more than about 8 per cent a few grains may also show linear partings parallel to $\{02\bar{2}1\}$, easily recognized by their cozonal relation to $\{01\bar{1}2\}$ and $\{0001\}$ and by their interfacial angle of 63° to the c axis. The orientation of these $\{02\bar{2}1\}$ "lamellae" has been plotted in several cases and has been found to be regularly related to the direction of applied stress.

The closeness of spacing of $\{01\bar{1}2\}$ lamellae of different orientations varies greatly in any given specimen. To record such variation a "spacing index"—the number of lamellae per millimeter as measured normal to the plane of the lamellae in question—is determined for each set of visible lamellae in every measured grain of selected sections. (*Cf.* Turner and Ch'ih, 1950.) Such indices are not individually precise, for they are subject to error arising from the personal factor in counting lamellae. Nevertheless, especially where all such measurements are made by one observer, the wide range of recorded values for lamellae in any

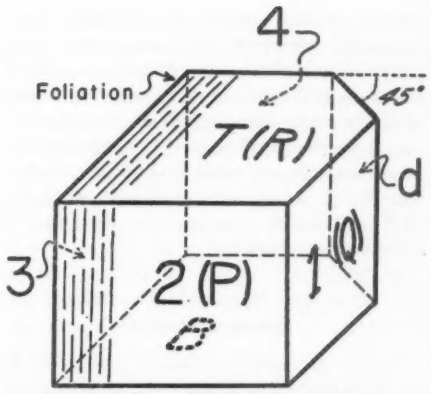

Figure 1.—Yule Marble, Block No. 3

Showing probable orientation of faces 1, 2, 3, 4, T, B, in relation to P, Q, and R planes of other blocks.

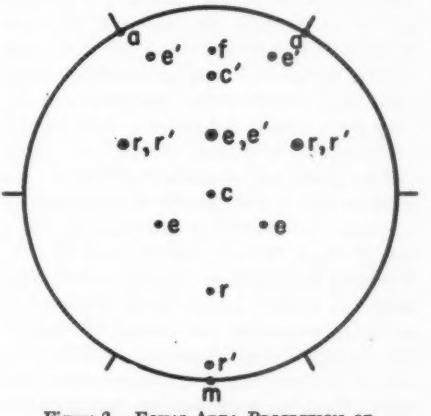

Figure 2.—Equal-Area Projection of Calcite Lattice

Showing poles (solid black) of planes $\{0001\} = c$, $\{10\bar{1}1\} = r$, $\{01\bar{1}2\} = e$, in a calcite lattice. Open circles lettered c', r', e' represent poles of corresponding planes in a second lattice twinned on a common $\{01\bar{1}2\}$ plane $= e$, e', with respect to the first lattice. Adjacent poles of the first lattice—namely, appropriate faces of $\{10\bar{1}0\} = m$, $\{11\bar{2}0\} = a$ and $\{02\bar{2}1\} = f$—are also shown.

section greatly exceeds the probable error. Statistical treatment of spacing-index data yields reproducible results that seem to be of considerable significance in correlating degree of deformation of grains with stress vectors. In specimens elongated by more than 12 to 15 per cent (depending on orientation of the cylinder) lamellae are so profusely developed in all grains that it becomes impossible to determine a reliable spacing index.

Microscopic Measurements on Strongly Deformed Material

Highly deformed specimens (elongated or shortened by 12 to 30 per cent) in most cases present special difficulties in fabric analysis. Lamellae of at least one set per grain are so closely spaced that, even allowing for the minute thickness of each lamella, it is possible that a considerable proportion of the total material in a given grain may be in twinned relation (or possibly in a generally disordered state) with respect to the space lattice of the same grain prior to deformation. Whether this interpretation is correct or not, the highly lamellar grains are internally disturbed to such a degree that it is impossible in most cases to determine the position of the *c* axis by direct optical means. To meet this situation all well-developed lamellae and cleavage traces, commonly six or eight sets in all, are measured as accurately as possible and plotted on a projection. From interfacial angles and zonal relations between the plotted poles a unique position for the *c* axis of the grain may be determined in some instances; and this can be checked to some extent by observing the extinction behavior of the grain. More commonly, especially where there are five or more measured crystal planes, interpretation of the crystallographic data is attended by some ambiguity. Here a limited number of lamellae and partings (*e.g.*, those labeled *r* and *e* in Fig. 2) may be recognized as belonging to $\{10\bar{1}1\}$ or $\{01\bar{1}2\}$ in a crystal lattice, whose *c* axis is thereby located. The ambiguity just mentioned concerns other, typically somewhat less perfect, partings, the poles of which are situated at 70° to 90° from *c* (*e.g.*, *e'*, *r'*, Fig. 2). From their interfacial angles Knopf (1949, p. 547, 554) has tentatively identified comparably situated partings in calcite grains of compressed Yule marble as belonging either to the prism *m* $\{10\bar{1}0\}$ or to the steep rhombohedron *f* $\{02\bar{2}1\}$. The corresponding interfacial angles (*c* to *f* = 63°; *c* to *m* = 90°) are compatible with this interpretation, especially as in such densely lamellar grains interfacial angles can be determined only to within ± 5°. Moreover definite $\{02\bar{2}1\}$ lamellae have been observed in somewhat less deformed material.

For calcite grains in the deformed marbles studied by us, we prefer for most lamellae an alternative identification based on the assumption that in a highly deformed grain $\{01\bar{1}2\}$ lamellae of at least one set become so densely spaced that a considerable proportion of the original crystal lattice is now reversed by twinning on this particular $\{01\bar{1}2\}$ plane. Two sets of visible partings (*e'* in Fig. 2) making angles of about 69° with the *c* axis of the original lattice are identified as secondary $\{01\bar{1}2\}$ lamellae forming within the newly developed twinned lattice, the *c* axis of which is located as *c'* in Figure 2. While the angle between poles *e'* and the *c* axis of the original lattice is not significantly different from the interfacial angle *c* to *f* (= 63°,) the zonal relations of *e'* to *c*, *e* and *r* of Figure 2 preclude identification of *e'* as *f* $\{02\bar{2}1\}$ of the original lattice. Two planes of the form $\{10\bar{1}1\}$ (*r* = *r'* in Fig. 2) coincide in the original and the twinned lattices; the pole of the third $\{10\bar{1}1\}$ plane of the twinned lattice is situated at 82° to the *c* axis of the original lattice and is thus indistinguishable from a plane *m* $\{10\bar{1}0\}$ in the latter.

In accordance with the above interpretation, most lamellae and partings observed in the highly deformed specimens are identified as belonging to $\{10\bar{1}1\}$ or to $\{01\bar{1}2\}$, either within the original crystal lattice or within a newly developing crystal structure formed by twinning on a plane $\{01\bar{1}2\}$ of the original lattice. This allows identification of two, and in some cases even three, *c* axes in a single highly deformed grain. In specimens that have been elongated or shortened by 20 per cent or less one such *c* axis is situated within the general area of *c* axis concentration as determined for the undeformed specimen. This is assumed to be the axis of the original crystal lattice. In most cases *e* and *r* lamellae of this lattice are

more conspicuously and continuously developed than lamellae assigned to the secondary lattice.

Results of Petrofabric Analysis

Preferred Orientation of Optic Axis c

Variation in undeformed specimens.—The fabric of Yule marble is remarkably homogeneous, in that the same general pattern of preferred orientation of optic axes, *c*, emerges from all the dozen or so fabric analyses made to date by several investigators working on differently oriented sections cut from four blocks of the marble. Invariably the *c* axes show a marked tendency to lie at high angles (55° to 90°) to the foliation. Nevertheless minor variations in pattern are obvious. Thus Knopf (1949, p. 450) finds that, within this general area of axes concentration, a maximum persistently appears at 65° to the foliation in diagrams prepared for *P*, *Q*, and *R* sections cut from block No. 1; but location of equally strong adjacent maxima varies from one diagram to another. (*Cf.* Knopf, 1949, p. 451, 453, Figs. 7, 8.) Turner (1949, p. 602, 603, Figs. 5–8), working on *P*, *Q*, and *R* sections of block No. 2, records considerable variation in detailed distribution of maxima but finds that in all cases over 50 per cent of the measured axes are inclined at between 55° and 90° to the foliation.

What concerns us now is the degree of variation that may arise in comparing plots of 100 axes measured in individual sections of similar orientation (*R*) cut from different parts of the single block (No. 3) employed in the present series of experiments. Accordingly six diagrams, each representing 100 axes measured at random in one section, have been prepared from five sections of four undeformed cylinders (Fig. 3).

All these show a general concentration of axes around the pole of the foliation. Within the concentration sector are maxima which vary somewhat in their precise location, but in all cases show the same degree of concentration of axes (5 to 10 per cent per 1 per cent area of the diagrams). Variation in detail among diagrams drawn for similarly oriented sections of different specimens (Fig. 3: B, C, E) is apparently of the same order as the differences between diagrams prepared from differently oriented sections of one specimen (Fig. 3: E, F) or between diagrams depicting measurements made by different observers working on the same section (Fig. 3: C, D). It would seem that most of the variation displayed by Figure 3 is due to variation in sampling rather than to inhomogeneity of fabric. Greater uniformity could be obtained by measuring 300 or 400 axes in each section; but in view of the large number of fabric analyses necessary in this type of research this was not considered practicable. Measurement of 100 grains brings out the essential features of the fabric and certainly is sufficient to allow detection of any considerable change in fabric during deformation.

Counts of plotted axes in all six cases represented in Figure 3 yields additional consistent details of preferred orientation as follows:

(1) The percentage of axes inclined at between 55° and 90° to the foliation (*e.g.*, within the broken arcs of Fig. 3, A) ranges from 56 to 62 in five cases and is 74 in the sixth. The mean value is 61 per cent.

(2) The percentage of axes lying within an angular distance of 45° from the center of the diagram ranges between 7 and 11. The mean value is 9.

(3) The percentage of *c* axes inclined at angles of 30° or less to the foliation ranges between 9 and 19. The mean value is 14.

Orientation data for deformed specimens.—The extent to which the pattern of preferred orientation of the optic axis changes during deformation is illustrated in Plate 1. From these diagrams and corresponding fabric analyses we have made these inferences:

(1) The orientation pattern is little changed in specimens elongated or shortened to only a moderate degree—of the order of 10–12 per cent or less. Axes remain concentrated at high angles to the foliation, and within this sector of concentration individual maxima—of the same general intensity as those of Figure 3—vary as regards position much as in diagrams representing the undeformed fabric.

(2) Further statistical data for the fabrics of these same moderately and slightly deformed specimens are given in Table 1. It is possible,

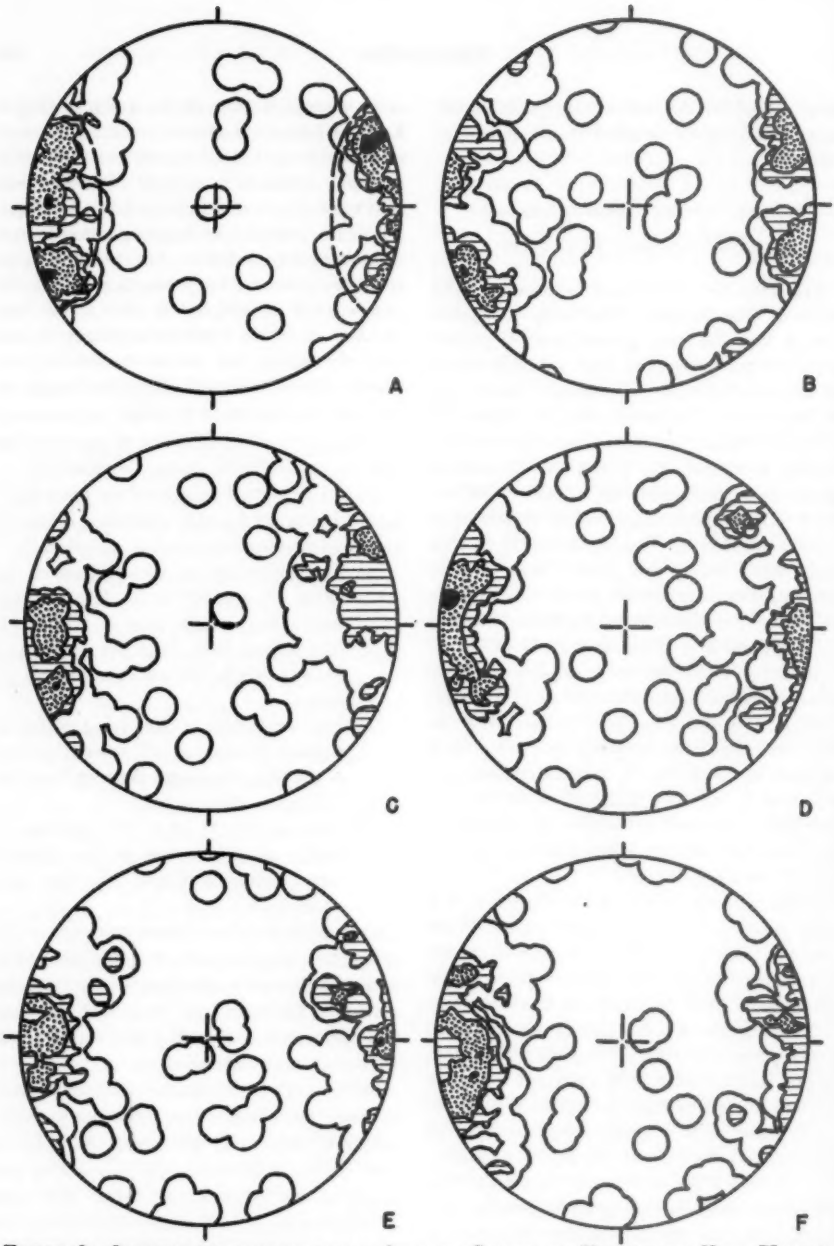

FIGURE 3.—ORIENTATION DIAGRAMS FOR *c* AXES OF CALCITE IN UNDEFORMED YULE MARBLE

100 grains per diagram. Contours 1, 3, 5, 10%, per 1% area. All diagrams are similarly oriented with the pole of the *B* surface of the block at the center (lower hemisphere). Foliation is normal to plane of diagrams, parallel to N–S diameters.

A: Specimen 172 (measurements by I. Borg).
B: Specimen 158 (measurements by C. S. Ch'ih).
C: Specimen 154 (measurements by C. S. Ch'ih).
D: Specimen 154 (measurements by I. Borg).
E: Specimen 231 (measurements by C. S. Ch'ih on *T* section).
F: Specimen 231 (measurements by C. S. Ch'ih on 1 Section; poles rotated into plane T).

but by no means certain, that these figures may be significant in the following respects:

(a) Extension (of *R* cylinders) parallel to the foliation is accompanied by slight reduction in the number of axes initially inclined at low angles (0°–35°) to the axis of stress. The possibility that this apparent change is real is enhanced by the fact that 20-per cent elongation of an *R* cylinder is accompanied by elimination of all optic axes within 45° of the axis of applied stress. (*Cf.* Pl. 1, D.)

(b) Extension (of *Q* cylinders) perpendicular to the foliation (Pl. 1, F–H) has no obvious effect on preferred orientation of optic axes.

(c) Extension (of *d* cylinders) at 45° to the foliation gives rise to slight but significant disturbance of the initial pattern: the number of axes in the original sector of concentration falls off, and axes begin to become more concentrated in a zone normal to the applied stress.

(d) Compression (of *R* cylinders) parallel to the foliation does not obviously change the *c*-axis diagram. However, in each grain one set of $\{01\bar{1}2\}$ lamellae is very profusely developed; and, if the *c* axes within such lamellae (assuming twinning) are determined graphically, they are found to be conspicuously concentrated between 15° and 50° to the axis of applied stress (Pl. 1, A). Two of the 30 grains on which Plate 1A is based have ambiguous orientation, though in each case the optic axis must lie somewhere in the central portion of the diagram. The relative positions of measured lamellae and cleavages in each are such that the grain may be interpreted alternatively as a relatively slightly deformed crystal whose optic axis retains its initial orientation, or as an almost completely twinned grain whose optic axis is now in twinned position with regard to the peripherally situated axis of the original grain. In one case, represented by the cross in Plate 1A, the latter alternative seems more likely. In the other, there are several possible positions for the

TABLE 1.—ADDITIONAL DATA ON DISTRIBUTION OF OPTIC AXES IN PLATE 1

Mean values for fabrics of undeformed marble (Fig. 3) are given in italics.

Applied stress	Specimen number	Percentage strain	Percentages of optic axes oriented as follows:			
			55°–90° to foliation plane	0°–30° to foliation plane	0°–35° to axis of applied stress	55°–90° to axis of applied stress
Extension parallel to foliation (*R* cylinders)	158	5	67 (*61*)	10 (*14*)	1 (*5*)	
	154	6.4	63	12	4	
	159	7.2	68	8	2	
Extension perpendicular to foliation (*Q* cylinders)	231	6.8	77 (*61*)	7 (*14*)		
	232	9.2	63	13		
	234	12	65	15		
Extension at 45° to foliation (*d* cylinders	281	7	50 (*61*)	13 (*14*)	25 (*29*)	41 (*36*)
	280	12.2	52	12	18	46
Compression parallel to foliation (*R* cylinders)	173	10.5	53 (*61*)	7 (*14*)	7 (*29*)	
Compression perpendicular to foliation (*Q* cylinders)	235	10.5	65 (*61*)	9 (*14*)		
Compression at 45° to foliation (*d* cylinders)	283	6	50 (*61*)	13 (*14*)	28 (*29*)	37 (*36*)
	282	11	69	12	28	42

optic axis, and this has therefore been omitted from the diagram. All other grains are uniquely oriented.

(e) Compression (of *Q* cylinders) normal to the foliation possibly results in reduction in the number of axes inclined at high angles to the axis of shortening.

(f) Compression (of *d* cylinders) at 45° to the foliation fails to give consistent results. In one of the two cases investigated (No. 283; Pl. 1, J) the percentage of axes in the initial zone of concentration is reduced by the same factor as was recorded for specimens of similar orientation deformed by extension. [*Cf.* (c).]

(3) Where strain is of the order of 20 per cent or more, the orientation pattern of optic axes is much more strongly affected; but the densely lamellar condition of many grains in some cases renders it impossible to determine optic axes for every grain and hence to present orientation data in the form of orientation diagrams comparable with those of Plate 1.

(a) The most obvious feature of the diagram (Pl. 1, D) for an *R* cylinder (167) elongated 20.5 per cent parallel to the foliation is complete absence of optic axes from the central zone within 45° of the axis of elongation. [*Cf.* 2(a).]

(b) With regard to extension at right angles to the foliation, reference must be made to the orientation data published by Balsley (1941) from measurements on a *Q* cylinder (125) elongated 22 per cent.

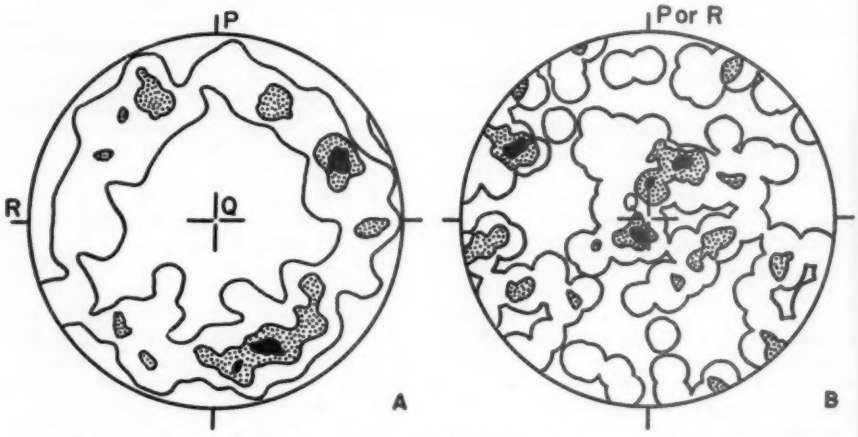

FIGURE 4.—ORIENTATION DIAGRAMS FOR *c* AXES OF CALCITE IN *Q* CYLINDER (125) OF YULE MARBLE
Projections on *Q* plane. Contours 1, 3, 5% per 1% area.
A: 200 axes determined by J. Balsley (1941).
B: 113 axes determined by C. S. Ch'ih in 50 grains selected from Balsley's group of 200 grains.

He has kindly made available to us his measurements, thin sections, and photomicrographs on which he had recorded the positions of all grains measured by him. His orientation diagram is shown as Figure 4A. We have remeasured 50 of these same grains, using the time-consuming technique outlined in the section on measurement of strongly deformed material. Our results (Fig. 4, B) differ strikingly from those of Balsley. We find that in every grain we can locate at least two *c* axes in mutually twinned position. In some grains there are three such axes, a condition implying densely spaced lamellar twinning on two of the three $\{01\bar{1}2\}$ planes of the original crystal lattice. Figure 4B is based on 113 *c* axes located in 50 grains. It shows a central area of concentration presumably occupied by the original *c* axes, and a peripheral girdle within which fall *c* axes of what are interpreted as lattices newly developed by twinning on $\{01\bar{1}2\}$ of the

original lattice. From the very dense spacing of corresponding observed $\{01\bar{1}2\}$ lamellae, it might be assumed further that twinning has proceeded to between one-third and two-thirds of the way to completion. Balsley's diagram (Fig. 4, A) shows an annular area of concentration which almost coincides with the area of minimal concentration of our diagram.

(c) A single *d* cylinder (No. 284) elongated 21 per cent at 45° to the foliation proved unsatisfactory for microscopic investigation. The *c* axes, accurately measured in 10 grains chosen at random, show a similar distribution to that discussed under 2(c) for less-deformed materials of similar orientation. Five axes lie within the original concentration sector (55° to 90° to foliation); none fall within 35° of the axis of applied stress; seven are inclined steeply (55° to 90°) to the axis of stress.

(d) No further work has been done on specimens strongly deformed by compression parallel to the foliation. Knopf's measurements on the fabric of an *R* cylinder shortened by 20 per cent (Knopf, 1949, p. 546–548, Figs. 34–36) indicate a tendency for *c* axes to become reoriented at angles of 45° or less to the axis of compression. This is consistent with the mode of development of $\{01\bar{1}2\}$ lamellae in less-deformed specimens of similar orientation in the present series, as described later.

(e) In a *Q* cylinder (No. 246) shortened 20 per cent by compression perpendicular to the foliation, the grains can still be measured accurately. Out of 10 axes selected at random, 8 occur in the original area of concentration (55° to 90° to foliation). The few axes originally inclined to the axis of shortening at high angles apparently have become reoriented. [*Cf.* 2(e).]

(f) In a section of a *d* cylinder (No. 285) shortened 20 per cent at 45° to the foliation, lamellae were so densely spaced as to preclude measurement of optic axes in many grains.

Preferred Orientation of Axes a_1, a_2, a_3

The positions of the three crystal axes a_1, a_2, and a_3 were determined in 100 grains in each of 16 representative sections of undeformed and deformed material. Corresponding orientation diagrams are reproduced on Plate 2. Presence of three cozonal maxima separated from one another by angular intervals of 60° suggests some degree of preferred orientation a_1, a_2, and a_3 in some cases.

The pattern for undeformed marble (Pl. 2: A, F, L) is weak; it indicates a faint tendency for one of the three *a* axes to be aligned at right angles to the *R* face (corresponding to the subcentral maxima of the figures).

Extension (of *R* cylinders) parallel to the foliation consistently results in a new and somewhat stronger orientation pattern with one *a* axis normal to the axis of elongation and the other two symmetrically inclined to it at 30° (Pl. 2: B–D). All diagrams, including one not reproduced here, show this feature; and it is most strongly developed in the diagram (Pl. 2, D) constructed for the most strongly deformed cylinder (No. 167; elongation 20.5%). Moreover, a comparable pattern never appears in diagrams drawn for cylinders deformed in any other manner.

There is little regularity in the other diagrams. The original weak pattern may become either slightly intensified (*e.g.*, Pl. 2, G) or partially disrupted, (Pl. 2, N). It is perhaps significant that, where stress is applied at 45° to the foliation, the pattern persists in the case of compression (Pl. 2: J, K) but begins to disintegrate under the influence of extension (Pl. 2: M, N).

The reality of the on-the-whole weak patterns of Plate 2 is confirmed by laboratory experience which shows that adjacent grains in groups of four or five frequently show a more decided tendency toward parallel orientation than characterizes the fabric as a whole.

Development and Preferred Orientation of $\{01\bar{1}2\}$ Lamellae

General statement.—The pattern of any orientation diagram for $\{01\bar{1}2\}$ lamellae in calcite depends on several factors:

(1) The pattern of preferred orientation of the calcite space lattice.
(2) The relative degrees of development of the three sets of $\{01\bar{1}2\}$ lamellae in every grain, as determined by relative positions of each lamella, the *c* axis, and the direction of applied stress.
(3) Relative accessibility of lamellae to observation in a given section viewed in a particular direction.
(4) The extent to which other partings such as $\{10\bar{1}1\}$ cleavage and $\{02\bar{2}1\}$ lamellae have been confused with $\{01\bar{1}2\}$ lamellae.

Since the state of preferred orientation of the space lattice is more satisfactorily demonstrated by orientation diagrams for *c* axis and for a_1, a_2, and a_3 axes, the only reasonable object of recording orientation diagrams for $\{01\bar{1}2\}$ lamellae must be to evaluate factor (2) above. In our opinion where, as in the present case, directions of applied stress are known, a satisfactory assessment of this factor is possible by other means which will be discussed later.

Lamellae orientation diagrams.—Six conventional orientation diagrams for $\{01\bar{1}2\}$ lamellae are here reproduced (Fig. 5). These represent typical cases of moderate (6%–12%) shortening and elongation parallel normal and at 45° to the original foliation. Measurements were made in every case on sections of similar orientation (cut perpendicular to the foliation). This was such as to render almost every possible $\{01\bar{1}2\}$ plane of every grain accessible to direct measurement. Each recorded lamella was specifically identified as $\{01\bar{1}2\}$ by its angular relation to the *c* axis and its zonal relations to other lamellae and cleavages. The influence of the third and fourth factors mentioned above upon the lamellae diagrams thus is reduced to a minimum.

In the undeformed fabric the great majority of possible (not necessarily visible) $\{01\bar{1}2\}$ poles fall within about 45° of the pole of the foliation plane (*Q*). Since moderate deformation scarcely disturbs the original pattern of space-lattice orientation in Yule marble, preferred-orientation patterns for $\{01\bar{1}2\}$ lamellae observed in deformed specimens must also show maxima located within this same general zone—*i.e.*, near the right and left margins of diagrams in Figure 5.

Some of the differences between the recorded diagrams may be correlated with the extent to which weakly developed lamellae have been omitted from consideration. Thus the pattern of Figure 5E, based on 271 lamellae in 100 grains, is distinctly weaker than those of some other diagrams (Fig. 5, B; 187 lamellae) where attention was focused especially on a smaller percentage of lamellae characterized by high spacing index. Nevertheless there is at least one consistently recognizable feature that must have some deeper significance. In all diagrams, including others not reproduced here, maxima are displaced either away from the axis of extension or toward the axis of compression. Note, for example, how maxima are sharpened peripherally in Figures 5B and 5D, weakened and dispersed from the margin in Figures 5A and 5E, and rotated about the center in Figures 5C and 5F. This feature is consistent with the hypothesis that development of conspicuously visible $\{01\bar{1}2\}$ lamellae involves intracrystalline gliding (whether by twinning or translation) in the same direction and sense as is effective in artificially produced mechanical twinning on $\{01\bar{1}2\}$. The diagrams also conform to the common assumption of structural petrologists that the symmetry of an orientation diagram reflects the symmetry of deforming movements and stresses responsible for the orientation pattern.

Spacing index data.—In all moderately deformed specimens $\{01\bar{1}2\}$ lamellae are much

FIGURE 5.—ORIENTATION DIAGRAMS FOR OBSERVED CONSPICUOUS $\{01\bar{1}2\}$ LAMELLAE IN CALCITE OF DEFORMED YULE MARBLE

100 grains in each case, except A. Contours 0.5, 2.5, 4%, per 1% area. All diagrams similarly oriented, by projection on *R* plane; trace of foliation plane (= *Q*) is parallel to N-S diameters.
A: Specimen 173, *R*, shortened 10.5%; 28 sets of lamellae in 28 grains.
B: Specimen 235, *Q*, shortened 10.5%; 187 sets of lamellae.
C: Specimen 282, *d*, shortened 11%; 213 sets of lamellae.
D: Specimen 154, *R*, elongated 6.4%; 230 sets of lamellae.
E: Specimen 232, *Q*, elongated 9.2%; 271 sets of lamellae.
F: Specimen 280, *d*, elongated 12.2%; 225 sets of lamellae.

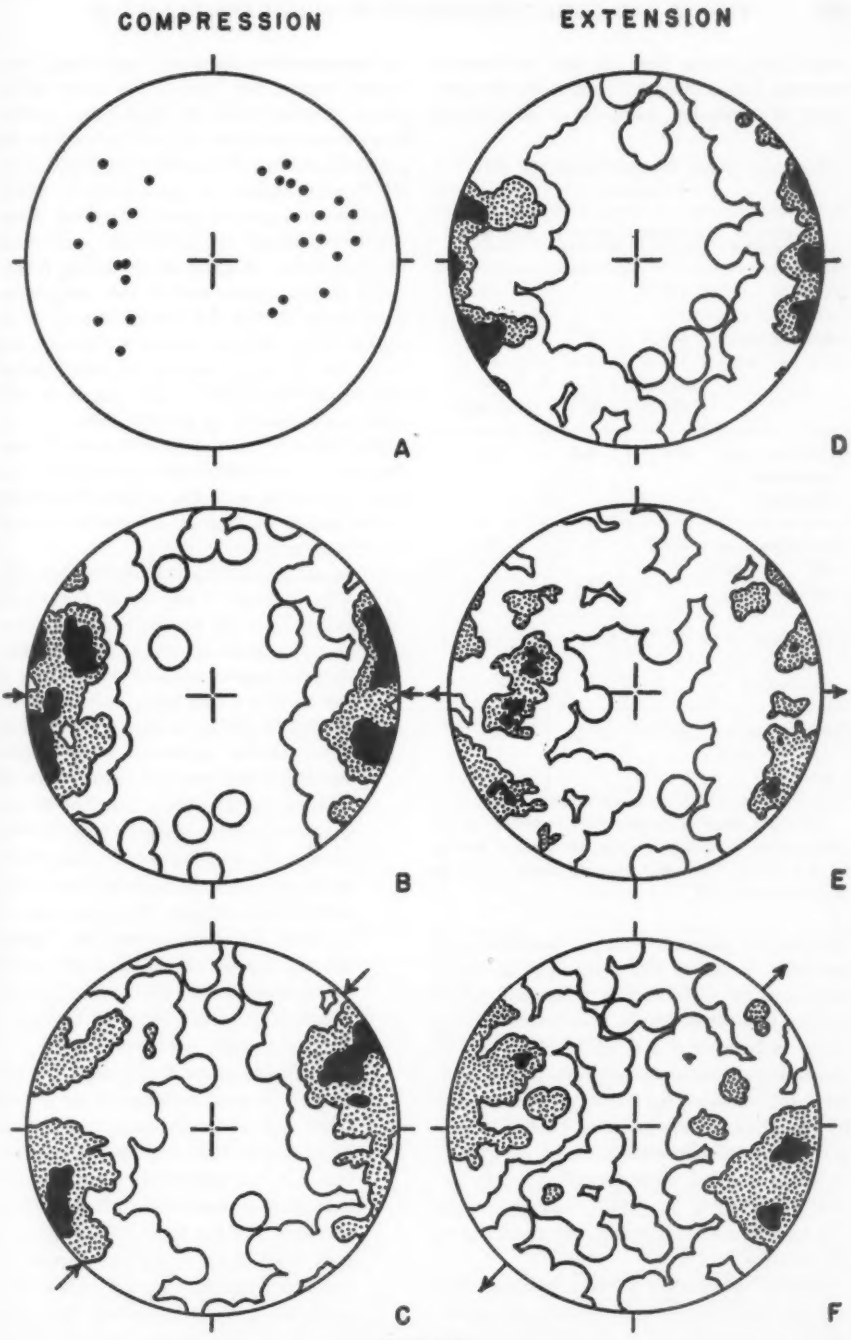

FIGURE 5

more conspicuous than in the undeformed material. This is due principally to the development of increasing numbers of lamellae as deformation proceeds—not to broadening of individual lamellae. The mean spacing index, calculated for all three sets of lamellae within a given number of grains, thus increases by a factor of between 5 and 10 for elongation or shortening of the order of 5 to 12 per cent. Some typical values (all based on measurements by one observer) are given in Table 2. For a given degree of deformation, the lowest spacing indices correspond to stress conditions unfavorable for twinning on $\{01\bar{1}2\}$—namely, extension parallel and compression perpendicular to the foliation.

TABLE 2.—MEAN SPACING INDEX FOR $\{01\bar{1}2\}$ LAMELLAE

Direction of applied stress	Specimen number	Percentage strain	Mean spacing index
No stress	158 *R*	0	9
Extension parallel to foliation	128 *R*	4	42
	154 *R*	6.4	71
	159 *R*	7.2	70
	167 *R*	20.5	Very high*
Extension perpendicular to foliation	231 *Q*	6.8	86
Extension at 45° to foliation	281 *d*	7	130
Compression perpendicular to foliation	235 *Q*	10.5	66
Compression at 45° to foliation	282 *d*	11	83

* At this stage of deformation, lamellae of at least one set in most grains are too densely spaced to be counted. The mean spacing index might be of the order of 200.

Possible relationship between spacing index and resolved shear stress in the direction appropriate for twin gliding on $\{01\bar{1}2\}$ was tested in six representative cases with surprisingly consistent results. For each of the three $\{01\bar{1}2\}$ planes of about 20 to 40 grains, the resolved shear-stress coefficient was determined by the graphical method of Handin and Griggs (Part II). Spacing indices of corresponding $\{01\bar{1}2\}$ lamellae were plotted against resolved shear-stress coefficient; a distinction was made between values of shear stress falling respectively in the tension and in the compression fields of the Handin and Griggs diagram. Some typical results are reproduced in Figures 6 and 7, in the left-hand sections of which points representing the three $\{01\bar{1}2\}$ planes of each grain are connected by straight lines.

The following characteristic features of these diagrams are so consistently reproducible that they are obvious in a plot of data determined on any sample of 20 grains selected at random in a given section:

(1) In extension of a *Q* cylinder (No. 231, Fig. 6) the great majority of the plotted points lie in the tension field. All corresponding lamellae are so oriented that they are subject to shear stress acting in the direction and sense appropriate to cause twin gliding. Figure 6 (231) brings out a marked correlation between spacing index and resolved shear-stress coefficient for the three lamellae of any grain: in each grain the lamellae tend to develop most profusely on the $\{01\bar{1}2\}$ plane for which the resolved shear-stress coefficient is highest. However, there is no such correlation when the highest spacing indices of all measured grains are compared, for the open circles in Figure 6 (231) are scattered through a broad essentially horizontal belt.

(2) In extension of an *R* cylinder (No. 154, Fig. 6) the great majority of the plotted points fall within the compression field, indicating that the corresponding $\{01\bar{1}2\}$ lamellae are unfavorably situated for twin gliding when the applied stress is tensional. For the three $\{01\bar{1}2\}$ planes of each grain there is obvious correlation between lamellae spacing index and proximity to the tension field. The spacing index is close to zero for those $\{01\bar{1}2\}$

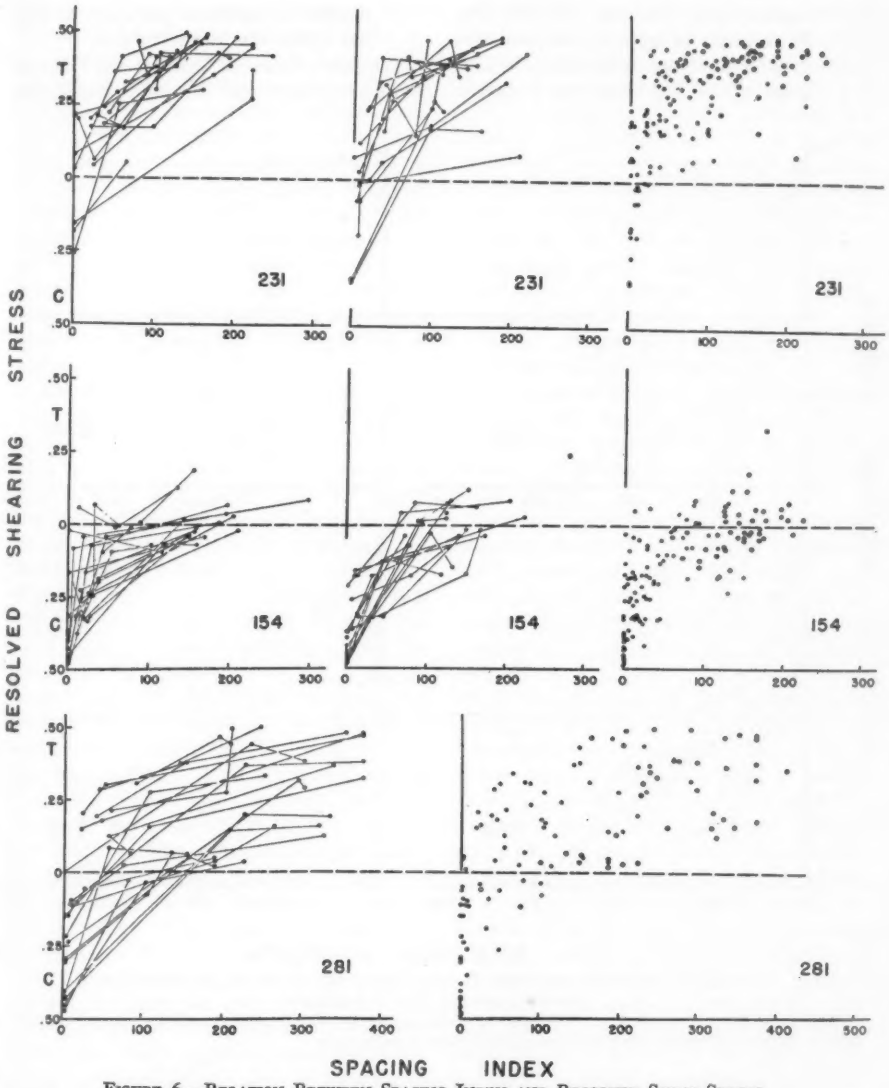

FIGURE 6.—RELATION BETWEEN SPACING INDEX AND RESOLVED SHEAR-STRESS COEFFICIENT FOR {01$\bar{1}$2} LAMELLAE

Specimens 231 (*Q*), 154 (*R*), and 281 (*d*), deformed by extension. In right-hand sections open circles represent the set of lamellae with maximum spacing index in each grain.

planes subject to the highest stress—but within the field of compression.

(3) In extension of a *d* cylinder (No. 281, Fig. 6) the same general relationships are apparent. Spacing indices near zero correlate with high shear stress in the compression field; and high spacing indices are characteristic of points falling within or very close to the tension field.

(4) Data for compression show comparable

characteristics (No. 235, No. 282, Fig. 7). As might be expected, comparison of data for the three $\{01\bar{1}2\}$ planes of each grain in No. 235 brings out a distinct resolved shear-stress coefficient is high but within the field of tension.

The data collected in Figures 6 and 7 demonstrate two points which bear on the mechanism

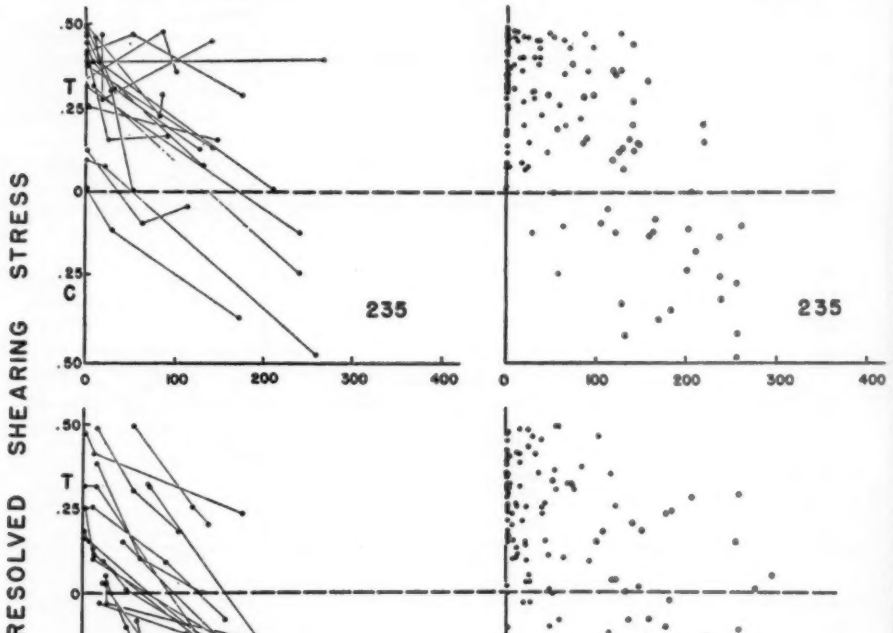

FIGURE 7.—RELATION BETWEEN SPACING INDEX AND RESOLVED SHEAR-STRESS COEFFICIENT FOR $\{01\bar{1}2\}$ LAMELLAE

Specimens 235 (*Q*) and 282 (*d*), deformed by compression. In the right-hand sections, open circles represent the set of lamellae with maximum spacing index in each grain.

correlation between spacing index and proximity to the compression field. In the case of specimen No. 282 more points fall within the compression field; and here the highest spacing index for a given grain tends to be that for which the resolved shear-stress coefficient, too, is high. In both figures zero spacing index is characteristic of planes for which the of deformation. (1) Development of visible lamellae can be correlated with shear stress acting in the same sense and direction as is known to cause twin gliding under ordinary pressures. (2) Broad correlation between resolved shear-stress coefficient and spacing index indicates that the stress pattern for any one grain is determined principally by the type and

direction of applied stress and is not greatly influenced by behavior of adjacent grains.

Preferred orientation of edges [e:e'].—As in the case of naturally deformed marbles (Turner, 1949, p. 608), a clear and reproducible orientation pattern is obvious in any plot of the edges [e:e'] between intersecting well-developed sets of {01$\bar{1}$2} lamellae. Some typical orientation diagrams are reproduced as Figure 8. The patterns of these are in no way influenced by the state of preferred orientation of [e:e'] prior to deformation, for any lamellae persisting from the original fabric would be too sparsely spaced to be included as "well-developed lamellae" in the deformed fabric.

Though there is an obvious relation between areas of concentration of edges [e:e'] and the nature and direction of applied stress, the state of preferred orientation of c crystal axes also influences the patterns of Figure 8. In any crystal, edges of this type are inclined at 76° to the c axis. Since in all the moderately deformed fabrics corresponding to diagrams of Figure 8 the c axes are concentrated within 30° of the pole of faces 1 and 3, it follows that [e:e'] edges must tend to lie within a broad belt (bounded by broken arcs in Fig. 8: C, E) extending on each side of the vertical diameter of the orientation diagram. Within this belt of possible concentration the positions of the [e:e'] maxima are related to the direction of applied stress. Where the stress is "tensional", the maxima lie as close as possible to the axis of stress; the result is a single maximum in Figure 8A and B, a cleft girdle pattern in Figure 8C, and an asymmetrically situated maximum in Figure 8D. Where the applied stress is compressional, [e:e'] maxima tend to develop nearly perpendicular to the stress axis, giving a simple girdle pattern in Figure 8E and an asymmetrical girdle in Figure 8F. These results are so consistent that they suggest a possible means for dynamic interpretation of some of the simpler patterns of preferred orientation in naturally deformed marbles.

Development and Preferred Orientation of {02$\bar{2}$1} Lamellae

In most of the moderately and highly deformed specimens, partings ("lamellae") parallel to {02$\bar{2}$1} appear in some grains. Typically only one of the three possible sets of {02$\bar{2}$1} planes is visible in any grain. Partings or lamellae of this type are insignificant compared with {01$\bar{1}$2} lamellae in the same specimens. For example, in specimen No. 282 (d cylinder, shortened 11 per cent) only 23 sets of {02$\bar{2}$1} lamellae were observed in 100 grains; individual spacing indices for most of these are between 10 and 40, with 65 as the maximum recorded value (mean spacing index for {01$\bar{1}$2} in the same grains is 83, with many individual values exceeding 200).

In any section too few lamellae have been measured to justify plotting a contoured orientation diagram. Figure 9 shows two scatter diagrams with contrasted orientation patterns for specimens deformed respectively in compression and in extension applied at 45° to the foliation plane.

Lamellar twinning on {02$\bar{2}$1}, generally interpreted as the result of gliding in a direction perpendicular to the edge between {02$\bar{2}$1} and {0001}, is well known in dolomite, though not in calcite (Fairbairn, 1949, p. 28). The {02$\bar{2}$1} lamellae now observed in calcite of deformed Yule marble we attribute to either twin or translation gliding in the direction and sense appropriate for twinning; for, although optically recognizable twin lamellae were not observed in any case, the influence of sense as well as direction upon development of visible {02$\bar{2}$1} lamellae is clearly brought out when spacing indices are plotted against resolved shear-stress coefficient, with due regard to opposite effects of tension and compression. For example, in the case of No. 282 deformed in compression, all plotted points lie well within the compression field, and corresponding values of resolved shear-stress coefficient invariably are high (0.3 to 0.5). Moreover, in any individual grain, visible lamellae correspond to that {02$\bar{2}$1} plane for which the resolved shear-stress coefficient is a maximum.

Interpretation of Fabric Data

Mechanism of Deformation

In Part I Griggs and Miller have discussed the bearing of their experimental work on Yule marble upon each of two hypotheses which

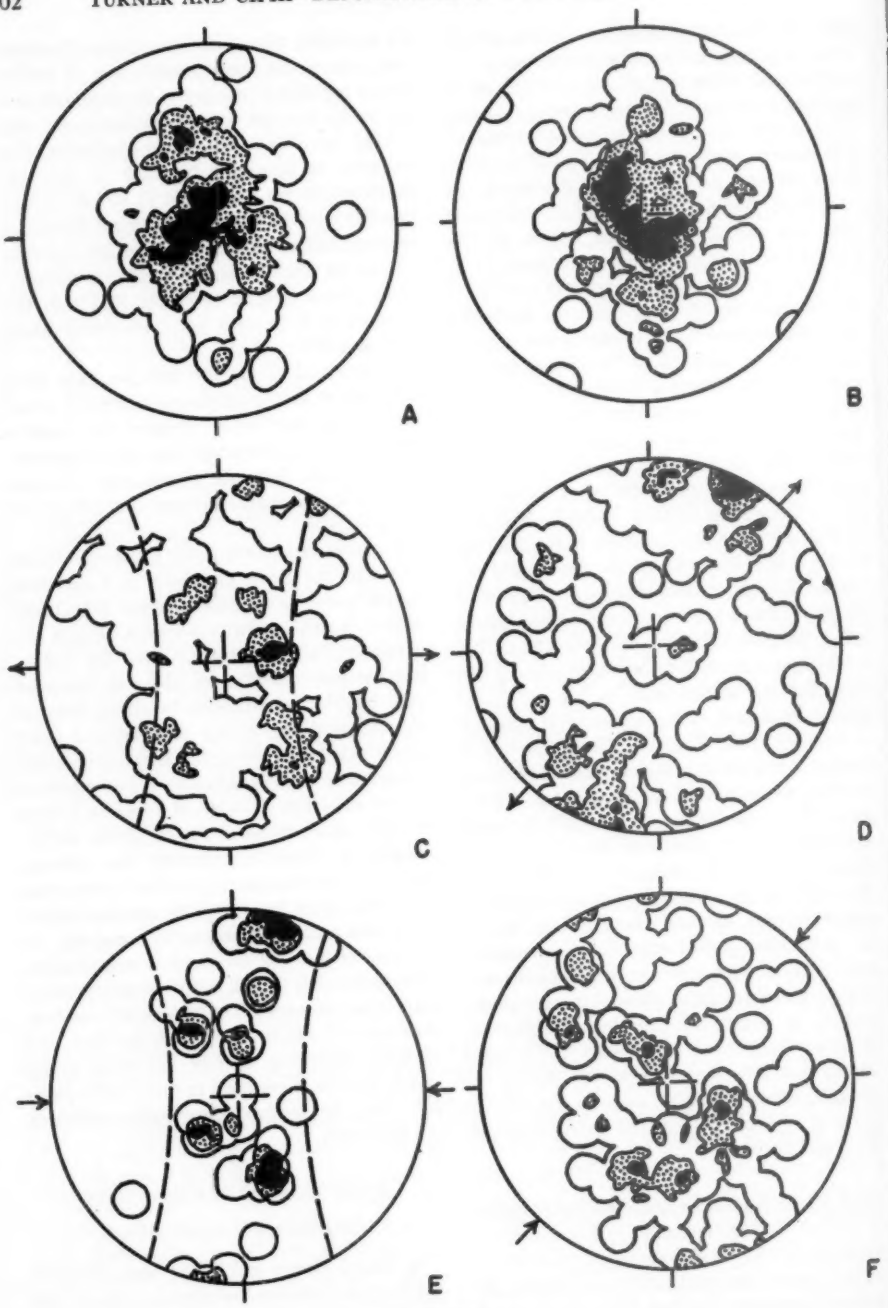

FIGURE 8

have been advanced by metallurgists to account for the plastic deformation of polycrystalline aggregates:

(1) The hypothesis of "heterogeneous deformation" assumes that each individual grain deforms to a different degree in response to the external stress field; effects of neighboring grains upon it are ignored.

(2) The hypothesis of "homogeneous deformation" on the other hand assumes that each grain is strained to the same degree as are the surrounding grains, and the behavior of any grain is conditioned by that of adjacent grains.

It has not been suggested that either hypothesis is strictly applicable to the present case. However, Griggs and Miller have found that their experimental data are most consistent with a mechanism of deformation that approaches hypothesis (2) rather than (1). In Part II, Handin and Griggs, starting with a series of representative orientation data determined for undeformed marble, have deduced the extent and manner of change in fabric to be expected for strain of various degrees, on the basis of each hypothesis.

The observed changes in pattern of preferred orientation of *c* axes (Pl. 1; Fig. 4), as pointed out by Handin and Griggs in Part II, are remarkably similar, both as regards trend and magnitude of change, to those predicted by Handin and Griggs on the hypothesis of homogeneous deformation. On the other hand they do not accord nearly so satisfactorily with fabrics predicted on the hypothesis of heterogeneous deformation. On this latter hypothesis if twinning on $\{01\bar{1}2\}$ be assumed, the trend of

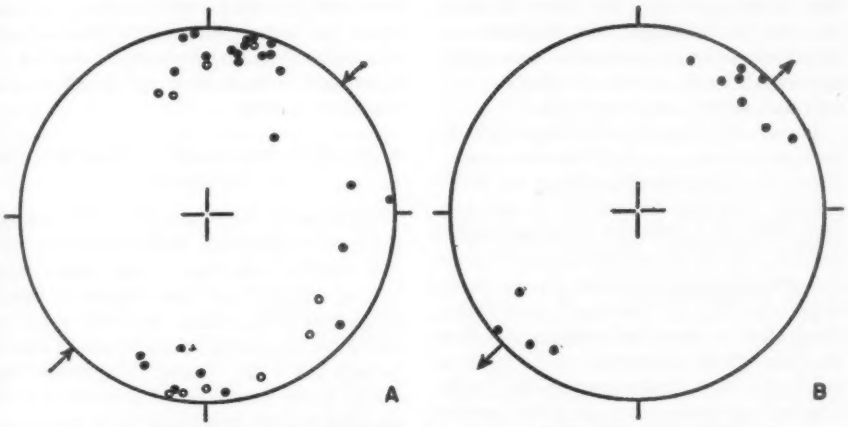

FIGURE 9.—ORIENTATION OF POLES OF ALL OBSERVED $\{02\bar{2}1\}$ LAMELLAE IN THREE *d* CYLINDERS OF DEFORMED YULE MARBLE

Plane of diagrams is parallel to *R*; trace of foliation plane (= *Q*) is parallel to N-S diameters.
A: Specimen 282, 25 lamellae, full black circles. Specimen 283, 10 lamellae, open circles. Axis of shortening indicated by arrows.
B: Specimen 280, 12 lamellae. Axis of elongation indicated by arrows.

FIGURE 8.—ORIENTATION DIAGRAMS FOR EDGES [*e*:*e'*] IN CALCITE OF DEFORMED YULE MARBLE

Contours 1, 3, 6%, per 1% area. All diagrams similarly oriented by projection on *R* plane; trace of foliation plane (= *Q*) is parallel to N-S diameters.
A: Specimen 158, *R*, elongated 5%; 107 edges in 100 grains.
B: Specimen 154, *R*, elongated 6.4%; 102 edges in 100 grains.
C: Specimen 231, *Q*, elongated 6.8%; 152 edges in 100 grains.
D: Specimen 280, *d*, elongated 12.2%; 128 edges in 100 grains.
E: Specimen 235, *Q*, shortened 10.5%; 33 edges in 50 grains.
F: Specimen 282, *d*, shortened 11%; 91 edges in 100 grains.

predicted change is somewhat similar to that observed, but the magnitude of predicted change is much too great; while if translation on $\{01\bar{1}2\}$ be assumed the predicted change is of the right order of magnitude, but in some cases follows a trend markedly different from that actually observed. We agree, therefore, with Handin and Griggs, that deformation in the present series of experiments has probably approximated fairly closely to what has here been termed the homogeneous type.

As defined by Handin and Griggs (Part II) the homogeneous type of deformation is accomplished by intracrystalline gliding on $\{01\bar{1}2\}$ parallel to the edge between $\{01\bar{1}2\}$ and adjacent $\{10\bar{1}1\}$ faces. Gliding in one sense involves twinning, but in the opposite sense pure translation. The hypothesis predicts that for certain stress conditions (R cylinders in compression, Q cylinders in extension) twinning should be the main gliding mechanism, while for other orientations (R cylinders in extension, Q cylinders in compression) gliding is chiefly by translation. Close agreement between predicted and observed fabrics at all stages of deformation consequently is strong evidence supporting the hypothesis that twinning occurs wherever the stress system allows it, and that wherever the stress system is unfavorable for twinning translation predominates.*

From the demonstrated relationship between spacing index for $\{01\bar{1}2\}$ lamellae and resolved shear-stress coefficient, it has been suggested that development of visible lamellae is promoted by shear stress acting in the direction and sense appropriate for twinning. Thus the visible lamellae may perhaps be very thin twin lamellae; or alternatively they may possibly be surfaces of translation gliding activated and rendered visible by preliminary development of a film of twinned material over the translation surfaces. The visible lamellae cannot, however, be due to translation on $\{01\bar{1}2\}$ in the sense opposite to that appropriate for twinning; for we have found consistently that the spacing index approaches zero (*i.e.*, lamellae tend not to develop) in the case of $\{01\bar{1}2\}$ planes for which the resolved shear-stress coefficient is maximal but in the sense opposed to twinning. It is on just such planes that translation gliding should be most effective. We are forced therefore to conclude that where translation gliding occurs in the sense opposed to twinning, and even where it is the dominant mechanism of deformation, it leaves no microscopically visible trace of its activity.

Application to Interpretation of Petrofabric Data in General

Conditions of our experiments—low temperature, very high stress, absence of water—depart notably from those under which most natural marbles have been deformed. Direct comparison of our fabric data with those recorded for marble tectonites therefore cannot be expected to be fruitful. Nevertheless our results would seem capable of useful indirect application to the vexed problem of interpretation of petrofabric data in general. Several suggestions are put forward in this connection:

(1) Even where experimental deformation has been carried out under conditions favoring profuse development of visible glide lamellae, we are forced to conclude that some other type of intracrystalline movement, leaving no visible trace of its activity, has played a part in deformation. To interpret the fabric of marble tectonites (especially if recrystallization has probably been important) entirely in terms of visible $\{01\bar{1}2\}$ lamellae—as has been done by many structural petrologists—is surely unjustified in many cases.

(2) The value of many published orientation diagrams for "$\{01\bar{1}2\}$ lamellae" in marbles is highly questionable. Not only is the development of visible lamellae possibly of comparatively minor significance in the evolution of some fabrics, but, unless the angle between each lamella pole and the c axis is checked, the identity of recorded lamellae is in doubt; there is, moreover, the statistical error which so commonly arises from selecting and recording only such lamellae as happen to be clearly visible in first examination of each grain. Deductions drawn from the relative positions of maxima in lamella diagrams and those in c

* In an abstract of this paper (Turner, Griggs and Ch'ih, 1950) the conclusion was stated that "half, or more, of the deformation is due to translation gliding on $\{01\bar{1}2\}$." This possibly overemphasizes the role of translation gliding; for under favorable circumstances twinning appears to outweigh translation in the opposite sense.

axis diagrams for the same rock probably are seldom justified, unless confirmed by comparing relative positions of lamellae and *c* axis in each individual grain.

(3) Postulation of assumed "glide mechanisms," unsupported by experimental evidence, to explain different orientation patterns commonly exhibited by calcite, quartz, mica, and so on, is especially dangerous. The long list of such "orienting mechanisms" proposed for quartz (*cf.* Turner, 1948, p. 255–266) illustrates the confusion that arises when the imagination is allowed unrestricted play in this field. [Hypotheses so developed are least likely to be of value in the case of coarse monomineralic rocks (many marbles and quartzites) whose fabrics appear to be products of recrystallization of initially finer-grained materials.]

(4) The most significant petrofabric data for marble tectonites seem to be those relating to orientation of *c* axis, orientation of a_1, a_2, and a_3 axes, spacing index of $\{01\bar{1}2\}$ lamellae, and in some cases orientation of edges $[e{:}e']$ between two strong sets of lamellae per grain. It may prove possible in some cases to use spacing-index data and $[e{:}e']$ diagrams to reconstruct stress conditions operating at the close of deformation.

(5) The long-accepted principle that symmetry of fabric tends to reflect symmetry of deforming movements seems generally applicable to our petrofabric data. In our material the predeformational pattern of space-lattice orientation has proved remarkably persistent. The patterns recorded in this paper can be regarded as those of a predeformational fabric, still recognizable, but becoming modified to conform to the symmetry of the system of applied stress.

(6) Partially developed girdle patterns for *c* axes of calcite, and hence probably those for crystal axes of quartz or other minerals, need not necessarily indicate existence of an axis of rotation (*B* axis) normal to the girdle in question. Under the conditions of our experiments, *c* axes of calcite tend to develop girdles normal to the axis of extension. Associated visible $\{01\bar{1}2\}$ lamellae likewise show distinct girdle patterns in such cases.

References Cited

Balsley, J. R. (1941) *Deformation of marble under tension at high pressures*, Am. Geophys. Union, Tr., pt. 2, p. 519–525.

Fairbairn, H. W. (1949) *Structural petrology of deformed rocks*, Addison-Wesley, Cambridge, Mass.

Griggs, David (1936) *Deformation of rocks under high confining pressures*, Jour. Geol., vol. 44, p. 541–577.

Knopf, E. B. (1949) *Fabric changes in Yule marble after deformation in compression*, Am. Jour. Sci., vol. 247, p. 433–461, 537–569.

Turner, F. J. (1948) *Mineralogical and structural evolution of the metamorphic rocks*, Geol. Soc. Am., Mem. 30.

—— (1949) *Preferred orientation of calcite in Yule marble*, Am. Jour. Sci., vol. 247, p. 593–621.

—— and Ch'ih, C. S. (1950) *Note on survival of fabric characters in Yule marble after heating to 700°C*, Am. Jour. Sci., vol. 248, p. 347–354.

——, Griggs, D. T., and Ch'ih, C. S. (1950) *Fabric of Yule marble deformed experimentally at ordinary temperatures in absence of water* (Abstract), Geol. Soc. Am., Bull., vol. 61, p. 1512.

University of California, Berkeley 4, Calif.; National Tsing Hwa University, Peking, China.

Manuscript Received by the Secretary of the Society, January 9, 1951.

COMPRESSION

EXPLANATION OF DIAGRAM

A: Specimen, 158, *undeformed.*

B: Specimen 154, R, elongated 6.4%.

C: Specimen 159, R, elongated 7.2%.

D: Specimen 167, R, elongated 20.5%.

E: Specimen 235, Q, shortened 10.5%.

F: Specimen 231, *undeformed.*

G: Specimen 231, Q, elongated 6.8%.

H: Specimen 232, Q, elongated 9.2%.

I: Specimen 234, Q, elongated 12%.

J: Specimen 282, *d*, shortened 11%.

K: Specimen 283, *d*, shortened 6%.

L: Specimen 154, *undeformed.*

M: Specimen 281, *d*, elongated 7%.

N: Specimen 280, *d*, elongated 12.2%.

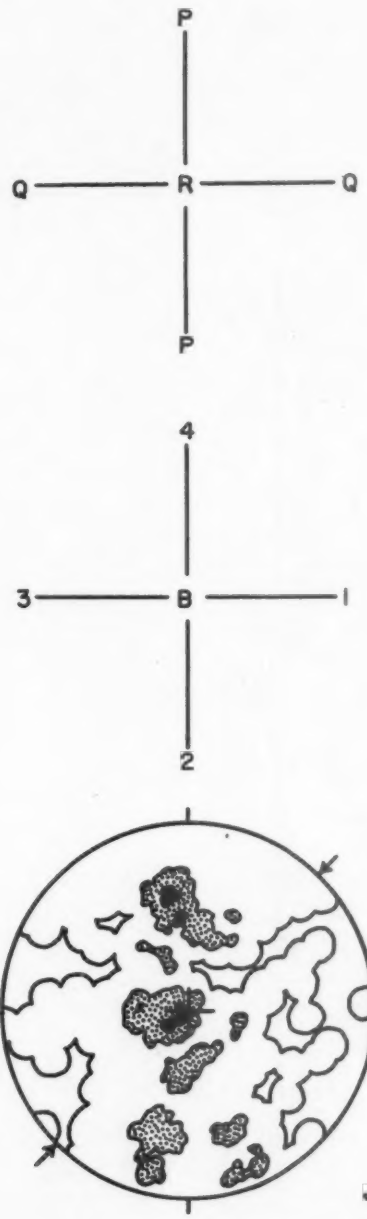

ORIENTATION

ESSION

UNDEFORMED

EXTENSION

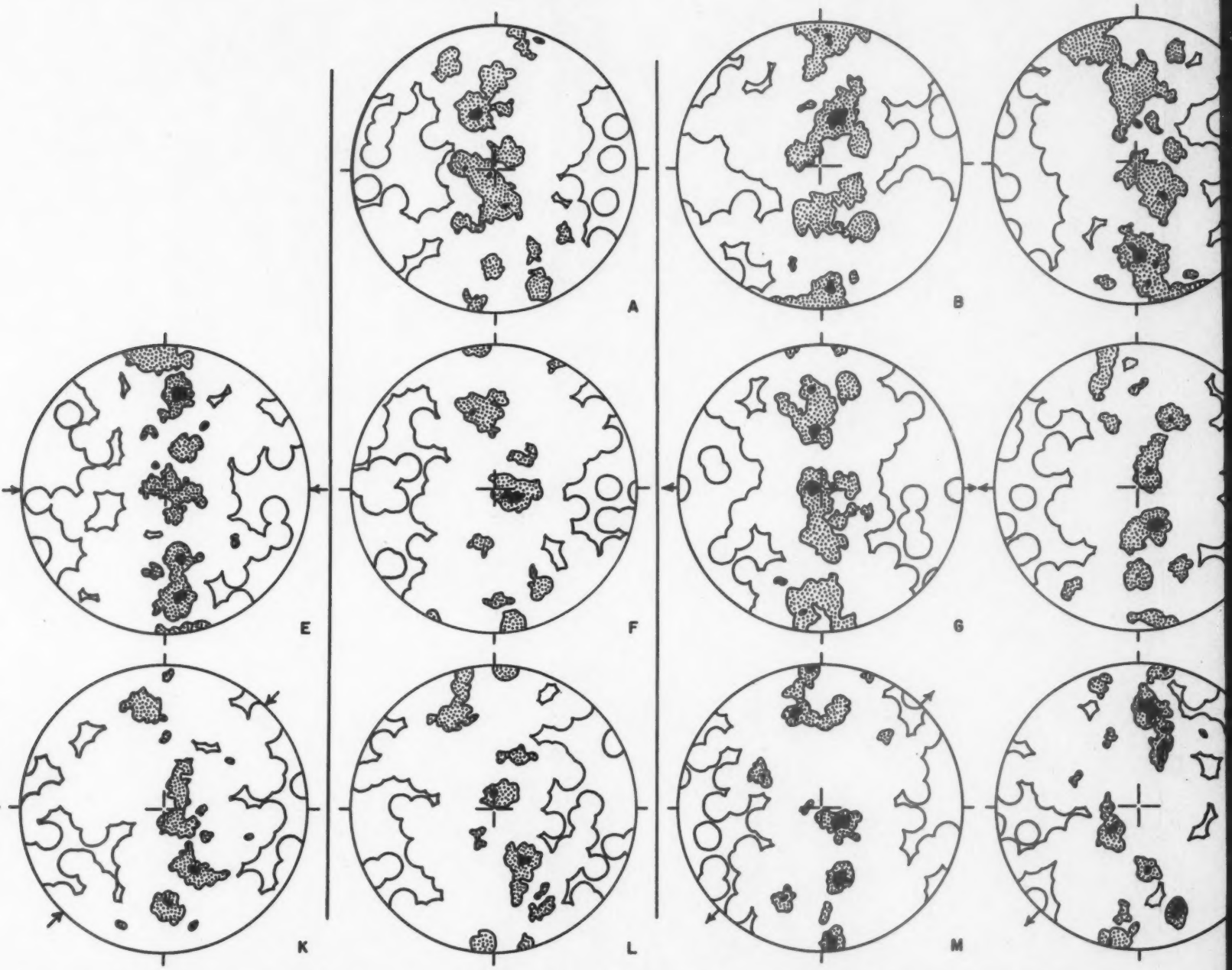

TION DIAGRAMS FOR a_1, a_2, a_3 AXES OF CALCITE IN UNDEFORMED AND IN DEFORMED

Each diagram represents 300 axes in 100 grains. Contours 0.3, 2, 4%, per 1% area. All diagrams similarly oriented, by projection on R plane; trace of foliation plane ($=Q$) is parallel to N-S diameters.

COMPRESSION

UNDEFORMED

ORIENTATION DIAGRAMS FOR a_1, a_2, a_3 AXES OF CA

Each diagram represents 300 axes in 100 gra
oriented, by projection on R plane; trace of foliati

RMED

EXTENSION

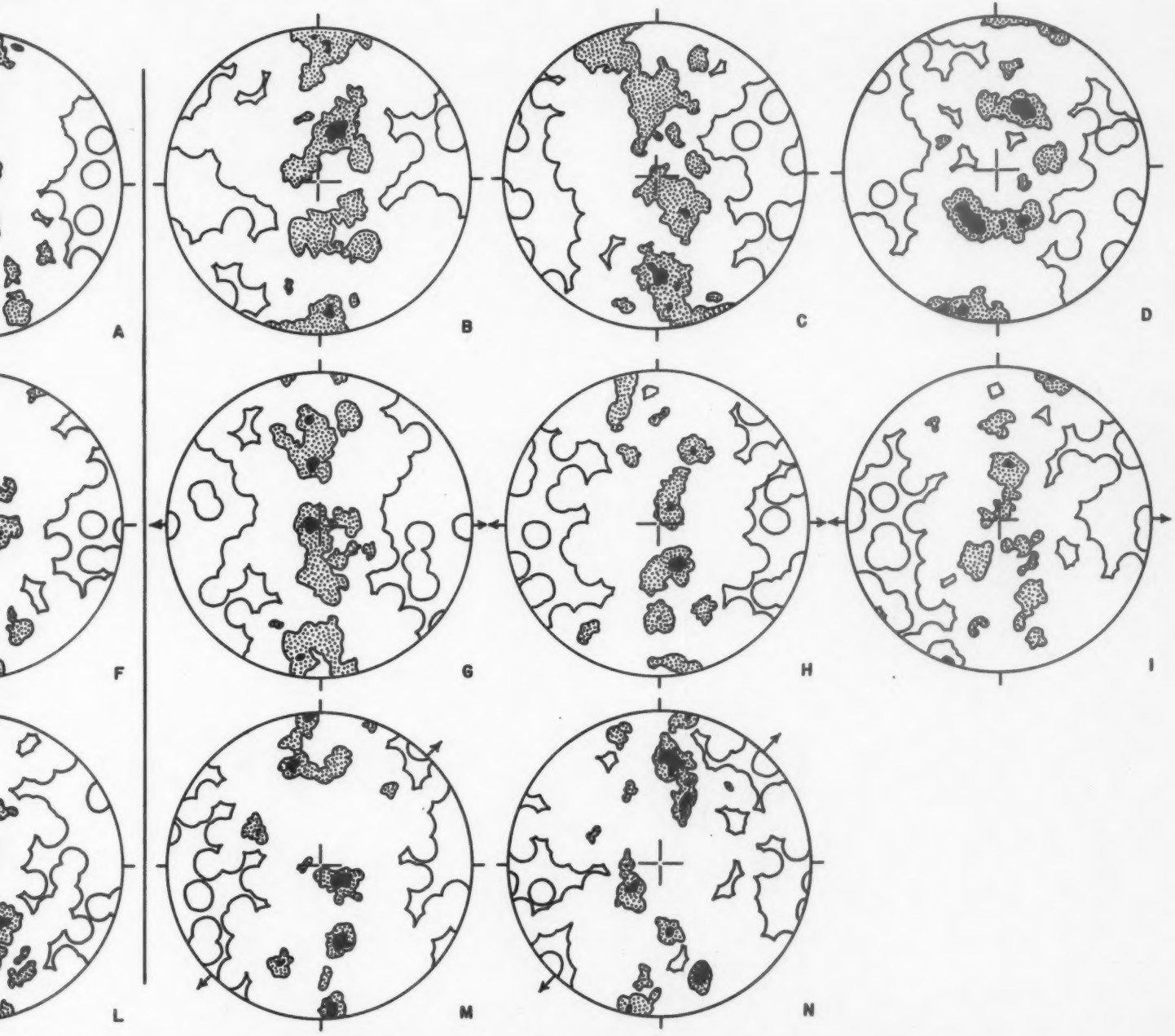

OF CALCITE IN UNDEFORMED AND IN DEFORMED YULE MARBLE

es in 100 grains. Contours 0.3, 2, 4%, per 1% area. All diagrams similarly
ace of foliation plane (= Q) is parallel to N-S diameters.

BULLETIN OF THE GEOLOGICAL SOCIETY OF AMERICA
VOL. 62, PP. 907-918, 4 FIGS., 2 PLS. AUGUST 1951

MOLD OF A RHINOCEROS IN BASALT, LOWER GRAND COULEE, WASHINGTON

By WALTER M. CHAPPELL, J. WYATT DURHAM AND DONALD E. SAVAGE

ABSTRACT

The occurrence of the mold of a rhinoceros in the pillows at the base of a basalt flow of the Columbia River Basalts near Blue Lake, Washington, is described and discussed. It is concluded that preservation of the rhinoceros mold is due to the special conditions causing the formation of the pillows in the base of the flow. Apparently the advancing lava flow encountered a shallow body of water, with a dead and bloated rhinoceros either upon the shore or floating on the water. The water caused the formation of the pillows at the base of the flow. The pillows retained sufficient plasticity to pack around the body of the animal but were rapidly cooled by the water so that they became rigid enough to preserve the mold thus formed. The entombed rhinoceros appears to be referable to the genus *Diceratherium*, suggesting an upper Oligocene or lower Miocene age for the containing lava. A restoration of the animal, based upon the mold, is presented.

CONTENTS

	Page		Page
Abstract	907	Mode of preservation	911
Introduction	907	Description of the bones	913
Acknowledgments	908	Comparisons	915
The Mold	908	Description of the cast	915
Location	908	Age significance	918
Description of the mold	908	References cited	918
Contents of the mold	910		

ILLUSTRATIONS

Figure	Page	Figure	Page
1. Locality map	909	4. Restoration	917
2. Diagrammatic sketch of site of rhinoceros mold	912	Plate	Facing page
3. The skeletal material	914	1. Leg casts	916
		2. Views of the cast	917

TABLES

Table	Page	Table	Page
1. Spectrographic analyses	910	3. Comparative measurements of the cheek-tooth length	915
2. Comparative measurements of the jaw and teeth	914		

INTRODUCTION

The mold and associated bones which are the subject of the present paper have been known since 1935 and have been the topic of much informal discussion and controversy. Despite its past history, however, the only papers published on this mold are those of Beck (1935; 1937) and Chappell, Durham, and Savage (1949). Several unpublished reports and memoranda were submitted to the National Park Service in the interval from 1935 to 1937.

HISTORY AND DISCOVERY: The cavity here discussed is in the northeast quarter of Section 22, Township 24 North, Range 27 East of the Williamette Meridian, on property owned by H. B. Hayden. It is an opening in the basalt of the west wall of Jasper Canyon, a few feet above the talus slope that borders an arm of Blue Lake, in the Lower Grand Coulee, Grant County, Washington. This site has been given University of California, Museum of Paleontology No. V5108.

According to information furnished by Professor George F. Beck of the Central Washington College of Education at Ellensburg, and members of the discovery party, the general history of its discovery is as follows:

A tramping party consisting of Mr. and Mrs. H. B. Friele and Mr. and Mrs. G. B. Peabody, all of Seattle, Washington, found the cavity in the summer of 1935. Mr. Friele entered it and noted that numerous fragments of bone were scattered on the floor. From an extension of the main cavity opposite the entrance, he removed fragments of a jaw, in one side of which teeth were still set. The specimens were given to Mrs. Peabody who took them to Seattle and presented them to the University of Washington. Soon thereafter Beck learned of the discovery and, consistent with his interest in local geology, asked Mrs. Peabody for information about it. The University released the bones to Beck in order that he might submit them to a vertebrate paleontologist for identification. Soon afterward, Mr. Beck visited the cave with an assistant, Mr. Frechette, who collected bones from small pipe-like extensions at the side of the main cavity. Beck did not enter the main cavity, being at that time partially incapacitated, but directed the work from the outside. The bones collected by Beck and Frechette were badly broken, but, together with the pieces of jaw obtained from the University, they were sent to the late Dr. Chester Stock, California Institute of Technology, for identification. Stock subsequently identified them as an *Aphelops*-like rhinoceros. In a paper published in Northwest Science, Beck (1935) included a brief statement regarding the discovery of the cavity and his interpretation that it may be the mold of a rhinoceros.

During the next 2 years, several visits were made to the site by different people, who offered various interpretations about the origin of the cavity. Wartime activities disrupted plans for a serious study of the mold, so that it was not until the summer of 1948 that the junior authors were able to visit the site, make a cast of the mold, and study the remaining evidence regarding the authenticity of the feature. In 1949, Durham visited the locality again, taking additional impressions of certain critical features.

The present paper is the result of investigations in the field by Chappell in 1936, as well as the subsequent examinations and laboratory studies by Durham and Savage. Savage is responsible for the morphologic descriptions of the cast of the mold, the study of the bone fragments, and the restoration of the animal. The remainder of the paper is the work of Chappell and Durham, but has been contributed to by Savage as well.

Acknowledgments

All line drawings except the locality map were prepared by Mr. Owen J. Poe, Staff Artist of the Museum of Paleontology of the University of California. Grateful acknowledgment is made to Dr. R. A Stirton for his aid and advice in the investigation.

The Mold

Location

The cave or cavity, hereafter called the mold, is located in a cliff of basalt along the southwest wall of Jasper Canyon, just beyond the end of that arm of Blue Lake. The opening to the mold is on a ledge about 200 feet or more above the level of the lake, with a vertical cliff of basalt rising at least that much higher above it. The bottom of the actual entrance in the cliff is a few inches above a thin layer of sediments marking the contact of two distinct lava flows (Fig. 2). The opening is just large enough to permit one's shoulders to pass, if it is entered in a nearly horizontal position.

Description of the Mold

Upon entering the mold and examining it, one is impressed by its rhinoceros-like shape. The form is gently curved and lacks the rough and irregular projections and hollows that commonly characterize cavities formed in lava by steam action. The opening on the face of the cliff cuts across the rump and practically obliterates the impression of the left hind leg. The body is aligned almost normal to the face of the cliff, but it inclines upward at an angle of about 30°. The animal is lying on the left side and its short legs project outward in a way characteris-

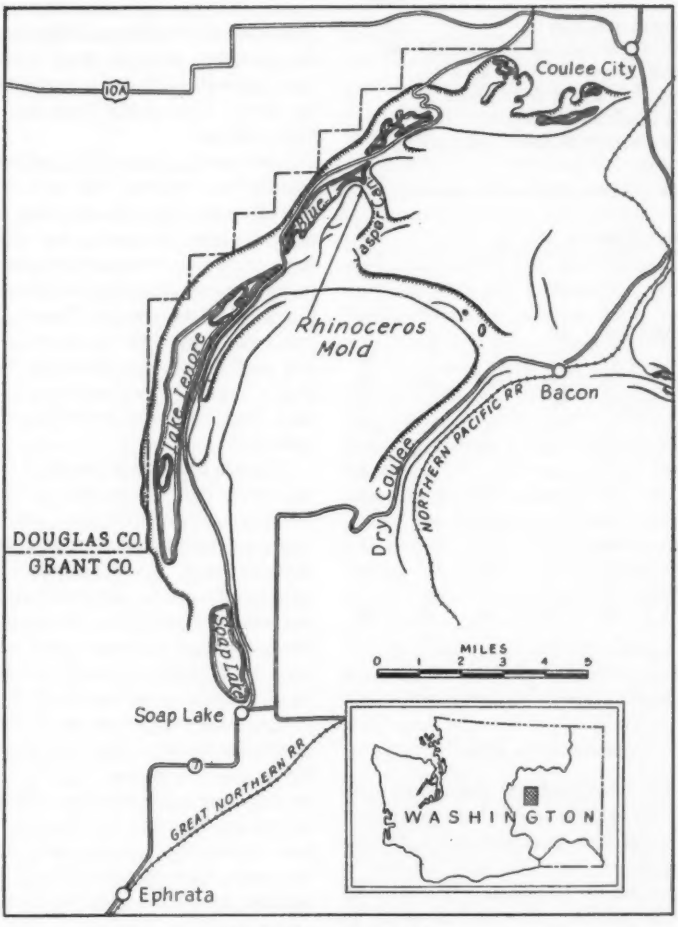

FIGURE 1.—LOCALITY MAP

tic of an animal in rigor mortis. The legs are properly placed with respect to the plane of body symmetry, with the front legs closer together than the hind legs. The body mold resembles that of an animal of heavy build. The head is long and somewhat pointed. The ventral[1] part of the neck has weak transverse marks that suggest impressions made by folds in the skin. Following are various measurements of the mold:

[1] Our orientation of the mold follows the standard orientation terminology for a quadrupedal mammal.

(Base of neck taken as a surface perpendicular to anteroposterior axis and at a point 19 inches anterior to line connecting centers of entrances of front legs into body cavity.)

	Inches
Base of neck to rump (estimated)	66
Center of front legs to center of hind legs	44
Maximum transverse diameter of body cavity	32
Maximum dorsoventral diameter of body cavity	33
Base of neck, transverse diameter	15
Base of neck, dorsoventral diameter	12

	Inches
Length of head and neck	28
Total length of head and body (estimated)[1]	94
Proximodistal length of right hind leg (measured from line of body profile to center of distal surface of foot)	15
Proximodistal length of right front leg	17

TABLE 1.—SPECTROGRAPHIC ANALYSES

	Sediment	Pillow Basalt	Basalt	Matrix	Bone	John Day bone
Si	PC	PC	PC	PC	10–20	10+
P	—	—	—	—	10	10+
Al	10–20	PC	PC	1	1	2
Mg	2	2	2	2	2	.50
Mn	.05	.10	.10	.02	.01	.10
Fe	10	PC	PC	10	10	.5
V	.05	.10	.10	—	.01	.001
Cu	.05	<.02	.10	<.02	<.02	.01
Na	.30	1–5	.50	—	—	.50
Ti	1	.50	.50	<.10	<.10	.10
Ni	—	.01	.05	—	—	—
K	1	1–10	1–10	1	.1	—
Ca	.50	10	10	.20	PC	10+
Cr	.005	.01	.01	—	—	—
Ba	.10	.50	.50	.10	.3	.20
Y	—	—	—	—	—	1

Above figures cited as approximate per cent composition; PC indicating a principal constituent.

Contents of the Mold

When first discovered, the mold must have contained considerable broken bone in addition to the jaw and limb fragments and teeth that were recovered at about that time, for even in 1948 a number of fragments were gathered (sufficient to partially fill a 10-inch sack). In addition, portions of the lower limb bones are still in the left front leg, having been left there because of the difficulty of removing them.

In an attempt to explain the cavity as something other than the mold of an animal preserved in lava, it has been suggested that the bones were brought into the cavity by some carnivore or other animal. This suggestion is controverted, however, by an examination of the loose bone fragments and of the bone still imbedded in the leg cavity. At the time of the 1948 visit, the site was carefully examined with this possibility in mind. Bone is still imbedded in a matrix filling the lower part of the left front leg cavity. Part of this bone and matrix has been removed.

Subsequently, bone which had been removed from this leg, together with some of the matrix, the adjacent pillow basalt, some of the sedimentary layer separating the adjacent lava flows, and some non-vesicular basalt from higher in the flow, was examined spectrographically by George M. Gordon of the Department of Mineral Technology of the University of California. The analysis of a bone from the John Day region is included for comparison (Table 1). This John Day bone was imbedded in tuffaceous sediments.

Although the bone is porous, it is quite hard, and, as can be seen from the analysis, it is silicified and has been infiltrated with certain elements (notably iron and magnesium) from the adjacent basalt. The abundance of calcium and phosphorous can be attributed to the original composition of the bone. The matrix is high in silica, iron, and magnesium and seems to have been largely derived from the adjacent basalts by percolating waters—certainly it does not appear to have had its source in the sediments underlying the flow. This last point is interesting inasmuch as the lowest parts of the mold lie no more than a few inches at most and perhaps are not more than an inch above the base of the flow. Apparently the cavity was not in free communication (between the pillows) with the underlying soil. If a connection had existed, the cavity would have been either partially or completely filled with sediment forced in by the weight of the overlying flow. It is interesting to note that the sample of fossil bone from the John Day region has been infiltrated with much less iron and magnesium and more aluminum.

In similar fashion to the left front leg bone, which was actually imbedded in matrix *in situ* when collected, all the innumerable small scattered bone fragments collected from the floor and small crevices in the bottom of the mold are silicified and have the same type of preservation. These small fragments are all parts of larger bones and appear to have been subjected to the action of heat and steam, or some other

[1] In taking this measurement, the point of the rump, which was broken off in the cliff face, had to be estimated from the curvature of the posterior part of the body. The measurement is probably not more than 2 or 3 inches in error.

agent which would fragmentize and warp them. Although silicified, most of the bone fragments are still porous, further indicating that the entire cavity had not been filled by any solid matrix.

Mode of Preservation

The mold is imbedded in the base of a thick flow of basalt and is surrounded by pillows. This layer of pillow basalt is persistent along the base of the flow, usually about 2 feet thick, but where the base of the flow encloses cavities (molds of tree trunks and the rhinoceros mold), this layer is thicker and extends about 2 feet above the top of the cavity (Fig. 2). The pillows are vesicular and grade upward into the massive basalt. Some pillows are hollow or have a fine to coarse, ropy surface preserved, but most have adjusted their surfaces fairly closely to those adjacent.

Underneath the layer of pillow basalt is a thin layer of sandy silt (Fig. 2), varying from 2 to over 5 inches in thickness, with the average thickness perhaps nearer the latter figure. These sediments pinch and swell along the strike and, as may be seen from the spectrographic analysis, are probably derived from the underlying basalt flow. Macroscopically at least, the silt shows little or no effect of baking by the overlying flow. The top of the underlying lava is highly vesicular, shows marked flow structure through a thickness of more than 5 feet, and then grades into massive fractured basalt below.

When the site is viewed from the floor of the opposite side of the canyon, it appears that the flow, at a point approximately 250 yards to the south, is only about half as thick as at the site of the mold, suggesting that the flow was partially dammed up in the area of the mold.

Two specific objections have been raised against the interpretation of the cavity as the mold of an animal buried in the base of the flow. First, it is commonly accepted that lava of this type is fluid only above 900°C., and that such temperatures would supposedly destroy the skin, flesh, and bones of an engulfed animal. Second, because of the diverse specific gravities of lava and the body of a mammal, the latter should float to the surface where, if it had survived burning, it would be destroyed by weathering. This reasoning is sound, but it does not take into consideration all of the conditions under which this flow of lava formed and congealed. These special conditions are:

1. The opening to the cave is only a few inches above a horizontal layer of sandy sediments that may be traced for some distance along the side of the cliffs in this vicinity. The sedimentary layer averages nearly 5 inches thick and rests on the vesicular surface of a lava flow. Accordingly, there seems to be little question that the sediments accumulated between the time of eruption of these two flows, and that the cave is near the base of the higher flow.

2. At several places near the cave, fossilized logs and stumps surrounded by basalt may be seen resting on sedimentary layers separating flows. Cylindrical cavities that appear to be log molds are likewise rather abundant. In the latter cases it seems that the wood, having failed to petrify, has subsequently been removed. Several such cavities lie near the rhinoceros mold but are not connected with it (Fig. 2). If the specific conditions postulated by opponents had prevailed at the base of the flow, then the logs and stumps also should have been burned or floated to the surface of the lava.

3. Pillow or ellipsoidal lava forms a persistent layer along the base of the lava flow enclosing the cavity. The ellipsoids completely surround the cavity (Fig. 2) and extend about 2 feet above it. The upper surface of this zone is approximately horizontal and grades through a limited thickness into the overlying massive lava. Such pillow structure has been frequently observed in basaltic lavas and is very abundant in certain portions of the Columbia Plateau region. Fuller's studies (1931) of pillow basalt and other structures associated with it in the immediate region have supported the generally accepted opinion of geologists (Tyrrell, 1929, p. 37–39) that separation into these sack-like masses results when lavas enter water. Hence pillow structure in the base of the upper lava flow of this locality and forming the walls of the cave is regarded as evidence that this flow entered a shallow body of water.

4. If, as the evidence suggests, the lava entered water, one has a clue to the formation of the local log and stump molds, some of which contain fossilized wood. The numerous logs in

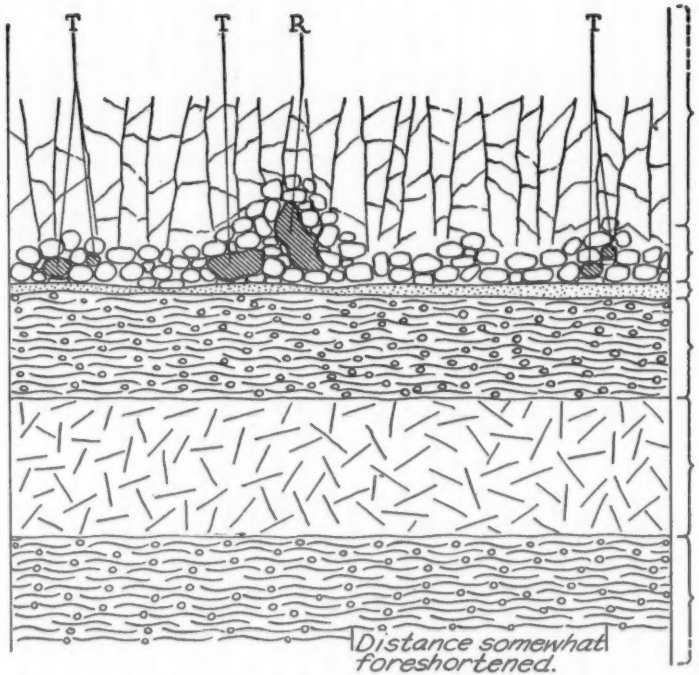
T
T
R
T
Massive, coarsely columnar basalt. Non-vesicular except at base. Over 100' thick.
Irregularly ellipsoidal vesicular pillow basalt about 2' thick except over trees and rhinoceros.
Layer of moderately fine sandy sediments, pinching & swelling laterally, but usually 2"-5" thick.
Highly vesicular basalt with well developed flow structure, ±5'.
Massive, irregularly fractured basalt, ±6'.
Highly vesicular basalt with well developed flow structure, +10'.
Distance somewhat foreshortened.
Sketched by J.W.D
T = Opening to molds of tree trunks; R = Opening to rhinoceros mold.

FIGURE 2.—DIAGRAMMATIC SKETCH OF SITE OF RHINOCEROS MOLD

the vicinity of Ginkgo Petrified Forest State Park, 50 miles to the southwest, are likewise enclosed by pillow lavas. Wood burns at temperatures much lower than those of liquid basaltic lavas, and at such temperatures no remnant of the form or substance of the wood should have survived. Beside the trail by which the cave is reached and at the base of an older flow, the mold of a large standing tree is conspicuous. Some fossil wood can be seen near the base of the mold and it is probable that much wood has been removed. The tree mold extends upward through the pillow lava at the base of the flow, but it ends where the pillows are overlain by massive basalt. Since the fossil logs and stumps of this vicinity are found in pillow lava, this coincidence seems significant. It is conceivable that the advancing lava broke the tree off at this level, but it seems more probable that the upper part was burned away and that within the pillow zone the lava had been sufficiently chilled by the water to prevent the destruction of the wood by burning. The cool water and particularly its conversion to steam must have dissipated the heat with great rapidity. This seems a reasonable explanation of the fact that fossil trees of this part of the Columbia Plateau are invariably enclosed by pillow lava and none have yet been found in massive lava.

5. Since pillow lava enclosed and preserved the wood until it was later silicified, thus faithfully preserving the cell structure, there seems no valid reason why the body of a mammal might not be entombed in a similar manner. If petrifying solutions did not accompany or follow closely the entombment by the lava, the flesh would decompose, leaving only the bones and teeth.

The above listed field evidence and theoretical considerations suggest that the mode of burial may have been somewhat as follows:

Lava encountered the body of a rhinoceros in a shallow body of water. Possibly the animal was floating. On entering the water, the lava divided into bulbous ellipsoids. Chilling toughened the outer surface of these ellipsoids but their liquid interior gave them a certain degree of mobility. As they formed and settled by gravity to the bottom of the water, they still possessed enough mobility to adapt their outer surfaces of contact to one another and doubtless also to organic objects in the water. Possibly this may have taken place in much the same manner as loosely-filled sacks of sand might be packed about an object. Chilling was rapid, however, and by the time the main mass of lava advanced over the body of the animal, the ellipsoids were cooled sufficiently to support the weight of the overlying lava. The walls of the cave show that the pillows accumulated around and adjusted themselves to a rhinoceros-like form. Junctions between pillows are clearly marked and commonly openings still remain between their curved surfaces. One of the largest of these is across the nose, but opinions vary as to whether it has the form of a horn. It does not appear that chilled pillows of lava packed about the body of a mammal would have any great effect on the bones, but the highly fragmented and warped condition of most of the bones recovered may be owing in part to the action of heat.

Description of the Bones

An incomplete left lower jaw, fragment of the right lower jaw, pisiform, cancellous fragments of the skull, rib fragments, teeth fragments and many unidentifiable bone fragments have been collected from within the mold cavity and downslope from the opening of the cave. This material is now in the collections of the Museum of Paleontology at the University of California and has been given Museum No. 40307. All of the unidentifiable fragments are small, but there is nothing to suggest that these pieces belong to anything but a rhinoceros. No bones of small animals are represented.

LEFT LOWER JAW: Uniquely warped and cracked; slivers of bone of ventro-internal face of horizontal ramus literally curled or warped individually into cellular portion of ramus, forming an *en echelon* pattern; dorsal part of ascending ramus, including complete coronoid process and broken condyle, bent medially, causing much tensional fracturing of external surface; contains anterior root of P_3, both roots of P_4, both roots and small portion of crown of M_1, all of M_2 except marginal angles of occlusal surface.

Height of crown of M_2 suggests teeth were in

TABLE 2.—COMPARATIVE MEASUREMENTS OF THE JAW AND TEETH[a]

	Millimeters		
	Grand Coulee Jaw UCMP no. 40307	Diceratherium cooki UCMP no. 39249	*Subhyracodon trigonodum** AMNH no. 529
Anteroposterior length, cheek-teeth (P_2-M_3)	182.5	156.0	170
Estimated length of cheek-teeth in living animal	180	156.0	170
P_2, anteroposterior diameter	15.0 ± 1	19.2	21.5
P_2, maximum transverse diameter	Indeterminable	13.8	12.5
P_3, anteroposterior diameter	21.3 ± 1	23.4	23.5
P_3, maximum transverse diameter	18.0 ± 2	16.5	16
P_4, anteroposterior diameter	26.0 ± 3	25.8	24
P_4, maximum transverse diameter	Indeterminable	18.7	18
M_1, anteroposterior diameter	32.3 to 33	28.5	28.5
M_1, maximum transverse diameter	21.2 ± 1	21.5	27
M_2, anteroposterior diameter	34 to 35	32.6	37
M_2, maximum transverse diameter	22.1 ± 1	21.5	23
M_3, anteroposterior diameter	36.0 ± 3	36.2	40.5
M_3, maximum transverse diameter	23.0 ± 2	20.5	22
Length, P_2 to P_4 inclusive	68.8 to 69.2	64.2	66
Length, M_1 to M_3 inclusive	115.0 ± 3	94.1	103.5

* Measurements from Wood, 1927, Table VI.

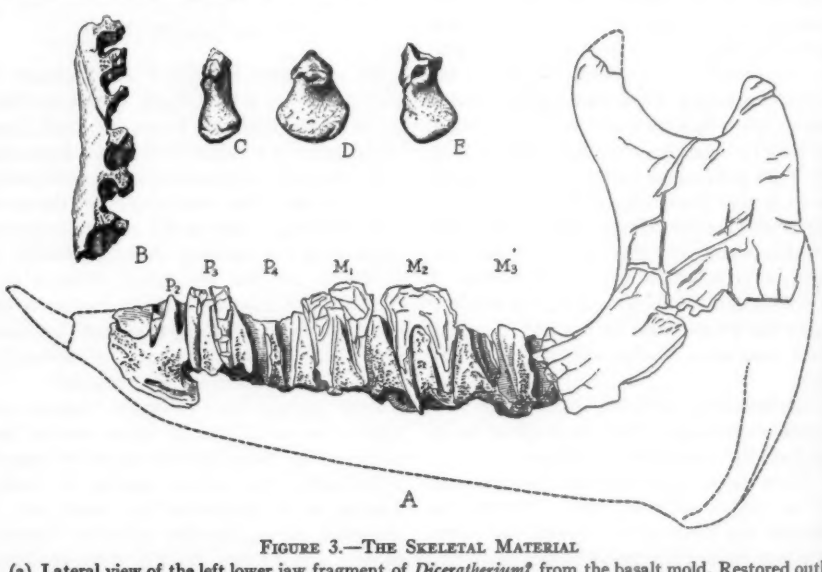

FIGURE 3.—THE SKELETAL MATERIAL

(a) Lateral view of the left lower jaw fragment of *Diceratherium?* from the basalt mold. Restored outline based on *Diceratherium annectens* and *D. cooki*. (b) Occlusal view of the right lower jaw fragment of *Diceratherium?* from the basalt mold. (c) Lateral view of the pisiform of *Diceratherium?* from the basalt mold. (d) Lateral view of the pisiform of *Diceratherium cooki*, Univ. of Calif. Mus. Paleont. no. 39960. (e) Lateral view of the pisiform of *Tapirus*, Univ. Calif. Mus. Paleont. no. 22880.

[a] Dr. H. E. Wood visited the University of California in the summer of 1949 and examined all of the rhinoceros mold materials. His unrivaled experience in the biometrics and evaluation of Tertiary rhinocerotids was utilized; many of the measurements were corroborated by him.

mature stage of wear at time of animal's death; enough of dorsal border of horizontal ramus anterior to P_2 is preserved to demonstrate presence of diastem and absence of P_1.

RIGHT LOWER JAW FRAGMENT: Lingual surface partially preserved; contains alveoli for teeth in center of cheek-tooth row; entire bone warped and cracked.

PISIFORM: Relatively slender as compared with *Diceratherium cooki* Peterson; proximodistal length—40.2 mm. (40.2 mm. in adult *D. cooki*); maximum dorsoventral height of distal boss—20.0 mm. (33.2 mm. in adult *D. cooki*); maximum transverse diameter of distal boss—9.6 mm. (17.7 mm. in adult *D. cooki*); part of proximal articular facets broken away.

The bone is extremely slender, particularly in dorsoventral diameter. There has been some distortion and perhaps shrinking, but this possible distortion is not great enough to account for the total slenderness. This pisiform more closely resembles that of the Recent *Tapirus* than any of the compared rhinoceroses (see Fig. 3c, 3d, and 3e).

Comparisons

The North American rhinocerotids with same lower cheek-tooth formula and with species of comparable size are *Diceratherium*, *Subhyracodon* and perhaps *Aphelops* and *Teleoceras*. Both *Aphelops* and *Teleoceras* (middle or upper Miocene to middle Pliocene) have been characterized by their stocky, rhinocerotid skeleton. (*See*, for example, Matthew 1931, p. 8–9; 1932, p. 414–416.) The slenderness and tapiroid attributes of the pisiform of the Grand Coulee rhinoceros, therefore, tend to separate it from these genera. The jaw from Washington is most diceratherine in general appearance, although the small species of *Aphelops*, such as *A. meridianus* (Leidy), are poorly known and might prove to be similar if they could be directly compared. Most of the species of *Diceratherium* and *Subhyracodon* have been based on skulls or upper cheek teeth. Mandibular portions or lower cheek teeth have merited little or no attention in the literature. Wood (1927, p. 59) has noted that *Subhyracodon* represents a group of rhinoceroses which merge into *Diceratherium*.

The Grand Coulee jaw is equal in size to *Diceratherium annectens* Marsh from the John Day fauna and is larger than the well known *D. cooki* from Agate Springs, Nebraska. It may be about equal in size to *Subhyracodon copei* (Osborn), but *S. copei* is known from the upper cheek teeth alone.

Most of the figured mandibles of *Subhyracodon* show that a slightly obtuse angle is formed between the plane through the occlusal surfaces of the cheek teeth and the plane along the anterior edge of the coronoid process. The Grand Coulee jaw conforms with all compared mandibles of *Diceratherium* by the acute angle thus developed. This appearance suggests that the Grand Coulee specimen is a *Diceratherium*, but it does not seem likely that such a distinct separation in morphology between *Diceratherium* and *Subhyracodon* exists. Probably other specimens will show more gradation between the two genera in this character.

TABLE 3.—COMPARATIVE MEASUREMENTS OF THE CHEEK-TOOTH LENGTH

(P_2–M_3 inclusive)

	Millimeters
Grand Coulee jaw, U.C.M.P. no. 40307	180 (est.)
Diceratherium annectens, U.C.M.P. no. 105	174.0
D. armatum, U.C.M.P. no. 462	216.0
D. cooki, U.C.M.P. no. 39249	158.0
Subhyracodon trigonodum, A.M.N.H. no. 529*	165
S. tridactylum, A.M.N.H. no. 538*	212 (approx.)

* Measurements taken from Obsorn (1898)

Description of the cast

A cast has been made of the rhinoceros mold in order that its shape and symmetry can be effectively illustrated. Since it was necessary to have a casting medium which could maintain a certain rigidity and at the same time be detached from the porous walls of the mold, it was decided that a plaster-and-burlap technique of casting was most feasible.

CASTING PROCEDURE: The entire mold was first brushed out; then jellied soap was applied to its walls. Next, a moderately thin layer of burlap strips impregnated with quick-setting plaster was laid and shaped to the entire wall surface. This plaster-burlap layer was pressed tightly to the mold wall but was jammed into

the crevices between the basalt pillows only enough to indicate the position of each crevice. Any attempt to make an exact cast of the inter-pillow crevices would have made removal of the cast impossible and would have contributed nothing to the study of the shape of the mold as a whole. A system of removable wooden struts was constructed in order that the cast could be re-assembled to controlled dimensions after it was removed from the mold. These removable struts were bolted to wooden posts which were, in turn, anchored to the plaster-burlap walls. We were able to arrange one brace running longitudinally from rump to snout, two braces running dorsoventrally through the belly cavity, and one brace running transversely through belly cavity. Accessory struts were constructed so as to create triangles and give rigidity to the entire wooden support assembly.

Lines were cut or chiseled in the casting after the struts had been removed, and the individual pieces thus formed were removed from the mold. The front leg cavities could not be successfully cast by this method and had to be duplicated by a latex rubber casting. The re-assembled cast (Pl. 2) does not absolutely match the inside measurements of the mold but does not depart significantly from any true diameter.

THE HEAD: There is a strikingly rhinoceros-like contour and outline of the head and neck portion of the cast from all viewing positions. The somewhat elevated position of the head and neck and resultant straightness of the dorsal profile suggests a contraction of the dorsal neck muscles accompanying rigor mortis. The incompleteness of the mold in the nose region, due to the large inter-pillow openings, prohibits definite statements as to the presence or absence of paired nasal horns on the original. There is ample room in this part of the mold for the accommodation of such horns, however; and they may have been present. At any rate, the dorsal contour of the head of the cast positively indicates that no horns were existent posterior to the nasal region. The poorness of the cast in the region of the anterior tip of the head prevents us from interpreting the anteromedial eminence as a suggestion of a large and protruding upper lip. Again it may be stated that there is ample room for such a structure in this part and certain views of the cast are very suggestive of such a feature. Perhaps the most rhinoceros-like attribute of the head and neck region of the cast is the molding of the ventral outline of the mandible. The area of the symphysis and bifurcation of the horizontal rami are all positively suggested by the configuration of the ventral surface of the cast and are in a completely natural orientation. Constriction of the throat part of the cast immediately behind the angle region of the mandible authenticates the contention that this part is a relatively true casting of the neck of a rhinoceros. A series of rather small transverse ridges on the postero-ventral area of the neck suggests skin folds.

THE BODY: The shape of the main portion of the body is in accord with the animal likeness of the other parts. We believe that the original animal was much thinner than the absolute outline of the cast indicates. Heavy ridges dorsally and laterally situated are indisputably the aftermath of incomplete molding by the basalt pillows. General bulbousness of the abdominal area, with extra-abdominal shortening of the leg outlines, is interpreted as evidence that the animal was bloated when molded.

THE FRONT FEET: We have not yet cast the left front leg cavity inasmuch as bone still remains *in situ* there. The cast of the right front foot presents certain characteristics which are most allusive. Figures 3 and 4 of Plate 1 show the similarity of the cast to the foot of a modern rhinoceros. Strongest point of resemblance is the trace of a three-toed structure on the cast.

PLATE 1.—LEG CASTS

FIGURE 1. LATERAL VIEW OF CAST OF RIGHT HIND LEG OF *Diceratherium*? FROM THE BASALT MOLD × 1/6 approximately.

FIGURE 2. OUTLINE OF LEFT HIND LEG OF *Diceratherium annectens* (YALE UNIV. PEABODY MUS. NO. 730), IMPOSED ON OUTLINE OF CAST OF RIGHT HIND LEG OF *Diceratherium*? FROM BASALT MOLD × 1/4.

FIGURE 3. ANTERIOR VIEW OF CAST OF RIGHT FRONT LEG OF *Diceratherium*? FROM BASALT MOLD × 1/6 approximately.

FIGURE 4. DORSO-ANTERIOR VIEW OF FOOT OF A RECENT RHINOCEROS × 1/4 approximately.

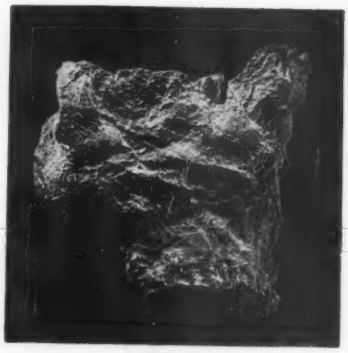

FIGURE 1

FIGURE 2

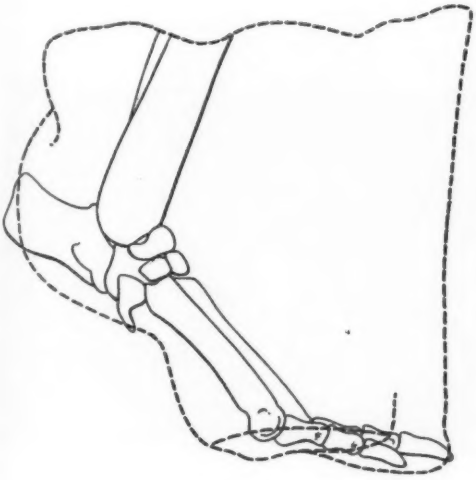

FIGURE 3

FIGURE 4

LEG CASTS

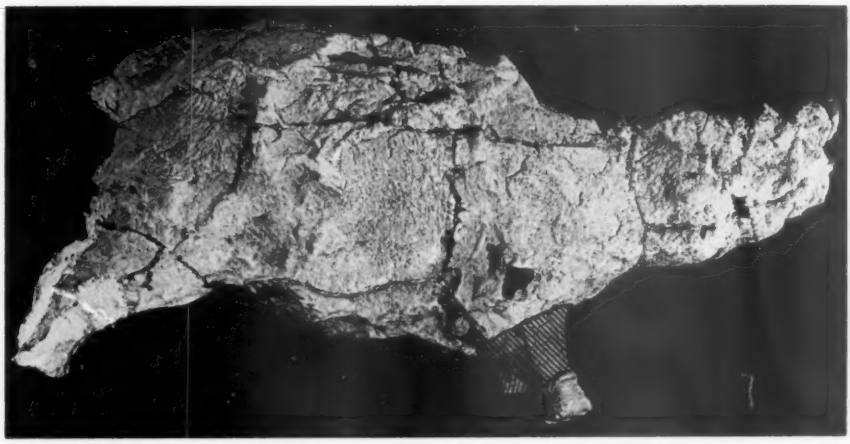

FIGURE 1

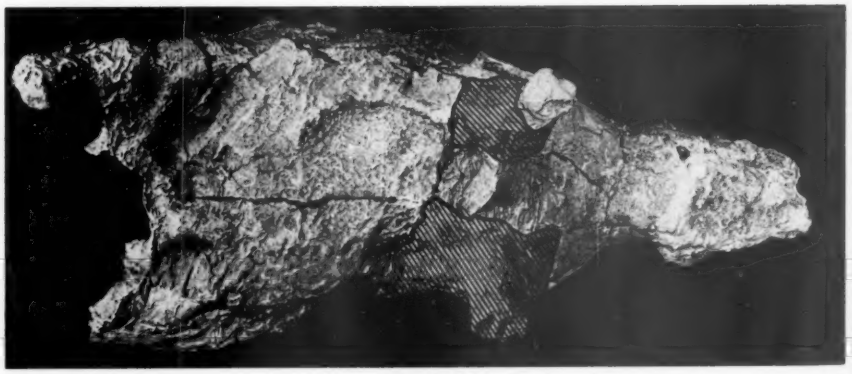

FIGURE 2

VIEWS OF THE CAST

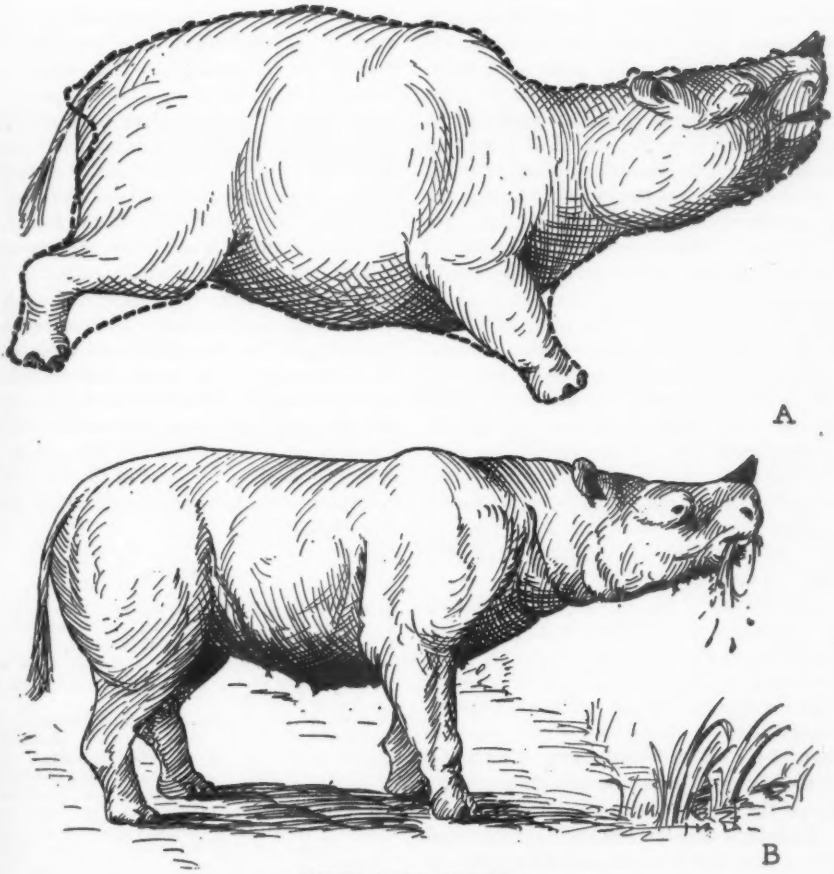

FIGURE 4.—RESTORATIONS

a. Possible bloated, death-pose of the Grand Coulee rhinoceros. Heavy dashed line represents actual outline of the cast. b. Possible appearance of the living Grand Coulee rhinoceros.

The lack of splay in the toe region of the cast may be accredited to comparative slenderness of the fossil beast and to the compressive effect of the molding lava. The front foot cast, however, does not alone offer incontrovertible proof of the rhinocerotoid quality of the mold.

THE HIND FOOT: The cast of the right hind foot is also very suggestive but is not convincing in itself (Pl. 1, fig. 1). The posterior knob clearly resembles the hock or tarsal joint; it is oriented as would be expected in a sturdily built, semi-rectigrade, sub-digitigrade, ambulatory quadruped. There is also a strong indication of a tripartite hoof shown in the distal surface of the cast. This hind leg cast seems to be a bit too short to match the proportions of a moderately built and fairly long-limbed dicerathere, such as is suggested by the accompanying bone frag-

PLATE 2.—VIEWS OF THE CAST

× 1/15 approximately

FIGURE 1. LATERAL VIEW OF THE CAST OF *Diceratherium?* FROM THE BASALT MOLD

FIGURE 2. VENTRAL VIEW OF THE CAST

Hachured areas are restored.

ments. Dr. Joseph T. Gregory of the Peabody Museum at Yale University has kindly allowed us to study a specimen of a left hind leg of *Diceratherium annectens* Marsh from the John Day fauna of Oregon. Figure 2 of Plate 1 shows an outline view of the foot of *D. annectens*, based on the Yale specimen, imposed upon the outline of the Grand Coulee cast. Although the *D. annectens* foot can be crowded into the area of the cast, it seems more likely that the Grand Coulee rhinoceros had a shorter metatarsus. In the position of alignment of bones in *D. annectens*, the distance from the back of the calcaneum to the distal tip of ungual phalanges is about equal to the distance from the back of the calcaneum to the knee joint (tibial length). The relative tibial length must have been greater on the Grand Coulee rhinoceros. We can only attempt to account for the stubbiness of the entire hind leg cast by postulating a bloated condition and a somewhat doubled-up or cramped-in position of the hind leg in the original animal.

RESTORATION OF THE ANIMAL: Figure 4a shows our restoration of the bloated death-pose of the rhinoceros in the mold; and Figure 4b is our concept of the living animal. It is most apparent that imagination must be exercised in the reconstruction of proportions of the proximal parts of the limbs, natural degree of rotundity of the abdominal region, and in the configuration of the eyes and ears.

We believe that the amazingly rhinocerotoid lines of the head and neck and the undeniably quadruped-like arrangement and proportions of the leg areas of the mold and cast—combined with the creditable record of the diceratherelike mandibular fragments from the mold cavity—offer convincing proof of our thesis that here is truly represented the lava mold of a rhinoceros.

Age Significance

Any assignment of geologic age to the lava flow which trapped the rhinoceros herein described must, of necessity, be only as precise as the categorical distinction of the entombed animal. By means of the osteological characters previously described, it has been concluded that the Grand Coulee rhinoceros is probably to be referred to the genus *Diceratherium*. Animals referred to the genus *Diceratherium* have been found in deposits ranging from Late Oligocene through Early Miocene in age. These attenuated criteria indicate, therefore, a Late Oligocene or Early Miocene age for the basalt enclosing the rhinoceros mold. The geologic relationships of this basalt to the "Excelsior Surface" of Scheid (1947) are unknown, but the age indications of this rhinoceros call attention to the fact that the Columbia River Basalts may range through a long time span, as originally suggested by Russel, rather than being restricted to the middle Miocene as is indicated by most present-day authors. The rhinoceros mold apparently occurs, however, within the upper few hundred feet of a basaltic series doubtless thousands of feet thick within the main lava basin. Thus, if our provisional identification of the animal is correct, even the later flows of this sequence, in this area, may be somewhat older than heretofore supposed.

REFERENCES

Beck, G. F. (1935) *Fossil-bearing basalts, more particularly the Yakima basalts of Central Washington*, Northwest Sci., vol. 9, no. 4, p. 4–7.

—— (1937) *Remarkable west American fossil, the Blue Lake rhino*, Mineralogist, vol. 5, no. 8 p. 7–8, p. 20–21.

Chappell, W. M., Durham, J. W., and Savage, D. E. (1949) *Rhinoceros mold in basalt*, Geol. Soc. Am. Bull., vol. 60, p. 1949 (abstract).

Fuller, R. E. (1931) *The aqueous chilling of basaltic lava on the Columbia Plateau*, Am. Jour. Sci., ser. 5, vol. 21, p. 281–300.

Matthew, W. D. (1931) *Critical observations on the phylogeny of the rhinoceroses*, Univ. Calif. Pub., Bull. Dept. Geol. Sci., vol. 20, pp. 1–2.

—— (1932) *A review of the rhinoceroses with a description of* Aphelops *material from the Pliocene of Texas*, Univ. Calif. Pub., Bull. Dept. Geol. Sci., vol. 20, p. 411–480 (Edited by R. A. Stirton).

Osborn, H. F. (1898) *The extinct rhinoceroses*, Am. Mus. Nat. Hist., Mem., vol. 1, p. 75–164.

Scheid, V. E. (1947) *Excelsior Surface—an Intra-Columbia River Basalt Weathering Surface*, Geol. Soc. Am. Bull., vol. 58, p. 1224–1225 (abstract).

Tyrrell, G. W. (1929) *The Principles of Petrology*, New York: P. Dutton and Company, Inc., pp. 1–349.

Wood, H. E. (1927) *Some early Tertiary rhinoceroses and hyracodonts*, Am. Paleont. Bull., vol. 13, p. 3–89.

CARACAS, VENEZUELA; MUSEUM OF PALEONTOLOGY, UNIVERSITY OF CALIFORNIA, BERKELEY, CALIFORNIA; MUSEUM OF PALEONTOLOGY, UNIVERSITY OF CALIFORNIA, BERKELEY, CALIFORNIA.

MANUSCRIPT RECEIVED BY THE SECRETARY OF THE SOCIETY, FEBRUARY 27, 1951.

BULLETIN OF THE GEOLOGICAL SOCIETY OF AMERICA
VOL. 62, PP. 919-930, 2 FIGS. AUGUST 1951

FURTHER BIOGEOCHEMICAL DATA FROM THE SAN MANUEL COPPER DEPOSIT, PINAL COUNTY, ARIZONA

By HARRY V. WARREN, ROBERT E. DELAVAULT, AND RUTH I. IRISH

ABSTRACT

Although the copper and zinc contents of plants in the vicinity of the San Manuel Copper Deposit are not particularly high, they are much higher than those of similar species in similar climatic areas remote from copper mineralization.

Some plants, notably California Poppy, Poppy, Paloverde, Creosote bush, and Scrub oak may be useful to the biogeochemist. Others, such as the Saguaro and Ocotillo, appear from this preliminary study to be less promising.

CONTENTS

	Page
Introduction	919
Acknowledgments	919
Analytical results	920
Discussion of results	923
Conclusions	924
References cited	924
Appendix	925

ILLUSTRATIONS

Figure	Page
1. Location of samples taken from the vicinity of San Manuel Outcrop	927
2. Approximate location of control samples taken in Arizona Desert	929

INTRODUCTION

In 1948 Dr. O. S. Lovekin called on the authors to discuss the general validity of biogeochemistry, some of our publications having been referred to in the daily press.

After some discussion, in the course of which we indicated our need for samples collected over copper ore bodies situated in a dry climate and our inability to collect any for ourselves, Dr. Lovekin volunteered to collect a suite for us.

In due course a suite from the San Manuel Mine and vicinity arrived. The analyses were made in routine fashion. When the resulting data had been correlated, they were most suggestive. Dr. Lovekin was informed of the results and a second collection of samples soon arrived. This collection contained samples from negative areas. The results of the earlier tests were confirmed and amplified.

We hesitated to publish without ourselves having even been on the ground, but the stimulating and valuable paper of Lovering, Huff, and Almond (1950) contained sufficient plant analyses to indicate that our work might be of interest.

ACKNOWLEDGMENTS

The authors are deeply indebted to Dr. O. S. Lovekin who went to a great deal of trouble to collect all the samples on which this paper is based, and to the officials of the San Manuel Mine who gave him permission to collect the samples.

The authors are also deeply indebted to The Geological Society of America for grants from the Penrose Bequest. These funds, together with more modest assistance from the President's Committee on Research of the University of British Columbia, and the cooperation of Dr. M. Y. Williams of the Department of Geology and Geography of the above University made this work possible.

Dr. H. E. Hawkes of the United States Geological Survey discussed the general problems of San Manuel with us and has throughout all our biogeochemical researches afforded us every kindness and consideration. The authors, however, assume full responsibility for all the ana-

lytical work and for the general conclusions arrived at in this paper.

Analytical Results

Samples were collected of plants growing (A) on the outcrops of oxidized San Manuel, (B) on areas nearby and on "washes" draining the oxidized ground, and (C) on ground thought to be free from any mineralization of economic significance.

In all the tables results are given in both parts per million—p.p.m.—of dried plant material and in p.p.m. of ash. Where Lovering, Huff, and Almond (1950) have given results which are comparable, they are inserted in braces. Following our own custom, we also give the copper: zinc ratios, which is consistently higher in this relatively dry area than in most parts of British Columbia.

(a) California Poppy. (*Eschscholtzia mexicana*)

Sample No.	Organ	p.p.m. of dry plant Cu	p.p.m. of dry plant Zn	Ratio Cu:Zn	p.p.m. of Ash Cu	p.p.m. of Ash Zn	% Ash
		A. Over Oxidized Outcrop					
P.1.	Flowers	32	52	.62	310	500	10.3
P.2.	Leaves & Stems	32	66	.48	210	420	15.6
{ ?		75	50	1.50	—	—	— }
		C. Remote from Known Mineralization					
P. 4.	Flowers	11	63	.17	110	630	10.1
P. 3.	Leaves & Stems	12	153	.08	80	1000	15.0

It will be noted that the positive samples contain two to three times the copper content of the negative ones and that the copper to zinc ratio is even more conspicuously higher.

(b) Palo Verde (*Cercidium microphyllum*)

Sample No.	Organ	p.p.m. of dry plant Cu	p.p.m. of dry plant Zn	Ratio Cu:Zn	p.p.m. of ash Cu	p.p.m. of ash Zn	% Ash
		A. Over Oxidized Outcrop.					
P.V.I.	6″ tips	11	19	.58	180	300	6.2
{ ?		30	15	2.00	300		}
P.V.I.	Prickles 1″ or less	10	14	.91	130	190	7.5
		C. Remote from Known Mineralization.					
P.V.2.	6″ tips	6	26	.23	130	550	4.7
P.V.9.	4″ or less tips	7	40	.17	170	1000	4.0
P.V.9.	Prickles 1″ or less	7	38	.18	170	900	4.1
P.V.9.	Bark	3	11	.27	14	100	10.6
P.V.10	4″ or less tips	7	18	.42	190	450	4.0
P.V.10	Prickles 1″ or less	7	17	.41	170	410	4.1
P.V.10	Bark	5	19	.26	40	170	11.4
P.V.12	4″ or less tips	6	14	.40	55	130	11.0
P.V.12	Bark	4	10	.45	30	70	15.0

It should be noted that, although the copper content of the ash of the two sets of samples is not very different, the copper content of the dry plant and the copper:zinc ratio of the two sets do differ. Furthermore these differences are of the same general order, upwards of 50 per cent above the "normals" for the area, as we have found in British Columbia.

(c) Creosote bush (*Larrea tridentata*)

Sample No.	Organ	p.p.m. of dry plant Cu	p.p.m. of dry plant Zn	Ratio Cu:Zn	p.p.m. of ash Cu	p.p.m. of ash Zn	% Ash
		A. Over Oxidized Outcrop.					
G. 1	Stems of tips <4″	30	17	1.82	410	230	7.25
G. 1	Leaves of tips <4″	28	20	1.36	290	210	9.7
?		35	25		350		
G. 15	Tips 1″ long, No flowers or fruit	27	24	1.1	370	330	7.2
G. 15	Leaves	41	28	1.50	410	280	9.9

B. Areas near Oxidized Outcrops.

Sample No.	Organ	p.p.m. of dry plant Cu	p.p.m. of dry plant Zn	Ratio Cu:Zn	p.p.m. of ash Cu	p.p.m. of ash Zn	% Ash
G. 2	Stems of tips <4″ long	15	18	.86	210	250	7.0
G. 2	Leaves from above	14	17	.82	180	220	7.85
G. 3	Stems of tips <4″ long	35	31	1.11	420	380	8.25
G. 3	Leaves from above	25	24	1.04	260	250	9.8
G. 4	Stems of tips <4″ long	18	15	1.24	210	170	8.5
G. 4	Leaves from above	13	16	.84	150	180	8.7
G. 13	Tips 1″ long +	21	35	.60	210	350	10.2
G. 13	Leaves	28	29	.96	220	230	12.5
G. 14	Tips 1″ long +	35	32	1.10	330	300	10.5
G. 14	Leaves	30	16	1.90	270	140	11.1
G. 16	Tips 1″ long +	20	50	.40	210	520	9.5
G. 16	Leaves	18	20	.90	190	210	9.6
G. 17	Tips 1″ long +	19	22	.85	230	260	8.4
G. 17	Stems 1–6 years old	25	25	1.00	270	270	7.8
G. 17	Leaves	23	27	.62	250	400	9.3
G. 18	Tips 1″ long +	14	19	.74	190	260	7.4
G. 18	Stems 1–6 years old	24	27	.89	310	350	7.7
G. 18	Leaves	8	19	.42	90	210	9.0
G. 19	Tips 1″ long +	31	30	1.00	370	360	8.4
G. 19	Stems of last 2 years	26	34	.78	340	430	7.7
G. 19	Stems 3–7 years old	34	31	1.10	390	360	8.6
G. 19	Leaves	37	38	1.00	380	390	9.6
G. 20	Tips 1″ long +	40	29	1.40	460	340	8.6
G. 20	Stems of last 2 years	30	68	.44	360	810	8.4
G. 20	Stems 3–7 years old	43	22	2.00	610	310	7.0
G. 20	Leaves	46	23	2.00	410	220	11.2

Note: + containing no flowers or fruit.

*C. Areas Remote from Known Mineralization**

Sample No.	Organ	p.p.m. of dry plant Cu	Zn	Ratio Cu:Zn	p.p.m. of ash Cu	Zn	% Ash
G. 5	Stems of tips <4″ long	10	17	.61	140	230	7.25
G. 5	Leaves from above	10	20	.50	140	280	7.25
G. 6	Stems of tips <4″ long	10	16	.62	140	230	7.05
G. 6	Leaves from above	11	18	.61	120	220	8.8
G. 7	Stems of tips <4″ long	26	16	1.68	380	220	6.9
G. 7	Leaves from above	20	17	1.20	250	210	8.15
G. 8	Tips 1″ long +	10	53	.19	140	730	7.2
G. 8	Stems of last 2 years	8	54	.15	140	930	5.8
G. 8	Stems 3–7 years old	7	46	.15	150	1000	4.5
G. 8	Leaves	6	42	.14	60	440	9.5
G. 9	Tips 1″ long +	6	17	.35	75	210	7.9
G. 9	Stems of last 2 years	8	50	.16	120	730	6.8
G. 9	Stems 3–7 years old	7	52	.13	130	1000	5.6
G. 9	Leaves	3	17	.18	35	200	8.5
G. 10	Tips 1″ long +	9	32	.28	110	400	8.1
G. 10	Stems of last 2 years	10	20	.50	100	200	6.8
G. 10	Stems 3–7 years old	10	23	.45	140	300	7.7
G. 10	Leaves	7	22	.32	80	240	9.0
G. 12	Tips 1″ long +	5	20	.25	70	270	7.4
G. 12	Stems of last 2 years	8	37	.23	110	490	7.5
G. 12	Stems 3–7 years old	9	29	.31	120	390	7.4
G. 12	Leaves	4	22	.18	45	250	7.4
G. 21	Tips 1″ long +	14	18	.78	120	160	11.5
G. 21	Stems 1–6 years old	9	22	.40	90	210	10.4
G. 21	Leaves	10	24	.42	70	170	14.3
G. 22	Tips 1″ long	16	27	.60	200	330	8.2
G. 22	Stems 1–6 years old	18	34	.53	230	430	7.8
G. 22	Leaves	14	27	.52	130	260	10.4
G. 23	Tips 1″ long	27	42	.64	240	370	11.3
G. 23	Stems 1–6 years old	22	22	1.00	210	210	10.4
G. 23	Leaves	24	31	.77	180	230	13.6

Notes. + containing no flowers or fruit.

* Although at the time these samples were taken they were all thought to be from negative areas, Dr. Lovekin has since ascertained that samples No. 7 and 22 definitely come from a locality where drilling has disclosed significant copper mineralization. Number 23 came from the dry bed of the Gila River which drains a large area of south Arizona, including many mineralized areas. The values from this sample, therefore, probably simply show that there is copper somewhere upstream—an obvious fact.

(d) Scrub Oak (*Quercus turbinella*)

Sample No.		p.p.m. of dry plant Cu	Zn	Ratio Cu:Zn	p.p.m. of ash Cu	Zn	% Ash
		A. Over Oxidized Outcrop					
Oak 1.	Leaves	42	27	1.5	1100	700	3.9
"	Stems, new	38	40	.95	1100	1100	3.6
"	Stems 1 year old	36	32	1.1	800	700	4.4
"	Stems 2 years old	30	24	1.2	800	600	3.8
		15	20	.75	500		
		C. Remote from Mineralization					
Oak 2.	Leaves	9	23	.4	250	640	3.6
"	Stems, new	6	14	.4	150	340	4.1
"	Stems 1 year old	6	18	.3	150	450	4.0
"	Stems 2 years old	7	22	.3	190	600	3.7

We understand that only one oak was growing over the oxidized outcrop, so that it was not practical to collect a more representative positive sample. However the above results are comparable with those obtained under such entirely different climatic conditions in British Columbia and it would seem worthwhile to investigate further the oak tree as a biogeochemical tool in relatively arid areas.

(e) Saguaro (*Cereus giganteus*)

B. From Areas near Oxidized Outcrop and "Washes" Draining Oxidized Outcrops

Sample No.	Organ	p.p.m. of dry plant Cu	Zn	Ratio Cu:Zn	p.p.m. of ash Cu	Zn	% Ash
S. 1.	¼″ thin prickles	15	45	0.33	260	780	5.75
S. 1.	Marrow	24	6	4.0	160	40	15.0
S. 1.	Bark	18	7	2.6	190	70	9.3
S. 2.	2″ prickles	5	27	0.2	420	2100	1.3
S. 2.	1″–2″ prickles	14	45	0.31	610	1900	2.3
S. 2.	¼″ thin prickles	10	27	0.4	400	1200	2.25
S. 2.	Marrow	21	10	2.1	70	30	30.0
S. 2.	Bark	8	26	0.31	60	180	14.1
?		60	55		350		

The high ash content of the marrow material and the relatively low copper content of both ash and marrow are of interest and indicate the need for designating the organ which is being sampled.

The sample analysed by Lovering and his associates contains comparable amounts of copper to the samples collected by Lovekin.

(f) Ocotillo (*Fouquieria splendens*)

B. From Areas near Oxidized Outcrop and "Washes" Draining Oxidized Outcrops

Sample No.	Organ	p.p.m. of dry plant Cu	Zn	Ratio Cu:Zn	p.p.m. of Ash Cu	Zn	% Ash
Oc. 1.	Stem	24	18	1.3	620	470	3.85
"	Leaves	15	25	.6	120	190	13.0
Oc. 2.	Stem	26	40	.65	320	490	8.1
"	Leaves	14	20	.7	110	160	12.8
	C. From Areas Supposedly Uncontaminated by Mineralization						
Oc. 3.	Stem	9	15	.58	190	330	4.7
"	Leaves	25	23	1.1	170	150	15.0

The above three samples are useful only to indicate how in a general way this species of cactus apparently tends to carry similar amounts of copper and zinc to the Saguaro.

Discussion of Results

This investigation was undertaken primarily to test whether extra supplies of trace elements in the soil would be reflected in the vegetation of an arid area in the same manner as they are in a humid area.

The plants which we investigated fit into three groups: (1) The Poppy, Creosote bush, and Scrub oak are similar in build to plants in areas of average humidity. They, or close relations, can all grow in relatively humid areas. All of these species appear to respond in much the same manner as all the species so far investigated in Canada. (2) The Paloverde, a practically leafless thorny plant has in common with the preceding group special adaptations for drought conditions by its ability to reduce water losses and by fetching water from far

underground. Its boughs could be expected to behave like the preceding group, and they appear to do so. (3) The two cacti sampled, Ocotillo and Saguaro, both soak up quickly any water which may come their way and then store it most efficiently. It is difficult to know what organ to sample and how to go about sampling it. Furthermore they cannot really be compared with those plants which have an entirely different type of water circulation. We had no specimens from the oxidized outcrop area and too few samples for any final conclusions to be drawn. Nevertheless it seems that the copper and zinc content of their organs is comparable to that found in the organs of the plants found in humid areas.

It should be evident from the small number of samples taken that we had no ambition to undertake a survey of the area but only to make a modest experiment on the possibility of extending the uses of biogeochemistry to a new climate. So far no copper mine has been discovered in the drier areas of British Columbia, so these experiments could not be conducted there.

Thus even in an area like San Manuel, where Lovering and his associates have demonstrated that soil testing probably is superior to biogeochemistry in searching for hidden ore, biogeochemistry should not be overlooked as a potential prospecting tool.

Conclusions

The California poppy, the Scrub oak, the Paloverde, and the Creosote bush all tend to show variations in their copper content over a mineralized area as contrasted to nonmineralized areas. These variations are of the same general order of magnitude as those found in many species of trees and lesser plants similarly located in humid areas.

In carrying out biogeochemical investigations, it is important always to make comparisons between the mineral content of specific organs because the mineral content of the various organs varies greatly.

References Cited

Lovering, T. S., Huff, L. C., and Almond, H. (1950) *Dispersion of Copper from the San Manuel Copper Deposit, Pinal County, Arizona.* Econ. Geol., vol. 45, No. 6, p. 493–514.

The University of British Columbia, Vancouver, B. C., Canada

Manuscript Received by the Secretary of the Society, February 15, 1951.
Project Grant 499-46-S47

APPENDIX

*Localities from which Specimens were Collected**

* All samples collected April 24, 1949, except those numbered 1 to 7, which were collected on March 13, 1949.

A. Samples from Vicinity of San Manuel Outcrop.

"G".....creosote bush, or "grease-wood"
"PV".....Palo verde
"Oc".....Ocotillo
"S".....Saguaro
"Oak"....Oak.

G 1 PV 1	From outcrop at S.E. corner.
S 1	From dry wash draining S.E. part of outcrop area, about 150 yards below G 1.
G 13	From same dry wash, about 200 yards below G 1.
Oc 1	From same dry wash, about 300 yards below G 1.
G 18	From crest of ridge about 200 yards S.W. from G 13. No drainage from outcrop area affects this location. The main ore body is beneath it but presumably so deep that no plant roots would reach it.
G 14 Oc 2	From top of hill above outcrop area, about 30 yards from its S.W. border. Same comment as for G 18.
G 15	From outcrop at its N.W. border. Immediately under this bush is an excavation about 15 feet deep showing the ore. The drainage from this pit, however, is away from the bush, down the wash.
Oak 1	From North edge of outcrop. A short tunnel has been drilled into the ore in the hillside right beside this tree, and the wash draining the south side of the outcrop area also goes right by it.
G 16	From wash draining North side of outcrop, about 200 yards below Oak 1.
G 19	From wash around the corner of the small ridge to North of outcrop area. Presumably no part of the outcrop drains into this wash.
G 20 S 2	From hillside of "Red Hill" about 200 yards N.E. of G 19.
G 17	From wash on S.E. side of "Red Hill".
G 2	From hillside about 300 to 400 yards down the ridge from the outcrop.
G 3	From wash, 30 or 40 feet below G 2. This wash receives the one draining the south and west side of the outcrop.
G 4	From wash about half a mile below outcrop.
G 5	From hillside 50 to 60 feet above G 4.

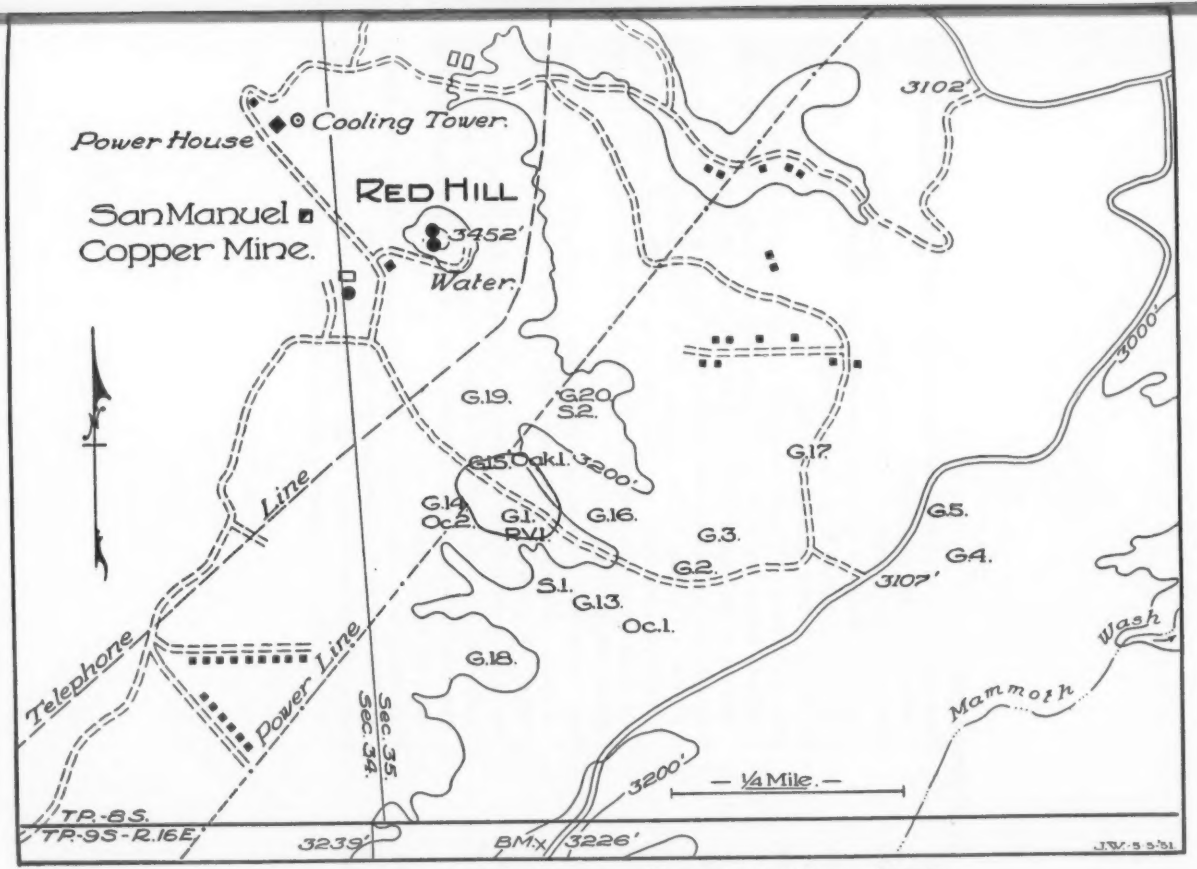

F GURE 1. LOCATION OF SAMPLES TAKEN FROM VICINITY OF SAN MANUEL OUTCROP
Shaded portion near center of map.
The map is a photographic enlargement of U. S. Geological Survey Map, Mammoth, Arizona, 1949 edition. Symbols as given in appendix.

B. Control Samples, Arizona Desert.

G 6	From roadside about 5 miles out of Tucson, on Oracle Road. Exact location not noted, but it was on a hillside.
G 21	From north side of road, 7.7 miles N.W. of Oracle Junction on Route 89. On a gently sloping plain, no washes in the immediate vicinity.
G 22	Same, but 8.1 miles N.W. of Oracle Junction.
G 7	Believed to be from area close to G 22.
G 23	From north bank of Gila River, about an eighth of a mile downstream from highway bridge just north of Florence. (The first clump of creosote bushes growing on the bank, downstream from the bridge.) Alluvial silt soil.
G 8	From alluvial plain in lower Gila River Valley, several miles distant from either the Gila or Colorado Rivers, 9.4 miles east of Yuma on Highway 80. Alluvial silt soil. No watercourse near. (Distances from "Yuma" refer to distances from the Plant Quarantine Inspection station at the western end of the Colorado River bridge, in California.)
G 9 PV 9	From bottom of dry wash south of road at foot of Telegraph Pass, 19.9 miles east of Yuma. This wash drains surrounding hills for a distance of two or three miles. Soil: gravel and silt.
G 10 PV 10 Oc 3	From steep, rocky hillside south of road in Telegraph Pass, about 75 feet above wash. Drainage from small area of hillside only. Location 21.3 miles east of Yuma on Highway 80, also .7 miles west of summit of Telegraph Pass. Soil: rocks and hillside gravel.
G 12 PV 12	From wash at south side of Highway 80, 128.4 miles east of Yuma. Soil: Alluvial silt. This wash drains a large area of neighbouring desert.
Oak 2	From gently sloping hillside 1.1 miles north of Oracle Post Office on Route 77. Soil: apparently decomposed granite. No known mineral near.

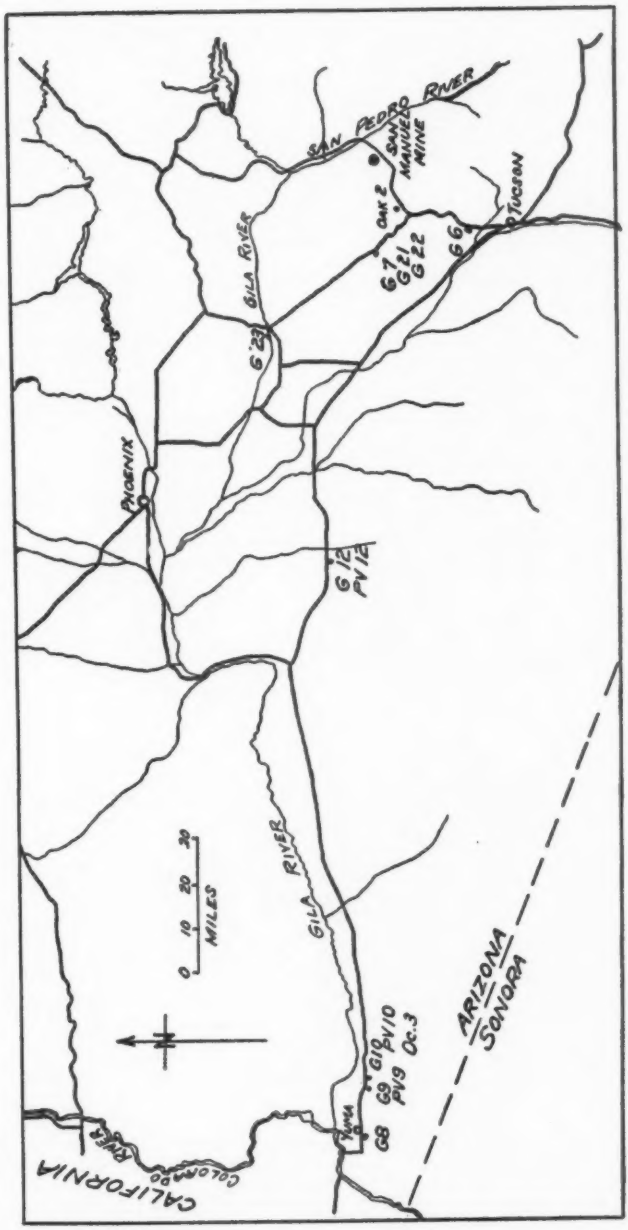

FIGURE 2. APPROXIMATE LOCATION OF CONTROL SAMPLES TAKEN IN ARIZONA DESERT.
Symbols as given in appendix.

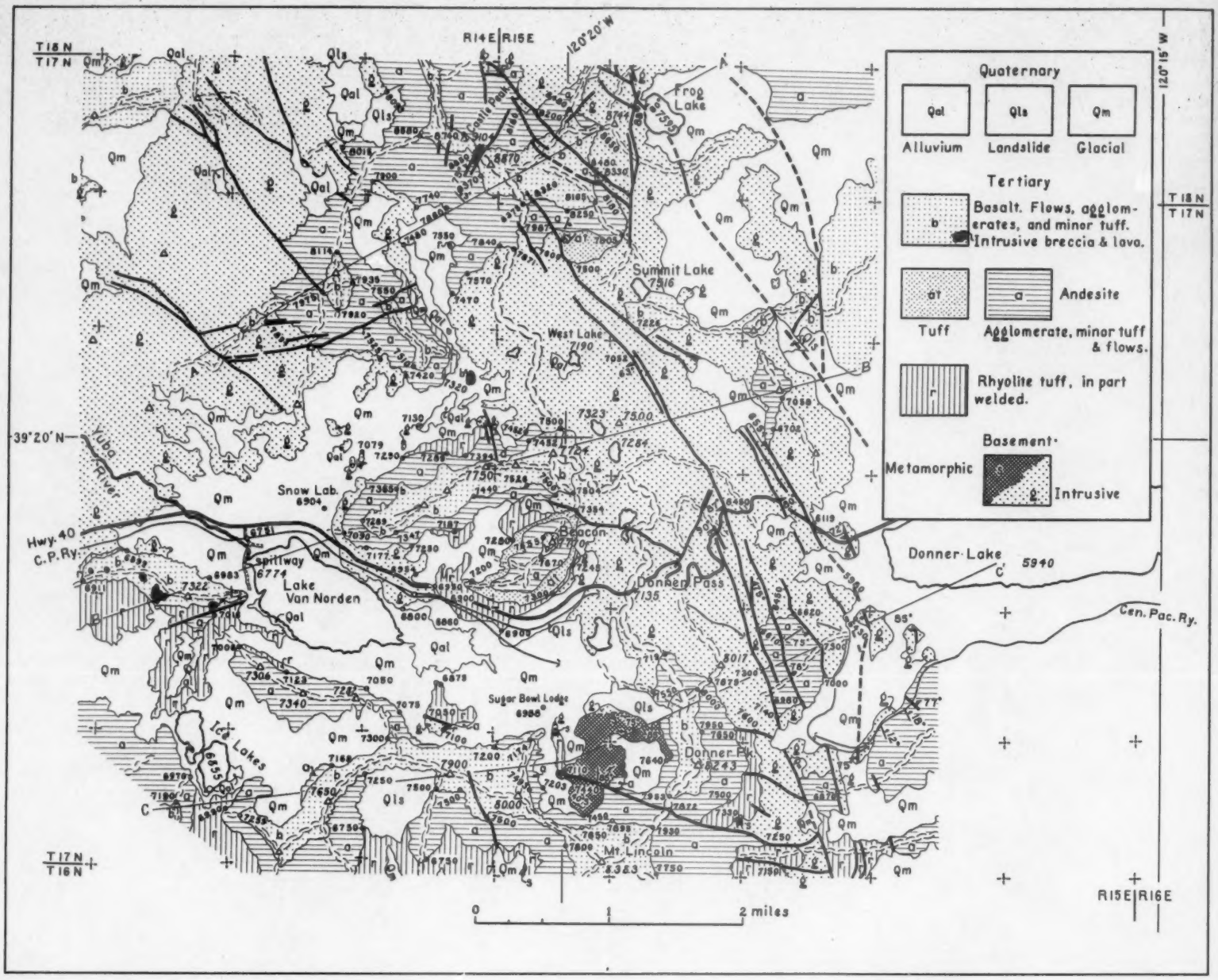

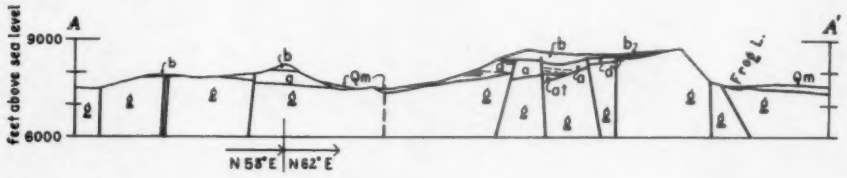

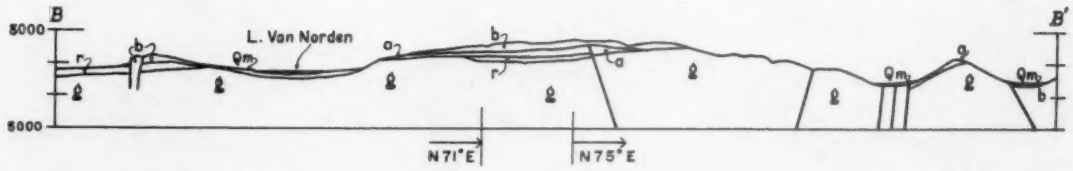

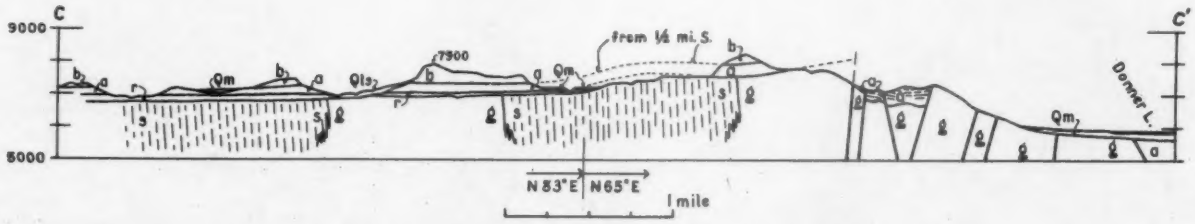

GEOLOGIC MAP AND STRUCTURE SECTIONS OF MT. LINCOLN - CASTLE PEAK AREA

BULLETIN OF THE GEOLOGICAL SOCIETY OF AMERICA
VOL. 62, PP. 931-952 2 FIGS., 2 PLS. AUGUST 1951

MOUNT LINCOLN-CASTLE PEAK AREA SIERRA NEVADA, CALIFORNIA

BY F. S. HUDSON

ABSTRACT

The formations of this region are separated by major unconformities into three divisions of equal areal extent: (1) Basement, composed of metamorphosed sediments intruded by granite and more basic rocks, (2) Tertiary, including middle Eocene stream gravel, overlain by rhyolitic, andesitic, and basaltic deposits, of middle Eocene, Miocene, and Pliocene age, and (3) Quaternary, made up of glacial, landslide, and alluvial materials.

The Tertiary volcanic deposits are separated by lesser unconformities. These, and the major post-basalt unconformity, resulted from episodes of compressive deformation which recurred from middle Tertiary to post-Pliocene time along the Donner zone, which extends north-northwest for 15 miles or more along the crest of the range. Median in this zone, but not persisting throughout its length, is its dominant element, a west-dipping reverse fault, on either side of which are genetically related faults and folds.

Bounding the Donner zone on the east is a belt of east-dipping normal faults, some 2 miles wide, which originated in late Quaternary time, after the last compressive deformation.

The Donner zone originated as a fold in metamorphic rock. With progressive deformation, the surrounding granite accommodated itself by reverse faulting which was thereafter the dominant activity. During compressive episodes there was folding of both Tertiary and basement where the latter is metamorphic rock, and faulting of both where the basement is granite. However, where younger Tertiary rests unconformably on previously faulted older Tertiary, the younger formation was deformed by folding as well as faulting.

CONTENTS

	Page
Introduction	932
Acknowledgements	933
Topography and drainage	933
Geologic formations	933
General statement	933
Basement rocks	933
Pre-volcanic Tertiary gravel	934
Rhyolite	936
Post-rhyolite erosion	939
Andesite tuff	939
Pre-andesitic agglomerate deformation and erosion	939
Pre-agglomerate surface	940
Andesite agglomerate, with minor tuffs and flows	940
Post-agglomerate deformation and erosion	941
Basalt of the Truckee Quadrangle	941
Basalt of Mt. Lincoln-Castle Peak area	942
Geologic age of the volcanic series	943
Quaternary deposits	945
Structure	946
General statement	946
Basement structure	946
Donner Pass zone	946
General description	946
Main reverse fault	948
Donner zone east of main fault	948
Donner zone west of main fault	948
Dates of activity of main fault	949
Castle Peak faults	949
Normal Faulting east of Donner zone	950
Late normal faulting within Donner zone	950
Summary of orogenic events in Donner zone	950
Conclusions	950
References cited	952

ILLUSTRATIONS

Figure	Page
Key map. Central Sierra Nevada	932
Structure sketch. Squaw Peak-Castle Peak area	935

Plate	Facing page
1. Geologic map and structure sections of Mt. Lincoln-Castle Peak area	931
2. Castle Peak	932

Introduction

Donner Pass and the adjacent Summit Valley on the west afford the most direct route from the east to the Great Valley of California. One of the main wagon trails of the Argonauts used it; the builders of the first transcontinental railway found it preferable to lower passes to the north; and it is now traversed by Highway 40, the principal road from San Francisco to Nevada and other states to the east.

Few who travel through the pass pause long enough to appreciate the grandeur of the well-named Castle Peak, a few miles to the north, or the rugged bulk of Mt. Lincoln to the south. The region suffered even greater neglect by geologists for many years following Lindgren's (1897) work. This is surprising because not only is the landscape grand, but the geologic features are worthy of careful study.

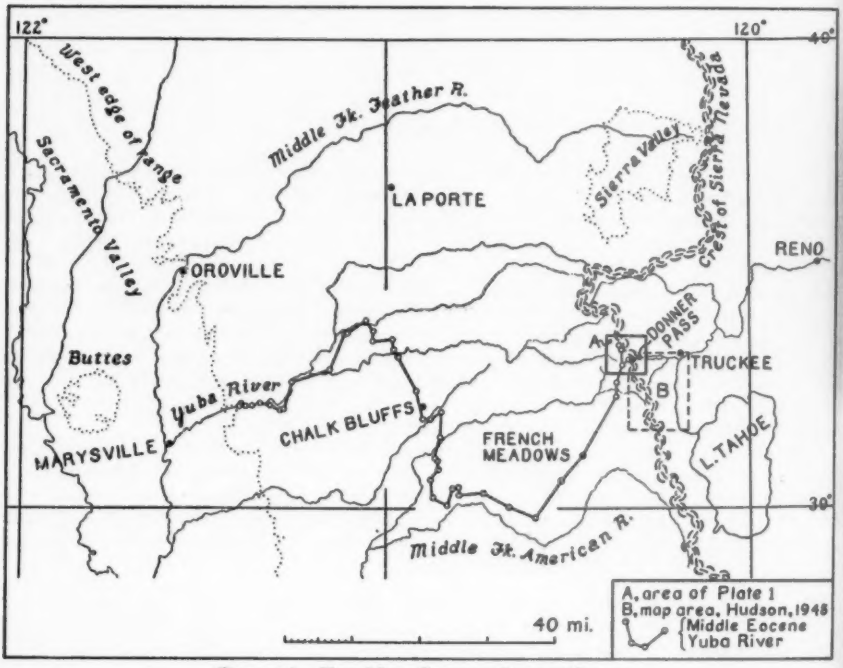

FIGURE 1.—KEY MAP. CENTRAL SIERRA NEVADA

This paper deals especially with an area of the summit region of the Sierra Nevada extending northerly from Mt. Lincoln across the pass to Castle Peak, a distance of 6 miles (Fig. 1; Pl. 1). The main objective was to carry on to the north the study of deformation of the Tertiary formations in the region south of the pass (Hudson, 1948). It was found that the structural problems could not be solved without a thorough investigation of the nature and age relationships of the Tertiary volcanics and

PLATE 2. CASTLE PEAK

View from 2.4 miles south. f_1 = Castle Peak faults, f_2 = minor faults; b = basalt, a = andesite agglomerate, g = granite

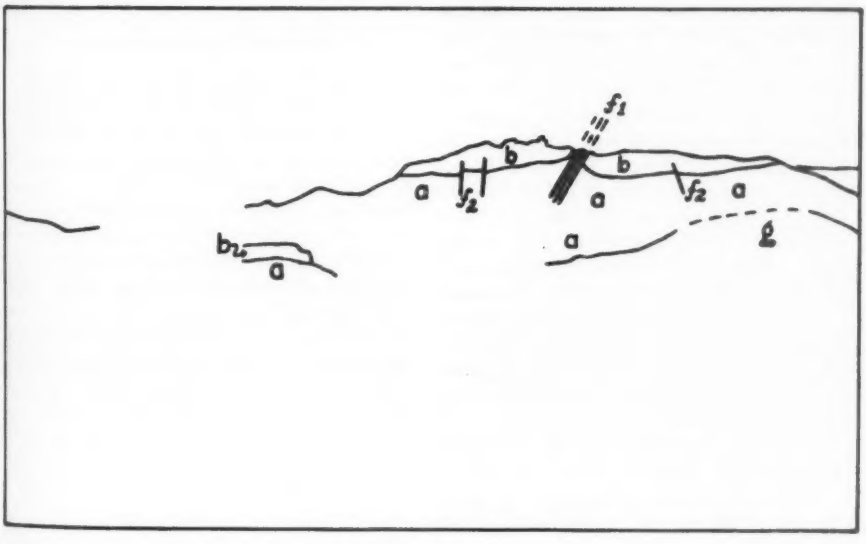

CASTLE PEAK

stream
objectiv
There
which a
geologic
the field
graphs
net of
Forest
part fro
Survey,
Enginee
ings adj

The
discussi
C. Dur
Olaf P.
Turner.
The
work w
Geologi

The
water p
Pacific
westerly
area (P
of peaks
by sadd
level. T
those o
north si
cipitous
glacial
declivity
east of
8744-foo
1149 fe
Rugg
of the p
bifurcat
3 miles
which
are shor
the peal
There
valleys

stream gravels, so this was made the second objective.

There are no contour maps of the region which are useful for detailed geologic work. The geologic map (Pl. 1) was made by transferring the field observations recorded on aerial photographs to a base prepared from the geographic net of the Donner Pass quadrangle of U. S. Forest Service. The elevations shown are in part from determinations by U. S. Geological Survey, Central Pacific Railway, and U. S. Engineers, and in part from barometric readings adjusted to the former, more precise data.

Acknowledgements

The writer is grateful for ideas gained in discussions with R. W. Chaney, A. C. Daley, C. Durrell, C. M. Gilbert, C. P. Holdredge, Olaf P. Jenkins, N. L. Taliaferro and F. J. Turner.

The expense of the greater part of the field work was defrayed through a grant of the Geological Society of America.

Topography and Drainage

The summit line of the Sierra Nevada, the water parting between the Great Basin and the Pacific Ocean, passes with sinuous north-northwesterly course through the center of the map area (Pl. 1). This divide is made up of a series of peaks, 7724–9104 feet in elevation, separated by saddles which lie 7135–7872 feet above sea-level. The higher peaks have the steeper flanks, those on the south side of Castle Peak and the north side of Mt. Lincoln being especially precipitous. These localities are at the heads of glacial cirques, as is also a place of even greater declivity which overlooks Frog Lake, a mile east of the divide. Here the descent from the 8744-foot peak to the west edge of the lake is 1149 feet in less than a quarter of a mile.

Rugged spur ridges extend westerly from all of the peaks save Donner. Most of these ridges bifurcate one or more times in passing some 3 miles west to the edge of the map. The spurs which diverge eastward from the main divide are shorter and steeper, and do not originate at the peaks.

There are lacustral basins in the principal valleys between the spurs on both sides of the divide. Bodies of water have persisted in three of these: Donner, Frog, and Ice lakes. The others have been emptied through recent downcutting of the glacial deposits or granite which formed their lips. Summit Valley, the largest west of the divide, is the head of South Fork of Yuba river. It is now partially occupied by the artificial Lake Van Norden.

All of the area east of the divide drains into Truckee river. Most of the runoff west of the summit goes into the Yuba river, but Ice Lakes and the country south of the Mt. Lincoln spur ridge feed the American river.

Geologic Formations

General Statement

The general sequence of formations of the northern Sierra Nevada was established 50 odd years ago by Lindgren and Turner in their series of Gold Belt folios (Lindgren and Turner, 1895; Turner, 1897, 1898). They divided the rocks into the pre-Tertiary Bed Rock Series, composed of Jura-Trias and Paleozoic metamorphosed sediments and volcanics invaded by deep-seated intrusives, and, above a great unconformity, the Superjacent Series. The latter included in ascending order pre-volcanic auriferous gravels, rhyolite, older basalt, andesite, and younger basalt. They believed the younger basalt to be Pleistocene and the older members of the Superjacent Series to be Neocene. It now appears that this series extends from middle Eocene through Pliocene. In the present paper, *basement* is used for the pre-Tertiary rocks and *Tertiary* for the Superjacent Series.

In the Donner-Castle Peak region all of the basement and Tertiary formations recognized by Lindgren and Turner are present, except the older basalt. These are overlain by Quaternary deposits of glacial, landslide and alluvial origin.

The three major divisions, basement, Tertiary and Quaternary, each occupy about a third of the ground surface within the map area (Pl. 1).

Basement Rocks

Metamorphic (s) rocks are exposed at three localities in the area. The largest exposure, immediately west of Donner Peak, extends

half a square mile and exhibits thinly bedded calcareous shale, limestone, and quartzite, which have suffered the hornfels type of alteration. It is overlain to the south by the thick pile of Tertiary volcanics that forms Mt. Lincoln, and is doubtless coextensive with the small outcrop of metamorphic rock which appears under the volcanics three-fourths of a mile west of that peak and with the large mass of metamorphics whose outcrop extends 6 miles southeasterly from the south side of the peak (Hudson, 1948, Pl. 1). The correlation of these metamorphic rocks by Lindgren (1897, p. 2) with his Jura-Trias Sailor Canyon formation seems sound.

The third occurrence of metamorphic rocks is immediately below the rhyolite, half a mile S.60°E. of Donner Peak. Here is a sliver of quartz-biotite schist enclosed in granitoid rock. This schist is quite different from the Sailor Canyon hornfels. It is thought that it is of pre-Mesozoic age, having become schistose before the invasion of the enclosing rock.

The predominant rock of the deep-seated intrusives is granite, but other types occur, ranging in composition from quartz diorite to gabbro. Rocks devoid of quartz were seen in only two areas, too small to show on the map. At one of these, on the highway seven-eighths of a mile west of Donner Pass, the road cuts through a landslide to expose rhyolite tuff underlain by diorite. The other is in the midst of morainal deposits, three-eighths of a mile south of Sugar Bowl Lodge, where gabbro and metamorphic rock are exposed in the creek channel.

The prevailing rock for a mile north and northeast of Donner Pass is granite. It is in part porphyritic, with phenocrysts of orthoclase as large as half an inch in maximum diameter, in a groundmass of medium granularity, composed of quartz, biotite, orthoclase and sparse oligoclase. To the east, as far as Donner Lake, quartz diorite is the prevalent rock. Much of it is porphyritic, with plagioclase phenocrysts up to three-quarters inch maximum diameter in a medium to coarse groundmass of quartz, plagioclase and biotite. It is cut by dikes of pegmatite, which consist of albite, quartz and, rarely, black tourmaline.

On the east, south, and southwest edges of the auto park, half a mile east of the pass, there are numerous dark inclusions in the granodiorite. Their outlines are usually rounded, and even when angular, are nearly equant, with diameters ranging from 3 to 18 inches. They consist of a mixture of biotite, quartz, and feldspar, with grain much finer than that of the host rock. There seems to be no linear or planar arrangement, save that the base of the zone of abundant segregations dips northwest at a moderate angle. These inclusions appear similar to those of the Big Bend locality, 10 miles west of the pass on south side of Yuba river (Pabst, 1928).

The terms granite and granitic rock are used for all quartz-bearing, holocrystalline, intrusive rocks, with the unexpressed qualification that such rocks may be more basic than granite.

Pre-Volcanic Tertiary Gravel

This was seen at only one locality, in an outcrop too small to show on the map, immediately beneath the 7245-foot elevation station, a quarter of a mile southeast of Beacon Peak. Here, 13 feet of coarse gravel rests on granite at 7232 feet above sea level. It is overlain by rhyolite tuff which laps onto the granite within short distances to north and south. The tuff is the lower formation of a series of volcanic deposits which, with the basement surface, dips southwest at appreciable angles, 4.8° for the basement and 2.9° for a cliff-forming member of welded rhyolite tuff.

The lower part of the gravel is made up of rounded boulders of granite, up to 3 feet in diameter, in coarse granite grit. Higher in the deposit, the boulders are progressively smaller, and the highest part of the gravel consists of well-rounded pebbles and boulders, up to 3 inches in diameter, of quartz and quartzose granite.

The less quartzose of the large boulders are decayed to the point of crumbling readily, as is the basement granite; the more quartzose large boulders seem quite fresh. There is, however, no development of clay or anauxite, bleaching of the biotite, or other sign of chemical decay in either basement or boulders. The shocks incident to transportation would reduce such decayed boulders to sand in a few feet of travel. Obviously the decomposition of the

boulders occurred after their deposition. The decay of the basement being physically similar to that of the boulders, it, too, probably happened after the gravel transportation ceased. These conclusions are contrary to the prevalent idea that the pre-volcanic streams of the Sierra Nevada flowed through country which had suffered deep chemical decay.

The Beacon Peak locality is a newly discovered point on a stream of the pre-volcanic river system. Another, and perhaps more important channel of this system had its course in the Donner-Castle Peak area. Lindgren (1897, p. 4) described it as beginning a short distance south of Castle Peak and continuing south by way of Summit Valley and Onion Creek, forming the "headwaters of the Neocene North Fork of the American River." From the map and river profile of a later publication (1911, Plates I and X), it appears that Lindgren came

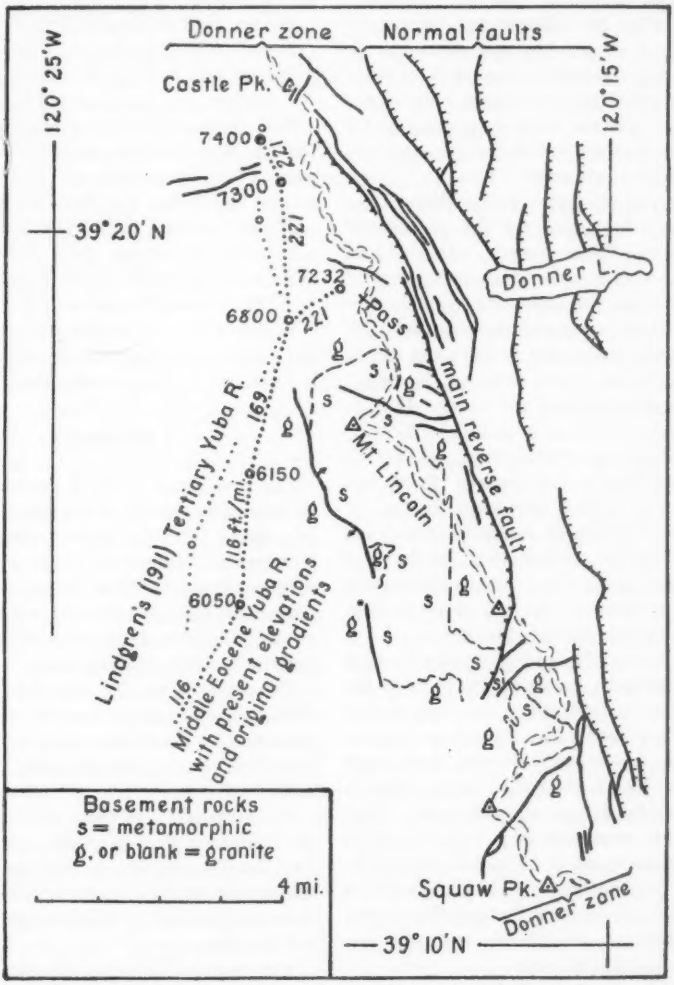

FIGURE 2.—STRUCTURE SKETCH. SQUAW PEAK—CASTLE PEAK AREA

to believe that this stream is a part of the main fork of the pre-volcanic Yuba river. This view is shared by the present writer (Fig. 1).

This channel, in the map area, is almost entirely hidden by volcanic and Quaternary deposits, but its reaches and turns can be determined by cross-section studies of the shape of the basement surface. Figure 2 shows the ideas of Lindgren and the present writer on the course of the stream within the map area and for some miles to the south.

AGE OF THE GRAVELS: The authors of the Gold Belt folios correlated the pre-volcanic gravels of the Sierra Nevada with the Ione formation. This is a sequence of non-marine clays and sands, with layers of coal and impure iron ore, which is exposed along the east side of Sacramento Valley and on the south side of Marysville Buttes in the center of the valley. They thought (Lindgren and Turner, 1895, p. 1) the the Ione overlay Tejon (marine Eocene) and, following usage of those days, assigned the gravels and Ione to the Neocene. In his last paper on this subject, Lindgren (1911, p. 23) stated that the deepest auriferous gravels are probably Eocene, because they are in some places overlapped by Ione, whereas the younger (but still pre-volcanic) bench gravels are Miocene, because they merge with the Ione.

Later work by other geologists, notably Allen (1929, p. 395–402), leaves no doubt as to the interfingering of both bench and deep gravels with the Ione, but it has also led to the conclusion (*see*, for instance, Stewart, 1949, sheet 2) that the Ione is older than Tejon, being in fact of middle Eocene age. Moreover, MacGinitie (1941, cross section, p. 19) found plant remains, determined to be middle Eocene, in both the deep channel and bench gravels at Chalk Bluffs, on the main Tertiary Yuba river, midway between the mouth and presently known head of the stream.

The middle Eocene age of the pre-volcanic gravels seems well established.

MIDDLE EOCENE LAND SURFACE: The geologic map and cross-sections (Pl. 1) show that this was a surface of rather strong relief, but much less rugged than the present terrain. Slopes of the valley sides ranged from 100 feet per mile to as much as 800 feet per mile. The gradients of the streams also indicate strong relief. The original (middle Eocene) gradients can be calculated by a method described (Hudson, unpublished paper) at the 1948 meeting of the Cordilleran Section. These (Fig. 2) are:

Beacon Peak to Summit Valley	221 ft./mi.
Summit Valley to Onion Creek	169
Onion Creek to 2 mi. W. of Soda Springs	116

Such gradients are not necessarily proof that the headwaters of the middle Eocene Yuba were in the Donner-Castle Peak area. The present day Yuba and American rivers have gradients in excess of 200 feet per mile along noteworthy extents of their channels as far down as the 3500-foot level, at localities from 13 to 20 miles west of the main divide.

In summary, the middle Eocene surface of the map area had moderately high relief and had suffered little chemical decay.

Rhyolite (r)

The rhyolitic deposits of the map area are entirely the product of eruptions of volcanic ash, there being no agglomerates or flows. Evidence of transport by water was found in only a few places. These deposits range from incoherent, through tuffs with varying degrees of lithification, to dense rocks with dull stony luster and, rarely, vitreous luster.

The denser types were thought by Lindgren (1897, p. 3) to be the product of lava flows. The present writer shared this belief, until Professor Durrell convinced him that they are actually welded tuffs.

The areal extent of their outcrops may give the impression that the stony type predominates, but a compacted crystal fragment tuff is the most abundant as to mass. This is followed, in decreasing order, by the stony, the incoherent and the glassy types.

The best developed section of the rhyolite is to be seen on the southeast flank of Beacon Peak and for a mile to the west along the north side of the highway. Following is the sequence of the entire volcanic series exposed on the side of the peak.

	Thickness
Basalt agglomerate	100 feet
Andesite agglomerate	150

	Thickness	
Andesite tuff		
Fine-grained, thinly bedded, and apparently water-laid. Compact, but neither cemented nor welded.....		140
Rhyolite tuff		
Pink welded tuff, with dull stony luster	30	
Black welded tuff, with glassy fracture and luster	5	
Gray compacted, but not welded, tuff	2	
Gray, incoherent tuff, with ¼″ grains of orthoclase and granite..	1	38
--------elevation 7245 feet--------		
Pre-volcanic gravel		13
Granite		

A third of a mile north, the andesite tuff overlaps the rhyolite and rests directly on granite. The andesitic deposits thicken to the west, the tuff to 200 feet in three-quarters of a mile, the agglomerate to 200 feet in half a mile. The rhyolite also thickens westward, attaining a maximum of 250 feet near the highway three-quarters of a mile southwest of the Beacon. This is due to the occurrence of layers of older, massive, compacted tuff which are progressively overlapped to the east by younger layers. West of the place of its maximum thickness, in less than half a mile, both the rhyolite and andesite tuffs are overlapped by andesite agglomerate.

From the foregoing and the general distribution of the formations (Pl. 1), it is seen that these volcanic deposits lie in a north-northwest trending trough in the basement. Figure 2 shows that the westerly of the two branches of middle Eocene Yuba river flowed along the axis of the trough, and that the place of maximum thickness of rhyolite is near the confluence of the two branches. The trough has been tilted westward about 2.5°, as may be seen on that part of structure section B-B′ (Pl. 1), which lies from three-quarters to 1¼ miles northeast of Lake Van Norden.

The ultimate maximum of rhyolite thickness in the region, and perhaps in the entire Sierra Nevada, is to be seen 2 miles southwest of Mt. Lincoln, where about 1000 feet of rhyolite lies in a basement trough and is overlapped by andesite to west, south, and east (Lindgren, 1897, map). This trough also is on the course of middle Eocene Yuba river. A part of its rhyolitic deposits are coextensive with those of the trough northeast of Lake Van Norden and those to be seen southeast of Donner Peak.

Ill Compacted Tuffs: These are generally of white or cream color, rarely show bedding, and are made up of fine ash with varying amounts of pumice fragments up to an inch in maximum dimension.

Compacted Crystal Fragment Tuffs: There are good exposures of this variety in the cuts on Highway 40, northeast of Lake Van Norden, 1¼ mile west of Donner Pass. The rock here is massive, rather competent, and separated into thick layers by partings which dip 7° S.E. Part of it has a rude columnar structure with columns, up to 6 feet in diameter, pitching 80° N.W., so as to be perpendicular to the gently inclined partings. The main mass of this rock is coarse tuff sand, consisting of flakes of biotite, broken crystals of clear albite-oligoclase, chips of brown glass, and fine pale-brown pumice fragments. In this granular mass are fragments of cream-colored pumice up to 6 inches in maximum diameter, only slightly collapsed. The refractive index of the glass of the large pumice fragments is less than 1.495, whereas that of the glass chips is 1.505. From W. O. George's work (1924), the chips are on the border line between dacite and rhyolite and the pumice is rhyolite. It seems proper to call the whole rock rhyolite tuff.

Near the eastern end of the road-cut exposures, the massive buff tuff is overlain by a thin sequence of alternating quarter-inch layers of pale, smashed pumice fragments, and yellow granular tuff sand. Above this is a 1-foot layer of massive, compacted, maroon tuff, followed by 10 feet of massive buff tuff with pumice fragments smaller and rarer than in the main mass of buff tuff. The maroon layer and the underlying thinly layered sequence dip 25° to S. 70° E. This layering does not seem to be due to water action, but the maroon layer does contain evidence of transportation and sorting by water. It is composed of fragments of pumice, flakes of biotite, perfect and broken feldspar crystals, chips of amygdaloidal rhyolite glass, and rounded and subrounded grains, up to 3 mm. in diameter, of quartz and varicolored rocks. There is an imperfect, fine banding, due

to alternate layers of different granularity. This, with the presence of the detrital grains, indicates deposition by water action. The bedding must have been originally near horizontal, and the present inclination indicates tilt to the southeast. The parallelism of the bedding to the underlying layering in the tuff shows that this too was originally horizontal. This suggests that the gentle southeast dip of the partings of the underlying columnar tuff also indicates tilting. Gilbert's observation (1938, p. 1835), that, with compaction, the pumice fragments of the Bishop tuff become aligned in the horizontal, is pertinent.

WELDED TUFFS: The predominant type of welded tuff has a dull stony luster, is found in a wide variety of colors, but generally gray, pink, or buff; and is enough lithified to ring under the hammer and to dress into building stones with fairly smooth faces. The rare type of welded tuff has a glassy luster and fracture and was seen with pale-gray, brown, and black color.

Layers of the glassy type, ranging from 3 to 20 feet thick, were found at four localities in the map area beneath thicker bodies of stony welded tuff. These occurrences are near but never at the base of the rhyolite deposits, the glassy rock being separated from the pre-volcanic base by 1 to 75 feet of non-welded tuff. A sample of the black glassy rock from the 5-foot layer that overlies the pre-volcanic gravel southeast of Beacon Peak consists of broken crystals of albite and quartz, up to a quarter of an inch longer dimension, and collapsed pumice fragments up to an eighth of an inch long in a matrix of dark-brown glass. The glass of the ground mass consists of very small, elongated fragments, packed in parallel arrangement and completely welded. Its index of refraction is 1.500, which according to George (1924) indicates 72 per cent silica. The rock is therefore rhyolitic.

The stony welded tuff which occurs in a 30-foot layer above the glassy rock southeast of Beacon Peak is made up of crystal fragments of orthoclase, albite, quartz, and biotite in a ground mass of thoroughly welded, elongated fragments of collapsed pumice. The larger of these pumice fragments, seen in thin section, measure 0.2 x 4.0 mm., the smallest discernible are 0.01 x 0.20 mm., and there is a complete range of intermediate sizes. The fragments are packed in layers with their longer dimensions parallel, and the layers bend around the crystal fragments in a manner resembling flow structure. All of the pumice fragments show at least slight birefringence. The stronger effects of this sort are due to the presence of tiny birefringent fibers which extend inward from the walls of the fragments. Part of these fibers are in parallel clusters, standing perpendicular to the walls, while other fibers are in clusters radiating from single points on the walls.

The minerals of these fibers or their origin were not determined. Such work would have been superfluous, as similar structures have been thoroughly studied by Marshall (1935) in the welded tuffs of New Zealand and by Gilbert (1938) in the Bishop tuff of Mono County, California. They found the fibers to be composed of feldspar and tridymite and showed that they developed in the glass after the depodeposition, compaction and welding of the fragments.

The ratio of thickness to major diameter of the pumice fragments suggest that the present 35 feet of stony and glassy welded tuff of the Beacon Peak locality came from an original deposit 100 feet or more thick. The stony rock is similar in degree of welding, compaction, and divitrification to rocks of the Bishop tuff which Gilbert (1938, p. 1835) showed could form only 350 to 400 feet below the tops of ash deposits from single or rapidly successive eruptions of the *nuée ardente* type. This seems to be a conclusion of general applicability, and accordingly it is thought that the Beacon Peak rhyolite deposit originally measured 500 feet above the base of the welded tuff; that the lower 100 feet of this mass was compacted to 35 feet thickness; and that the upper, non-welded part, after furnishing the insulation and weight required to compact and weld the lower part, was removed by erosion.

PRE-RHYOLITE SURFACE: This must be identical with the middle Eocene surface, described previously as one of moderately high relief with little chemical decay. At all places save one, where the contact of rhyolite on basement was seen, the underlying diorite or granite is disintegrated to the point of being crumbly, but

without chemical alteration. The exceptional case was observed on the west side of the creek, 1½ mile south-southwest from Castle Peak. Here the granite is overlain by a foot of non-lithified tuff, above which is 6 feet of black, vitreous, welded tuff, in turn overlain by pink, stony, welded tuff. The upper foot of the granite is altered to a blue-gray, clayey material. If this represented pre-rhyolite decay, one would expect to find it generally under the rhyolite. It is suggested that this chemical alteration is post-rhyolitic, and perhaps the work of emanations from the hot volcanic ash.

SOURCE OF THE RHYOLITE: No direct evidence was found in the map area for the location of the vents from which the tuff was thrown. Two probable loci of the rhyolite of Truckee quadrangle are mentioned by Lindgren (1897, p.. 3). One of these, 3 miles north-northwest of Castle Peak, on the south-east side of White Rock Lake, appears from the aerial photographs to be merely a mass of tuff in fault contact with the basement and younger volcanic rocks. The other is an isolated mass of rhyolite on a hilltop, 3 miles north of Rubicon Springs and 19 miles south of Donner Pass. It is clearly a flat-lying body of columnar welded tuff.

The ash clouds could not have traveled far if they were to deliver their load at a glowing hot temperature at the place of deposition. Presumably they might have traveled several miles, or even several tens of miles, as they are known to move down slopes with high velocity and to surmount slight acclivities. But the failure to find the tuffs outside the troughs of the region, and the great thickness of ash deposited in the troughs, suggests that the vents were in the troughs.

Post-Rhyolite Erosion

It has been shown that several hundred feet of rhyolite tuff was stripped from the Beacon Peak region before the deposition of the andesite tuff. With one minor exception, these two formations do not occur together elsewhere in the map area, so that generally the effects of this period of erosion cannot be discriminated from those of the period which followed the laying down of the andesite tuff.

Andesite Tuff (at)

There are three widely separated localities in the map area where bodies of fine-grained, generally thinly bedded andesite tuff occur beneath the lowest members of the sequence of andesitic agglomerates, flows, and tuff sands. The most important is the 140 feet of ash which lies between the rhyolite and the andesite agglomerate in the Beacon Peak mass of volcanics. This is a thinly bedded, fine, even-grained, seemingly water-laid material, which is compact but breaks readily between one's fingers. It is composed of particles of plagioclase, brown biotite, white and pale-brown clear glass, pale-brown divitrified glass, and opaque particles of pink, yellow, brown and black color. The plagioclase is mostly andesine, with albite rare. Quartz is lacking. All of the varieties of glass have indices of refraction of about 1.515. From George's data (1924), this indicates 65 per cent silica, and hence dacite. But the predominance of andesine and the lack of quartz and potash feldspar are taken to indicate that the rock as a whole is andesitic.

The kinship of this rock with dacite may be of importance with respect to its geologic age, discussed in a later section.

A mile southeast of Castle Peak is an exposure of pale-gray, fine, thinly bedded, andesite tuff, overlain unconformably by a sequence of andesitic tuff sands and fine agglomerates. The thickness of the tuff decreases from 250 feet on the west end of the exposure, where it is in fault contact with basement, to nil on the east where it is overlapped by agglomerate.

In the small area mapped as andesite (a), west of Lake Van Norden, fine, white, andesite tuff intervenes between rhyolite and coarser, andesitic deposits. This tuff contains no glass being composed of fragments of andesine in a matrix of small rock fragments in which the only discernible constituent is a feltwork of tiny feldspar crystals.

Pre-Andesitic Agglomerate Deformation And Erosion

The character of the andesite tuff, its occurrence at three widely separated places, and its overlap from rhyolite onto basement show that

it once formed a sheet comparable in extent to that of the rhyolite. The scarcity of andesite tuff that is preserved under the cover of agglomerate attests an important period of erosion following the deposition of the tuff.

There was also faulting prior to the laying down of the agglomerate. So little of the andesite tuff remains that it is not possible to decide what part of this faulting occurred before, and what part after, the deposition of this formation. At least a part took place in the latter period, as shown by the pre-agglomerate faulting of the andesite tuff a mile southeast of Castle Peak (section A-A′, Pl. 1).

Pre-Agglomerate Surface

In most of the map area, this surface had less relief than that of the post-rhyolite period. In the region south of Castle Peak, however, erosion that followed the deposition of the andesite tuff had exhumed the pre-rhyolite basement surface, and the relief of that surface had probably been increased by deformation, prior to the deposition of the agglomerate.

On the north side of the ridge, seven-eighths of a mile west-southwest from Castle Peak, the upper 15 feet of the granite under the agglomerate is a yellow, decayed material, easily penetrated by the pick. The biotite of the granite seems, however, to have suffered no alteration. Wherever seen elsewhere in the map area, both the granite and other rocks at the base of the agglomerate are quite fresh.

Andesite Agglomerate, With Minor Tuff and Flows

These rocks once formed a sheet over the entire map area, with the possible exception of the high granite ridges west of Frog Lake. Like the rhyolite, the greatest accumulation of the agglomerate was along the course of the prevolcanic Yuba river. The maximum thickness is 1100 feet, exposed on the southwest flank of Castle Peak (section A-A′, Pl. 1).

Fully 2000 feet of andesite agglomerates and flows was deposited east of the main divide in the Tahoe-Truckee depression. The western edge of this thick mass is represented in the map area by the 800-foot prism within the Donner fault zone, southeast of Donner Pass (section C-C′, Pl. 1).

Flows consitute a notable part of the thick andesitic deposits north and east of Donner Lake, but, within the map area the to west, they occur in thin layers at only three localities. One of these is on the ridge, 1¼ mile southwest of Castle Peak, where a 20-foot layer of massive lava lies within a sequence of agglomerates. Another locality is on the crest and southwest flank of a ridge, 1¾ mile northeast of Donner Pass, where a sheet of spheroidal weathering, coarse lava rests on granite. It dips 27° west and abuts on granite along the eastern member of a group of three north-northwest trending faults. The third exposure of andesitic lava, too small to show on the map, is immediately east of the same fault at the 5980-foot elevation station, southwest of the west end of Donner Lake. The rock here is massive hornblende andesite in which the arrangement of phenocrysts and parting planes indicate a dip of 70° W.S.W.

The agglomerates are composed of fragments of lava in a matrix of tuff sand, which is often well cemented. The lava fragments are generally angular, but are sometimes sub-rounded and rarely well rounded. The size of the fragments, and their abundance relative to the matrix, increase eastward across the map area. Rarely there are layers of fine tuff, never exceeding 1 foot in thickness.

The lavas of both flows and agglomerates are hornblende andesites, with phenocrysts of brown hornblende and oligoclase or andesine. In some of these rocks, the goundmass is a mixture of small plagioclase crystals and glass; in others, it is a feltwork of small plagioclase prisms.

Source: No dikes or plugs of andesitic material have been found in this region, but there is reason to believe that there were vents for the lavas and agglomerates both within and adjacent to the map area. On the south face of Castle Peak (section A-A′, Pl. 1), the agglomerates dip northeast, whereas the underlying basement surface dips west, suggesting that the thick agglomerates of that locality came from a nearby vent to the southwest, now hidden by Quaternary deposits.

The increase of coarseness and angularity in

the agglomerates in passing eastward and the higher proportion of flows to agglomerates east of the main divide suggest that part of the deposits west of the pass came from eruptive loci to the east.

Post-Agglomerate Deformation and Erosion

Unconformity between the andesite agglomerate and the overlying basalt is shown by angular discordance, and by the presence of post-agglomerate faults along which there was little or no movement after the deposition of the basalt. In most of the map area, this unconformity is less severe than any of those lower in the geologic column. But, in the region west and northwest of Lake Van Norden, a considerable thickness of agglomerate was swept away to allow the deposition of the basalt on a surface of granite and rhyolite.

Basalt of the Truckee Quadrangle

According to Lindgren's map (1897), there is a great difference between the amount of basalt along the main divide and western slope of the range and that present immediately to the east in the Tahoe-Truckee depression. In the 14-mile extent of the main ridge, from Squaw Peak north-northwest to Castle Peak, basalt is shown at only one locality as a mass of 200-feet thickness capping 300 feet of andesite on the west-trending spur a mile north of Beacon Peak. In striking contrast are the amounts shown in the lower country to the east: northwest of Truckee, 800 feet of basalt on 1400 feet of andesite; south and southwest of Truckee, 1000 feet of basalt on 1500 feet of andesite; north of Lake Tahoe, 900 feet of basalt on 2000 feet of andesite.

Another noteworthy contrast to be seen on this map is in the distribution of basalt and andesite on the two sides of Truckee river from its head at the Lake Tahoe outlet, downstream 12 miles to the town of Truckee. On the east side, three thick masses of basalt are shown capping andesite to form eminences from 1000 to 1700 feet above the stream, and dipping west or south into the canyon. One of these masses is delineated as terminating at the river, the others as extending short distances west of and a few hundred feet above the channel. On the west side of Truckee river there are peaks with shapes similar to the basaltic peaks of the east side, but rising about 1000 feet higher. These are shown as entirely andesitic.

With such relations of basalt to andesite, one is likely to conclude that the Tahoe-Truckee depression existed as a topographic feature at the time of the deposition of the basalt, and that the pre-basalt surface had great local relief. Such, indeed, was Lindgren's conclusion:

> "After the close of the volcanic (andesitic) period and its orographic disturbances followed a period of rest. The western range during this time became deeply scored by canyons, and Truckee River deepened its canyon all along to its present level and drained the Truckee basin. Then followed the basaltic eruptions which obstructed Truckee River in at least three places.... The Glacial epoch, probably begun before the basaltic eruptions, continued long after their close" (1897, p. 6).

There come to mind questions which are difficult to answer, such as: If post-glacial erosion has failed to remove a good part of the glacial deposits, how could it efface the volcanoes from which the basalt came? Why do we find basalt plastered on one side of the canyon and not on the other?

We need not try to answer these questions. The conclusions which evoke them are based on false premises. The basalt is not distributed in bizarre fashion. Actually there is about as much basalt on the west side of the river as on the east side and there are great masses of it on the main divide. All of the higher peaks from Tinker Knob north to Castle Peak are capped with basalt, resting with depositional contact on andesite. These deposits are not as thick as those in the Tahoe-Truckee depression, but the ratio of basalt to andesite in the peaks equals or exceeds that observed in the lower country to the east. The thicknesses of basalt and andesite in Castle Peak are 525 and 1110 feet, in Mt. Lincoln 500 and 500 feet, in Donner Peak 300 and 450 feet, and in the 8000-foot peak west of Mt. Lincoln 700 and 750 feet.

The basalt of the Truckee quadrangle was deposited in a continuous sheet on a surface of low relief which was in no way the ancestor of the present rugged terraine. It was then severely deformed and dissected prior to glaciation. The recognition that a large part of what

was once called andesite is really basalt is not merely a fine distinction that may be interesting to petrologists. It is a useful key to the structure of the region, as the base of the basalt is a widespread, readily recognizable unconformity.

Basalt of Mt. Lincoln-Castle Peak Area

The basalts of this area include lava flows, agglomerates, tuffs and plug intrusions of lava and breccia. The best exposed section of the flows and agglomerates, that on the steep south slope of Castle Peak, is summarized below:

	Thickness
Crag-forming, dark-gray agglomerate of the peak, composed of angular blocks of hypersthene basalt up to 3 feet in diameter, in a matrix of firmly cemented tuff sand	75 feet
Pale-gray, ill-cemented, basalt agglomerate, forming 1:2 slope from the base of the summit crags	200
Cliff-forming, platy, rudely columnar, slightly vesicular, olivine basalt	200
Basal cliff-forming member. It is black, columnar, olivine basalt at its western end, and basalt agglomerate at its eastern end	50
	525 feet
----------unconformity----------	
Coarse, hornblende andesite agglomerate.	

The basalt deposits of the map area display great lateral variation. For instance, the 175 feet of platy lava, which is the basal member of the basalt sequence in the high pass southwest of Donner Peak is overlapped by basalt agglomerate half a mile to the north. Again, the basal member on the south side of the same pass is an alternation of thin lava flows and layers of brown-weathered tuff, and less than half a mile to the west, massive cliff-forming lava forms the base of the series.

SOURCE: Three places of basalt intrusion were found within the map area. It is not certain that these mark the vents from which the extrusive basalts came, but there seems no reason to doubt that the surficial lavas were erupted either from them or from near-by, connected channels.

Of least volcanic importance, but giving evidence of value for dating orogenic events, is a dike exposed in the highway cut, a mile northeast of Donner Pass, 200 feet east of the 6450 foot elevation station. It is 24 to 30 inches wide and composed of olivine basalt which is irregularly fractured but neither sheared nor crushed. The country rock is granite, at the eastern edge of the zone of crushing and shearing along the main reverse fault of the Donner zone, and the N. 25° W. strike and 87° W. dip of the dike conform with the local attitude of that fault.

Next in importance is the small exposure surrounded by glacial deposits, three-quarters of a mile west of West Lake. Although its contacts with older rocks are hidden, it is believed to be a plug, because of its lack of accord in elevation with the bases of near-by extrusive masses, the turmoil of its flow structure, and its 2:1 ratio of phenocrysts to ground mass, which is much greater than that of the known extrusive rocks.

The most important of the intrusive basalt occurrences is the series of seven plugs on the ridge which extends west from Lake Van Norden. The four westerly plugs cut extrusive basalt, whereas the three easterly ones cut both that rock and rhyolite. The extrusive rocks adjacent to the three easterly plugs include platy lavas, and bodies of tuff and breccia. On the ridge these dip south at angles at high as 70°, whereas a few hundred feet to the north their inclination is 55° north.

The rock of the plugs is a breccia of fragments of olivine-hypersthene basalt in a matrix of massive basalt of the same composition. The grain size of the matrix is generally less than that of the fragments, but locally it is coarser, with feldspar phenocrysts as large as a quarter of an inch diameter.

The high angle of dip observed in the extrusive rocks suggests that the plugs are the roots of a volcanic cone which covered an area somewhat larger than that now occupied by the basalt complex. Such a volcano could not have been the only vent that furnished basalt to the Lake Van Norden area, because the basal member of the basalt sequence, seen resting on rhyolite at the west edge of the map, a short distance south of the railway, is a conglomerate with well rounded cobbles of basalt.

Extrusive rocks composed of basalt fragments in a lava matrix have not been observed in the region, either as lava sheets or as boulders in

agglomerates. This might suggest that the vents west of Lake Van Norden did not contribute much, if any, to the extrusive deposits to the east and north. But the plugs as seen today merely show the last material that flowed through these vents, and no such general conclusion should be based on their physical constitution.

PETROLOGY OF THE BASALTS: Ten samples of these rocks were examined microscopically in both thin section and mineral grain, and several additional samples were studied by the grain method alone. The purpose of this work was to make certain of the propriety of the revision of large areas of Lindgren's map (1897) from andesite to basalt. Accordingly, the work was restricted to determination of the feldspars and ferromagnesian silicates, that occur as phenocrysts and as larger crystals of the groundmass.

Macdonald (1949, p. 1544) used the term basalt for rocks of the Hawaiian petrographic province in which the average feldspar is labradorite or bytownite, and the term andesite for rocks whose average feldspar is andesine or oligoclase. Adopting these criteria, the rocks shown as basalt on the Donner-Castle Peak map (Pl. 1) yielded samples which, with one possible exception, are indicative of basalt. This exceptional sample is a dark-gray, fine-grained, slightly amygdaloidal rock, from the top of the basalt-capped ridge, 1¼ mile west of Beacon Peak. It is composed of basic andesine, olivine, iddingsite (after olivine), hypersthene, and monoclinic pyroxene, in a brown groundmass in which tiny feldspars are arranged in pilotaxitic structure. The olivine and hypersthene suggest basalt rather than andesite, so it is possible that the feldspar of the ground mass is more calcic than that of the phenocrysts. If so, the rock would be truly basalt as the ratio of ground mass to phenocrysts is 20:1. Curiously enough, this sample came from the single area along the main divide which is shown as basalt on Lindgren's map (1897).

All other samples from rocks shown as basalt are undoubtedly basaltic. The plagioclase of the various specimens ranges from medium labradorite to bytownite, the average being basic labradorite. Olivine and hypersthene are essential constituents, one or the other or both being present in all samples. Monoclinic pyroxene was found in about half, and brown hornblende in about an eighth of the specimens. In the samples collected for laboratory study, olivine occurs with slightly less frequency and abundance than hypersthene, but from field observations it is thought that olivine is the prime essential of these basalts.

Geologic Age of the Volcanic Series

It having been shown that the pre-volcanic gravels of the Sierra Nevada are middle Eocene, the oldest Tertiary volcanic deposits can be no older than middle Eocene.

The basalt capping the volcanic series of the Truckee quadrangle is pre-glacial, was laid down on a surface of low relief which has no relation to the rugged terrain of the glacial and present periods, and was severely deformed prior to the glaciation of the region. It seems reasonable to believe that the basalt is no younger than Pliocene. Accordingly, the various parts of the volcanic sequence must be assigned ages within the range middle Eocene to and including upper Pliocene.

After Lindgren and Turner, the first work on this problem was that of Louderback (1924, p. 17–19) whose conclusion—"that the period of great Tertiary andesitic erruptions of the Sierra Nevada is "Middle Neocene" that is, Lower Pliocene or Upper Miocene, perhaps bridging the gap between these two epochs."—was based on the fact that the San Pablo formation, where it occurs in the Coast Range of California, west of the area of Sierran andesitic deposits, contains large amounts of andesitic detritus. The San Pablo carries a marine fauna, considered at that time to represent either upper Miocene or lower Pliocene.

The present consensus of workers in invertebrate paleontology of the California Tertiary is that the San Pablo formation is upper Miocene. But vertebrate remains collected from andesitic deposits of the Sierra foothills have been determined by Stirton and Goeriz (1942, p. 455) as middle Pliocene for one locality and lower Pliocene for two other sites. They state (p. 470) that Axelrod studied a flora from the middle Pliocene vertebrate locality and reached a like conclusion as to age. The contradiction is probably one of names and not of facts.

Stirton and Goeriz (p. 462) state that a species of horse found in one of their lower Pliocene foothill faunas occurs also in the Mint Canyon formation of southern California, beneath a marine formation carrying upper San Pablo invertebrates. The difficulty then is not one of physical correlation, but arises from lack of accord between the vertebrate and invertebrate time scales. This is essentially the same as the current idea of Dr. Stirton (personal communication).

Since Louderback's work, an older andesitic deposit, the Wheatland formation, has been found in the Sierra foothills and determined as upper Eocene or lower Oligocene by Clark and Anderson (1938). With this in mind, and excluding also the pre-agglomerate andesite tuff of the Donner-Castle Peak area, it appears that recent work has substantiated Louderback's conclusion that the great mass of andesitic agglomerates and flows of the Sierra Nevada are upper Miocene or lower Pliocene.

The rhyolite and andesite tuffs of the map area remain for consideration. Most of the large deposits of auriferous gravels of the northern Sierra Nevada owe their preservation to a cover of volcanic tuffs and agglomerates, removed in part by post-volcanic erosion. In many of these deposits, the basal formation of the volcanic series is white tuff, generally mapped as rhyolite, but sometimes actually dacite. Andesitic agglomerates overlie the white tuffs and often overlap them so as to rest directly on the gravels.

Fossils have been described from only one locality in the white tuffs, the Dutch Diggings hydraulic mine, 1¼ miles northwest of La Porte, Plumas County, about 45 miles northwest of the Donner area. The gravels here are in a tributary from the north to the middle Eocene Yuba river. According to Lindgren (1911, p. 105), they are overlain by 50 feet of sands and carbonaceous clays, and these in turn by a "heavy cap of andesitic tuff". Plant remains collected from the tuff were determined by Potbury (1935) to be upper Eocene or lower Oligocene, and called the La Porte flora. She states that the tuff rests unconformably on the carbonaceous clay and that it is actually a hypersthene dacite vitric tuff, made up of 95 per cent glass, 3 per cent oligoclase, 2 per cent quartz, and 0.01 per cent each of hypersthene and ilmenite. A specimen of the matrix of the fossil plants, given to me by Dr. Chaney, was found to consist largely of two types of glass. The more abundant is slightly divitrified and has a refractive index of 1.515, the same as all types of glass in the andesite tuff of Beacon Peak in the Donner area, and, from George's work (1924), indicative of dacite. The less abundant glass of the La Porte tuff is clear and isotropic, and has an index of 1.505, which, according to George, determines it as carrying 70 per cent silica, thus placing it on the border between rhyolite and dacite. These results, together with the crystal content, show that the tuff is surely dacitic.

The facts that the andesite tuff of the Donner area overlies the rhyolite tuff unconformably and that it verges on dacite in composition suggest, on one hand, that it is appreciably younger than the rhyolite, and, on the other hand, that it may be the correlative of the La Porte dacite tuff. If these notions and Miss Potbury's age determination of the La Porte tuff are sound, the andesite tuff is upper Eocene or lower Oligocene and the underlying rhyolite is middle or upper Eocene.

The familiar rhyolite-andesite-basalt sequence is found not only in the Sierra Nevada, but also in the western Great Basin. Such a volcanic sequence overlies the lacustrine and fluviatile sediments of the Esmeralda formation in the Cedar Mountain region, 150 miles southeast of the Donner area. From the work of Buwalda (1914), Merriam (1916), and Stirton (1939) on the vertebrate fauna and of Axelrod (1940) on the flora, the age of the Esmeralda appears to be well established as lower Pliocene. The rhyolite here can be no older than lower Pliocene, an age widely descrepant from the Eocene age that seems proper for the rhyolite of the western slope of the Sierra. One cannot appeal to a lack of accord of different time scales here. We must be dealing with two distinct rhyolites. This idea is substantiated by evidence from another Great Basin locality, the Virginia City region, only 35 miles east of the Donner area. In a paper read at the Cordilleran Section meeting in 1949, Axelrod described the Alta andesite, the country rock of the Comstock lode, as resting on rhyolite and overlain

by a younger andesite, called the Kate Peak. A flora collected from a tuff member of the Alta andesite was determined by him as no younger than Oligocene and possibly as old as Eocene. It would appear from this that the land surfaces it was decided that as much as 200 feet of glacial materials underlies Lake Van Norden, Donner Lake, and the country immediately east of Frog Lake, and that about 100 feet of these deposits are present in the Ice

TABLE 1.—SUMMARY OF CORRELATIONS OF THE VOLCANIC SERIES

	Donner-Castle Peak Area	Western Slope of Sierra Nevada	Virginia City, Western Great Basin
Pliocene	Basalt		
	- - - unconformity - - -		
Pliocene Upper Miocene	Andesite agglomerate	Andesite agglomerate	Kate Peak andesite
	- major unconformity -		
Lower Oligocene or Upper Eocene	Andesite tuff	La Porte tuff	Alta andesite
	- - - unconformity - - -		
Middle Eocene	Rhyolite tuff Pre-volcanic gravel	Rhyolite tuff Pre-volcanic (auriferous) gravel	Rhyolite

underlying rhyolite is either Eocene or lower Oligocene, and not far from exactly correlative with the rhyolite of the western slope of the mountains.

It is possible to say with some assurance that the andesite tuff of the Donner area is Oligocene or upper Eocene and that the rhyolite tuff is middle Eocene.

The correlations are summarized in Table 1.

Quaternary Deposits

After the accumulation of the basaltic deposits came the sequence of orogenic movements which, with the accompanying glacial and aqueous erosion produced the present rugged land surface. The deposits of this period cover a third of the map area and are shown on Plate 1 as glacial materials (Qm), landslides (Qls), and alluvium (Qal).

GLACIAL DEPOSITS: These are so little dissected that neither the details of their composition nor their maximum thickness can be determined exactly. By projecting adjacent bare Lakes area. Elsewhere within the map area, they measure no more than a few tens of feet.

Their predominant component is granitic debris, in all sizes from fine sand to 20-foot boulders. In some places sub-rounded boulders of welded rhyolite tuff, up to 3½ feet in diameter are a prominent constituent. More rarely one finds detritus from the andesitic and basaltic formations.

Blackwelder (1931, p. 870–877) showed that there were four distinct periods of glaciation in this region. It is probable that special study will show that deposits of all these periods exist in the Mt. Lincoln-Castle Peak area, but the writer recognized with certainty only the materials of the two late Pleistocene stages, the Tahoe and Tioga. The latter include gravel, sand, and silt of the cirques and valleys, and the fresh, coarse morainal material of the stream valleys. The older, Tahoe deposits are soil-mantled, lateral moraines in which most of the detritus is decayed.

LANDSLIDES: These appear to have formed at the last recession of the glaciers, when the

lateral support of the steep valley walls by the ice ceased. The hummocky surfaces of the slides and the fresh scars in the undisturbed rock at their heads attest their recency. All of the slides came from the volcanic formations and are composed solely of the rhyolite, andesite, or basalt from which they sprang.

ALLUVIUM: This includes the sand and gravel in transit in the streams, and the post-glacial silt, sand, and fine gravel deposited in existing or recently drained lakes. Only the latter is shown on the map.

STRUCTURE

General Statement

It has been shown that there were intervals of erosion after the deposition of each of the four volcanic formations and that earth movements occurred in connection with at least three of these intervals. The least important of these orogenic episodes occurred between the times of accumulation of the andesite agglomerate and the basalt. The most important followed the laying down of the basalt at the beginning of the great Quaternary revolution, which, from the evidence of earthquakes along the eastern side of the Sierra Nevada, is still in progress.

The structural features might be described in conformity with a classification based on their geologic age. But the most important deformation of the area is along the Donner Pass zone, on which movement recurred from Middle Tertiary to early Quaternary time. Accordingly, for purposes of description, a genetic classification is used: (1) Primary structures of the basement rocks; (2) Structures along the Donner Pass zone of deformation, largely due to compression; and (3) The results of normal faulting, east of that zone.

Basement Structure

In the mass of metamorphic rock which outcrops west of Donner Peak, the general dip of the foliation is east-northeast at a high angle. In the small area of schist, southeast of the peak, the dip is 70° west. The former attitude conforms with the general attitude of the metamorphic rocks of the Truckee and Colfax quadrangles (Lindgren, 1897; 1900; Cloos, 1936, fig. 5) and accordingly it was adopted in representing those rocks, where masked by Tertiary deposits, on structure section C-C' (Pl. 1).

Table 2 summarizes observations made on the attitude of joint planes in the granite.

The dominant joints are those of set 1, vertical with N.-S. strike, and set 4 which strike N.E. and dip N.W. at angles ranging from near horizontal to 55°. Next in importance are those of set 3, vertical joints with N.W. strike, and set 2 which strike E.N.E. and dip steeply N.

The base of the previously described zone of dark inclusions in the granite, half a mile east of Donner Pass, dips N.W. at a moderate angle, thus conforming with the joints of set 4.

Donner Pass Zone

General description.—This was defined in the writer's earlier paper (1948, p. 797–799) as a zone of uplift extending S. 15° E., along the crest and east flank of the range, from the vicinity of Donner Pass to Squaw Peak, a distance of 10 miles. The zone was thought to have originated as an anticlinal fold, which was accentuated later by reverse faulting on its east limb. The first movements were believed to have been no earlier than Pliocene and possibly as recent as late Pliocene. The west-northwest trending faults on the west side of the reverse fault near Donner Peak were thought to be older than the reverse faulting but younger than the folding. Two loci of maximum deformation were recognized: (1) the Northern Uplift, near Donner Pass, and (2) the Southern Uplift, 8 miles to the south near Squaw Peak.

The conclusions from the later work are that the structures in this zone are due to compression, that the initial result was folding of the less rigid part of the basement, but that, as deformation progressed, the dominant activity through most of the zone came to be reverse faulting. This was accompanied by folding where the underlying rocks yielded to compression in such a way that the overlying strata could fold. Finally, it is evident now that there were recurring movements along the zone, ranging in date from as early as Middle Miocene to Quaternary.

The suggestion that the zone extends far beyond the limits of earlier study (1948, p. 799) is confirmed as to northerly prolongation. The detailed mapping (Pl. 1) proves that it passes through Castle Peak, and a study of the relation of Tertiary volcanics to basement on Lindgren's Truckee map (1897) shows that it reaches at least 5 miles further north along the main divide. On the basis of present elevation of the contact of Tertiary on basement, the uplift is greater in the Castle Peak area than at the previously defined locus of maximum deformation of the Northern Uplift in the vicinity of Donner Pass. However, the evidence of the course of the Middle Eocene Yuba River shows that the Castle Peak area was high land in early Tertiary time. Furthermore, the differential movements in the zone in Middle and late Tertiary time were much less in the Castle Peak area than in the vicinity of the pass, confirming that the latter is the place of maximum deformation.

TABLE 2.—STRIKE AND DIP OF NOTEWORTHY JOINTS

Locality:	Set:				
	1	2	3	4	5
West of main reverse fault immediately S.W. of Donner Pass	N. 10° E.* vert.			N. 40° E.* 42° N.W.	
Highway 40, ⅜ mi. N.E. of Pass		N. 60° E. steep N.	N. 40° W.* vert.		
Highway 40, adjacent to fault	N. 10° E.* vert.	E.–W. vert.		N. 45° E. low N.W.	
Old road, ½ mi. due E. of Pass	N.–S. 82° W.		N. 55° W. 87° S.	N. 10° E.* 55° W.	N. 30° W. 50° E.
1¾ mi., S. 38° E. from Donner Peak	N. 20° W.* vert.	N. 85° E. steep N.		N. 70° E. 7° N.	
East of fault 1 mi. S. 80° E. from Donner Peak	N. 5° W.* 75° W.				N.–S. 33° E.
½ mi. east of West Lake	N. 5° W. 86° E.				

* denotes the stronger set or sets at each locality.

The dominant element of the Northern Uplift is a reverse fault, which dips steeply westward. Its trace was described (Hudson, 1948, p. 798) as extending along the east side of the range from the vicinity of the pass for 6 miles south-southeast and then turning southwesterly across the main divide. It is now known to extend 3 miles northwest of the pass to the vicinity of Castle Peak.

The Donner Pass zone is defined as the crustal block of this area within which the rocks were notably deformed by compressive forces in Tertiary and Quaternary time (Fig. 2). It encompasses the main reverse fault and extends northward beyond the termination of that feature. The eastern boundary of the zone is

marked by the westernmost of the system of normal faults which extend southeast from Frog Lake through Donner Lake. The western boundary is the limit of noteworthy faulting and folding 2½ miles from the main reverse fault.

Main reverse fault.—Coming into the map area from the southeast, this fault extends N. 20° W. to a point a mile northeast of Donner Pass, where it turns and follows a N. 40° W. course to the vicinity of Castle Peak. It is compound, being made up of three overlapping parts, with the northern and southern segments lying a few hundred feet west of the middle one. The southern segment, in its course from the latitude of the pass to the edge of the map, dips 80° W. Beyond that, to the south-southeast, the dip decreases to about 70° W. The middle segment, where crossed by Highway 40, east of the pass, dips 87° W. No other attitude was observed on it, but its dip doubtless decreases in passing north, because east of West Lake, where the middle and northern segments overlap, the latter dips 63° W.

The greatest movement is in the latitude of the pass where the dip is steepest. Here the contact of andesite on basement is 1250 feet lower on the east side of the two fault segments than its projected position on the west side (structure section C-C′, Pl. 1). The separation is in two steps, 900 feet on the western break and 350 feet on the eastern one.

North of Donner Pass, the fault trace is in granite to the locality where it crosses the base of the andesite agglomerate, a mile southeast of Castle Peak. Here the contact has been depressed 300 feet on the east side of the fault with respect to its position on the west side. The slight anticlinal bend in the basalt, half a mile to the northwest (section A-A′, Pl. 1) suggests that the fault continues toward the peak as a pre-basalt break which became the locus of post-basalt flexing.

A mile south of the place of maximum movement, the vertical separation of the base of the andesite is 850 feet. Direct measurements are not possible south of this point. However, from the shape of the contact of rhyolite on basement, it is evident that the faulting decreases several hundred feet in passing to the structural sag between the two oblique faults at the edge of the map, and attains a submaximum a mile further south (Hudson, 1948, p. 799).

At the 7052-foot elevation station on the fault, half a mile east of West Lake, the movement was along a 1-foot zone of parallel shear planes, striking N. 20° W. and dipping 63° W. Striations on the shear planes pitch 82° S. No other pertinent evidence, of this or other nature, having been seen elsewhere along the fault, it is presumed that the direction of movement was nowhere far from the line of dip.

Donner zone east of the main fault.—Adjacent to the fault is a graben flanked on the east by a horst. These elements of the zone are strongest in the region of greatest movement on the main fault and decrease in prominence both north and south of that locality, indicating the close genetic relationship of all three features. Southeast of the pass there is faulting and synclinal folding of the andesitic agglomerate within the graben (section C-C′). In the Caste Peak region (section A-A′), the agglomerate and andesite tuff in the graben are faulted, whereas the overlying basalt is synclinally folded and only slightly faulted.

Donner zone west of the main fault.—The principal features produced by deformation in this block are gentle folds in the middle and upper Tertiary formations, minor faults parallel to the main fault, and oblique faults with strikes deviating about 55° west from the trace of near by parts of the main fault.

The folds are best developed in the southeastern part of the map area, in the vicinity of section C-C′. The andesite agglomerate and basalt of the Donner Peak ridge lie in a slightly folded syncline. Half a mile west these formations pass over an anticline with relatively steep west limb. A mile and a quarter further west, and just east of the 7900-foot peak, is a barely perceptible syncline, followed in a half mile by an equally slight anticline.

Folding is much less important in the central and northern parts of the map area. Along section B-B′ there is slight folding of the andesitic agglomerate, and the overlying basalt is bowed up where it crosses the pre-basalt fault just east of the 7750-foot peak. Along section A-A′, the andesitic agglomerate and basalt west of the main fault lie in an internally faulted struc-

tural depression. This might be the result of sagging of the basement, but, as it is bounded by reverse faults, it is believed that compression was responsible, at least in part, for its origin.

The oblique faults are best exemplified by the group of five parallel faults in the vicinity of Donner Peak. These dip steeply south and strike N. 75° W., or 55° westerly from the trace of the main fault, from which they extend one-half to 2 miles westward. The two more important faults are normal, whereas the others are reverse. Four of the faults affect basement and rhyolite but not the overlying andesite agglomerate. The fifth and longest of the faults affects andesite through most of its course but had only pre-andesite movement at its western end. Its trace has been denuded of basalt, but, from the near-by elevations of the base of that formation, it is believed that there was no post-basalt movement. The two southerly faults bound the structural low which separates the maximum and sub-maximum highs of the Northern Uplift. The contact of rhyolite on basement is 450 feet lower in this depression than its position northeast of Donner Peak. Only about 150 feet of this drop is due to movement on the faults, the balance being the result of southerly dip of the contact, so there was probably folding in addition to faulting.

The fault which traverses the high pass north of the Beacon is similar to those of the Donner Peak group in dipping steeply south and having a strike deviating 55° west from that of the nearest part of the main fault. It is a reverse fault, affecting the basalt and earlier formations northeast of the Beacon, but within a short distance to the west it either terminates or passes into a pre-andesite agglomerate break.

The oblique faults 2 miles southwest of Castle Peak strike S. 75° W., deviating 65° westerly from the N. 40° W. trace of the nearest part of the main fault. They are normal faults, dipping steeply south, and had post-basalt movements at their eastern ends but only pre-basalt activity to the west.

All of the oblique faults have the same orientation with respect to the main fault, and all show waning activity with increasing distance from the major break. This indicates a close genetic relationship, not only between the various oblique faults, but between them and the main fault. It is concluded that all are the result of compressive forces which affected the region from time to time, and that the movements on the oblique faults were concurrent with activity of near-by parts of the main fault.

In his earlier work (1948, Pl. 1), the writer thought that four of the five oblique faults of the Donner Peak area cut all of the formations of the volcanic sequence and concluded that these faults were younger than the folding of the volcanic rocks of that area. It is now known that only one of these faults cuts rocks younger than rhyolite and that it is pre-basalt in age. The folding of the andesite and basalt was necessarily post-basalt and hence later than the oblique faulting of this area.

The Beacon Peak oblique fault and those southwest of Castle Peak originated in pre-basalt time, but their greater activity was post-basalt and on those parts of their courses closest to the main fault. The folding in this part of the map area was post-basalt and noteworthy only near the main fault, so it is believed that it was concurrent with the later phase of the oblique faulting.

Dates of activity of the main reverse fault.— From the foregoing it is evident that the first movement on this fault of which there is definite geologic record was in pre-andesitic agglomerate (middle Miocene) time and was accompanied by the greater part of the oblique faulting of the Donner Peak region. The last movement was in post-basalt (early Quaternary) time. To these must be added a third, the pre-basalt (middle or upper Pliocene) episode, attested by direct evidence of the main fault in the area southeast of Castle Peak (section A-1′).

It is possible that the pre-andesitic agglomerate period of deformation and erosion actually includes two periods: a later one immediately prior to the laying down of the agglomerate, and an earlier one between the times of accumulation of the rhyolite and andesite tuffs. If so, it would suggest a fourth date of activity on the main fault in late Eocene time.

Castle Peak faults.— An eighth of a mile southeast of Castle Peak, a zone of reverse faulting passes north-northest across the main divide (Pl. 2). It is composed of three closely spaced faults which dip 75° west. The vertical separation of the basalt-andesite contact, from

one side of the zone to the other, is 450 feet. This zone lies athwart the last seen trace of the main reverse fault. It is an element foreign to the otherwise orderly scheme of deformation of the map area and may be the southern part of a fault which, in the region to the north, plays a role in the Donner Pass zone similar to that of the main reverse fault to the south.

Normal Faulting East of the Donner Zone

Post-andesitic faulting along the east side of the main divide was discovered by Louderback (1924, p. 23–24), who presented evidence of normal faults with 1500 feet aggregate downthrow to the east on the southeast flank of Squaw Peak. These faults form a north-northwest trending belt which passes through Donner Lake and thence, with more northwesterly course, extends past Frog Lake. (Fig. 2; Pl 1). They dip east at angles ranging from 60° to nearly vertical. North of Donner Lake, the base of the basalt is about 1500 feet lower on the east side of the belt than on the west side. It is believed that all of this normal faulting is younger than the latest of the reverse faulting, because: (1) north of Squaw Peak the western member of the belt cuts three members of the reverse fault group, and (2) glacial deposits are not affected by the reverse faulting, whereas, on the ridges north and south of the east end of Donner Lake, lateral moraines of Tahoe age have been downthrown 200 feet against basalt along the easternmost of the normal faults shown on Figure 2.

Late Normal Faulting Within Donner Zone

The 6554-foot elevation station, 1¼ miles northeast of Donner Pass is on the eastern of three closely spaced parallel faults within the Donner zone. Immediately to the west are two patches of glacial detritus of Tahoe aspect, which are too small to show on the map. These form the treads of topographic steps, delimited by the three faults. The risers on the west sides of the two treads are of bare granite and slope westward in excess of 35°. The eastern riser is 15 feet high and the western one 55 feet. They are thought to be fault scarps and indicative of post-Tahoe normal faulting with downthrow on the west. The earlier movements on these faults were of reverse character, the granite on the west having risen with respect to the andesite on the east. (See structure section B-B′.)

Summary of Orogenic Events in Donner Zone

There were three or four episodes of deformation due to compression. These were genetically related to activity on the dominant structural feature, a reverse fault which dips west at angles ranging from 63° to vertical. The maximum movement on the main fault took place in the latitude of Donner Pass where the dip is steepest. Here the vertical separation of the base of the andesite agglomerate is 1250 feet.

East of the main fault there is a graben, flanked on the east by a horst. These features are strongest adjacent to the place of maximum movement on the main fault.

Following is a summary of events in the area west of the main fault:

Late Eocene: Probable deformation and subsequent erosion but, if so, the results are inextricably mixed with those of the next episode.

Middle Miocene: Activity on main fault and on southern group of oblique faults.

Middle or upper Pliocene: Activity on main fault. Movement on minor faults parallel to main fault in Castle Peak area (section A-A′) and on northerly group and one member of southerly group of oblique faults.

Pre-glacial Quaternary: Movement on main fault, on parallel minor faults and on northern group of oblique faults. Folding and minor faulting of the basalt in Castle Peak region (section A-A′), and stronger folding of andesite agglomerate and basalt in Mt. Lincoln area (section C-C′).

Conclusions

The principal conclusion of the writer's earlier paper (1948, p. 799) was that the tilting of the Sierra Nevada as a rigid block cannot explain the structure of the Tertiary deposits. This is corroborated by the results of the later work. The range in the Donner Pass region was subjected to recurring compressional deformations, producing structures that could not have been formed by block tilting. It is improbable that the subsequent normal faulting was accompanied by tilting of the range, as its ability to

act as a rigid block must have been greatly reduced by the reverse faults of the earlier periods.

RELATION OF DEFORMATION TO NATURE OF BASEMENT: The character of deformation of a conformable sequence of superincumbent deposits was controlled by the nature of the basement. Where foliated metamorphic rock forms the basement, there was folding; where granite is the subjacent rock, there was faulting. This demonstrates that an old rule (Reed, 1933, p. 29) for the deformation of the post-Jurassic formations of the California Coast Ranges also applies to the Tertiary of the Sierra Nevada.

In the Mt. Lincoln-Donner Peak region (section C-C′) where the basement is largely foliated rock, the 1000-foot sequence of andesite agglomerate and basalt, together with the basement, yielded by folding in the early Quaternary episode. In the Castle Peak area (section A-A′) where the basement is granite, the deformation of the 500-foot cover of andesite agglomerate in the Pliocene orogenic event was entirely by faulting.

Minor exceptions to this rule are to be seen in the structure sections. Along section B-B′, immediately east of Lake Van Norden, the andesite agglomerate is gently folded and its contact on the granite is represented as conforming with this folding. Doubtless, under certain conditions, granite will fold, but it is improbable that such conditions prevailed during the Tertiary in the basement rocks now exposed to view. The appearance of folding may be due to undetected minor faulting. The other exceptions are on section C-C′, where the syncline under Donner Peak and the barely perceptible anticline and syncline on either side of the 7900-foot peak have their axial planes in granite. These axes are close to granite-metamorphic contacts, and the seeming folding of the basement is probably the result of tilting of blocks of the more rigid granite through yielding of the adjacent, more plastic, foliated rock.

DEFORMATION OF AN UNCONFORMABLE SEQUENCE OF TERTIARY OF WHICH THE LOWER MEMBER WAS PREVIOUSLY FAULTED: Such a sequence yielded by folding and minor faulting, even where the basement rock is granite.

The lower formation, which had been faulted in the earlier orogenic episode, appears to have acted as a mattress which distributed the stresses of the later compressive event so as to facilitate folding of the superjacent rocks while the granite was yielding by faulting. The relative importance of folding to faulting in the Tertiary rocks during the later earth movements is recorded in the structure of the deformed unconformity.

This is well exemplified in the central part of structure section A-A′. Here the andesite tuff and andesite agglomerate were displaced along four faults in the Pliocene orogeny, but, in the early Quaternary episode, the unconformity at the base of the basalt cover was displaced by fault movements along only two of these breaks, and the sequence as a whole suffered more folding than faulting.

Another example is shown in the central part of section B-B′, where a fault that was active in both the middle Miocene and Pliocene orogenies was the locus of anticlinal folding in the post-basalt, early Quaternary revolution.

APPLICATION OF FOREGOING CONCLUSIONS TO DONNER ZONE SOUTH OF MT. LINCOLN: In the writer's earlier paper, the volcanic sequence of the Squaw Peak region was represented as faulted as well as folded, whereas that of the area 2 miles southeast of Mt. Lincoln was shown as simply folded (1948, Pl. 1, sections C-C′ and B-B′). In both of these areas the subjacent basement was depicted as granite. These sections now appear contradictory to one another, and the northerly one, B-B′, fails to conform to the recent conclusion that Tertiary lying directly on granite is faulted during compressional deformation.

These areas have not been revisited, but a satisfactory explanation was gained from a study of the aerial photographs. Metamorphic rock was identified under the volcanics, at the western edge of the area of granite outcrop, 2 miles southeast of Mt. Lincoln (1948, Pl. 1). This is not proof, but it suggests strongly that the volcanic cover of the main divide for some 4 miles southeast of Mt. Lincoln rests on foliated basement rock rather than, as previously thought, on granite. If so, the folding of the volcanics in the regions of section B-B′ (1948) conformed to the rule for the area to the north.

It was shown in the earlier paper that some of the faults of the Squaw Peak area extend upward from the granite only part way through the volcanic sequence. It is believed now that there is at least one unconformity here within

the volcanics, and that restudy in the field would show that the structure is similar to that of the Castle Peak region—a mattress of faulted Tertiary with a folded cover.

RELATION OF DONNER ZONE TO STRUCTURE OF BASEMENT: The faults conform in no way to the joint system of the granite. The only fault which forms a contact between granite and metamorphic rock is that at the western edge of the zone, west and south of Mt. Lincoln (Fig. 2). On the other hand, the mere geographic relation of the zone of deformation to the body of foliated basement rock suggests that the two are genetically related and that the parallelism of the main reverse fault to the eastern boundary of the metamorphic rock is not fortuitous. Moreover, it has been shown that this rock yielded plasticly in the Tertiary and early Quaternary compressional episodes.

It is concluded that the metamorphic mass determined the position of the Donner zone, which had its inception as an anticlinal fold in that rock; that the granite to the north and south along the zone and the granite east of the original anticlinal axis, being unable to fold, accommodated itself to the increasing deformation of the metamorphic rock by faulting; and that, with further deformation, reverse faulting on the eastern breaks became the dominant activity, accompanied, however, by folding where metamorphic rock forms the basement.

REVERSAL FROM COMPRESSIONAL DEFORMATION TO NORMAL FAULTING DURING THE QUATERNARY: The cause is a matter of speculation beyond the scope of this paper, but it is noteworthy that this region, after recurrent periods of reverse faulting and folding, from middle Tertiary to early Quaternary in age, became in the recent past the scene of important normal faulting.

REFERENCES CITED

Allen, Victor T. (1929) *The Ione formation of California*, Univ. Calif. Pub., Bull. Dept. Geol. Sci., vol. 18, no. 14, p. 347–448.

Axelrod, D. I. (1940) *The Pliocene Esmeralda formation of west-central Nevada*, Wash. Acad. Sci., Jour., vol. 30, no. 4, p. 163–174.

Blackwelder, Eliot (1931) *Pleistocene glaciation in the Sierra Nevada and Basin Ranges*, Geol. Soc. Am., Bull., vol. 42, p. 865–922.

Buwalda, J. P. (1914) *Tertiary mammal beds of Stewart and Ione valleys in west-central Nevada*, Univ. Calif. Pub., Bull. Dept. Geol. Sci., vol. 8, p. 335–363.

Clark, B. L., and Anderson, C. A. (1938) *The Wheatland formation and its relation to early Tertiary andesites of the Sierra Nevada*, Geol. Soc. Am., Bull., vol. 49, p. 931–956.

Cloos, E. (1936) *Der Sierra-Nevada-Pluton in Californien*, Neuen Jahrb. Mineral., Beil. Bd. 76, Abt. B. 1936, p. 355–450.

George, W. O. (1924) *The relation of the physical properties of natural glasses to their chemical compositions*, Jour. Geol., vol. 32, no. 5, p. 353–372.

Gilbert, Chas. M. (1938) *Welded tuff in eastern California*, Geol. Soc. Am. Bull., vol. 49, p. 1829–1861.

Hudson, Frank S. (1948) *Donner Pass zone of deformation, Sierra Nevada, California*, Geol. Soc. Am., Bull., vol. 59, p. 795–800.

Lindgren, W. (1897) *Truckee folio, California*, U. S. Geol. Survey, Folio 39.

—— (1900) *Colfax folio, California*, U. S. Geol. Survey, Folio 66.

—— (1911) *The Tertiary gravels of the Sierra Nevada of California*, U. S. Geol. Survey, Prof. Paper 73.

—— and Turner, H. W., (1895) *Smartsville folio, California*, U. S. Geol. Survey, Folio 18.

Louderback, G. D. (1924) *Period of scarp production in the Great Basin*, Univ. Calif. Pub., Bull. Dept. Geol. Sci., vol. 15, no. 1, p. 1–44.

Macdonald, Gordon A. (1949) *Hawaiian Petrographic Province*, Geol. Soc. Am., Bull., vol. 60, p. 1541–1596.

Mac Ginitie, Harry D. (1941) *A middle Eocene flora from the central Sierra Nevada*, Carnegie Inst. Wash., Pub. 534.

Marshall, P. (1935) *Acid rocks of the Taupo-Rotorua volcanic district*, Royal Soc. New Zealand, Tr. and Pr., vol. 64, p. 323–366.

Merriam, J. C. (1916) *Tertiary vertebrate fauna from the Cedar Mountain region of western Nevada*, Univ. Calif. Pub., Bull. Dept. Geol. Sci., vol. 9, p. 161–198.

Pabst, Adolf (1928) *Observations on inclusions in the granitic rocks of the Sierra Nevada*, Univ. Calif. Pub., Bull. Dept. Geol. Sci., vol. 17, no. 10, p. 325–386.

Potbury, Susan S. (1935) *The La Porte flora of Plumas county, California*, Carnegie Inst. Wash., Pub. 465, II.

Reed, R. D. (1933) *The geology of California*, Am. Assoc. Petrol. Geol.

Stewart, Ralph (1949) Chart 34, U. S. Geol. Survey, Oil and gas Inv.

Stirton, R. A. (1939) *The Nevada Miocene and Pliocene mammalian faunas as faunal units*, 6th Pac. Sci. Cong., Pr., p. 627–640.

Stirton, R. A., and Goeriz, H. F. (1942) *Fossil vertebrates from the superjacent deposits near Knights Ferry, California*, Univ. Cal. Pub., Bull. Dept. Geol. Sci., vol. 26, no. 5, p. 447–472.

Turner, H. W. (1897) *Downieville folio, California*, U. S. Geol. Survey, Folio 37.

—— (1898) *Bidwell Bar folio, California*, U. S. Geol. Survey, Folio 43.

3036 DIVISADERO STREET, SAN FRANCISCO 23, CALIFORNIA

MANUSCRIPT RECEIVED BY THE SECRETARY OF THE SOCIETY, SEPTEMBER 5, 1950

PROJECT GRANT 518-47

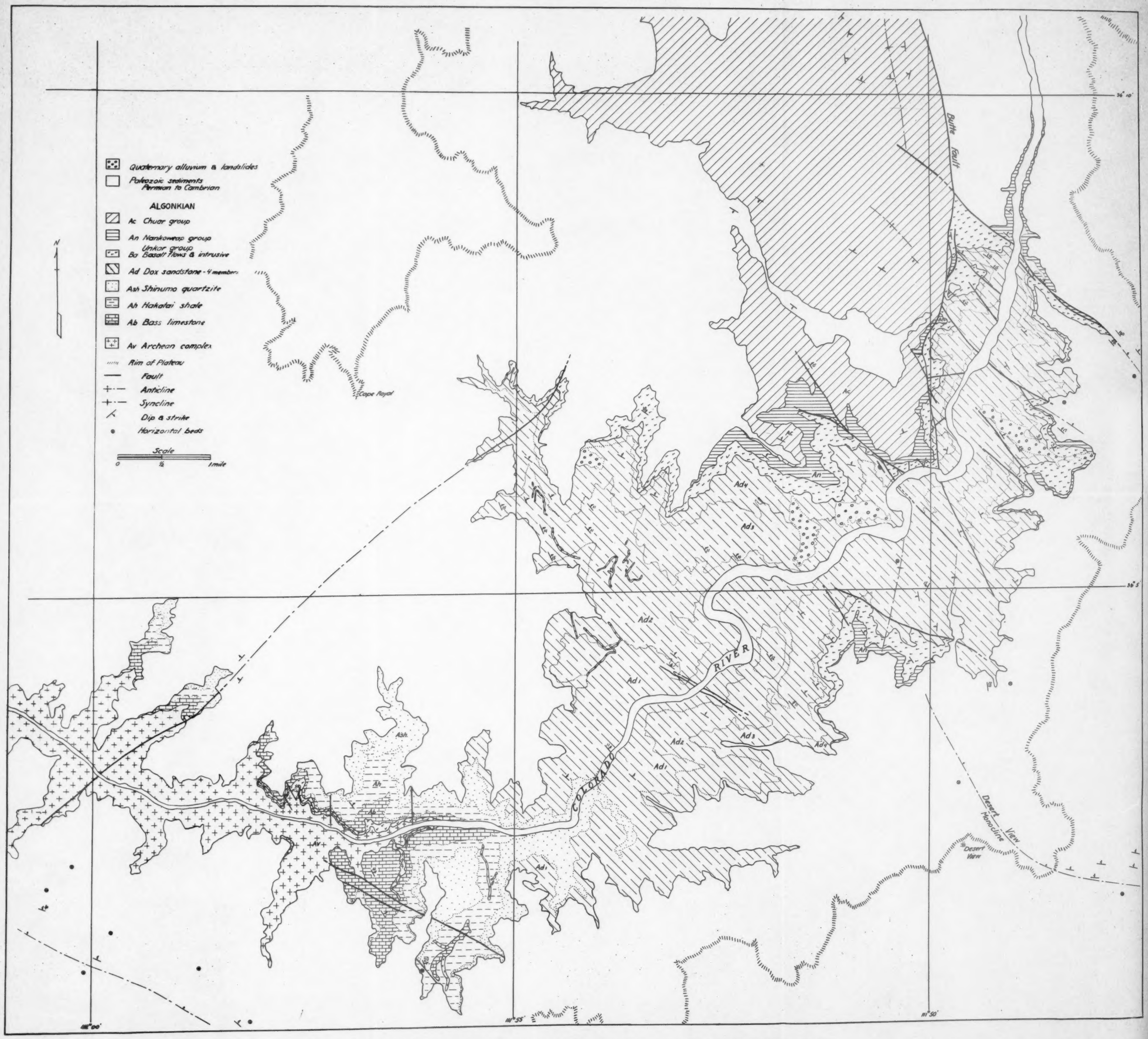

GEOLOGIC MAP SHOWING DISTRIBUTION OF NANKOWEAP GROUP IN BIG BEND AREA, EASTERN GRAND CANYON

BULLETIN OF THE GEOLOGICAL SOCIETY OF AMERICA
VOL. 62, PP. 953-959 2. FIGS., 3 PLS. AUGUST 1951

NANKOWEAP GROUP OF THE GRAND CANYON ALGONKIAN OF ARIZONA

By C. E. Van Gundy

Abstract

The investigation and mapping of the Algonkian rock of the Grand Canyon of Arizona disclosed that a group of sediments should be separated from the Unkar and Chuar groups described by C. D. Walcott in 1895. This intermediate group, called Nankoweap, includes the lower member of the Chuar group as described by Walcott and the upper portion of his Unkar group. The sediments of the Nankoweap group are 330 feet thick and are separated from both the Unkar and Chuar groups by erosional unconformities. A fossil jellyfish medusa found in the Nankoweap sediments suggests that a portion of the Nankoweap has been deposited in an ocean, bay, or estuary.

CONTENTS

	Page
General statement	953
Geology of Nankoweap group	953
Petrography and source of material	957
Fossil jellyfish	957
Depositional environment	958
References cited	959

ILLUSTRATIONS

Figure	Page
1. Sketch map of eastern Grand Canyon	955
2. Geologic map of Nankoweap Valley	956

Plate	Facing page
1. Geologic map showing distribution of Nankoweap group in Big Bend area, eastern Grand Canyon	953
2. Nankoweap group	954
3. Jellyfish medusa	955

General Statement

The Grand Canyon Algonkian rocks include more than 12,000 feet of sediments, diabase, and basalts known as the Grand Canyon series. This series has been differentiated into the Unkar and Chuar groups. Investigation and mapping of the Algonkian rocks during 1933 and 1934 has resulted in the separation of an intermediate group, called Nankoweap, which includes the lower member of the Chuar group, as described by Walcott, and the upper portion of his Unkar group. It is a pleasure to acknowledge the assistance of R. A. Bramkamp in the field and the counsel of members of the University of California Geological Department at Berkeley during the investigation. R. A. Bramkamp and R. S. Bassler assisted with the paleontology. The Carnegie Institution of Washington contributed financial support in the field. The National Park Service and particularly E. D. McKee extended numerous courtesies. The Nankoweap group has been described previously in part by Van Gundy (1937) (1946) and by Hinds (1938).

Geology of Nankoweap Group

Exposures of the Nankoweap sediments are confined to the eastern part of the Grand Canyon. A small area in Nankoweap Valley contains exposures of 200 feet of the group (Fig. 2). The best section, which is the type section, is found in Basalt Canyon where 330 feet of Nankoweap sediments are exposed. Partial sections are exposed southward along the Colorado River from a point 2 miles south of the mouth of the Little Colorado River to Basalt Canyon and westward to Unkar Creek. Partial sections are also exposed on the south side of the Colorado River in the canyon of Comanche Creek and in the first canyon west of Tanner Canyon (Pl. 1). Thicknesses of the Grand Canyon series units and a measured

section of the Nankoweap group in Basalt Canyon follows:

	Thickness Feet
Chuar group	5098–5323
Disconformity	
Nankoweap group	
Sandy limestone, light gray, thin-bedded, with laminae of green shale	23
Sandstones, white and purple, well stratified, thin-bedded; reddish brown sandstone with thin-bedded purple and red shales which show ripple marks and cross-bedding	52
Sandstone, purple, which is well cemented, thin-bedded, cross bedded, and ripple marked; massive brown sandstone subordinate	80
Sandstones, white, purple and brown. Thin-bedded with numerous ripple marks and mud cracks	147
Siliceous sandstone, white, light brown and purple. Local conglomerate base	28
	330
Disconformity	
Unkar group	5684–6138

The sediments of the Nankoweap group (Pl. 2, fig. 1) are brown or gray when viewed from a distance; close examination of fresh surfaces discloses a predominance of brown, red, or purple. The basal beds of the group, in most places, are composed of conglomerate or coarse sandstone. The conglomerate is 1 foot or less thick and contains well rounded pebbles and cobbles, up to 8 inches across, imbedded in a matrix of sand grains composed of quartz, feldspar, and fine basaltic debris. Eighty-five per cent of the material in the conglomerate, larger than half a centimeter in diameter, is composed of amygdules from the lavas. The amygdules consist of granular quartz and chalcedonic material in shades of cream, red, or black. The remaining 15 per cent of the coarse debris is red or pink siliceous sandstone. The basal conglomerate is present in the canyon of Unkar Creek and Chuar Lava Butte, but is absent at Basalt Canyon and at the valley of Nankoweap Creek. At Chuar Lava Hill, half a mile north of Lava Butte, and Comanche Creek, sandstone dikes extend into the underlying lavas. In Basalt Canyon, the Nankoweap beds include thin-bedded light-brown, purple, and white medium to coarse-grained sandstone, red sandstone alternating with red and gray sandy shale, and thin-bedded gray sandstone. This latter sandstone grades into pure-white, very fine-grained siliceous sandstone which contains laminae of blue-green serpentine debris and chlorite. These sandstones are overlain by thin-bedded buff and green shales which disappear in a short distance along the strike of the beds.

Ripple marks, mud cracks, and crossbedding are very common throughout most of the Nankoweap sediments. Deoxidation spheres are present but rather uncommon. Casts and molds of salt crystals, present in several members of the Unkar group, were not observed in the Nankoweap group.

One of the most distinct unconformities within the Grand Canyon series is located between the Nankoweap sediments and the basaltic lava flows. This contact marks the upper limit of Precambrian volcanic activity in this region. The surface of the basaltic flows has been eroded to an irregular surface. The basal conglomerate of the Nankoweap group, which rests upon this erosional surface, contains debris which has been derived from basalt and sandstone, indicating that the material in the conglomerate has been derived from a diversified source. A second conglomerate, the basal Chuar, rests upon an irregular erosional surface 330 feet stratigraphically above the Nankoweap-Unkar contact, and grades into a coarse-grained sandstone which in turn grades into a

PLATE 2. NANKOWEAP GROUP

FIGURE 1. NANKOWEAP SEDIMENTS, NORTH SIDE OF BASALT CANYON
Ba—basalt, An—Nankoweap group, Ac—Chuar group
FIGURE 2. MUD CRACKS FROM NANKOWEAP GROUP

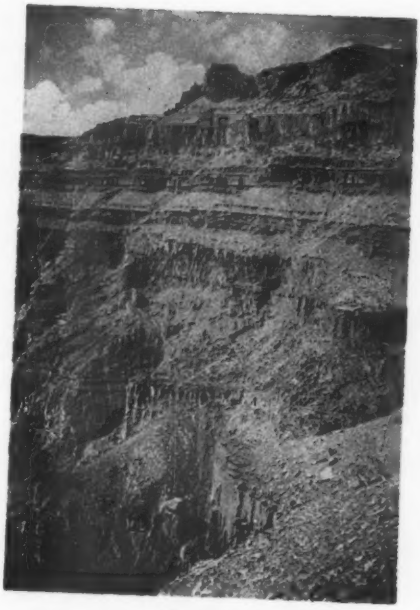

FIGURE 1

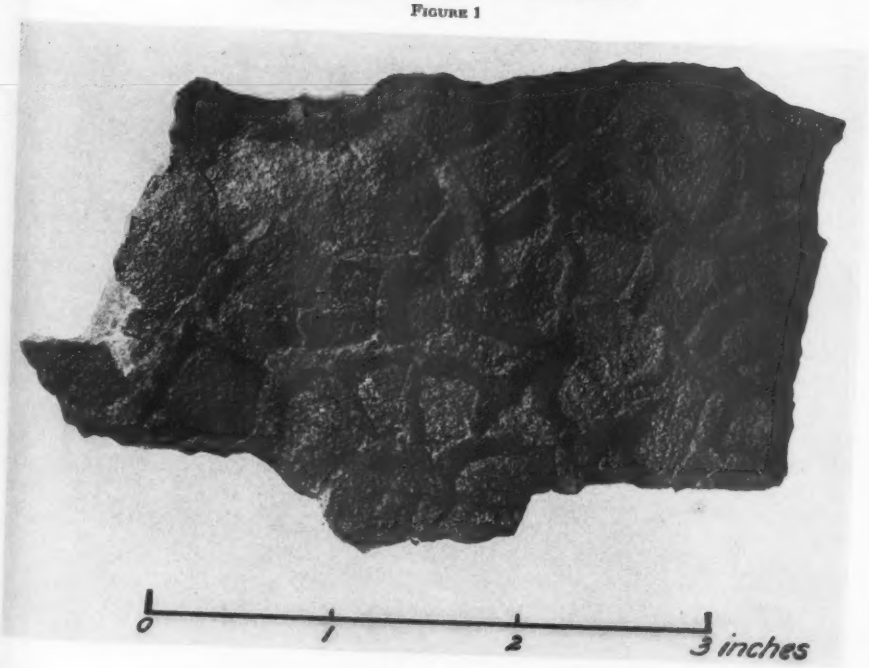

FIGURE 2

NANKOWEAP GROUP

FIGURE 1

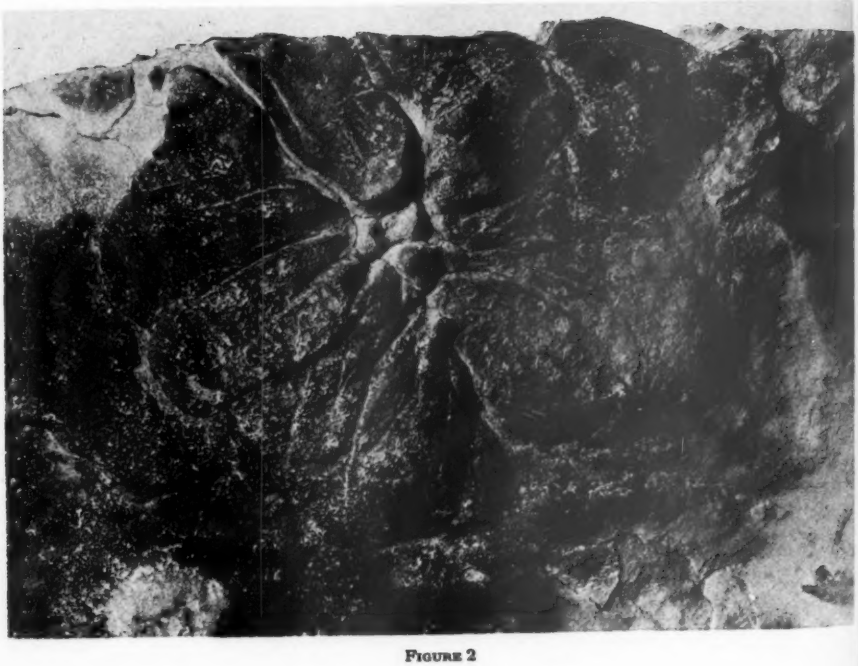

FIGURE 2

JELLYFISH MEDUSA

massive, cliff-forming, magnesian limestone. The erosion surface, conglomerate, and magnesian limestone were observed in the vicinity of Basalt Canyon and at Nankoweap Creek, some 10 miles north of Basalt Canyon. The Nankoweap sediments resemble the sediments of the Unkar group more than those of the Chuar group and were mapped by the writer as the uppermost member of the Unkar group until the unconformity at the top of the

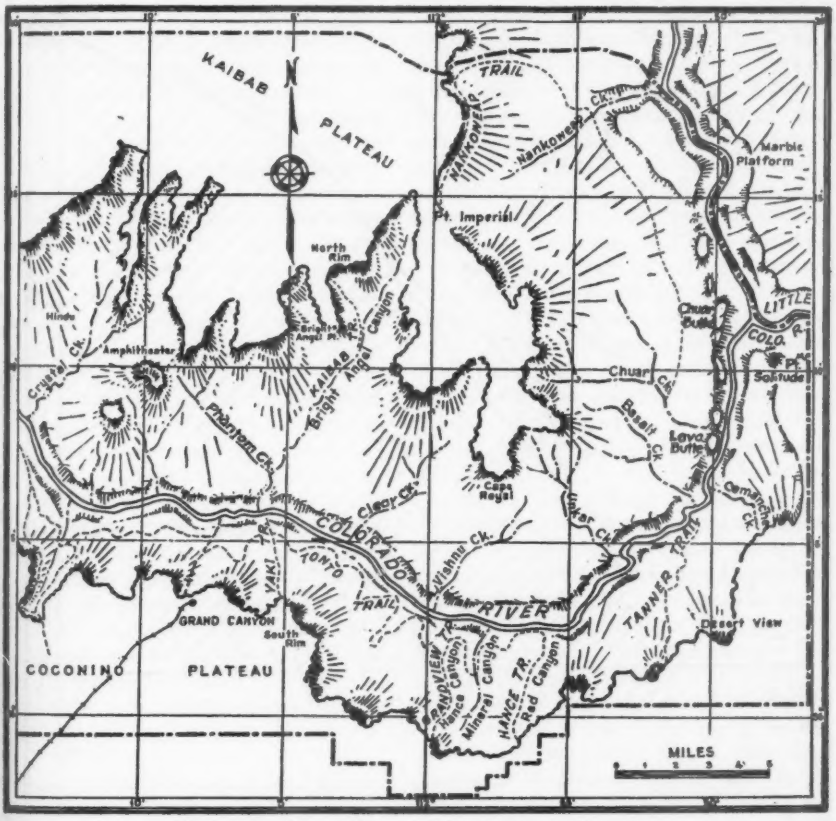

FIGURE 1.—SKETCH MAP OF EASTERN GRAND CANYON

Nankoweap-Chuar erosional unconformity, therefore, is not a local feature. The evidence indicates that the Nankoweap sediments form a distinct and mappable unit separated from the adjacent rocks by disconformities.

basalt was recognized. Walcott (1895) noted this similarity and included these sediments in the Unkar group. The Nankoweap was subsequently considered a transition unit between the basalts and the Chuar group, until an

PLATE 3. JELLYFISH MEDUSA

FIGURE 1. FOSSIL IMPRESSION OF UNDER SIDE OF JELLYFISH MEDUSA
From Nankoweap group. ⅓×

FIGURE 2. A PORTION OF JELLYFISH MEDUSA
Natural size

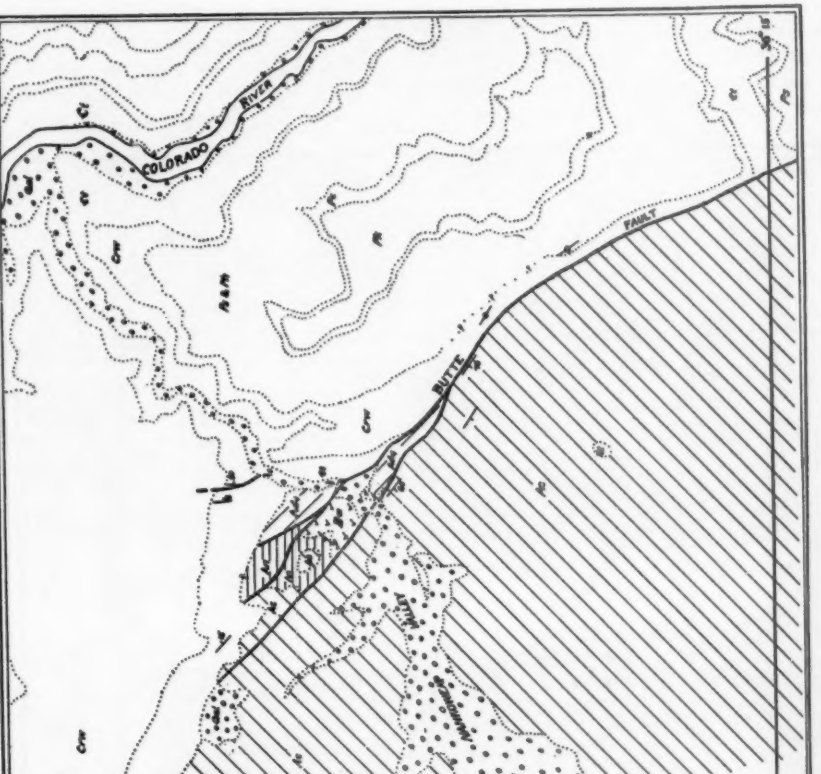

FIGURE 2.—GEOLOGIC MAP OF NANKOWEAP VALLEY

erosional unconformity was found at the base of the Chuar magnesian limestone. The field evidence, in the writer's opinion, does not justify assignment of the Nankoweap sediments to either the Unkar group or the Chuar group or classification as a transition unit. Since this unit separated from, and is located between, two established groups of sediments, it must necessarily be classed as a group. The writer hesitates to designate a mappable unit only 330 feet thick as a group, but some justification for doing this can be derived by comparing the Nankoweap with the Paleozoic sediments which are exposed in the walls of eastern Grand Canyon. Here, the sediments which occur within the Cambrian-Carboniferous interval in the area mapped are less than 300 feet thick and have been assigned to the Devonian period. Furthermore, the overlying Carboniferous sediments show no appreciable angular discordance with either the Devonian or Cambrian sediments. The Ordovician and Silurian periods are not known to be represented by sediments in eastern Grand Canyon although more than 6000 feet of sediments assigned to the Cambrian-Carboniferous interval have been reported in western Grand Canyon and Nevada. The amount of time represented in the Cambrian-Carboniferous interval therefore is much longer than the field relationships alone would indicate. The field relationship of the Chuar-Unkar interval is practically identical with that of the Cambrian-Carboniferous interval and may represent a considerable interval of geological time.

FIGURE 2.—GEOLOGIC MAP OF NANKOWEAP VALLEY

PETROGRAPHY AND SOURCE OF MATERIAL

Microscopic examination of the sedimentary rocks of the Nankoweap group discloses that 91-96 per cent of the mineral grains are quartz and 4-9 per cent are feldspar represented by microcline, orthoclase, and plagioclase (oligoclase-andesine). The remaining minerals include muscovite, sericite, biotite, chlorite, augite, green hornblende, epidote, allanite, tourmaline, zircon, titanite, rutile, magnetite, ilmenite, hydrous (?) iron oxide, leucoxene, serpentine (antigorite), and rock fragments. The rock fragments consist of micrographic intergrowths, quartz aggregates, and argillaceous material. Silica is the predominant cementing material, although some calcium carbonate occurs in the uppermost beds. The grains are predominantly well rounded although sub-angular grains are common. The sediments of the Nankoweap group are, in general, well sorted.

Quartz grains from the Nankoweap show strain shadows and contain numerous inclusions which indicate that the sediments have been derived fro metamorphosed rocks. Microcline, orthoclase, micrographic intergrowths, and tourmaline indicate that acidic igneous rocks have contributed some material. Pegmatite dikes are common in the Archean and the minerals undoubtedly have been derived, at least in part, from them. The Unkar group has contributed some material to the sediments of the Nankoweap group. Amygdules, basalt fragments, augite, chlorite, and antigorite are believed to have been derived from the basaltic rocks of the Unkar group, although some of the antigorite and chlorite may have been derived from other sources. It is doubtful that the Dox sandstone contributed an appreciable amount of material to the Nankoweap group. Mica is sparse in the Nankoweap sediments but is universally present in the Dox sandstone. If the Dox sandstone had contributed appreciably to the Nankoweap sediments, one would expect to find more than an occasional grain of mica, regardless of the mode of transportation. The fragments of siliceous sandstone in the basal conglomerate do not show the effects of metamorphism. The areal extent of deposition of the Nankoweap group is not known and the siliceous sandstone pebbles show no distinctive characteristics, therefore their derivation is not known. The sediments of the Nankoweap group, in general, appear to have been derived from the Unkar basaltic rocks, metamorphic rocks, and acidic igneous rocks.

FOSSIL JELLYFISH

The impression of a jellyfish medusa (Pl. 3) was found in the Nankoweap sediments in Basalt Canyon, 150 feet above the base of the group. This fossil is preserved in a thin-bedded, fine-to very fine-grained brown silty sandstone, which is well-bedded, well-sorted and well-cemented with siliceous cement. Neither ripple

marks nor mud cracks were observed although they are quite common in the other sediments of the Nankoweap group. Only one fossil specimen has been found although a thorough search was made in these and adjacent sediments. The impression measures 18 centimeters across and shows the sub-umbrella or underside of the animal. The outer marginal part of the sub-umbrella is lobed. While only slightly more than half of the animal is present, three distinct lobes and possibly a fourth lobe are shown, indicating that at least six and probably eight lobes were formed on the animal. Marginal tentacles have not been preserved. The central disc is more or less circular and measures 6 centimeters across. It is composed of five principal lobes and three secondary lobes which are 2.5 centimeters long and approximately 1 centimeter wide. The mouth is 1 centimeter across. The Nankoweap specimen does not correspond very closely to any of the types figured in Walcott's monograph (1898) and, according to R. S. Bassler (personal communication) appears to be a new form.

This fossil jellyfish gives positive proof that biologic phyla had become differentiated into types more specialized than the Protozoa prior to the Cambrian, since the Coelenterata, which include jellyfish, represent a highly specialized Phylum. Furthermore, the presence of this fossil in the Algonkian rocks implies that forms intermediate to the Protozoa and Coelenterata must have existed prior to the Cambrian. There is little evidence to support the possibility that the Grand Canyon Algonkian might be Lower Cambrian in age. The Tonto group, which overlies the Grand Canyon Algonkian, is not younger than Middle Cambrian. Lower Cambrian fossils are reported by McKee (1945) from the Bright Angel shale of the Tonto group at localities several miles west of the exposures of the Nankoweap group. Furthermore, considerable tectonic movement has disturbed the area and more than 12,000 feet of Algonkian sediments have been removed in this region during the interval between the Grand Canyon Algonkian and the Tonto group.

The jellyfish has been examined by Dr. Bassler, who writes (1936)

"I really do not know whether your fossil medusae represents a marine or fresh water type, but from all I have seen of the marine species and of the fossil ones that occur with regular marine fossils, I would say that yours undoubtedly indicated the marine type."

Many impressions of medusae have been described from rocks ranging in age from Cambrian to Recent, but none, to the writer's knowledge, have been found hitherto in rocks older than Lower Cambrian. In the Cambrian and Ordovician sediments, the medusae are associated with marine fossils. Hydrozoa medusae are known today from fresh waters throughout the world, and a colonial type (Obelia) is found on seaweed. These forms, however, are small (less than 4 centimeters across) while the Scyphomedusae, which include the jellyfish, are commonly from 1 inch to 6 feet across. *Cyanea artica* has a body 6 feet in diameter and oral arms 130 feet long. These medusae are all marine, and most of them are pelagic floaters and swimmers, although some forms are reported to have been found at depths of 1200 feet below the surface. At the present time, some medusae are found in cold Arctic waters and others in tropical climates. The preservation of the comparatively fragile jellyfish structures in a fine-grained sandstone must have taken place under very ideal conditions, perhaps on the sea floor where strong translatory waves were not active, or possibly in an estuary, bay or lagoon, where the animal floated, became submerged, and was buried rapidly by sediments. The evidence, in the writer's opinion, favors a marine habitat for this animal.

Depositional Environment

The sediments of the Nankoweap group appear to have been deposited in shallow water, either a marine basin or a body of water connected thereto.

The ripple marks, found in many places in the Nankoweap group, include both symmetrical and asymmetrical types. According to Kindle (1925), a ratio of the amplitude to wave length of 1:4 to 1:10 is characteristic of water-formed ripples. All of the ripple marks examined in the Nankoweap group have a ratio of 1:2.5 to 1:10 which indicates that the sediments in which they occur were deposited in water. Some of the ripple marks indicate a

current flowing from south to north; however, in the upper member of this group, a 12-inch thickness of beds contains ripple marks with strikes varying through 360°, indicating that the direction of the currents was quite variable. Interference ripples, or "tadpole nests," in the Nankoweap sediments indicate that local changes in current direction were effective. The occurrence of oscillation ripple marks suggests that at least some of the beds were not deposited on a flood plain or delta, although those showing asymmetric ripples may have had this origin. The deposition must have taken place in a basin where waves of oscillation were active, either the open ocean, a sea, an estuary, lagoon, bay, or a closed basin.

Mud cracks are found in the Nankoweap group (Pl. 2, fig. 2). These indicate that the sediments were deposited in water shallow enough to allow periodic exposure of the sediments to the atmosphere. The mud cracks are developed in sandstones which contain very little argillaceous or colloidal material so that syneresis, advocated by Jungst (1934) as a possible method of producing mud cracks, could not have been effective. Mud cracks have been used as criteria to distinguish fresh-water deposits from salt water deposits, on the theory that, if the edges of the mud crack polygons were convex upward, they were of salt-water origin, but, if the edges of the polygons curled upward, the cracks were considered to have been formed in fresh water. Bradley (1933) has shown that either type of curvature may be formed in salt water and that the main factors which control the curvature are the vertical grain size gradient, the presence of incipient salt crystals toward the upper surface which may produce larger-sized grains than are present in the original clastic material, and the rate of drying. The mud cracks in the sediments of the Nankoweap group show both types of curvature.

Casts or molds of salt crystals were not observed in the sediments of the Nankoweap group although abundant in the Unkar group. This suggests that the Unkar sediments were deposited in or saturated with water of high salt content whereas those of the Nankoweap group were not.

While the inorganic evidence does not show conclusively whether the Nankoweap sediments were deposited in a fresh water, marine, or a brackish water lake of low salt concentration, it does appear to exclude highly saline lakes as a site of deposition. The fossil jellyfish apparently lived in a marine environment, however; most of the Nankoweap sediments appear to have been deposited where they were intermittently submerged by brackish water and where waves of oscillation were active.

The evidence therefore leads to the conclusion that these sediments were deposited in shallow water, possibly an ocean or mediterranean but probably in a body of water connected with the ocean such as a lagoon, bay, or estuary where mud flats or tidal flats existed.

References Cited

Bradley, W. H. (1933) *Curvature of mud cracks*, Am. Jour. Sci., 5th ser., vol. 26, p. 55.

Hinds, N. E. A. (1938) *Algonkian jellyfish from Grand Canyon of the Colorado*, Science, n. ser., vol. 88, p. 186.

Jungst, H. (1934) *Der Geologische Bedeutung der Synarese*, Geol. Rund., Bd. XXV, p. 225.

Kindle, E. M. (1925) *Recent and fossil ripple marks*, Geol. Survey Canada, Mus. Bull. No. 25.

Van Gundy, C. E. (1937) *Jellyfish from Grand Canyon Algonkian*, Science, n. ser., vol. 85, p. 314.

—— (1946) *Faulting in East part of Grand Canyon Canyon of Arizona*, Am. Assoc. Petrol. Geol. Bull., vol. 30, No. 11, p. 1902.

Walcott, C. D. (1883) *Pre-Carboniferous strata in the Grand Canyon of the Colorado, Arizona*, Am. Jour. Sci., 3rd ser., vol. 26, p. 440.

—— (1886) *Second contribution to the studies on the Cambrian faunas of North America*, U. S. Geol. Survey, Bull. 30.

—— (1886) *Classification of the Cambrian System of North America*, Am. Jour. Sci., 3rd ser., vol. 32.

—— (1895) *Algonkian rocks of the Grand Canyon of the Colorado*, Jour. Geol., vol. 3, p. 312.

1190 North Los Robles Avenue, Pasadena, California.

Presented before Cordilleran section, April, 1936.

Manuscript Received by the Secretary of the Society, Jan. 28, 1949

BULLETIN OF THE GEOLOGICAL SOCIETY OF AMERICA
VOL. 62, PP. 961-966 AUGUST 1951

Short Notes

DEEP-SEA SANDS AND SUBMARINE CANYONS[1]

BY D. B. ERICSON, MAURICE EWING, AND BRUCE C. HEEZEN

Well-sorted sands at abyssal depths far from land were first discovered in the South Atlantic by the Gazelle Expedition of 1874 to 1876 (Andree, 1920). Since then other occurrences have been recorded from time to time, but until recently the significance and importance of these interesting sediments have not been appreciated.

In 1947 a bottom-sediment core (150-35) was taken by the research vessel ATLANTIS at a point 750 kilometers (400 nautical miles) southeast of New York City where the depth of water was 4755 meters (2600 fathoms). It contained several layers of well-sorted sand interbedded with clay and globigerina ooze. In the following year another core (152-135) 9 meters long was taken in the same region. It also contained sand layers, one of which was more than a meter thick.

In the meantime much was being learned about the topography and sediments of the Hudson Canyon region. It was found that the canyon could be traced with certainty to a distance of about 280 km (150 nautical miles) southeast of the edge of the continental shelf. Beyond this point the regional topography assumed the form of a broad plain gently sloping to the southeast in which the Hudson Canyon was so little entrenched that it could no longer be followed with assurance. It was on this plain that the two cores containing sand had been taken. This association of coarse, well-sorted sediment with a topographical feature resembling an alluvial plain extending out beyond the Hudson Canyon strongly suggested a genetic connection between type of sediment and topography. In order to test the theory that the plain was in fact a submarine delta, a co-ordinated coring and topographic survey was tentatively planned. The much-hoped-for opportunity to carry out the plan came in the summer of 1950 when a scheduled survey by the R/V ATLANTIS in the Hudson Canyon region was interrupted for several days by unavoidable delay in the arrival of another vessel the assistance of which was required in completing the work.

By means of a piston coring tube 10 additional cores having an average length of 6.8 meters were taken on the plain. The numbers of these cores, the positions of which are shown on the accompanying chart, are included in the series 164-13 to 164-24. No cores were obtained at stations 164-18 and 164-21. Although study of these cores has not been completed, preliminary work on them has already yielded so much new evidence having an important bearing on submarine erosion and deep-sea sedimentation that a short note at this time is felt to be justified.

The 12 cores from the plain outline an area of about 15,500 square kilometers or 6000 square nautical miles. Depths of the core stations vary from 4370 meters (2390 fathoms) to 4940 meters (2700 fathoms). All the cores, except one, 164-17, contain sand layers. The layers range in thickness from mere films of clean quartz silt to beds more than 6 meters thick. On the average about 30 per cent of the thickness of sediment penetrated is sand. The sediment interbedded with the sands is largely clay of abyssal facies. The number of sand layers and their positions in the cores differ greatly from core to core. The lower contacts of the individual layers where they rest on abyssal clay are very sharply defined. Graded bedding is evident in some of the sands. In others, where graded bedding is less obvious, it can be shown to be present by sieve analyses. In exceptional layers there is complete gradation from sand through silt into gray clay containing an abnormally large amount of calcium car-

[1] Investigation supported by Government Research Contracts numbered NObsr43355 and N6-onr271 Task Order 24.

bonate for the depth of water of the area. However, in the majority of cases the upper contacts of the sand layers show abrupt change from sand to normal deep-sea sediment. Sorting

important fraction which includes various feldspars, micas, ferromagnesian minerals, and heavy minerals. Glauconite is nearly always present, and frequently there are also a few

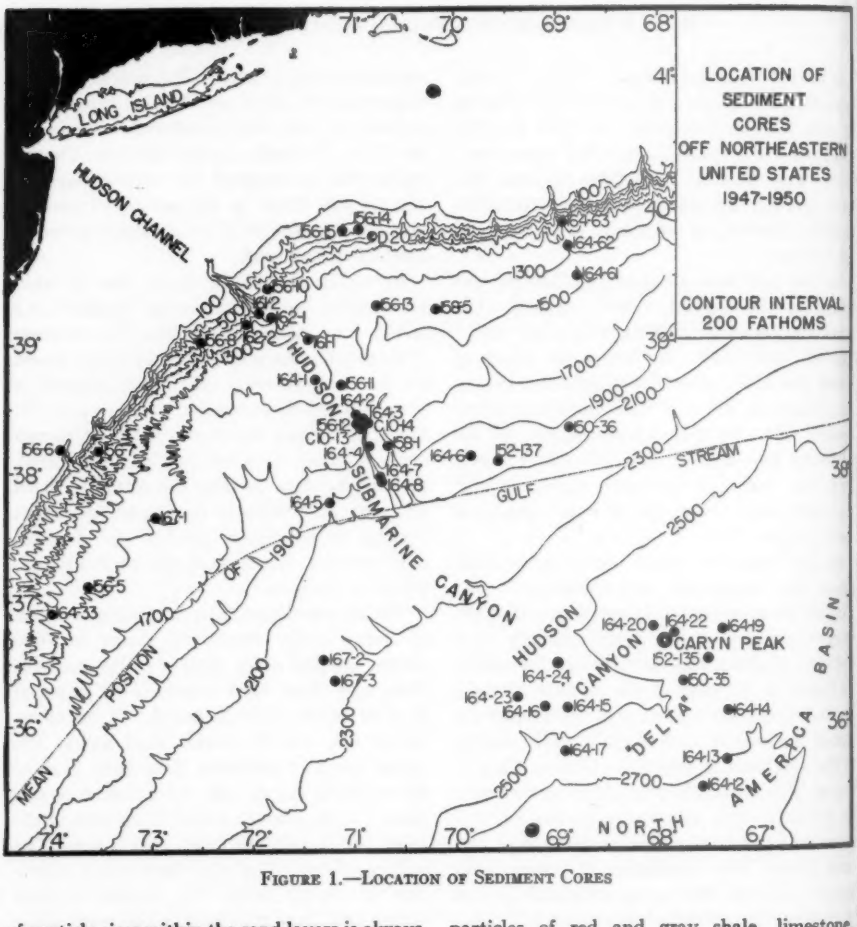

FIGURE 1.—LOCATION OF SEDIMENT CORES

of particle sizes within the sand layers is always good. The small proportion of clay-size material in the sand layers is shown by their remarkable fluidity while still saturated with water. When dry many layers are no more coherent than beach sands.

Although all degrees of rounding, polishing, and frosting are found among the sand particles, angularity predominates. Quartz is the most abundant mineral, but there is usually an

particles of red and gray shale, limestone, chert, fine-grained sandstone, and mica schist. Staining of some of the grains of quartz and feldspar by red iron oxide is not uncommon.

A number of short cores taken in 1947 by the R/V BALANUS on the continental shelf in the vicinity of the head of the Hudson Canyon have been studied at the Lamont Geological Observatory. The coarse fractions of these shelf sediments are remarkably similar in min-

eral composition to the sands of the deep cores. Even the iron-oxide stain on quartz and feldspar grains is present in the shallow-water sediments. The only important difference is in the poor particle-size sorting of the shelf sediments in contrast to the good sorting of the deep-sea sands.

Foraminifera, though never abundant, are usually present in the coarser sands. In addition to the usual planktonic species there are almost without exception a few species which are characteristic of the continental shelf and slope sediments, such as *Elphidium incertum*, *Globobulimina auriculata*, and *Nonion labradoricum*. Not infrequently particles of vegetal matter are also present.

Faunal evidence from the sands and interbedded clays shows that none of the cores reaches sediment as old as the Sangamon interglacial stage of the Pleistocene. Although most of the sand layers must have been deposited during the Wisconsin Glacial stage, there is clear proof that a few have been laid down in post-Wisconsin time. Very recent deposition of sand is shown convincingly in core 164-14. Here a graded sand layer 72 cm thick overlies 38 cm of clay of abyssal facies containing the normal post-Wisconsin assemblage of Foraminifera known to be living in the region at the present time. This 38-cm layer in turn overlies dark-red clay containing a cold-water fauna. No trace of normal deep-water sediment overlies the sand layer. Further evidence that the sand was deposited only a short time ago is provided by the thickness of the post-Wisconsin zone beneath the sand. Its thickness compared with the thicknesses of corresponding layers in other cores from this region shows that it must represent very nearly all of post-Wisconsin time.

Except for one or two doubtful cases correlation of sand layers between even the most closely spaced cores—that is, about 10 miles apart—has not been successful. On the contrary, much disparity from core to core in the thicknesses of interbedded deep-water clay layers, presumably deposited at constant rate throughout the region, shows that the sand layers must be of only local extent, and not continuous sheets blanketing the entire area.

Other important suites of cores have been taken in the region of the Hudson Submarine Canyon to the northwest of the plain. In this area of greater relief there is a close correspondence between type of sediment and topography. On this basis the cores may be divided into three groups. First there are those taken outside of the canyon on the gentle slope into which the canyon has been cut, which contain an upper layer, usually less than 50 cm thick, of abundantly foraminiferal clay resting on clay containing a meager fauna of cold-water species. No sand layers are present or any other sediment at all abnormal for the depth, between 2500 meters (1370 fathoms) and 4000 meters (2190 fathoms), and the distance from the continent. Examples of such cores are numbers 158-5, 164-5, and 164-6.

The second group of cores comes from the canyon walls. These contain a compact green pyritic clay with a Mio-Pliocene fauna. Recent cover, if present at all, amounts to no more than a few centimeters in thickness. Examples are numbers 164-2, 164-4, 164-8, and C10-13.

The third group includes cores taken on the canyon floor. These contain either sand or muddy to fairly clean gravel with abundant mollusk shells and shell fragments. The pebbles of diameters to 2 cm are largely composed of a variety of igneous, metamorphic, and hard sedimentary rocks. In addition there are cobble-size masses of the green clay from the canyon walls as well as pebbles of an upper Eocene chalk which has been cored in place in the canyon wall near the foot of the continental slope at a depth of 2170 meters (1185 fathoms) or more than 1000 meters higher than the gravel occurrences. Dr. Horace Richards, who has examined the mollusks, has reported that they are of Pleistocene age, but that the possibility of faunal mixing is suggested by the presence of a few deep-water forms among many shallow-water species. Study of the Foraminifera contained in the interstitial material supports Doctor Richards' conclusions. Cores containing gravel are numbers 156-12 and 164-7.

Several theories of the origin of deep-sea sands which have been advanced since their discovery 75 years ago can now be dismissed Among these is the theory that they are composed of material which has been carried out from the continent by strong winds. Even if

this mode of transportation could be admitted for the sands, it cannot explain the gravels. The good sorting and graded bedding are fatal to the theory of ice rafting as a mode of transportation for the sands.

Deposition at some time of greatly lowered sea level is disproved by the fact that in so many cases sand layers in certain cores can be shown to be equivalent to uninterrupted deposition of deep-sea clay in other cores. Furthermore, some of the sands have been laid down in Recent time, a fact difficult to reconcile with greatly lowered sea level, to say the least.

On the other hand, mineral and faunal similarity to the shelf sediments points to the continental shelf as the source of a large part of the material making up the sands. The presence of gravels containing shallow-water shells in the canyon bed, but nowhere on the divides outside the canyon, suggests that the route of transportation was through the canyon. Wide occurrence of sands in the sediments of the deep plain upon which the Hudson Canyon opens and absence of sands from the sediment of the gently sloping surface in which the canyon has been cut lead to the same conclusion. In view of the evidence it is the opinion of the authors that transportation by turbidity currents most satisfactorily explains the distribution of sands in the sediments of the plain as well as the occurrence of gravel on the canyon floor.

A conservative estimate of the volume of sand underlying the area of the plain which has actually been cored is in the order of 100 cubic kilometers. The passage of such a quantity of abrasive through the Hudson Canyon can hardly have taken place without more or less erosion of the relatively soft sediments forming the bed and walls. However, it is probable that the total amount of Pleistocene sand in the sediments of the plain is many times the amount estimated. Some erosion, at least, in the course of transportation of the gravel of the canyon is proven by inclusion in the gravel of the upper Eocene chalk pebbles and cobbles of green clay from the canyon walls.

The authors believe that the new evidence from the cores strongly supports the theory that erosion by turbidity currents has been an extremely important process, if not the only process, involved in the formation of the Hudson Canyon.

Several corollaries to these conclusions should be mentioned. If there is a genetic connection between the deep-sea sands of the plain and the Hudson Canyon, there ought to be similar submarine alluvial plains off other canyons of Eastern North America. Although no other area has been so thoroughly charted and cored as that of the Hudson Canyon, there is good evidence from cores and soundings that the Hudson submarine alluvial plain is only one of a series of coalescing alluvial plains which form a zone parallel to the continental slope. By the same reasoning coarse sediments should be found in the beds of other canyons. As yet gravels have not been cored elsewhere than in Hudson Canyon, but coarse sands have been found in other canyons.

If deep-sea sands have been transported by turbidity currents, large quantities of much finer sediment must have been carried out beyond the zone of alluvial plains to be deposited in the deep basins. Evidence of the deposition of this finer material has in fact been found. Some of the deepest cores taken in the North Atlantic contain layers of gray clay of abnormally high calcium carbonate content interbedded with red clay of normal deep-water facies. Frequently the lower contacts of such gray layers are marked by thin layers of clean silt. The gray layers, like the sand layers of the plain, fail to correlate from core to core. If these more calcareous layers were due to climatic changes during the Pleistocene, their lateral extension over fairly wide areas would be expectable. Furthermore, of two adjacent cores from different depths it is usually the deeper one which contains gray layers, while the other is quite likely to contain only normal red clay.

If our conclusion is correct that large quantities of sediment are carried to great distances along the sea bottom by turbidity currents it follows that the rate of deposition even in the deep basins must be much more rapid than has been supposed hitherto. An effect of such a depth-seeking process of sedimentation would be to fill depressions in the sea bottom most rapidly, thus eventually producing broad,

nearly featureless plains. Fathometer records made on board the R/V ATLANTIS in the North Atlantic show that deep-basin topography is often characterized by just such monotonous plains broken only here and there by abruptly rising seamounts presumably of tectonic or volcanic origin.

The evidence presented here provides an extension to the ideas on submarine slumping which have grown up during the past few decades by showing that some of the slumped material is transported to great distances by turbidity currents. Both slumping and turbidity currents have been suggested as processes active upon the ocean bottom primarily on evidence from exposed marine strata. It has now been demonstrated from deep-sea sediments that turbidity currents play a dominant role in marine sedimentation. They transport large amounts of sediment to mid-ocean, and they sort the sediments well during transportation. They deposit the sediments by a depth-seeking process, which tends to fill depressions and produce broad, almost featureless plains like those observed in the North Atlantic basin and on the flanks of the Mid-Atlantic Ridge (Tolstoy and Ewing, 1949). It follows that the rate of deposition in the deep basins must be more rapid than has been supposed hitherto, and that an important part of all deep-sea sediments has been transported, and thereby sorted, at least one time after initial deposition on the ocean floor.

REFERENCES CITED

Andree, Karl (1920) *Geologie des Meeresbodens*, 419–429.

Tolstoy, Ivan, and Maurice Ewing (1949) *North Atlantic hydrography and the Mid-Atlantic Ridge*, Geol. Soc. Am., Bull., vol. 60, p. 1527–1540.

LAMONT GEOPHYSICAL OBSERVATORY, COLUMBIA UNIVERSITY, Palisades, N. Y.
WOODS HOLE OCEANOGRAPHIC INSTITUTION CONTRIBUTION No. 575
LAMONT GEOLOGICAL OBSERVATORY CONTRIBUTION No. 33